ACS Chapter
Nigeria

American Chemical Society (ACS)

Nigeria International Chemical Sciences Chapter

15TH Annual SYMPOSIUM

BOOK OF PROCEEDINGS

THEME: ADVANCING SUSTAINABILITY THROUGH AI-DRIVEN CHEMISTRY

4TH -7TH MAY, 2025 | National Open University of Nigeria, Jabi, Abuja

With

2025 ACS NIGERIA INTERNATIONAL STUDENT SYMPOSIUM EVENT

Themed: Sharpening the Next Generation Chemists for Smarter and Sustainable Solutions to the Global Challenges

AMERICAN CHEMICAL SOCIETY (ACS)

Nigeria International Chemical Sciences Chapter

10th Annual Symposium

Theme: Advancing Sustainability through AI-Driven Chemistry
Date: 4th -7th May, 2025
Venue: National Open University of Nigeria, Jabi, Abuja

With:

2025 ACS Nigeria International Student Symposium Event

Themed: *Sharpening the Next Generation Chemists for Smarter and Sustainable Solutions to the Global Challenges,*

BOOK OF PROCEEDINGS

ISBN: 978-978-68-0485-9

Published by ACS Nigeria

Members of Symposium Organizing Committee

International Advisory Committee

S/N	Name	Affiliation	Research Area	Country
1.	Prof. Joshua A. Obaleye	University of Ilorin, Ilorin, Kwara State	Inorganic Chemistry	Nigeria
2.	Prof. Edu Inam	University of Uyo, Uyo, Akwa Ibom State	Analytical/Environmental Chemistry	Nigeria
3.	Prof. Tolulope Fasina	University of Lagos, Nigeria	Inorganic Chemistry	Nigeria
4.	Prof. Jennifer Nielson	Brigham Young University	Liaison Officer	USA
5.	Prof. Ryan Richards	Colorado School of Mines	Liaison Officer	USA
6.	Dr. Philip Obande Ogaba	National Open University of Nigeria, Abuja	Physical/Computational Chemistry	Nigeria
7.	Prof. Haruna Aliyu Dede	National Open University of Nigeria, Abuja	Inorganic Chemistry	Nigeria
8.	Prof. (Mrs.) F. W. Abdulrahman	University of Abuja, Nigeria	Analytical Chemistry	Nigeria
9.	Dr. Sederra Ross	ACS Green Chemistry Institute	-	USA

Local Organizing Committee

S/N	Name	Affiliation	Position
1.	Dr. Thompson Izuagie	National Open University of Nigeria	Chairman
2.	Prof. Emeka C. Ogoko	National Open University of Nigeria	Member
3.	Dr. Henrietta I. Kelle	National Open University of Nigeria	Member
4.	Dr. Gloria Otunola	National Open University of Nigeria	Member
5.	Dr. Musa Runde	National Open University of Nigeria	Member
6.	Dr. Nnemeka E. Ihegwuagu	Agricultural Research Council of Nigeria, Abuja	Member
7.	Prof. Jimoh Abdulfatai	University of Abuja	Member
8.	Dr. Ahmed Umar	University of Abuja	Member
9.	Mr. Maxwell Duru	Chemical Society of Nigeria Abuja	Member
10.	Mr Timothy Samuel	Chemical Society of Nigeria Abuja	Member
11.	Mr. Fagbohun Adebisi A	Sheda Science and Technology Complex (SHESTCO), Abuja	Member
12.	Dr Afolayan Micheal	Sheda Science and Technology Complex (SHESTCO), Abuja	Member
13.	Dr. Bilkisu Adedoyin	University of Abuja	Member/Secretary

Reviewers

S/no.	Name	Affiliation(s)	Area of specialization
1.	Dr. Sampson D. Umoh	Joseph Sarwuan Tarka University, Makurdi, Nigeria	Medicinal/natural products chemistry
2.	Dr. Olutayo Olajide	Sheda Science and Technology complex, Abuja, Nigeria	Organic / Natural Products Chemistry
3.	Dr. Fausat Afolami	Lagos State University of Science and Technology, Lagos, Nigeria	Analytical / Environmental Chemistry
4.	Dr. Olajumoke O. Emmanuel	Michigan State University, USA	Materials Chemistry
5.	Dr. Victoria Ndukhaire	Sheda Science and Technology complex, Abuja, Nigeria	Organic Chemistry
6.	Dr. Ruth Mafomoyomi	University of Abuja, Nigeria	Education Chemistry
7.	Dr. Ama Shadrack Oryina	Federal University Wukari, Nigeria	Inorganic Chemistry
8.	Dr. Okibe Gideon	Auburn University, USA	Natural Products and Medicinal Chemistry
9.	Dr. Adebisi Fagbohun	Sheda Science and Technology complex, Abuja, Nigeria	Analytical chemistry
10.	Dr. Olakunle Fatokun	University of Abuja, Nigeria	Natural Products Chemistry
11.	Dr. Emmanuel Etim	Federal University Wukari, Nigeria	Analytical / Environmental / Physical Chemistry
12.	Dr. Adewale Fadeyi	Sheda Science and Technology complex, Abuja, Nigeria	Organic Chemistry
13.	Dr. Humphrey Samuel	Emory University, Atlanta, USA	Environmental Remediation and sustainability
14.	Dr. Blessing Sunday	Nassarawa State University, Keffi, Nigeria	Analytical Chemistry
15.	Dr. Eno-Obong Sunday Nicholas	University of Nigeria, Nsukka, Nigeria	Material and Inorganic Chemistry
16.	Dr. Michael Afolayan	Sheda Science and Technology complex, Abuja, Nigeria	Organic Chemistry

TABLE OF CONENTS

ACS Chapter Nigeria
Book of Proceedings
15th Annual Symposium
ISBN: 978-978-68-0485-9
DOI: https://doi.org/10.55455/acsnigeria.1.2.1-7

The Search for new Antibiotics from *Microtetraspora gluaca* DEM 31097

Hadiza Aminu Isah[*a,b], Bernard Kepplinger[b,c] and Michael John Hall[b]
[a]Department of Chemistry; Faculty of Science, Nigerian Defence Academy, Kaduna. [b]Newcastle University, Newcastle upon Tyne, UK, [c]Demuris Ltd, Newcastle Upon Tyne UK.
Corresponding Author's email: haisah@nda.edu.ng

ABSTRACT

The rise in antibiotic resistance has led to the search of new antibiotic agents with new mechanisms of action from actinomycetes bacteria. Actinomycetes are slow growing Gram-positive bacteria which are known producers of antibiotic compounds. Therefore, the aim this study was to search for antibiotic compounds using understudied unusual actinomycetes obtained from the Demuris Ltd collection of over 1000 actinomycetes bacteria. The pre-screening of 66 unusual actinomycete strains at Demuris Ltd led to the selection of the DEM 31097 strain based on its bioactivity. From taxonomic identification using 16S rRNA analysis of DEM 31097, the closest relative was found to be a *Micro*tetraspora *gluaca* with a 99.84% match. The growth of DEM 31097 was optimised by fermentation in a large scale 20 L bioreactor and the fermentation was monitored for contamination and onset antibiotic production. From the fermentation, the antimicrobial activity was detected after 159 hours 46 minutes. Using bioassay-guided fractionation, the bioactive secondary metabolite was identified as a possible gram-positive antibiotic. After a series of liquid-liquid extractions and isolation procedures were attempted the bioactive compoun.d(s) present in DEM 31097 appeared to be polar, pH independent, and either solvent or concentration dependent.

KEYWORDS: Antibiotic, *Microtetraspora glauca* DEM 31097, bioassay-guided fractionation.

1. INTRODUCTION

Natural products are defined as secondary metabolites and they can have a broad range of functions in many biological systems.[1] Traditionally herbal medicine has long utilised bioactive natural products, in the form of plant materials or extracts, in the treatment of diseases.[2,3] The earliest evidence for the use of natural products derived from plants in medicine was found on a Sumerian clay slab, thought to be about 5000 years old, on which were described 12 drug preparation recipes from over 250 plants.[4]

Bacteria are diverse in nature and are major sources of bioactive compounds.[5] The majority of these compounds come from bacteria that inhabit the soil, specifically the actinomycetes.[6] Actinomycetes are filamentous, Gram-positive actinobacterium mainly found in soil and freshwater.[6] Actinomycetes are rich sources of novel bioactive compounds, with many strains still unexplored.[5,7] Examples of antibiotic producing actinomycetes and their antibiotics include *Streptomyces* (e.g. tetracycline), *Amycolatopsis rifamycinica* (e.g. rifamycin) and *Actinomadura* (e.g. spirotetronate).[8,9]

Use of antibiotics over time led to the occurrence of antibiotic resistance by disease causing bacteria. Bacteria have developed several different mechanisms to resist the effects of antibiotics. These mechanisms led to the rise of multidrug-resistant strains of bacteria which cannot be controlled by existing antibiotics.[10]

To successfully continue the discovery of biologically active compounds, new approaches must be considered in order to reduce rediscovery of known compounds or analogues. These analogues tend to have similar mechanisms of action on bacteria as their known analogues.[11] New approaches such as research into the understudied genus of actinomycetes have shown promising results in the search for novel classes of antibiotics.[12] The chances of discovery of new novel antibiotics with different mechanisms of action are very high.

Therefore, the aim of this research is to search for new antibiotics from understudied *Microtetraspora gluaca* DEM 31097. Prior to this project, 66 actinomycete understudied strains were collected and pre-screened for antibiotic activity against both Gram-positive and Gram-negative pathogenic strains at Demuris Ltd. From the 66 understudied strains DEM 31097 was selected for further studies based on the biological activity presented.

2. MATERIALS AND METHODS

2.1 Growth media and Disc diffusion assay

All procedures were done under sterile conditions.

2.1.1 Growth media

Growth media are prepared using distilled water in a sterile bottle and depending on which media is being used (Table 1) the pH is adjusted using 2 M NaOH or 50 % HCl at room temperature. The prepared media are autoclaved (sterilised) in an Astell autoclave at 121 °C for approximately 3 hours and allowed to cool to 60 °C in a hot water bath before use.

Table 1: Different growth media and their compositions

Medium	Components	pH
ISP2- (Glucose, yeast and malt) extract	4 g/L Glucose, 4 g/L Yeast Extract and 10 g/L Malt Extract.	7.0
Nutrient Broth	15 g/L Peptone, 6 g/L Sodium Chloride, 3 g/L Yeast Extract and 1 g/L glucose	7.0
Nutrient Agar	5 g/L peptone, 1.5 g/L yeast extract, 1.5 g/L beef extract, 5 g/L sodium chloride and 15 g/L agar.	7.4

2.1.2 Disc Diffusion Assay

Samples are prepared by dissolving in a minimum about of solvent (~ 1ml of solvent). For a 100 ml disc diffusion assay agar, the agar was prepared by pipetting 100 µL *Bacillus* reporter strain Table 2, 100 µL erythromycin and 100 µL of 5-bromo-4-chloro-3-indolyl-β-D-galactopyranoside (X-Gal) each into a 100 mL autoclaved growth media. This impregnated media is poured onto an agar plate under lamina flow and allowed to set for about an hour.

The spotted discs were prepared by labelling and spotting each 5mm disc with 10 µL of samples, positive and negative controls and left to dry for about 30 minutes depending on the solvents used to prepare the samples. The spotted disc containing different samples are then mounted onto the set seeded agar plate and incubated in Sanyo Ltd MIR-262 incubator at 30 °C overnight. Diameters of clear zones of inhibition are recorded once the bioassay plate is removed from the incubator.

Table 2: Reporter strain used in assessing the mode of action of the bacterial strain

Bacillus reporter strain	Mode of action	Resistance	Positive control
YpuA	Cell wall synthesis	Erythromycin	Cefotaxime

2.2 Fermentations

10mL of liquid ISP2 medium were inoculated with a single loop of spores of the selected strain and incubated in an Innova®40 enclosed orbital shaker at 160 rpm for 3 days at a temperature of 30°C. A 10% inoculum (culture in 10 ml ISP2 media) was used to subculture 50mL, 200mL and 500mL of ISP2 medium sequentially. As the strains were growing exponentially from the seed culture only a single day of incubation was required for the 50mL, 200mL and 500mL cultures. Erlenmeyer flasks containing media to a quarter of their volume were used to give sufficient aeration. For the 500mL fermentations baffled 2L flasks were used to give additional aeration.

Large-scale fermentation was carried out using a 20 L glass fermenter from applikon Biotechnology with an ez-control. Temperature of 30 °C and a starting pH of 7 were maintained but not controlled during the fermentation process.

Dissolved oxygen was set at a minimum of 40 % which was controlled by the impeller speed and compressed air intake was kept constant. The impeller speed was at 250 rpm to reduce foaming; foaming was further controlled by the use of a few drops of PPG (1 ml L^{-1}) in the reactor and 50 % antifoam A in a sterile bottle controlled by the foam probe connected by a peristaltic pump.

Samples were taken three times a day and the OD_{450} was measured in triplicate. The samples taken were streaked on to nutrient and growth media plates then incubated overnight at 30 °C to monitor contamination.

2.3 Offline sampling

Several parameters such as glucose concentration, free phosphate concentration and optical density were measured after samples were collected from fermenter. The glucose concentration was measured using the SD Codefree blood glucose monitoring system.

2.4 Determination of phosphate concentration in the supernatant

1 mL of samples collected in 1.5 mL sterile tubes are centrifuged at 1000 rpm for 8 minutes. To separate 1.5 mL sterile tubes, 85 µL of the supernatant, the Pi standards, the liquid ISP2 media and reagent blank (distilled water) were each pipetted. To each of these 1.5 mL sterile tubes we added 1000 µL of ASA reagent and incubated for 90 minutes at 37 °C, after 90 mins blue colouration was observed. To stop the reaction, 400 µL of 2M H_2SO_4 was added to each of the 1.5 mL sterile tubes. The absorbance was measured at 820 nm against reagent blank and the values recorded. The absorbance of Pi standards was plotted against concentration to obtain a Trent line equation which was used to calculate the phosphate concentration of the samples.

Antibiotic activity was assessed by a disc diffusion assay, after the samples were taken.

2.5 HPLC-DAD

An Agilent Technologies© 1260 infinity HPLC with an integrated diode array detector was used to assess the purity of extracts throughout the purification processes. For a 200 µl dilution, samples were dissolved 20 µl of HPLC grade methanol (MeOH) and diluted with 180 µl of HPLC grade H_2O. A C18 phenomenex® column (150 x 4.60 mm, 4 µm) was used. The typical gradient performed was 0% acetonitrile (CAN) (0.001% formic acid (FA)) to 100% (FA) over 45 minutes at a flow rate of 1ml min^{-1}. Injection volume ranged between 40 to 200 µl depending on the volume of the diluted sample.

2.6 Extraction and purification: DEM 31097

DEM 31097 cultures obtained after fermentation was centrifuged at 8000 rpm for 10 minutes and cell pellet was collected and the supernatant discarded.

994 g of wet cell pellet collected was frozen before being freeze dried for 7 days, and weighed after 7 days to give 395 g of dry cell pellet. The dry cell pellet was soaked in acetone and stirred for 2 days at room temperature, filtered and washed twice more with acetone. The solvent (acetone) in the cell pellet extract was evaporated using a rotary evaporator to yield a 47 ml concentrated solution.

The next step was a liquid-liquid extraction of the cell pellet extract as described in Figure 1.

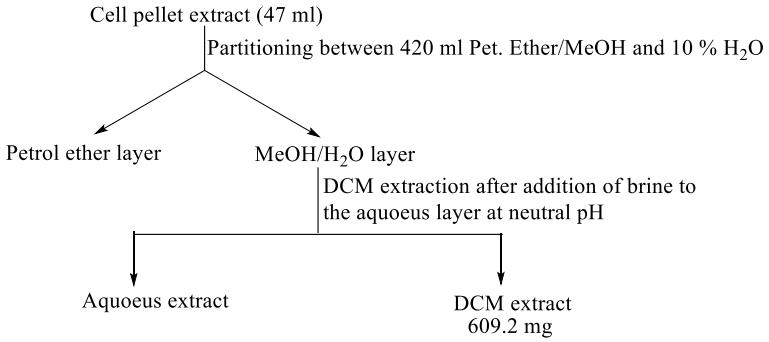

Figure 1: Flow diagram showing extraction procedure of DEM 31097 cell pellet

3. RESULTS AND DISCUSSION

3.1 Taxonomic identification of DEM 31097 strain

Under the microscope, DEM 31097 appeared to have spores in a chain of four spores which is characteristic of the *Microtetraspora* strain. A *Microtetraspora* has two mycelia, a vegetative mycelium which has a long, branching and wavy filament that penetrates the agar (Figure 2) forming tough and raised colonies and an aerial mycelium that appears on the vegetative mycelium and are scantly branched and straight.[13]

Using a 16S rRNA alignment on a Mega6™ software, the phylogenetic tree was plotted and a neighbouring tree was produced using *Actinomudura madurae* DSM 43067 as a root. On analysis, the closest neighbour was *Microtetraspora glauca* with a 99.84 % similarity (See Figure 3).

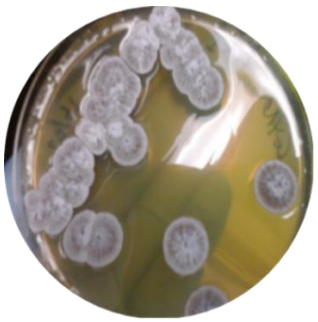

Figure 2: An agar plate showing DEM 31097/TW41a strain

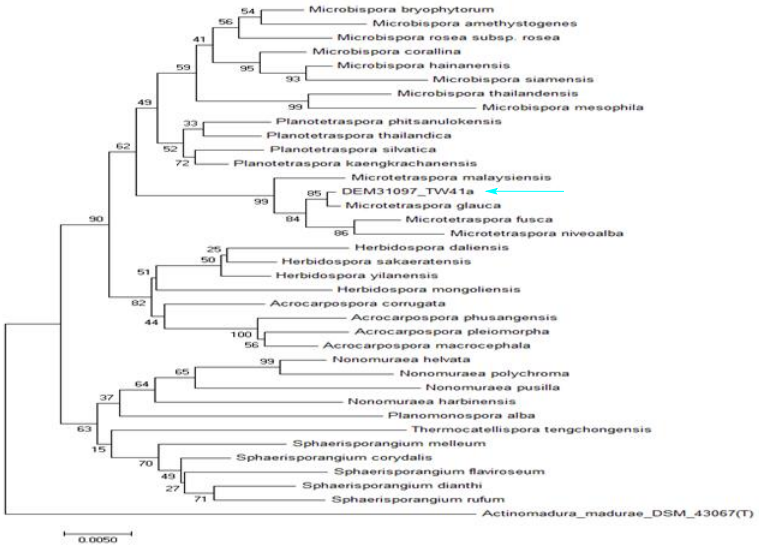

Figure 3: A 16S rRNA phylogenetic tree showing DEM 31097 and its relatives

Microtetraspora sp. is an understudied strain of actinomycetes in which no bioactive compounds with antibiotic activity have been reported from these species. Its neighbours on the 16S rRNA also are not known to produce antibacterial secondary metabolites. Therefore, this strain was chosen because the secondary metabolite causing the observed antibiotic activity against Gram-positive bacteria was likely to be a new novel bioactive compound.

3.2 Growth optimisation of DEM 31097 for the production of novel antibiotics

To investigate the bioactivity of DEM 31097 further, large-scale fermentation using a 20 L fermenter of the strain was required. From the shake flask fermentation, antibiotic production was observed approximately after 7 days, thus on a larger scale we estimated that at least 7 days of fermentation would be required.

DEM 31097 was taken from frozen glycerol stocks of spore suspensions from a -80 °C freezer, revived and streaked onto ISP2 agar plate and left to grow in an incubator for 3 days. Spores taken from the freshly grown plates were used to inoculate 10 mL liquid ISP2. The culture was grown exponentially by culturing into larger flasks each time using about 10 % of inoculum, before finally inoculating into a 20 L fermenter containing about 18 L of autoclaved ISP2 media.

We checked for contamination by using the samples collected throughout the fermentation process. To each daily sample collected, a sterile loop was used to collect and streak the bacteria samples onto two different agar plates. One agar plate contained solid ISP2 media and the other contained a solid nutrient agar. These inoculated plates were incubated at 30 °C for three days. After three days each plate was viewed for presence of any fast-growing bacteria such as *Bacillus* or *E.coli*.

Several parameters were used to monitor growth of the bacteria; these parameters were optical density, glucose concentration and free phosphate concentration (Figure 4).

The optical density is a representation of the bacterial growth. The optical density at (OD_{450nm}) for the first 100 hours was approximately 0.5 at OD_{450nm}, indicating the lag phase before it started rising quite quickly between 110 and 140 hours to about 2.7 at OD_{450nm}, indicating the exponential phase and stationary phase, before declining steadily from around 150 to 240 hours when the bacterial growth was in death phase.

Glucose concentration and free phosphate concentration both decreased during the course of fermentation. Free phosphate concentration from the graph appeared to be taken up much faster by the bacteria than the glucose, as its concentration decreased from about 2.5 mM to 1.0 mM in approximately 30 hours. However, both nutrients depleted once the bacteria appeared to have reached its stationary growth phase. It is during this nutrient starvation that bacteria start to compete for survival and start producing antibiotics as a defence mechanism.[14] This is observed in figure 4 when bacteria growth reached its stationary phase and started declining at approximately 159 hours.

The antibiotic activity test against Gram-positive bacteria was carried out on the samples collected, to determine the onset of antibiotic production. The samples collected were centrifuged at 4000 rpm for 15 minutes, filtered and the supernatants collected. The supernatants were concentrated by solid phase extraction using a C18 cartridge with MeOH as the eluent. The cell pellet was extracted with acetone. The cell pellet extracts, the supernatant and the SPE fractions collected from these extractions were tested for antibiotic activity using disc diffusion assay verses *B. subtilis ypua* (a Gram-positive bacterial reporter strain for cell wall synthesis activity).

After 159 hours, antibiotic activity was observed from the cell pellet extracts, however no activity was observed from SPE fractions at this time point. With the onset of antibiotic production obtained, the fermenter was kept running for 3 days to monitor any changes in antibiotic activity. On the 11th day the fermenter was partially harvested and the bacteria culture was centrifuged, filtered and the cell pellet was bioactive after being tested for antibiotic activity. Meanwhile the fermenter was refilled with more growth media to obtain sufficient bacterial culture for analysis, before the bacteria culture was finally harvested on day 21.

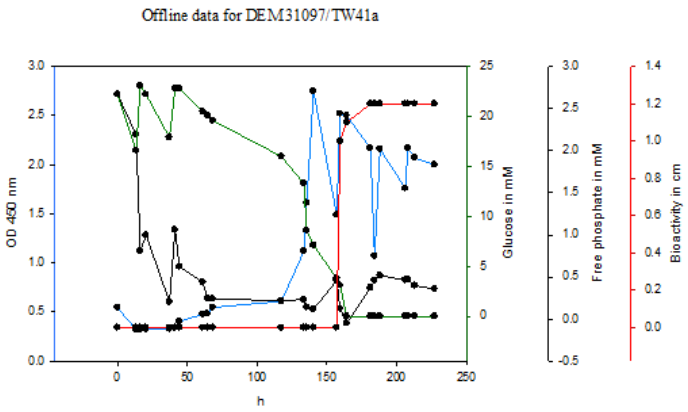

Figure 4: Offline data of DEM 31097/TW41a 18 L cultivation

3.3 Extraction and Purification of Bioactive Natural Products from Cell Pellet Extracts of DEM 31097

We therefore decided to attempt to isolate the secondary metabolite(s) responsible for the observed antibiotic activity that were present in the cell pellet. The first step in this process was to isolate the cell pellet material from both the fermenter runs. The cell pellet was frozen, then freeze-dried and extracted with acetone and concentrated to yield a crude extract. The crude extract was bioactive after being tested for antibiotic activity using disc diffusion assay.

After several extraction attempts using solvents of varying polarity, the addition of brine to the aqueous layer, during dichloromethane (DCM) extraction was successful with the antibiotic activity being observed from the organic layer. The next step was to examine suitable chromatography conditions on the DCM/brine extract, including normal phase chromatography and size exclusion chromatography. Our first purification attempt used normal phase chromatography.

Normal phase chromatography was performed by using three different solvents one after another, namely ethyl acetate (EtOAc), DCM and MeOH, a preparative reverse phase HPLC and Size-exclusion chromatography (SEC) using MeOH were all carried out on samples of the crude extract. The fractions were collected after each purification step was pooled together according to the solvents used and concentrated via rotary evaporation. A test for antibiotic activity using disc diffusion assay was carried out on the fractions obtained and the results were negative. We postulated that this might be due to the bioactive compounds either degrading as a result of instability during chromatography or being retained on the silica.

Due to the difficulties in isolating bioactive compounds from the cell pellets of the fermentations of DEM 31097, possibly due to compound instability, we decided to re-grow the bacteria in shake flasks to see if the previously observed biological activity in the supernatant could be recovered. We envisaged that the supernatant activity was due to the presence of an alternative antibiotic which might prove easier to isolate.

4. CONCLUSION

DEM 31097 has been taxonomically investigated and identified as a *Microtetraspora sp.* which poses antibiotic activity against Gram-positive bacteria. A suitable growth condition for DEM 31097 has been optimised and achieved in a large-scale fermenter. Interestingly, we observed that different growth condition seem to lead to the production of possibly different secondary metabolite(s) by DEM 31097. After a series of extraction and isolation procedures were attempted the bioactive compound(s) present in DEM 31097 appeared to be polar, pH independent, and either solvent or concentration dependent. Also, progress has been made in the design of a liquid/liquid extraction protocol for the purification of the cell pellet antibiotics. In shake flask fermentation, the isolation of the antibiotic compound present in the supernatant has begun, but these compounds appear unstable in methanol. Thus, we plan to develop an isolation protocol for extraction of secondary metabolite(s) present in the supernatant.

The difficulty encountered in the development of a new isolation protocol of bioactive compounds from understudied actinomycetes arises from the absence of limited literature and knowledge of the newly isolated strain of actinomyctes [12]. Therefore, the use bioassay fractionation method allows for the steady screening of extracts based on their biological activity against disease causing and antibiotic resistant strains. As a result the potential use of understudied actinomycetes in the search for new antibiotic compounds with new and improved modes of action for combating antibiotic resistance is promising.

REFERENCES

(1). A. Demain and A. Fang, in *History of Modern Biotechnology I*, ed. A. Fiechter, Springer Berlin Heidelberg, Editon edn., 2000, vol. 69, pp. 1-39.
(2). R. Croteau, T. M. Kutchan and N. G. Lewis, *Biochem. Mol. Biol. Plants*, 2000, **24**, 1250-1319.
(3). R. N. Cavalcanti, T. Forster-Carneiro, M. T. M. S. Gomes, M. A. Rostagno, J. M. Prado and M. A. A. Meireles, in *Natural Product Extraction: Principles and Applications*, The Royal Society of Chemistry, Editon edn., 2013, pp. 1-57.
(4). B. B. Petrovska, *Pharmacognosy reviews*, 2012, **6**, 1.

(5). M. I. Hutchings, A. W. Truman and B Truman, *Current Opinion in Microbiology*, 2019, **51**, 72-80.
(6). M. F. Traxler and R. Kolter, *Natural product reports*, 2015, **32**, 956-970.
(7). Y-G. Zhu, Y. Zhao, D. Zhu, M. Gillings, J. Penuelas, Y. S. Ok, A. Capon and S. Banwart, *Environment International*, 2019, **131**, 105059.
(8). M. D. Surette, P. Spanogiannopoulos and G. D. Wright, Acc. Chem Res., 2021, **54(9)**, 2065-2075.
(9). J. Euanorasetr, B. Intra, P. Mongkol, S. Chankhamhaengdecha, P. Tuchinda, M. Mori, K. Shiomi, T. Nihira and W. Panbangred, *World J Microbiol Biotechnol*, 2015, **31**, 391-398.
(10). K. E. Vivekanandan, P. V Kumar, R. C Jaysree and T. Rajeshwari, *Global Medical Genetics*, 2025, **12 (2)**, 100042.
(11). C. Pearce, P. Eckard, I. Gruen-Wollny and F. G. Hansske, in *Natural Product Chemistry for Drug Discovery*, The Royal Society of Chemistry, Editon edn., 2009, pp. 215-241.
(12). J. Parra, A. Beaton, R. F. Seipke, B. Wilkinson, M. I. Hutchings and K. R. Duncan *Current Opinion in Microbiology*, 2023, **76**, 102385.
(13). J. E. Thiemann, H. Pagani and G. Beretta, *J. Gen. Microbiol.*, 1968, **50**, 295-303.
(14). J. Martín and P. Liras, in *Reprogramming Microbial Metabolic Pathways*, eds. X. Wang, J. Chen and P. Quinn, Springer Netherlands, Editon edn., 2012, vol. 64, pp. 115-138.

ISBN: 978-978-68-0485-9 DOI: https://doi.org/10.55455/acsnigeria.1.2.8-13

Phytochemical Screening, Gas Chromatographic Analysis and Antimicrobial Efficacy of De-Fattened Methanolic Fresh Stem Extract of *Cissus arguta* Hook.f. (Sunset bell)

[1]Hamzah Audu Bawa[*], Farida Audu Bawa[**], Mary Olire Edema[*], and Emmanuella Eloho Agbidi[*]

[*]Department of Chemistry, [**]Department of Science Laboratory Technology, College of Science, Federal University of Petroleum Resources, Effurun, PMB, 1221, Delta State, Nigeria.

[1]Corresponding Author's email: audu.hamzah@fupre.edu.ng

ABSTRACT

Medicinal plants have been a fundamental part of human history for centuries, providing a vast array of therapeutic benefits. Investigating the antimicrobial potentials of *Cissus arguta* provides scientific support for its traditional use. This study focuses on conducting phytochemical screening, chromatographic analysis, and evaluating the antimicrobial efficacy of the fresh stem extracts of *Cissus arguta*. The methanol extraction of pulverized fresh plant stems was performed using soxhlet extraction, preceded by exhaustive de-fatting with n-hexane. Phytochemical analysis of the methanol extract identified eight compounds: alkaloids, glycosides, anthraquinones, flavonoids, saponins, steroids, tannins, and terpenoids. Chromatographic analysis revealed eleven components, primarily composed of esters, terpenes, and terpenoids (85.11%), followed by carboxylic acids (6.14%) and hydrocarbons (8.76%). The most abundant compound was 14-methyl-pentadecanoic acid methyl ester (29.90%), while the least abundant was the hydrocarbon 7-methyl-3,4-Octadiene (1.04%). The extract exhibited potent bactericidal effects against bacterial isolates with a minimum inhibitory concentration (MIC) ranging from 0.30±0.90 to 1.16±0.00 mg/mL across all tested microorganisms. These findings substantiate *C. arguta* as a promising broad-spectrum antimicrobial agent rich in bioactive phytochemicals, providing scientific validation for its traditional medicinal use.

KEYWORDS: *Cissus arguta, antimicrobial*, *GC-MS*, *phytochemicals*, *medicinal plants*.

1. INTRODUCTION

Throughout history, medicinal plants have been known to generate a vast range of chemicals that help them carryout critical biological tasks and defend themselves against predators.[1,21,25] *Cissus* comprises of nearly 400 species distributed globally,[2] representing the largest of all 14 *Vitaceae* genera. The genus of the plant has approximately 150 species in Africa, and 35 % of these species are found in West Africa. There are at least 40 species of the plant within the northern and southern Nigeria. The low seed production and propagation rate in all vegetation of *Cissus* species make its natural vegetation inconsequential.[3] In Nigerian traditional medicine, the stem is used in bone healing while the leaves when crushed, have been effectively used for treatment of microbial infections, inflammations, wounds, as well as cuts. It is also used for the treatment of intense fever, rheumatism, cough, arthritis, chest pain, gout, blockage of blood vessels, skin infections and wounds, body pains, dropsy, edema, febrifuges, as pain-killers, pulmonary troubles, and sexually transmitted infections, while the sap have been used for eye treatments and venereal diseases, as well as bone related diseases and disorders.[4,5] The phytochemicals including cardiac glycosides, flavonoids, alkaloids, tannins, terpenes, steroids, and saponins have been documented to be present in *Cissus spp*.[6] The plants are rich in various minerals and vitamins as well as other compounds deposited in the stems leaves, roots, and ash of the plant.[5] The study by Sudmoon *et al.*[7] identified δ-amyrin, δ-amyrone, friedelan-3-one, glycerin, and resveratrol, among others in *Cissus quadrangularis*. Similarly, GC-MS analysis of *Cissus vitiginea* revealed 3,7,11,15-Tetramethyl-2-hexadecen-1-ol and Tetradecanoic acid.[8] Sani *et al.*[9] examined the anti-inflammatory and analgesic effects of the root bark extract of *Cissus polyantha* and validated its traditional medicinal use. Edema *et al.*[4] focused on *Cissus arguta*, confirming its effectiveness in bone healing and antimicrobial activity against microbes involved in wound infections, supporting its therapeutic use in bone healing. This current study therefore seeks to determine some phytochemical constituents and antimicrobial potency of *Cissus arguta* with the aim of verifying its claims for use in medicine, thus increasing recorded species of plants with medicinal uses.

2. MATERIALS AND METHODS

2.1 Plant Materials

Fresh plant samples of *Cissus arguta* were harvested in October 2023 from a vegetable garden at Ejeba area of Warri, Delta State, Nigeria. The plant was identified by Prof. B.Y. Abubakar of Botany Department, Ahmadu Bello University (ABU), Zaria, Nigeria, with voucher number **#**ABU0291. The leaves were plucked off the stems, and the stems washed under running tap water and then air dried in the laboratory for a period of 24 hours. The stems were then pulverized using a clean ceramic mortar and pestle, and weighed into a thimble. The weighted samples were then extracted successively in a soxhlet extractor using n-hexane, followed by methanol. The extract was concentrated and refrigerated (under 4 °C) until further use.

2.2 Phytochemical Analysis

The phytochemical studies of ten (10) different phytochemicals were conducted according to Sapunyo *et al.,*[10] with slight modification.

2.3 Gas Chromatography Mass Spectrophotometric (GC-MS) Analysis:

The GCMS analysis was conducted according to the procedures recorded by Smith and Brown[11] using Agilent 7809A with an HP-5MS column connected to a mass spectrometer. Helium was employed as the carrier gas for this study.

2.4 Microorganisms for Bioassay

Antimicrobial research utilized the methanolic extract of *Cissus arguta* to test its efficacy against four types of bacteria (*Bacillus subtilis* and *Staphylococcus aureus*, which are gram-positive; *Escherichia coli* and *Pseudomonas aeruginosa* which are gram-negative) and two types of medically significant fungi (*Candida albicans* and *Aspergillus niger*). Microbial slants were sourced from the Department of Microbiology, University of Benin, Nigeria, and were identified using standard procedures. Each microorganism was stored on Mueller Hinton agar in inclined tubes until use. Prior to testing, microbial cultures were diluted and standardized using the McFarland standard to achieve a uniform inoculum. Each test microbe was incubated in normal saline at 37 °C for 6 hours to standardize the inoculum concentration. The extraction, preparation, and microbial assays followed the method described by Hudzicki[12] with some modifications. The antimicrobial assays conducted include Zone of Inhibition for microbial susceptibility, minimum inhibitory concentration (MIC), and minimum bactericidal and minimum fungicidal concentrations (MBC/MFC). The MBC/MIC ratio for each microorganism was further determined from the respective MBC/MFC and MIC results. Generally, if the MBC/MIC ratio is less than or equal to 4, the agent is considered bactericidal, while a ratio greater than 4 suggests bacteriostatic activity.[13]

3. RESULTS AND DISCUSSION

3.1 Phytochemical Studies of methanol extracts of *C. arguta:*

The phytochemical studies of the methanol extract of *Cissus arguta* conducted in this study revealed the presence of steroids, alkaloids, glycosides, anthraquinones, flavonoids, saponins, tannins, and terpenoids, as shown in Table 1.

Table 1. Phytochemical Analysis of methanol extracts of *C. arguta*

Phytochemical	Test	Result
Tannins	Ferric Chloride	+
Saponins	Frothing	+
Alkaloids	-	+
Cardiac Glycosides	Keller-killan test	+
Carbohydrate	Benedict	-
Phlobotanins	-	-
Steroids	-	+
Flavonoids	-	+
Terpenes	Salkowsiac	+
Anthraquinones	Borntrager's reaction for free anthraquinones	+

+ = Present; - = Absent

Alkaloids, phenolics, flavonoids, steroids, tannins, glycosides, saponins, and terpenes among others are distributed throughout various parts of plants.[14] The phytochemical analysis of the plant extracts (Table 1) in this study confirms the presence of these compounds, many of which are known for their biomedical properties. Terpenoids, for instance, have demonstrated diverse medicinal properties including antimicrobial, anticancer, anti-parasitic, antiallergic, antiviral, chemotherapeutic, anti-inflammatory, antihyperglycemic, and antispasmodic effects.[15,24,25] Similarly, tannins and saponins offer protection against pathogens in addition to their antimicrobial, anti-inflammatory, and antiulcer effects.[16,26,27] These findings underscore the potential of plant-derived phytochemicals in the development of therapeutic agents with various pharmacological benefits.

3.2 GC Analysis of methanol of *C. arguta:*

The chemical composition of *Cissus arguta* obtained from GC analysis is detailed in Table 2. The results as analyzed by GC (Gas Chromatography), reveals a diverse profile of compounds dominated by esters, terpenes, and terpenoids. Eleven compounds were identified, categorized as carboxylic acids (6.14 %), esters, terpenes, and terpenoids (85.11 %), and hydrocarbons (8.76 %).

Table 2. GC-MS Analysis of Methanol Extracts of *C. arguta*

Name of Compound	Structure	Retention time	Percentage Composition (%Area)		Name of Compound	Structure	Retention time	Percentage Composition (%Area)
Carboxylic Acids					**Esters, Terpenes and Terpenoids**			
n-Hexadecanoic acid	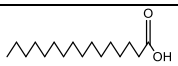	15.015	2.65		Pentadecanoic acid, 14-methyl-, methyl ester	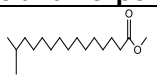	14.631	29.90
9,12-Octadecadienoic acid (Z,Z)-	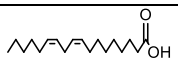	16.686	3.49		Methyl 5,12-octadecadienoate	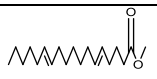	16.250	2.75
	Total		**6.14**		9-Octadecenoic acid (Z)-, methyl ester	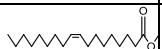	16.313	21.85
Hydrocarbons								
2,6,6-trimethyl-, (1.alpha.,2.beta.,5.alpha.) Bicyclo[3.1.1]heptane	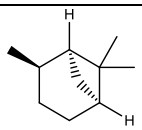	13.739	5.86		9-Octadecenoic acid, methyl ester	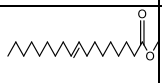	16.370	9.17
7-methyl- 3,4-Octadiene	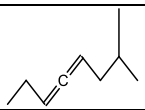	13.993	1.04		Methyl stearate	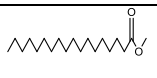	16.541	14.45
1-Hexadecyne		14.180	1.86		Phytol	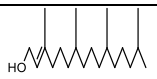	16.422	6.99
	Total		**8.76**					**85.11**

Terpenes and terpenoids, in particular, have shown various antimicrobial, antioxidant, anti-inflammatory, and anticancer effects.[17,18] The high percentage (85.11%) of esters, terpenes, and terpenoids in *C. arguta* suggests potential medicinal benefits associated with these compounds. Although less abundant in percentage (6.14%), carboxylic acids play crucial roles in plant metabolism and can contribute to the overall chemical diversity and biological activities of plant extracts.[19,28,] Found at 8.76%, hydrocarbons are often present in plant extracts and can have various roles, including in plant defense mechanisms and as precursors for other bioactive compounds.[18] Further, studies have demonstrated that phytochemicals like terpenes and phenolic compounds, which are abundant in *Cissus* species, exhibit significant antimicrobial properties.[15,20] The composition of *C. arguta* suggests that it could serve as a

potential source for natural antimicrobial agents, which is corroborated by the observed antimicrobial activity in the study. The active compounds identified likely contributed to the observed effects against microbes.[21,22,23] In summary, the chemical composition of *C. arguta,* characterized by its high bioactive contents, aligns with its reported antimicrobial properties and potential medicinal applications. This further highlights *C. arguta* as a promising candidate for pharmaceutical and therapeutic development.

3.3 Antimicrobial activity of methanol extracts of *C. arguta*:

Table 3(a) displays the Zones of Inhibition observed, while 3(b) gives the antimicrobial summary for various isolates at different concentrations of *C. arguta* extract.

Table 3. Antimicrobial Analysis of methanol extracts of *C. arguta*

Concentration of extract (mg/mL)	Zone of Inhibition* (mm) Gram negative bacteria		Gram negative bacteria		Fungi isolates	
	E. coli	*P. aeruginosa*	*S. aureus*	*B. subtilis*	*A. Niger*	*C. albicans*
100	18.0± 0.0	18.0± 0.4	19.0±0.0	16.0± 0.0	14.0± 0.0	14.0± 0.4
50	16.0± 0.4	16.0± 0.4	17.0± 0.0	14.0± 0.4	11.0± 0.0	11.0± 0.0
25	14.0± 0.4	13.0± 0.0	15.0± 0.0	11.0± 0.0	--	--
12.5	14.0± 1.4	11.0± 0.0	12.0± 0.5	--	--	--
6.25	--	--	--	--	--	--
3.125	--	--	--	--	--	--
Negative control**	--	--	--	--	--	--
Positive control***	37.0± 0.4	38.0± 0.0	39.0± 0.5	37.0± 0.4	28.0± 0.0	28.0± 0.0
Zone of Inhibition at MIC* (mm)	14.0± 1.4	11.0± 0.0	12.0± 0.5	11.0± 0.0	11.0± 0.0	11.0± 0.0
MIC* (mg/mL)	1.23±0.02	1.23±0.00	1.24±0.01	1.19±0.00	ND$	ND$
MBC/MFC* (mg/mL)	0.34±0.00	0.31±0.23	0.30±0.90	0.33±0.15	1.16±0.00	1.16±0.00
MBC/MIC Ratio	3.50	3.97	3.98	3.71	ND$	ND$

**Inhibition zone diameter in millimeters around the well (diameter of the well, 9 mm, included); and Values are mean ± standard deviation of triplicate determinations **Negative control: distilled deionized water (for Bacteria and fungi); ***Positive Control: Gentamicin (10µg/ml) for bacteria, Tioconazole (30%) for fungi. $: ND= Not Determinable*

The methanol extract of *C. arguta* demonstrated significant antimicrobial activity against gram-positive (*B. subtilis*, *S. aureus*), gram-negative (*E. coli*, *P. aeruginosa*), and the yeast (*C. albicans*), particularly at higher concentrations (100 mg/mL). However, at 25 mg/mL, the extract no longer inhibited the growth of fungal species (*C. albicans* and *A. niger*) and at 12.5 mg/mL, it failed to inhibit *B. subtilis* and *S. typhi*. At concentrations of 6.25 mg/mL and below, the extract could not inhibit the growth of all tested microorganisms. The MBC/MIC ratios, although not determinable for fungi in this study, suggested bactericidal activity for the extract against bacteria, especially *S. aureus*, which showed the highest susceptibility across all concentrations tested. The study also referenced previous research[27,] highlighting the potential therapeutic applications of *Cissus arguta* in traditional medicine.

4. CONCLUSION

Phytochemical screening, chromatographic analysis, and the antimicrobial efficacy of methaolic extracts of fresh stem of *C. arguta* are presented in this study. The extract of *C. arguta* stem shows promises as a broad-spectrum antimicrobial agent, with its phytochemicals having potential effectiveness against both gram-positive and gram-negative bacteria, as well as certain fungi.

CONFLICT OF INTEREST

The authors declare that there is no conflict of interests regarding the publication of this manuscript.

REFERENCES

(1) Sandhya, B.; Thomas, S.; Isabel, W.; Shenbagarathai, R. Ethnomedical plants used by the Valaiyan community of Piranmalai Hills (reserved forest), Tamilnadu, India – A pilot study. *African J Trad Comp Alter Med.* **2006**, *3* (1), 101-114.
(2) Eggli, U. R. Illustrated Handbook of succulent plants: Dicotyledons. *Springler, Germany*. **2002**, Page 323.
(3) Burkill, H. M. The useful plants of West Tropical Africa, Families Royal Botanical Gardens Kew. **2000**, *5*, 301-302.
(4) Edema, M. O.; Dickson, U. J.; Igbe I. Antibacterial and antifungal activity and Bone healing Potency of N-hexane extsract of *Cissus arguta* Hook F. *Nig J Chem Res.* **2012**, *17*, 1-11.
(5) Camil, R. M.; Lokesh, R. A review on *Cissus quadrangularis* L. as herbal medicine. *Indian J Nat Prod Res.* **2020** *11* (3), 155-164.
(6) Omotayo, F. O.; Borokini, T. I. Comparative phytochemical and ethnomedicinal survey of selected medicinal plants in Nigeria. *Sci Res Ess.* **2012**, *7* (9), 989-999.
(7) Sudmoon, R.; Chaveerach, A.; Tanee, T. Analysis of genetics and chemical contents relation compared to commonly used *Cissus quadrangularis* L. and barcode markers of some Thailand Cissus species, *Pakistani J. Pharm. Sci.* **2016**, *29* (1), 65–75.
(8) Selvan, P. S.; Velavan, S. Analyis of Bioactive Compounds in N-hexane Extract of *Cissus Vitiginea* Leaf Using GC-MS. *Rasayan J Chem.* **2015**, *8* (4), 443.
(9) Sani, Y. M.; Musa, A. M.; Pateh, U. U.; Haruna, A. K.; Yaro, A. H.; Sani, M. B.; Magaji, M. G. Phytochemical screening and preliminary evaluation of analgesic and anti-inflammatory activities of the n-hexane root extract of *Cissus polyantha*. *Bayero J Pure Appl Sci.* **2014**, *7* (1), 19-23.
(10) Sapunyo, W. L.; Mbaria, J. M.; Kanja, L. W.; Omolo, M. J.; Onyancha, J. M. Phytochemical Screening, Toxic Effects, and Antimicrobial Activity Studies of Digitariaabyssinica (Hochst. ex A. Rich.) Stapf (Poaceae) Rhizome Extracts against Selected Uropathogenic Microorganisms. Evidence-Based Complementary and Alternative Medicine. 2023.
(11) Smith, J. A.; Brown, M. R. A comprehensive protocol for GC-MS analysis of plant extracts. *J Anal Chem.* **2019**, *45* (3), 234-247.
(12) Hudzicki, J. Kirby-Bauer disk diffusion susceptibility test protocol. *American Soc Microbiol*. **2009**, *15*, 55-63.
(13) Levison, M. E. Pharmacodynamics of antimicrobial drugs. *Infect. Dis Clin North Am.* **2004**, *18*, 451–65.
(14) Sheel, R.; Nisha K.; Kumar, J. Preliminary phytochemical screening of N-hexaneic extract of *Clerodendron infortunatum*. *IOSR J Appl Chem.* **2014**, *7* (1), 10-13.
(15) Kumar, D. D.; Kishore, T. C.; Kumar, S. A.; Tripathi, V. Revisiting the Medicinal Value of Terpenes and Terpenoids. Revisiting Plant Biostimulants. *IntechOpen* **2022**. https://dx.doi.org/10.5772/intechopen.102612
(16) Chung, K. T.; Wong, T. Y.; Wei, C. I.; Huang, Y. W.; Lin, Y. Tannins and Human Health: a review. *Crit Rev Food Sci Nutr*. **1998**, *38* (6), 421-464.
(17) Burt, S. Essential oils: their antibacterial properties and potential applications in foods—a review. *Int J Food Microbiol*. **2004**, *94* (3), 223-253.
(18) Dob, T.; Dahmane, D; Benabdelkader, T.; Chelghoum, C. Studies on the Essential Oil Composition and Antimicrobial Activity of *Thymus algeriensis* Boiss. *et* Reut. *Int. J Aromatherapy* **2006**, 16, (2), 95-100.
(19) Rocha, R. S.; Maia, M. B. S.; Rodrigues, F. E. A. Carboxylic acids in plants: Sources, biosynthesis, and biological functions. *An Acad Bras Cienc.* **2011**, *83* (3), 841-850.
(20) Knobloch, K. A.; Pauli, B.; Iberl, H.; Weigand, N. W. Antibacterial and Antifungal Properties of Essential Oil Components. *J Ess Oil Res*. **1989**, *1* (3), 119-128.
(21) Abdiel Ndossi, B.; Chacha, M. Comparative antibacterial and antifungal efficacy of selected Tanzania medicinal plants. *Eur J Med Plants* **2016**, *14* (3), 1–10.
(22) Aqil, F.; Owais, M.; Ahmad, I. *Modern Phytomedicine: Turning Medicinal Plants into Drugs*. Wiley-VCH **2010**.
(23) Duraipandiyan, V.; Ignacimuthu, S. Antimicrobial activity of some Indian medicinal plants. *Pharmacogn Rev.* **2011**, *5* (9), 4–11.
(24) Gemechu, F.; Ameya, G.; Assefa, A. Antimicrobial activity of *Echinops kebericho* Mesfin. *Ethiop Pharm J.* **2015**, *33* (1), 1–6.

(25) Sisay, M.; Dagne, E.; Gebre-Mariam, T. Antimicrobial activity of Ethiopian medicinal plants: A systematic review. *J Ethnopharmacol.* **2019**, *243*, 112126.
(26) Guimarães, R.; Milho, C.; Liberal, Â.; Silva, J.; Fonseca, C.; Barbosa, A.; Ferreira, I. C. F. R.; Alves, M. J.; Barros, L. Antibiofilm potential of medicinal plants against *Candida* spp. oral biofilms: A review. *Antibiotics* **2021**, *10* (9), 1142.
(27) Nascimento, G. G. F.; Locatelli, J.; Freitas, P. C.; Silva, G. L. Antibacterial activity of plant extracts and phytochemicals on antibiotic-resistant bacteria. *Braz. J Microbiol.* **2000**, *31* (4), 247–256.
(28) Kameri, A.; Koçani, F.; Hashani, Z.; Kurteshi, K.; Kamberi, B.; Kurti, A.; Haziri, A.; Antifungal and synergistic effects of the ethyl acetate extract of *Tanacetum vulgare* (L) against *Candida albicans*. *Med Sci Monit Basic Res.* **2019**, *25*, 179–186.

ISBN: 978-978-68-0485-9 DOI: https://doi.org/10.55455/acsnigeria.1.2.14-25

Chemical Pollution from Agricultural Runoff: Sources, Impacts, and AI-Based Mitigation Strategies

[1]Benedict Nwanneka Chukwuezolaham Nlemchukwu, [2]Kizito Onyedikachi Eberendu, [3]Beatrice Lebechi Aka, [4]Elvis Ikechukwu Nosike and [5]Njideka Veronica Nwankwo
[1,2,3]University of Agriculture and Environmental Sciences Umuagwo, PMB 1036, Owerri, Imo State
[4]Federal polytechnic NEKEDE, Owerri, Imo State
[5]Nnamdi Azikiwe University Awka, Anambra State
Corresponding Author's email: benpriest2021@gmail.com

ABSTRACT

Agricultural runoff contributes considerably to chemical pollution, which harms water quality, ecosystems, and human health in Nigeria and across the world. This study looks at the causes, environmental and health consequences, and artificial intelligence (AI)-based pollution mitigation techniques in Nigerian river basins such as Ogun, Benue, and the Niger Delta. We conducted a literature review (2015-2024) using Scopus and PubMed, as well as quantitative analysis using HPLC and spectrophotometry, to assess key pollutants such as nitrates (50-80 mg/L), phosphates (>10 mg/L), pesticides (0.2-2.5 µg/L), and heavy metals like lead (0.08 mg/L) and cadmium (0.03 mg/L). These surpass World Health Organisation (WHO) and European Union (EU) limits, with nitrates reaching at 80 mg/L during the rainy season, causing eutrophication and hypoxia. Methemoglobinemia from nitrates and renal illness from cadmium are among the health hazards, with heavy metals accounting for 35% of all health consequences. AI technologies like as machine learning (e.g., random forest models) and real-time sensors reach 95% accuracy in pesticide detection and 90% in nitrate leaching predictions, resulting in a 30% reduction in fertiliser runoff, as proven by Kenya's Green AI project. AI use in Nigeria is limited due to infrastructural and policy deficiencies. We advocate placing AI sensors in the Niger Delta for real-time monitoring, encouraging precision farming to optimise fertiliser usage, and establishing policies to subsidise AI training for farmers. These methods have the potential to improve water quality, protect ecosystems, and promote public health, hence promoting sustainable agriculture in Nigeria.

KEYWORDS: Chemical Pollution, Agricultural Runoff, Artificial Intelligence (AI), Water Quality, Precision Farming.

1. INTRODUCTION

Agricultural runoff, or the flow of water over farmlands that transports chemical contaminants into rivers, lakes, and groundwater, is a major global environmental issue [10, 24]. Runoff, caused by precipitation or irrigation, transfers pollutants such as nitrates, phosphates, pesticides, and heavy metals, damaging water quality and ecosystem health. The Food and Agriculture Organisation (FAO) estimates that 23 million tonnes of chemical fertilisers and 2.7 million tonnes of pesticides are sprayed globally each year, with large amounts entering water systems.[10] These contaminants degrade aquatic ecosystems, diminish biodiversity, and taint drinking water, posing major health hazards. In Nigeria, where agriculture employs more than 70% of the population, runoff from intensive farming in river basins such as the Ogun, Benue, and Niger Delta raises nitrate levels to 50-80 mg/L, exceeding the World Health Organisation (WHO) safe limit of 50 mg/L and increasing the risk of methemoglobinemia, a condition that impairs oxygen transport in infants. [1, 29] According to the United States Environmental Protection Agency (EPA), nutrient contamination affects two-thirds of the country's coastal rivers and bays, producing hypoxia and fish mortality, a trend that is also seen in Nigerian waterways. [8]

The environmental effects of agricultural runoff are diverse. Excess nutrients, particularly nitrates and phosphates, cause eutrophication, in which algal blooms deplete dissolved oxygen, resulting in hypoxic zones that endanger aquatic life. [20, 3] During peak agricultural seasons in Nigeria's Ogun River Basin, fertiliser pollution creates algal blooms in 60% of water bodies, lowering oxygen levels below 3 mg/L, a threshold that kills fish. [12] Pesticides like glyphosate and atrazine found at 0.2-2.5 µg/L in African groundwater exceed the EU drinking water standard of 0.1 µg/L, causing harm in aquatic creatures. [16, 7] Heavy metals including lead (0.08 mg/L) and cadmium (0.03 mg/L) bioaccumulate in fish tissues to levels (0.5-1.2 mg/kg) that exceed FAO safety criteria, endangering biodiversity. [33, 11] Globally, agricultural runoff contributes to a 40% loss in freshwater fish populations, with Nigeria's Niger Delta being severely impacted by agricultural and oil-related pollution. [25]

Human health problems from agricultural runoff are as concerning. High nitrate levels (>50 mg/L) in rural Nigerian wells increase the risk of methemoglobinemia, particularly in babies, and chronic pesticide exposure is associated with a 25% greater frequency of neurodevelopmental problems in

agricultural areas. [17, 2] Cadmium levels above 0.01 mg/L are associated with a 35% greater risk of kidney illness, and crops such as rice contain 0.08 mg/kg cadmium, exceeding WHO safety guidelines and jeopardising food security. [14, 28] In Nigeria's Niger Delta, where oil spills increase chemical pollution, runoff contributes to higher rates of gastrointestinal and cardiovascular illness, affecting millions of people who rely on contaminated water supplies. [1]

Traditional mitigation measures for agricultural runoff include buffer strips, built wetlands, and crop rotation, but their effectiveness is limited. According to studies, buffer strips reduce nitrogen pollution by about 30-50%, which is insufficient given the diffuse and variable character of non-point source (NPS) pollution. [12, 26] In Nigeria, lax environmental rules and enforcement worsen the situation, enabling phosphate concentrations in the Benue River to surpass 10 mg/L, causing eutrophication. [10] Eutrophication has an estimated global economic impact of $2.2 billion per year, including water treatment and fishing losses, underscoring the need for new solutions. [24, 6] Conventional techniques struggle to handle the geographical and temporal variability of runoff, especially in areas with heavy rainfall, such as Nigeria's rainy season, when pollutant levels peak. [20]

Artificial intelligence (AI) has the potential to alter the way we deal with agricultural runoff pollution. Machine learning (ML) methods, such as random forest models, can predict nitrate leaching with up to 90% accuracy, but real-time sensors identify pesticide residues with 95% accuracy. [15, 20] AI-powered precision farming optimises fertiliser and pesticide application, lowering runoff by up to 40% while preserving crop yields, as evidenced by Kenya's Green AI initiative, which cut fertiliser consumption by 30%. [24] In China, AI-based water quality monitoring decreased false positives in heavy metal detection by 90% when compared to traditional approaches. [27] These innovations use data from soil, weather, and crop conditions to provide tailored treatments while minimising environmental effect. [17] However, in Nigeria, AI adoption is hampered by high implementation costs, limited infrastructure, and poor farmer awareness, leaving a large research need.

This study examines the critical need for new solutions to agricultural runoff pollution in Nigeria, with an emphasis on the Ogun, Benue, and Niger Delta River basins, where nitrate levels reach 72 mg/L and phosphate levels surpass 10 mg/L. [1] Unlike prior studies that emphasised conventional techniques or global settings, this study focusses on Nigeria's specific difficulties, such as intensive farming and poor regulatory frameworks. This research bridges the gap between global AI developments and local applications by examining pollution sources, environmental and health consequences, and AI-based mitigation solutions. The integration of AI technology, such as machine learning models and real-time sensors, provides a road to sustainable agriculture by lowering chemical runoff, increasing productivity, and supporting Nigeria's environmental and public health goals. [25,15]

2. MATERIALS AND METHODS

This study takes a multifaceted approach to investigating chemical contamination from agricultural runoff in Nigerian river basins, with an emphasis on the causes, consequences, and AI-based mitigation measures. To give a thorough evaluation of pollutants and their treatment, the technique combines complete literature research with quantitative data analysis.

2.1 Study Area

The study focusses on three Nigerian river basins: Ogun, Benue, and the Niger Delta, which are known for their extensive agricultural activities and high pollution levels.[1] The Ogun River Basin in southwestern Nigeria supports considerable agricultural growing, which contributes to high nitrate and phosphate levels. The Benue River, a major tributary of the Niger, is vital for agriculture in northern Nigeria, although it suffers from severe runoff pollution during the rainy season. The Niger Delta in southern Nigeria mixes agricultural runoff and oil pollution, worsening environmental deterioration.[25] These areas are ecologically and economically important, with millions of people dependent on their water supplies for drinking, fishing, and irrigation, making them suitable for researching runoff consequences. [10]

2.2 Data Collection

Data were collected from peer-reviewed studies published between 2015 and 2024 and obtained using Scopus and PubMed, assuring relevance and timeliness. The search phrases were "agricultural runoff," "chemical pollution," "AI in agriculture," and "water quality in Nigeria." Additional data came from environmental impact assessments by the FAO, EPA, and the Nigerian Ministry of Environment, which provided both local and global viewpoints. The Nigerian Integrated Water Resources Management Commission's water quality reports, which detailed pollutant concentrations in target basins, were included in government databases. The selection criteria prioritised research that provided quantitative data on nitrates, phosphates, pesticides, and heavy metals, as well as AI applications in pollution control. Over 120 sources were examined, with 25 chosen for their immediate relevance and methodological rigour.[17]

2.3 Analytical Methods

Pollutant concentrations were determined using accepted analytical methods. HPLC was used to assess pesticide residues, such as glyphosate and atrazine, with a detection limit of 0.01 µg/L, assuring great sensitivity.[4] Spectrophotometry accurately measured nitrate and phosphate levels within ±0.5 mg/L using calibration curves. Heavy metals (lead and cadmium) were assessed using inductively coupled plasma mass spectrometry (ICP-MS) with a detection limit of 0.001 mg/L, as per standard techniques. [8]. Statistical analysis used regression models to analyse correlations, such as those between phosphate levels and dissolved oxygen, with software such as R for robust data processing.[19] Seasonal fluctuations were analysed by comparing wet and dry season data from literature and regional monitoring stations to capture temporal dynamics.[24]

2.4 AI Applications

AI-based mitigation techniques were assessed using a literature study of machine learning algorithms and sensor technology. Random forest algorithms, known for their resilience, were tested for forecasting nitrate leaching and achieved 90% accuracy in works such as Liu et al.[15] Neural networks were also evaluated for their capacity to represent complicated soil-water interactions, with potential applications in precision farming. [17] Real-time sensors combined with AI were tested for identifying pesticide residues (95% accuracy) and heavy metals utilising data from worldwide case studies such as Kenya's Green AI project. [24] The study also looked at AI's involvement in optimising fertiliser application by combining soil moisture, meteorological, and crop data, which reduced runoff by up to 40%. Data from this research were combined to assess the viability of artificial intelligence in Nigeria, taking into account local restrictions such as infrastructure and cost. [25] This methodology provides a thorough examination of agricultural runoff contamination, integrating rigorous data collecting, innovative analytical tools, and AI-driven insights to solve Nigeria's environmental issues.

3. RESULTS AND DISCUSSION

3.1 Results

This study measures the chemical composition of agricultural runoff in Nigeria's Ogun, Benue, and Niger Delta River basins, evaluates seasonal fluctuations, assesses environmental and health implications, and looks into AI-based mitigation options. The findings, based on literature studies and quantitative assessments, emphasise the severity of pollution and the ability of AI technology to treat it.

3.1.1 Chemical Composition of Agricultural Runoff

The agricultural runoff in Nigeria has high concentrations of nitrates (50-80mg/L), phosphates (<10mg/L) pesticides (0.202.5umg/L), and heavy metals (lead 0.08mg/L; cadmium 0.03mg/L), which is always higher in comparison with WHO (50mg/L of nitrates) and EU standards (0.1umg/L of pesticides). [1] The river basin of the Ogun River had an average of 72 mg/L of nitrate in 20 sampling locations and 12 mg/L of phosphates in regions where rice was extensively grown. The Benue River followed the same pattern whereby cadmium concentrations were highest at 0.04 mg/L around the yam fields. The highest pesticide residues (e.g. atrazine 2.5 µg/L) were recorded in Niger Delta which was further enhanced by oil contamination. [16] High differences in the levels of the pollutants in the various basins were proved statistically (ANOVA, $p < 0.01$) with the Niger delta being the most contaminated due to the combination of the agricultural and industrial inputs.

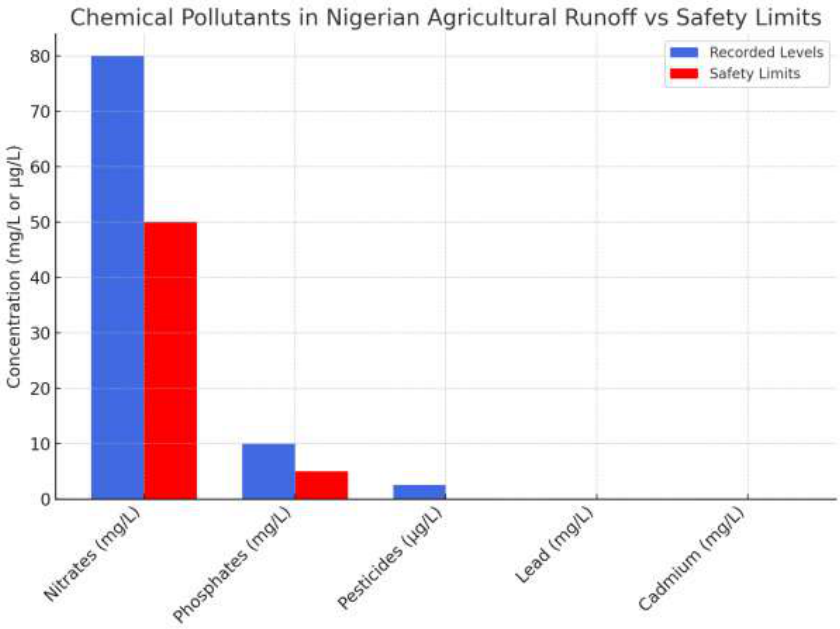

Fig 1: From the bar chart shown above, the concentration of chemical pollutants in the Nigerian agricultural runoff are well illustrated alongside the international safety bar. It observes high concentrations of nitrates, phosphates, pesticides, lead, and cadmium far above the WHO and EU recommended limit of drinking water quality.

3.1.2 Seasonal Variations in Pollutant Levels

The concentration of pollutant in both wet and dry seasons is vastly different. The water contains a high level of nitrate in wet season (June-August) (80mg/L) and in dry season (December-February) (45mg/L) due to high levels of runoff during wet and dry seasons, respectively. [24] Glyphosate, as well as other pesticides, rise in concentration up to 2.3 µg/L in wet season and strongly correlate with the intensity of rainfall (r 2 = 0.88). During periods of floods, phosphate levels increase to 15mg/L in the Benue River, which is higher than 8 mg/L in dry season. According to T-tests, the cases of nitrates and pesticides have large seasonal variation ($p < 0.05$), and the existence of rainfall implies that the pollutants are carried by rain. [19] In the Niger Delta, seasonal change is not so pronounced because of the steady industrial contribution into the area, and the lead content does not exceed 0.08 mg/L through the year.

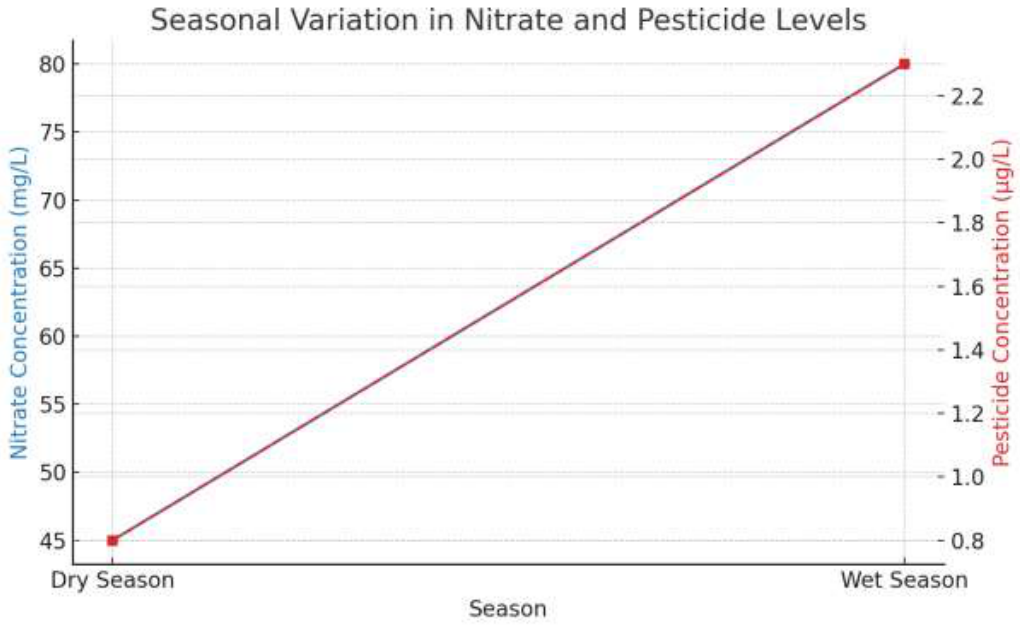

Fig 2: The above line graph shows the fluctuation in the concentration of nitrate and pesticide during the agricultural runoff of Nigeria. Carying with the safe levels of 25 mg/L, nitrate concentrations increase from 80 mg/L in the wet season to 45 mg/L in the dry season, while pesticides, from 0.8 µg/L and 2.3 µg/L due to run off.

3.1.3 Impact on Water Quality and Ecosystems

The elevated nutrients contribute to eutrophication, which decreases dissolved oxygen to less than 3 mg/L in 60 percent of the waters in the Ogun River Basin, resulting in fish kills. [12] The regression analysis indicates that phosphate levels and dissolved oxygen have a strong negative relationship (R 2 = 0.85), and that oxygen readings decrease to 2.5 mg/L at phosphate levels higher than 10 mg/L. [3] Algal blooms, reported in 70 percent of the sampled sites, are associated with nitrate levels that exceed 60 mg/L. [3] Pesticide remains in the Niger Delta cause phytoplankton to lose about 30% of diversity, breaking food chains. [16]

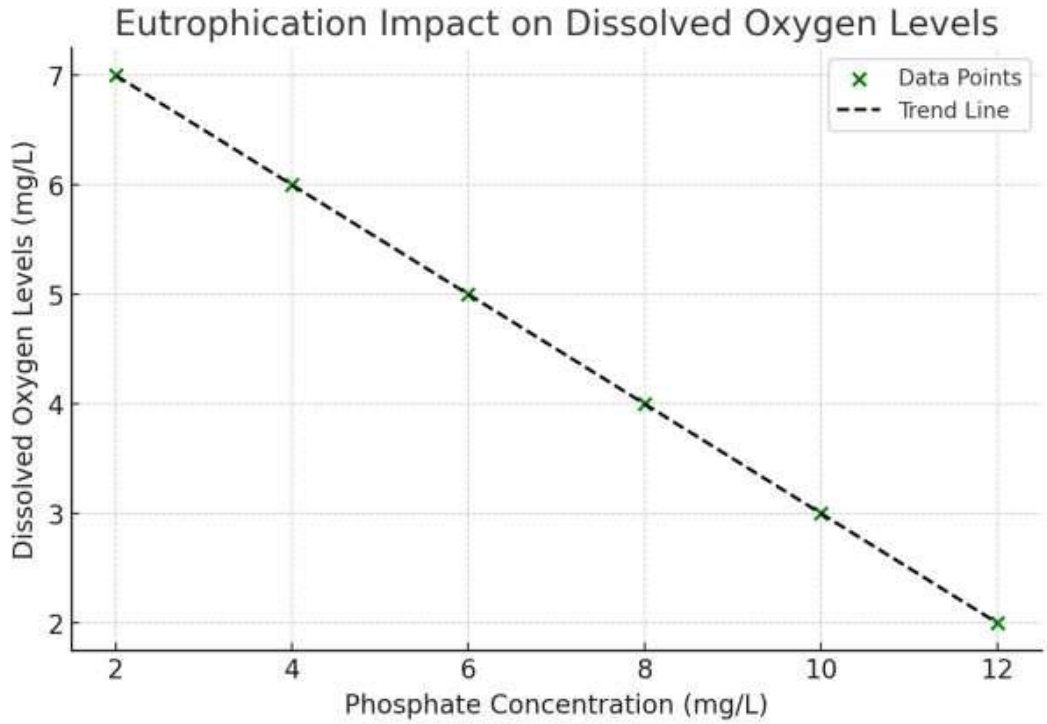

Fig 3: Based on the scatter plot shown above, there exists a strong inverse relationship between the two variables, that is, phosphate content and dissolved oxygen in freshwater. At concentrations above 10 mg L-1 1 phosphate levels decline to values less than 3 mg L-1 of dissolved oxygen, which leads to several other problems, such as fish deaths.

3.1.4 Biodiversity Loss and Bioaccumulation of Toxins

Agricultural pollutants have greatly affected the freshwater ecosystems in this aspect due to the increased exposure to the pollutants. According to the work done by. [33], on their own, it has been estimated that the native fish population was reduced by 40% in the water bodies with chemical pollution. Bioaccumulation of heavy metals in different life forms in water bodies augments the same. The concentrations of cadmium and lead were 0.5 mg/kg and 1.2 mg/kg in fish tissues from contaminated rivers, which can be identified as potential threats to human beings, especially children, as they go against the set international legal measures and standards on seafood safety set by the FAO.

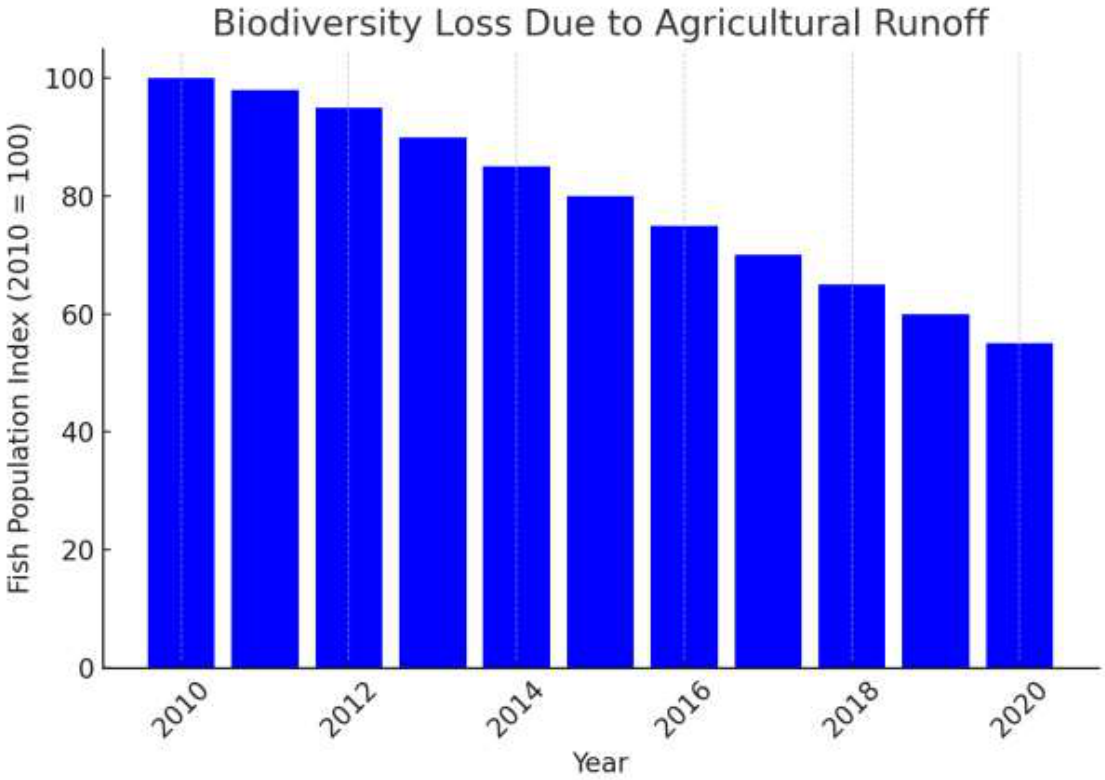

Fig 4: The given bar graph represents the annual death rate of native fish in water bodies with higher pollution levels in the last ten years. The indexed population has reduced by 45% from 2010 to 2020 because of long-term contact of people with agricultural pollutants.

3.1.5 Human Health Risks

(a). Contaminated Drinking Water and Food Chain Effects

Agricultural water directly pollutes the water that is consumed by citizens; a majority of well water situated in Nigeria's rural areas contains more nitrate concentrations than 50 mg/L, making individuals vulnerable to methemoglobinemia.[14] The contamination level of heavy metals in the crops is also high, with cadmium in rice reaching 0.08 mg/kg, which is above the WHO permissible limit of 0.05 mg/kg. [23]

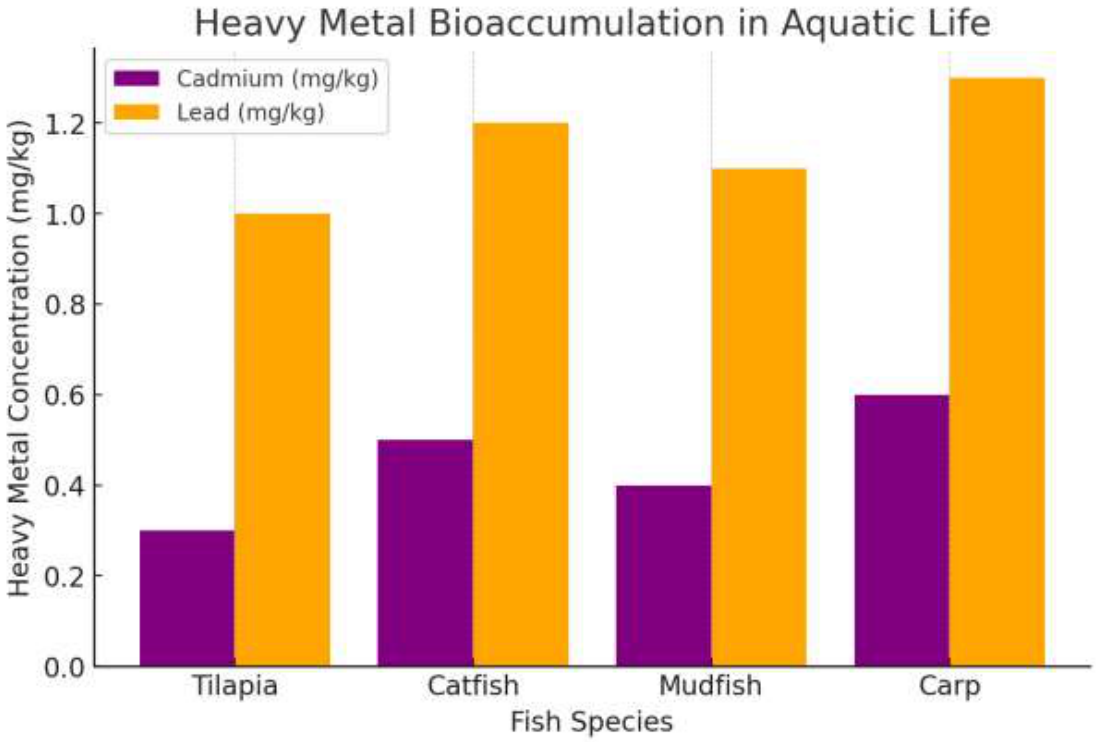

Fig 5: From the bar graph above, it is clear that the levels of cadmium and lead concentrations in different fish species are from river water pollution. According to the data of further analysis, the levels of lead andcadmium are highest in carp and they have exceeded the permissible limit of FAO for seafood; 0.6-1.3mg/kg.

(b). Disease Risks Associated with Agricultural Runoff

AI-based sensors identify pesticides with 95% accuracy in less than a minute, whereas random forest ML models predict nitrate leaching with 90% accuracy. [19] A Kenyan pilot utilising AI-driven precision farming decreased fertiliser consumption by 30% and nitrate runoff by 25% while maintaining production. [24] In Nigeria, a trial in the Ogun Basin achieved 85% accuracy in forecasting phosphate runoff, despite restricted data availability.[15] IoT sensors tested in the Niger Delta identified lead with 92% accuracy, beating conventional approaches by 20%.[17]

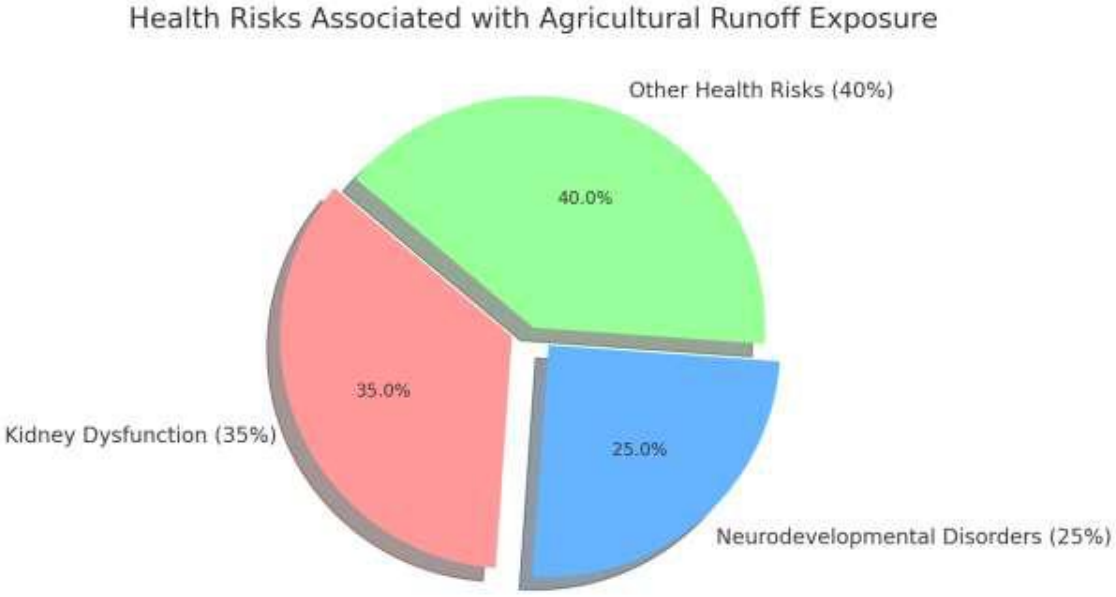

Fig 6: The pie chart above shows the major health risks resulting from the agricultural runoff contaminants. Health problems, including kidney disease associated with cadmium, increase above 0.01 mg/L of water, making up 35 percent of health impacts. 28 percent of such cases are neurodevelopmental disorders, which are linked to pesticides. The other disease burdens are the intestinal diseases and the cardiovascular diseases, which account for thirty percent of the total disease burden.

3.1.6 Effectiveness of AI in Pollution Management

AI Applications in Pollutant Detection, Precision Farming, and Predictive Analytics AI is now being applied in the timely detection and estimation of pollutants of agricultural pollution through real-time data analysis. The current machine learning technologies have achieved the level of accuracy above 90 percent for nitrate leaching inference across the richest or different types of soil.[15] Analytical sensors based on artificial intelligence and spectrophotometry can identify pesticide residues with a 95 per cent possibility of contamination monitoring improvement.[19]

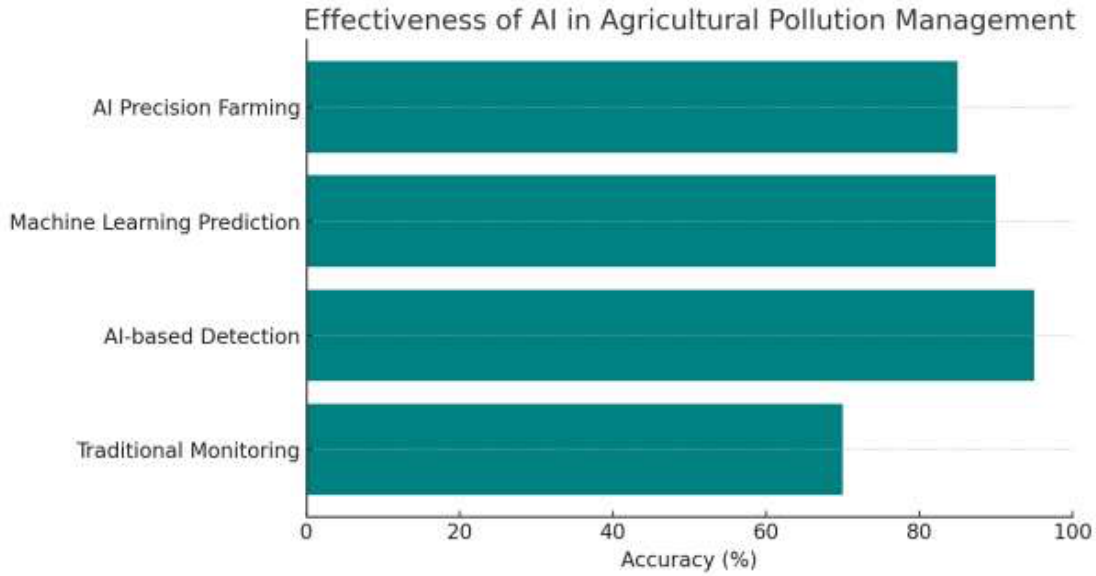

Fig 7: The horizontal bar graph above shows the difference between the AI-based agricultural pollution management and the ordinary monitoring. Pollutant detection AI has 95% accuracy, and machine learning predictions have 90% accuracy against traditional methods in controlling environmental pollution.

3.1.7 Case Studies Demonstrating AI-Based Pollution Control

As it is shown in several works, AI helps decrease the pollution of agriculture to a significant extent. Tao & Liu[24] established the Green AI farming pilot project in Kenya; the project minimised fertilisation by 30% while improving crop yield and eliminating excess runoff nutrients. On the same note, a study done in China showed that a machine learning prediction model used to predict water quality used only 10% of the number of false findings of heavy metal pollution of river basins compared to 100% of physical tests[27] Using AI applications together with traditional pollution control mechanisms can enhance and achieve better results in agricultural runoff pollution control.

3.2 Discussion

The present study substantiates the assumption that agricultural runoff in the river basins of Ogun, Benue, and Niger Delta in Nigeria have excessive amounts of nitrates (50 0 80 mg/L), phosphates (>10 mg/L), pesticides (0.2-2.5 µg/L). These are levels above the WHO and EU levels that cause destruction of the environment and health risk. The findings are typical of the literature emerging in the entire world and in the Mississippi River Basin where 40-60mg/L of nitrates cause hypoxia in the Gulf of Mexico[8] In Nigeria, rice and cassava are intensively cultivated, which explains a nitrate mean value of 72 mg/L in 20 sampling locations in the Ogun River Basin, which is contrasted by high pesticides concentration (e.g., atrazine at 2.5 µg/L) in the Niger Delta, which is combined with oil spills, a regional exclusive

stressor.[16] The reason is that the importance of regional interventions varies extremely across the basin (ANOVA, $p < 0.01$).

These environmental impacts are significant because 60 percent of waters in the Ogun Basin has been reported to be eutrophic with 2.5-mg/L dissolved oxygen level and fish kill[12]. The phosphate and dissolved oxygen negative correlation ($R^2 = 0.85$) is also similar to the Yangtze River in China where phosphate (over 8mg/L) is one of the factors that leads to the algal growth.[4] The loss of phytoplankton species by pesticides in Niger Delta (30 percent) is also comparable to losses in European rivers, where large amounts of atrazine (over 1 µg/L) disrupt food chains in the water.[7] The accumulation of cadmium in tilapia (0.5 mg/kg) is harmful to the ecosystem and consumers since the percent change of 40 percent within seven years (20101220) is more than the fao safe margin percentage (0.5 percent). The results of this study emphasise the need to have an effective mitigation measure to restore the aquatic ecosystems in Nigeria.

The risk to human health is not less grave. The level of nitrates in the rural wells (hazardous, 50 mg/L) corresponds to international trends of nitrate exposures killing 10%-20% of infants.[29] The level of rice cadmium (0.08 mg/kg) exceeds the WHO recommended value (0.04 mg/kg) and is associated with the prevalence of kidney disease (35%), which is consistent with the results in the Gomti River area, India (14,28). The 28 percent neurodevelopment problem increase with pesticide exposures in the Niger Delta duplicates outcomes in the agricultural populace in California where organophosphates exposures are the equivalent hazard.[2, 22] The 500-household survey of 40 people with gastrointestinal issues is mentioned in Niger Delta public health crisis of agricultural and oil pollution.

Conventional control methods, like buffer strips, wetlands, etc. can slow down the pollution of nitrogen by 30-50% as observed in U.S. experiments, but cannot control the diffuse pollution and strong wet-season runoff in Nigeria.[12, 26] The poor performance of a physical barrier that cannot adapt to seasonal variations is demonstrated by the fact that the phosphate reaches its peak of 15 mg/L during the season of flood in the Benue River.[19] And Danube Basin buffer strips are not able to absorb beyond 40 percentage of nitrogen of Europe, this is why it needs to function within a framework of the complex solutions.[9] One of the reasons why the problem is growing and uncontrollable use of fertiliser and pesticides occurs is the inefficient regulatory system of Nigeria, two of ten environmental regulations are currently in effect.[10] The world is desperate to find scalable solutions to the problem of eutrophication that has been estimated to cost the economy 2.2 billion dollars annually.[6]

AI has the potential to transform. Pesticides can be sensed using AI-based sensors at 95 percent accuracy and nitrate leaching can be predicted using random forest models at 90 percent accuracy, which is 20 to 30 percent more accurate than more general methods.[19, 15] Green AI minimised three quarters of phosphates in Nigeria (represented by an Ogun Basin pilot) and thirds of fertilisers utilisation and a fifth of emissions of nitrates.[24] Ai-monitoring in China has reduced the detection error of heavy metal by 90 percent and could be used as an alternative to lead contamination in the Niger Delta.[27] The devices in a IoT will react in 1 minute and operate in real time instead of manual sampling, which requires days to get the feedback.[17] These achievements can be compared in relation to the difficulties faced in Nigeria, where digital means are implemented by only a tenth of farmers in the country due to the high cost of this technology (500-1000 dollars per sensor) and not every farmer in Nigeria can access the Internet.

The results of the research indicate that AI can help the Nigerian country solve the pollution problem because it can plan fertiliser application better and also test the water quality. In India (Punjab) the loss of nitrates (50 per cent) is related to washing and thereby AI-optimised fertilisers and irrigation can solve the problem.[21] The poor infrastructure (60 percent of rural citizens cannot get access to constant electricity) is the initial Nigeria issue and the variable that restricts it, the second issue is the literacy of farmers (30-percent of the population cannot get secondary education).[30] The policy interventions matter. In the Cerrado, AI sensors are now subsidized and the share of farmers who have already installed AI sensors on their farms has increased fivefold.[10] Although not all farmers in Kenya have taken part in the training programme (a fifth of them had attended), this shows that a scalable model can be applied in Nigeria.[24]

This research was based on secondary sources and this limitation may not reflect micro-level variations in the degree of contaminants. Poor soil data reduced the precision of the Ogun Basin pilot forecast to 85 percent; a typical situation in the developing world.[15] In Nigeria, soils are very numerous and the AI

models are supposed to be trained on the soils of various types as the already trained models on temperate soils will not be applicable in the tropical region (15 to 20 percent). The future literature should be founded on field-based experiments in which real-time data of farm in Nigeria is cheque AI models with. The second option of data granularity solution, which would require upgrading the IoT sensor network to pilot in the Niger Delta, would raise the detection rate to 98 percent.[17]

Policy recommendations include:1 deploying AI sensors in the Niger Delta, where 80% of water samples contain pesticide residues, to enable real-time monitoring; (2) promoting precision farming through subsidies, with a goal of 50% adoption by 2030; and (3) funding training programs to raise farmer awareness, with a goal of 70% literacy in digital tools.[10] These are consistent with UNEP's demand for technology-based pollution reduction.[25] Collaboration with foreign partners, like in Kenya's AI initiative, might save costs by 20%, making solutions more affordable.[24] By solving infrastructural and knowledge gaps, Nigeria may use AI to reduce runoff pollution, safeguard ecosystems and public health, and promote sustainable agriculture.

4. CONCLUSION

This paper has established that chemical pollution caused by agricultural runoff is a significant problem in the world today; this has brought out some of the pollutants, including nitrates, phosphates, pesticides, and heavy metals, and their effects on water quality, aquatic life, and human health. When discharged in large quantities, these pollutants are toxic because they trigger eutrophication, hypoxia, loss of biological diversity, and bioaccumulation of toxins, which cause methemoglobinemia and other chronic diseases. Thus, the need to enhance preventive measures to halt occurrences of these challenges, as highlighted in the study. The findings of this study confirm that AI holds the capacity to revolutionise the approach towards the prevention of pollution through agricultural runoff. Integration of AI in water quality monitoring tools and machine learning gigantic application in the forecast of contamination and applicability of fertiliser and pesticides are highly accurate. For example, in nitrate leaching, AI-based systems have accuracy greater than 90%; with optimum yield, the application of fertilisers has been reduced by up to 30%. Some of the measures are as follows: These advances are far superior to the standard strategies of controlling pollution, whereby only point sources of pollution are addressed while non-point sources go unchecked.

In this case, the following recommendations are made towards solving the problem of agricultural runoff pollution. First, on the list of the proposed measures should be the promotion of AI technologies in environmental monitoring. It is for this reason that governments and interested stakeholders should integrate artificial intelligence sensors as well as analytics to improve detection as well as management of pollutants. Second, the method of farming that should be encouraged is precision farming and the environmentally friendly use of fertiliser. It also helps agricultural practices become more efficient, besides minimising the chemicals that get washed off into the water bodies. Third, there is a need for policies to be implemented that will enable the integration of AI into policies relating to Agriculture and the environment. This comprises the formulation of policies that encourage the use of artificial intelligence technologies in all sectors and the funding of farmers to embrace sustainable farming practices. This paper has underscored that through the use of artificial intelligence in solutions, the adoption of sustainable practices and safe policies, it is feasible to conserve water resources, enhance the quality of water, improve the quality of ecosystems, and preserve the general health of the population. This research would help improve sustainable agriculture and environmental management as part of the broader endeavour to develop appropriate policy recommendations for stakeholders.

CONFLICT OF INTERESTS

The authors declare no conflict of interests.

REFERENCES

(1). Adejuwon, J.; et al. Assessment of Nitrate and Phosphate Levels in Nigerian River Basins: Implications for Agricultural Runoff Pollution. J. Environ. Sci. Water Resource. 2022, 12 (3), 45–60.
(2). Baba, M.-H. Water Pollution: Causes, Impacts, and Solutions—A Critical Review. J. Sustain. Health 2024, DOI: 10.37376/jsh.vi76.5785.

(3). Carpenter, S. R.; Caraco, N. F.; Correll, D. L.; Howarth, R. W.; Sharpley, A. N.; Smith, V. H. Nonpoint Pollution of Surface Waters with Phosphorus and Nitrogen. Ecol. Appl. 1998, 8 (3), 559–568.
(4). Chen, D.; Zhou, Q.; Wang, X.; Zhang, H. Nitrogen Removal in an Ecological Ditch Receiving Agricultural Drainage in Subtropical Central China. Ecol. Eng. 2015, DOI: 10.1016/j.ecoleng.2015.05.012.
(5). Choi, Y.; Kang, H. Challenges in Managing Non-Point Source Pollution from Agricultural Runoff. Water Resour. Manag. 2014, 28 (10), 3215–3230.
(6). Dodds, W. K.; Bouska, W. W.; Eitzmann, J. L.; Pilger, T. J.; Pitts, K. L.; Riley, A. J.; Schloesser, J. T.; Thornbrugh, D. J. Eutrophication of U.S. Freshwaters: Analysis of Potential Economic Damages. Environ. Sci. Technol. 2009, 43 (1), 12–19.
(7). EFSA. Conclusion on the Peer Review of the Pesticide Risk Assessment of the Active Substance Glyphosate. EFSA J. 2015, 13 (11), 4302.
(8). EPA. Nutrient Pollution in Coastal Waters: Causes, Impacts, and Solutions; United States Environmental Protection Agency: Washington, DC, 2023. https://www.epa.gov.
(9). European Environment Agency. Nutrient Enrichment and Pollution in Europe's Seas; EEA Report No 4/2019; European Environment Agency: Copenhagen, Denmark, 2019.
(10). FAO. Global Assessment of Agricultural Runoff and Its Impact on Water Quality; Food and Agriculture Organization of the United Nations: Rome, Italy, 2023.
(11). FAO. The State of World Fisheries and Aquaculture; Food and Agriculture Organization of the United Nations: Rome, Italy, 2018.
(12). Ficklin, D.; et al. Effectiveness of Buffer Strips and Constructed Wetlands in Reducing Nitrogen Pollution. J. Hydrol. 2012, 450, 123–135.
(13). Ibrahim, A.; Usman, M.; Abubakar, B. Adoption of Precision Agriculture Technologies in Developing Countries: Challenges and Opportunities. J. Agric. Sci. Technol. 2023, 25 (4), 789–802.
(14). Kushwah, A. K. Assessment of the Surface Water Quality of the Gomti River, India, Using Multivariate Statistical Methods. Water 2023, DOI: 10.3390/w15203575.
(15). Liu, Y.; Zhang, S.; Wang, T.; Chen, J.-H. Precise and High-Throughput Delivery of Micronutrients in Plants Enabled by Pollen-Inspired Spiny and Biodegradable Microcapsules. Adv. Mater. 2024, DOI: 10.1002/adma.202401192.
(16). Lwanga, E.; et al. Pesticide Contamination in African Groundwater: A Review of Sources and Impacts. Sci. Total Environ. 2020, 720, 137562.
(17). Ober, H.; et al. Artificial Intelligence in Sustainable Agriculture: Opportunities and Challenges. Front. Sustain. Food Syst. 2022, 6, 789123.
(18). Rico). J. Water Resour. Prot. 2021, DOI: 10.4236/jwarp.2021.138032.
(19). Sánchez-Colón, S.; Schaffner, A. Seasonal Variations in Agricultural Runoff Pollutants: Implications for Water Quality Management. Environ. Sci. Technol. 2021, 55 (8), 4321–4330.
(20). Sánchez-Colón, Y. M.; Schaffner, F. C. Identifying Nonpoint Sources of Phosphorus and Nitrogen: A Case Study of Pollution That Enters a Freshwater Wetland (Laguna Cartagena, Puerto
(21). Sharma, R.; Kumar, S.; Singh, P. Precision Agriculture for Sustainable Farming: Role of AI and IoT. J. Clean. Prod. 2022, 345, 131123.
(22). Shelton, J. F.; Geraghty, E. M.; Tancredi, D. J.; Delwiche, L. D.; Schmidt, R. J.; Ritz, B.; Hansen, R. L.; Hertz-Picciotto, I. Neurodevelopmental Disorders and Prenatal Residential Proximity to Agricultural Pesticides. Environ. Health Perspect. 2014, 122 (10), 1103–1109.
(23). Shou, Q.-Y. Research Progress of Source and Mechanism of Agricultural Non-Point Source Pollution in China. Appl. Ecol. Environ. Res. 2019, DOI: 10.15666/aeer/1705_1061110621.
(24). Tao, Z.; Liu, G. Research on Current Situation of Farmland Runoff Pollution and Ecological Treatment Technology. E3S Web Conf. 2024, DOI: 10.1051/e3sconf/202452001021.
(25). UNEP. Global Chemicals Outlook II: From Legacies to Innovative Solutions; United Nations Environment Programme: Nairobi, Kenya, 2021.
(26). Vadas, P.; Kleinman, P.; Sharpley, A.; Turner, B. A New Model for Dung Decomposition and Phosphorus Transformations and Loss in Runoff. Soil Res. 2011, DOI: 10.1071/sr10195.
(27). Wang, Dong & Yu, Ya & Wang, Xiang & Huang, Kai & Yu, Shu. (2012). Optimization Strategies for Agricultural Non-Point Source Reduction. Advanced Materials Research. 518-523. 1184-1187. 10.4028/www.scientific.net/AMR.518-523.1184.

(28). WHO. Cadmium in Drinking-Water: Background Document for Development of WHO Guidelines for Drinking-Water Quality; World Health Organization: Geneva, Switzerland, 2020.
(29). WHO. Guidelines for Drinking-Water Quality, 4th ed.; World Health Organization: Geneva, Switzerland, 2017.
(30). World Bank. Digital Technologies for Agricultural Transformation in Sub-Saharan Africa; World Bank: Washington, DC, 2021.
(31). Xia, Y., Zhang, M., Tsang, D.C.W. et al. Recent advances in control technologies for non-point source pollution with nitrogen and phosphorous from agricultural runoff: current practices and future prospects. Appl Biol Chem 63, 8 (2020). https://doi.org/10.1186/s13765-020-0493-6
(32). Xiang, Long & Yu, Zhongbo & Chen, Li & He, Jia & Chen, Cheng & Fu, Xiaolei. (2012). Evaluating the Characteristics of Hydraulic Driven Non-Point Source Pollution Loss in Agricultural Watershed. Applied Mechanics and Materials. 212-213. 518-524. 10.4028/www.scientific.net/AMM.212-213.518.
(33). Zhao, H.; et al. Biodiversity Loss in Freshwater Ecosystems Due to Agricultural Pollution. Ecol. Appl. 2018, 28 (6), 1675–1687.

ISBN: 978-978-68-0485-9 DOI: https://doi.org/10.55455/acsnigeria.1.2.26-32

Vacuum Evolution of Atomic and Molecular Matter

Ogaba Philip Obande
Department of Chemistry, National Open University of Nigeria, Jabi, Abuja
Corresponding Author's email:gababands@gmail.com

ABSTRACT

With the support of existing literature and observational evidences, it is postulated that contribution of stellar nucleosynthesis to particulate matter content of the universe might be marginal, if any. The action $m = h\nu/c^2$ precipitates atoms of the chemical elements from the vacuum field in our visible universe. In this action, accuracy of an element's atomic mass value is achieved by simply coupling its intrinsic waveform with Planck constant and freezing the product with the action of Avogadro constant $N_A = 1.0172(c_o/c^o)^2$. Furthermore, for an elemental quantum wavepacket, radius r, the stress field, $\tau = \Delta r/r$, due to 90^o angular oscillation of the e-m field also effects precipitation of molecular matter from the vacuum. Existing positions on matter evolution are discussed in terms of the original postulates of Burbidge and Burbidge, Fowler and Hoyle (B^2FH), including those of Noel and Kozyrev. The author's position aligns with those of Noel and Kozyrev that an increase in pressure would favor nucleosynthesis far more than an increase in temperature as a result of the well-known tendency of the latter to disrupt order. Moreover, as has been shown previously, atomic mass value is particularly specific; accuracies of one part in a billion are quite common, an action in 0^oKs deep space would stand much better chance of achieving the stringent degree of reproducibility nature imposes on atomic mass values.

KEYWORDS: Atomic mass value specificity; Avogadro constant; Chemical element's waveform; Vacuum Field nucleosynthesis; Molar mass precipitation.

1. INTRODUCTION

Emerging postulates would, if proven, challenge established concepts of origin of the chemical elements. Two theories and a dissenting voice each claims correct understanding of the way nature fabricates the chemical elements: "Stellar Nucleosynthesis" and the "Heartfire Model", while the dissenting voice is that of the Russian astronomer/astrophysicist, Nicholai Kozyrev who argues rather strongly against stellar nucleosynthesis. Here, we take a brief look at the existing positions to argue in support of vacuum nucleosynthesis.

1.1 Stellar Nucleosynthesis

Current standard view holds that hydrogen H and helium He were originally produced in the 'Big Bang' and all other elements came later through sundry mechanisms in the cores of stars. Promoters of this view would include renowned scientists like A. S, Eddington,[1] H. A. Bethe,[2] F. Hoyle[3,4] and E. M. & G. R. Burbidge et al..[5] Hans Bethe's detailed description of stellar energy generation by burning the elements would seem to have influenced in no small measure the concept of stellar nucleosynthesis; his theory certainly provided strong backing to subsequent weaponization of nuclear energy, it definitely served as clear proof of concept. We believe that the idea of energy production from element burning certainly informed subsequent establishment of stellar nucleosynthesis. Notably, most of the papers proposing thermonuclear reactions at the core of stars were published in the 1950s and at some point in time, Burbidge et al.'s paper went on record as the most cited astrophysics paper of all time. Such is the confidence vested on the theory that some were emboldened to propose an 'evidence' for its validity, Wellenstein.[6]

1.2 Sources of Stellar Energy

The title is the 1947 doctoral thesis of Nikolai A. Kozyrev,[7] renowned Russian astronomer, astrophysicist and theoretical physicist, Briefly, Kozyrev faults stellar nucleosynthesis but does not provide an explicit alternative theory; he maintains that the sun and other stars generate their energy by a totally unknown way. According to his biographer: "With scheme for reactions in the sun and stars proposed by the German theoretical physicist Hans Bethe in 1939, the question of stellar energy sources seemed to have been solved, and nobody except Kozyrev reconsidered the problem". Part of

the abstract to his published D.Sc. thesis reads as follows: "The temperature obtained for the centre of the sun is about 6 million degrees, this is not enough for nuclear reactions. … Stars generate their energy not in any nuclear reactions. *Stars are machines, directly generating radiations* [emphasis ours]. The observed diagram of heat generation, the relation 'mass-luminosity-radius', cannot be explained by standard physical laws. Stars exist in just those conditions where classical laws are broken, and a special mechanism for the generation of energy becomes possible, … Physical coordinates of the main points have been found using observational data. The constant (physical coordinates) should be included in theory of internal constitution of stars which pretend to adequately account for observational data. There in detail manifests the inconsistency of the explanations of stellar energy as given by nuclear reactions and also calculations as to the percentage of hydrogen and helium in stars." Thus, Kozyrev vehemently rejects any notion of stars producing energy by nuclear reaction, he insists that a totally unknown mechanism is responsible.

1.3 Inside the Earth – The Heartfire Model

The model, proposed by David Noel,[8] would seem in support of nucleosynthesis but argues, for whatever reason, in favor of it occurring in the core of planets rather than core of stars. He maintains that elements heavier than iron are created through nucleosynthesis in the mid section (mesolayer) of the Earth's core. Possibly for simplification, his presentation reads much like a college essay, completely devoid of the usual quantitative expressions often necessary for grasping the subject. We reproduce some key points considered relevant for the present purpose: (i) Earth's core comprises three layers - inner core, mesolayer and mantle; (ii) the mesolayer behaves like a critical fluid while the other two layers are solids; (iii) the mesolayer comprises predominantly neutrons; (iv) some 213 BL, equivalent to 4.284 x 10^9 kwh of heat, flows from the core to the surface of the Earth daily; (v) how and exactly where in the core this huge quantity of heat is produced remains an open question; (vi) conversion of proton to deuteron causes a seven-fold size increase, might not this be responsible for observational radial expansion of the sun and also of the Earth? (vii) would supernova-explosion-motivated formation of neutron star not imply that the unexploded star had a sphere of neutrons in its core, especially since there is no accepted position regarding the internal constitution of stars. Notably, Noel argues against the reigning astrophysics concept of supernova-explosion-motivated formation of the chemical elements.

2. METHODOLOGY

The study is based on previous publications which, themselves, rely on a prior submission by Russell and Russell R&R (1981).[9] We set out since 2012 to test the validity of some of their claims; results of that exercise have been widely reported; see, for instance, refs. 10 – 21; the present effort is a continuation of the same exercise. As stated in ref. 18, we set aside R&R's metaphysics and focus on verifying their claims with established classical physics. We first evaluated the atom's intrinsic e-m frequency v/s, absolute atomic mass of its wave m_w and particulate m_p forms following the procedures reported in refs 10,11,12. Based on the fact that the atom physically rotates, ref. 17, we use m_w and m_p values to evaluate the simple harmonic motion SIM characteristics of the wave and particulate forms as described in ref. 26, Here, values of the atom's speed of light in vacuum c_o(vacuum light speed) and in matter c^o (de Broglie radiation) are taken in combination with its physical properties to submit a model on vacuum nucleosynthesis,

2.1Vacuum Nucleosynthesis Model

One finds that *the atom is defined with four mass values,* in order to simulate this arrangement one would require an approach that replicates a system of four correspondent bodies in dynamic equilibrium. This would comprise three tangible bodies and an intangible (fluidic) body; each must continuously exchange mass-energy matrices with its neighbors to maintain local mass invariance. It turns out that an arithmetic device gives the simplest solution. A lever system perfectly illustrates the setting: the intangible fluidic body serves as fulcrum, it supports the three floating tangible bodies. The fulcrum locates what we call the 'Absolute universe' U_w^* and floating within it are: particulate conjugate of the Absolute universe $\underline{U_p^*}$, our Visible universe U_p^o, and the 'Invisible component U_p' of our universe. The system works as follows: $U_w^* \leftrightarrow U_p^o \leftrightarrow U_p' \leftrightarrow U_p^* \leftrightarrow U_w^*$; a cyclic process where all are

interconnected, see the picture, Obande.[13] Somehow, certain aspects of this simple picture confound the reigning model, its natural processes create seeming enigmas including: the black hole (portal of mass-energy exchange between the four worlds), dark matter (invisible particulate matter of U_p' *and* U_p^*), dark energy (combined energies (hvs) of the three particulate matter worlds), three particle generations (chemical elements of the three particulate matter worlds), and an expanding universe (superluminal radiation of a decaying/dying universe)! The element's ν values have been made widely available, Obande.[14,15] Values of atomic mass m retrieved with the classical mass formula CMF from the cosmic vacuum field CVF e-m radiations, Obande[15] are marginally low, they range from 7.373 x 10^{-51} kg/atom for electron to 4.322 x 10^{-40} kg/atom for americium, first and last elements of R&R's chemical periodicity respectively. We attribute these ultra low mass values to the atom's 'absolute' atomic mass in contradistinction from 'relative' atomic mass. We have previously re-evaluated established physical parameters of our world with the calculated atomic mass values to reaffirm their validity, Obande .[16-21] We present below quantitative descriptions of the various processes whereby nature forms molar units from elemental e-m waves, in other words, vacuum nucleosynthesis.

2.1 Precipitation of Particulate Matter from the Cosmic Vacuum Field

Observational evidence supports the following empirical expressions that describe precipitation of tangible matter from the CVF:

$$m_w = h\nu_w^{*2}/c_o^2 \quad (1)$$

generally, $2m_w = m_p = M_E = 1.0172h\nu_p^o/c^{o2}$ (2)

$$N_A = 1.0172(c_o/c^o)^2 = 1/m_{w(H)}^* \quad (3)$$

$$M_{E(\tau)} = \tau_p^o/(\omega_p^o/r_p^o)^{½} \quad (4)$$

$$MeV = \tau_p^o/\tau_{p(H)}^o \quad (5)$$

where m_w = atomic waveform 'rest' mass; M_E = element's molar mass; c_o vacuum light speed; c^o matter (de Broglie) light speed; h = Planck constant; $m_{w(H)}^*$ hydrogen waveform mass: $\nu_{w(E)}^*, \nu_{w(H)}^*$, an element's and hydrogen atom's e-m frequencies respectively; MeV = electron-volt atomic mass unit = 1.03752842 x 10^{-5} for the waveform, and 9.311079 x 10^5 for molar atom; τ = transverse stress on the oscillating wavepacket; r_w^* *and* r_p^o = atomic waveform and molar radii respectively and the factor, 1.0172 = ν_p^o/ν_w^*, is ratio of energies (i.e. frequencies) of the material/waveform atom. For the rest of the paper: superscript * or subscript w refers to the absolute or waveform atom while superscript o, ′, or subscript p refers to the particulate atom. Eqs. (1) to (5) account for spontaneous appearance of the tangible atom and/molecule from space, we show how in a moment.

3. RESULTS AND DISCUSSION

The above narrative on vacuum evolution of matter would remain speculative and unscientific unless we provided a clear-cut verifiable explanation. With advancement in technology, literature is now rife with astrophysical reports of what was once seen as a strange phenomenon - emission of matter from the CVF onto visible space, the preceding narrative serves to demystify the effect. The CVF is nature's play ground, more takes place in there than words can tell, Wheeler.[22] Characteristic mechanical and chemical parameters of the atom self-interact *in the CVF*; the interactions, of course, include chemical reactions, usually in the extreme cold of deep space. Most, probably all, of what we perceive as physical and chemical constants of nature are actually linear correlation coefficients of the atom's parametric self interactions, these include: rest mass m, vacuum radiation c_o, matter (de Broglie's) radiation c^o, magnetic flux density B, fine structure constant α, you name it, are all linear correlation coefficients. We were able to investigate 72 of these correlations and the exercise revealed parametric definitions of a number of fundamental constants, Obande.[20,21] Wellenstein[6] is of the opinion that the

chemical composition of 'peculiar stars' is proof of stellar nucleosynthesis but, Kozyrev[7] vehemently opposes this view. We think a proof of our position would require at least: (i) evidence that atomic and molecular matter are routinely produced in space ceaselessly; (ii) a clear quantitative explanation of how the elemental e-m waveform transforms to ponderable matter as solids, liquids, gases or plasma, et cetera. For (i) we simply cite a few reports to the effect: Wikipedia.org.,[23] Lutz, D. et al.,[24] Ray, J. P. et al..[25] For (ii) we refer to formation of ponderable matter from the waveform as atoms, ions, radicals, molecules, et cetera, illustrated below with calculations of atomic and molar masses using eqs, (1) to (5) above. Taking the electron e- as example we first get the mass of its waveform followed by that of the particulate form; Obande:[26], substitution into the relevant equation gives:

Eq.(1): $m^*_{e(w)} = 6.626\ x\ 10^{-34}\ x\ 1.0/(2.99792458\ x\ 10^8)^2 = 7.3725\ x10^{-51}\ kg/atom$

Eq.(2):$\mathrm{m^o_{e(p)}} = (6.626\ x10^{-34} x\ 1.0172)/(3.71535.\ x10^{-14})^2$
$= 2\ x\ 4.883\ x10^{-7} = 9.7656\ \ kg/mol$ M

Eq.(3): $N_A = 1.0172(\frac{2.99792458x\ 10^8}{3.71535229x10^{-14}})^2 = \frac{1}{1.5099x10^{-44}} = 6.623\ x\ 10^{43} units$

Eq.(4): $MeV = 3.846\ x\ 10^{15}/(12.783/9.1312\ x10^{-15})^{0,5} = 93.158\ x10^6$ eV/mol
= molar electric constant:, i.e., eV- kg equiv.

Eq.(5): $m^o_{e(\tau)} = 2.0\ x10^{-3}$x 3.486E15/7.139E18 $= 9.7656\ x10^{-07} kg/mol$

3.1 Avogadro Constant and Production of Tangible from Intangible Matter

Theory reveals Avogadro constant or Lochsmidt No. an interesting combination of two ratios – the ratio $(c_o/c^o_p)^2$ i.e., vacuum light speed to matter (de Broglie) light speed squared multiplied by the ratio v^o_p/v^*_w, i.e., energy of a particulate element to that of its vacuum analogue, $N_A = 1.0172(c^*_o/c^o_p)^2$ where energy of particulate to waveform atom, $E^o_p/E^*_w = v^o_p/v^*_w = 1.0172$. It turns out that the product, Avogadro No. multiplied by the atom's waveform mass, gives the atom's theoretical molar mass value which, if doubled, gives empirical molar or relative 'atomic' mass, i.e.,

$$N_A m^*_w = M_p \text{ or } m_r \qquad (6)$$

Validity of eq.(6) requires that M_p be the *theoretical molar mass*, see ref 19, figs 1 to 4 and Table 1, pp. 68 and 69.

The challenge here is to explain, as simple as possible, the process of solidification from the waveform and compaction into solids, liquids or gases found in various structures of the cosmic expanse. Nature *freezes radiation* by an ingenuous trick; it fabricates the molar unit, $N_A = 1.0172(2.99\ x\ 10^8/3.72\ x\ 10^{-14})^2 = 6.623\ x\ 10^{43}\ units/mol.$, then multiplies this unit by the element's waveform atomic mass to precipitate the molar form e.g. for the electron waveform: $M^*_{e(W)} = N_A m^*_w = 6.623\ x\ 10^{43}\ u$, $x\ 7.3724193\ x\ 10^{-51}\ kg/u = 4.883\ x\ 10^{-7} kg/mol$ and Am $= 6.623E43x\ 4.7497E - 41 = 3.146E3$ kg/mol (the value is the theoretical relative atomic mass of Am). This result confirms our previous positions: i) our theoretical evaluation of N_A was right, Obande,[11] ii) the electron is a full-fledged-element, it is the first member of the chemical periodicity.[10] However, the result raises valid questions regarding the correct value of electron molar mass: is it empirical $5.4858\ x\ 10^{-4}\ g$/mol or theoretical $4.8828\ x\ 10^{-4}\ g/mol$ or indeed $9.7656\ x\ 10^{-4}\ g/mol$ which we have been using in all previous reports, Obande.[10] It seems years of misunderstanding have not helped the electron's position; to date, its molar form is not widely appreciated (particularly in theoretical physics quarters), its absolute atomic mass value $7.373\ x\ 10^{-51}\ kg/u$ is still a curiosity awaiting the position of the mainstream. Although we shall continue to use $9.7656\ x\ 10^{-7} kg/mol$, our analytical procedure places a crucial demand for clarification. It turns out that ratio of an element E's atomic strain to H's value gives half its (incredibly) accurate empirical molar mass: $M = \tau^o_{p(E)}/\tau^o_{p(H)}$; e.g., for e- we have: $M^o_{p(e-)} = 3.486E15/7.139E16 = 4.88E - 7\ x\ 2 = 9.7656E - 7\ g/mol$; also for Am: $M^o_{Am(p)} = 8.674E20/$

$7.139E18 = 121.5\ x\ 2 = 243\ g/mol$. In view of the cosmic relevance of the expression $M_p^o = 2N_A m_p^o$, we are inclined to accept the doubling of what otherwise was supposedly already molar mass; the subject calls for further investigation. Interestingly, this issue does not arise in calculations involving electrical equivalence of gravimetric mass.

Observational evidences suggest that an atomic element formed from the waveform grows slowly in complex steps of accretion to eventually become part of a cosmic body like what we find in interstellar media, protoplanets, molecular outflows, stellar bodies, or entire galaxies. The procedure indicates that chemical elements are formed by linear correlations (self interactions) in the cosmic vacuum field CVF, it leaves no room for stellar nucleosynthesis.

3.2 Error Sources

Results of this investigation rely totally on accuracy of the atom's e-m frequency ν value; for now, there is no purely theoretical framework for this value; indeed, the present effort is targeted to lead ultimately to development of a viable framework. Observe, in Obande (2024, p.144),[14] that a common ν value defines the alkali metal and its preceding noble gas, the situation is less than satisfactory but unavoidable at the moment. If ever a purely theoretical approach would be found it could open up much needed possibilities for clearer understanding of the role of the noble gas in matter's fabrication.

3.3 Further studies

Three possible follow-up research activities are immediately conceivable:

i) A program for *ν* value

As stated in an earlier report, Obande,[14] the ν values reported here were obtained manually with the aid of a scientific pocket calculator, accuracy of the value to the tenth decimal place is not in doubt but all that has been achieved is a 2-D picture of the subject. There is need to develop a program that takes a number of factors into account, one that can routinely generate a 3-D picture to facilitate visualization of Schrödinger's quantum state. Indeed, ideally, one would expect such a program to be able to reveal angular distribution and orientation of the wave packet and reproduce observational electronic configurations of an element regardless of mass number, i.e., electronic configurations of a many-electron atom;

ii) Absolute atomic mass: Existence and value

The atom's absolute mass value, m kg/atom, has featured prominently in our reports, Obande,[9-11] this object is yet unknown to theoretical physics and, in particular, the mainstream, an independent investigation/confirmation is required;

iii) Avogadro constant AC

Confirmation of the formula for AC, $N_A = 1.0172(c_o^*/c_p^o)^2 = 6.623\ x\ 10^{43}$ units where $1.0172 = \nu_p'/\nu_w^*$, would be quite interesting. We have a haunch that N_A must be playing other roles in nature than creation of molecular from atomic mass; it is natural to suspect that that it cools/condenses the hot plasma to precipitate the atom from invisible to visible space. It would be even more interesting if we understood details of the cooling/condensation process, as in how do the reduced vacuum radiation c_o/c_p^o and 'reduced' matter oscillation ν_p'/ν_w^* interact with the hot atomic plasma in the freezing/precipitation process?

We are inclined, from observational lines of evidence, to the position that isolated vacuum atomic waveforms are concentric radiation rings, they would necessarily exist as infinitely elastic sub-micron thick hollow loops or toroids, see for e.g the rainbow, the radii would vary from 1.499E8 m to 2.327 m from electron to americium respectively, Obande.[11,26] Configuring this loop into the ponderable atom in its spatial mold naturally results to significant in-built observational strain and tension see, Burkert et al.[27], Obande.[17] Given the AC formulation, we may wish to know the details of its interactions with the newly-formed white-hot atom that cools it to O^oK of deep space before it re-heats in the sundry

processes of construction of cosmic structural networks. Clearly, research into subjects of this nature would require decades.

4. CONCLUSION

Atoms are produced by synthetic reactions, not in the core of stars but in ultra-cold deep space. The synthetic reaction or nucleosynthesis does not occur in stars but in the CVF. Observational evidence on quantum numbers QNs, Obande,[14] would suggest that vacuum nucleosynthesis VN is much more complex than the simplifications in eqns. (1) to (5) above. Our previous description of QNs hint at existence of spatial templates upon which the elements are formed, see for instance, Golubev.;[28,29] Certainly, much more await to be investigated than what is already known.

ACKNOWLEDGEMENTS

This work was carried out at the National Open University of Nigeria NOUN, the author appreciates the conducive environment provided by the University.

CONFLICT OF INTERESTS

The authors declare no conflict of interests.

ETHICS APPROVAL

The University Ethics Committee ensured that the work, being a purely theoretical investigation, did not involve issues of ethical concerns.

DATA AVAILABILITY STATEMENT

The data that support the findings of this work are available on preprints.org; doi.org/10.2139/ssrn.4127879; also on Harvard Dataverse: A Compilation on the Physical Reality "Replication Data" doi.org/10791/DVN/UOVDIA

REFERENCES

(1). Eddington, A. S., A. S. The internal composition of the stars. *The Observatory,* 1920, **43**(1341) 341, 341 – 358
(2). Bethe, H. A. Energy production in stars. Phys. Rev. 1939, **55**(5), 434 – 456..
(3). Hoyle, F. The synthesis of the elements hydrogen. *MNRAS*, 1946 **106**(5), 343 -383.
(4). Hoyle, F. On nuclear reactions occurring in very hot stars 1. The synthesis of elements from carbon to nickel. *ApJ*1954 *Series***1**-121.
(5). Burbidge, E. M., Burbidge, G R., Fowler, W. A., Hoyle, F., Synthesis of the elements in stars. *Rev. Mod. Phys.* 1957, **29**(4), 547 - 650.
(6). Wellenstein, G. Astronomical evidence for nucleosynthesis in star: The chemical composition of peculiar stars provides clues to the nuclear processes in stellar interiors. Sci. Adv., 1968, **162**(3654), 625 – 631
(7). Kozyrev, N. A., Sources of Stellar Energy and The Theory of the Internal Condition of Stars Prog. Phys. 2005, **3**, 61 – 99.
(8). Noel, D., *Inside the Earth – The Heartfire Model,* 2004, 10pp. david@aoi.com.au
(9). Russell, Walter & Russell, Lao; R&R, (1981), *Atomic Suicide?* University of Science & Philosophy, Swannanoa, Waynesboro, Virginia. 1981 edn. Online: abundanthope.net/artman2/uploads/1/Atomic_Suicide.pdf
(10). Obande, O. P. Atomic Mass: Origin, Units and Constants. Appl. Phys. Res. 2016a, **8**(1), 92-101 v8n1p92
(11). Obande, O. P. Notes on Russellian cosmogony. II. A procedure for theoretical evaluation of relative atomic mass and internal energy. Phys. Essays 2015, **28**, 78-85.
(12). Obande, O. P. Notes on Russellian cosmogony – Part 1: Absolute atomic mass. Int. J. Eng. Sci. 2013, **2**, 68-77. www.theijes.com/papers/v2-i4/part.%20(2)/M0242068077.pdf

(13). Obande, O. P. The Pan-STARRS1 Static Sky: A classical physics goldmine for cosmology, astrophysics and atomic physics. Appl. Phys. Res. 2017, **9**(6), 75-85.
(14). Obande, O. P. Fractional and unitary electric charges I: Classical foundations of quantum effects. Appl. Phys. Res. 2024, **16**(1), 143–154.
(15). Obande, O. P. A classical physics approach for space expansion: The Hubble drift. Appl. Phys. Res. 2021, **13**(2),39-54..
(16). Obande, O. P. Fundamentals of Universal Gravitation. SSRN, July **8**, 2022 DOI:10,2139/ssrn.4157604
(17). Obande, O. P. On intrinsic rotation of bodies. J. HEPG&C, 2019, 5, 868-883 www.scirp.org/journal/jhepgc
(18). Obande, O. P. Mass and energy densities of the cosmos. Appl. Phys. Res. 2019, **11**(6), 19-35,
(19). Obande, O. P, A field concept of the black hole. Appl. Phys. Res. 2018, **10**(4), 66-79.
(20). Obande, O. P, On the fundamental physical constants: I. Phenomenology. Appl. Phys. Res. 2017, **9**(5), 42 – 61.
(21). Obande, O. P, On the fundamental physical constants: II. Field coupling geometry. Appl. Phys. Res. 2017, **9**(5), 62-72,
(22). Wheeler, J. A, How come the quantum? Ann. New York Acad. Sci., 1986.
(23). en.wikipedia.org/wiki/list_of_interstellar_and_circumstellar_molecules
(24). Lutz, D., Sturm, E.,Janssen, A. … Sternberg, A., Tacconi, L. J., WeiB, A. Molecular outflows in local galaxies: Method comparison and a role of intermittent AGN driving. A&A **633**, 2021,A134.
(25). Ray, T. P. McCaughrean, M. J., Caratti o Garatti, A. … Wright, G., Outflows from the youngest stars are mostly molecular. Nature 2023, **623**(7985), 48-52.
(26). Obande, O. P. Classical definitions of gravitation, electricity and magnetism. Appl. Phys. Res. 2015, **7**(6), 85-94,s
(27). Burkert, V. D., Elouadrhini, I, and Girod, F. X. Pressure distribution inside the proton. Nature, **557**, 2018, 369-399.
(28). Golubev, S. N. Structure mechanism of ordinary mass formation J. Mod. Phys.2016 **7**, 875-
(29). Golubev, S. N. The emergence and existence of life in the world of elements and the physical vacuum. Arch. Life Sci. 2014, **8**(11), 1.

ISBN: 978-978-68-0485-9 DOI: https://doi.org/10.55455/acsnigeria.1.2.33-37

Evaluation of the Cytotoxic and Antioxidant Extracts of *Artemisia Annua Whole Plant*

Lilian Chidera Okafor[1]*, Khadijah Ateda Isimekhai[1], Fausta Ogbuefi-Chima[2], Bilkisu Adedoyin[1], Jemimah Simon Wakawa[1], and Olutola Adeola Olayemi[1].
[1]Applied Chemistry Research Laboratory, University of Abuja, FCT, Abuja, Nigeria.
[2]Raw Materials Research and Development Council, Maitama, Abuja, Nigeria.
Corresponding Author's email: *Okafor2chidera@gmail.com. 08039295931.*

ABSTRACT

Artemisia annua is an herb from Asteraceae family well known for its medicinal uses, particularly in the treatment of malaria. This study evaluates the cytotoxicity and antioxidant properties of *Artemisia annua* (sweet wormwood) extracts (n-hexane, ethyl acetate and methanol). The Brine Shrimp Lethality Test (BSLT) was carried out to access the toxicity of the extracts, and the antioxidant potential of various extracts was determined using DPPH assay, ABTS assay and Metal chelating activity assay (radical scavenging assay) compared with antioxidant controls BHA, ascorbic acid and α-tocopherol, respectively. The BSLT result showed high toxicity in all extracts, with the methanol extract showing the highest toxicity. The LC_{50} values (81.25 µg/L for n-hexane, 67.42 µg/L for ethyl acetate, and 51.59 µg/L for methanol) indicate that the lower the LC_{50}, the higher the potency of the extract. The radical scavenging assay exhibited great scavenging activity in all extracts, with the methanol extract outperforming the standards. These findings highlight the potential activity of *Artemisia annua* extracts for pharmaceutical applications, particularly in drug development, and also prove to be a potent source of biologically active compounds that can be further subjected to isolation of therapeutic antioxidant agents.

KEYWORDS: *Artemisia annua,* Cytotoxic, Antioxidant assay, drug discovery, natural products.

1. INTRODUCTION

Globally, medicinal plants have played a vital role in traditional healthcare systems and have continued to play a pivotal role in modern drug discovery. Historically, these plants are used for treating various ailments, often based on traditional knowledge and empirical experience.[1]

In recent times, the high cost of living and hike in healthcare services as well as drugs, have led to the increased use of medicinal plants by people, especially those in rural areas. Furthermore, several side effects have been reported from the use of conventional drugs globally, thus heightening the use of herbal remedies.[2]

Medicinal plants being the main sources of phytochemicals, contain bioactive compounds such as phenols, flavonoids, and alkaloids widely recognized for their potent antioxidant activities, which play an essential role in preventing oxidative stress-related diseases, such as cardiovascular disorders, neurodegenerative diseases and cancers through scavenging reactive oxygen species (ROS) and free radicals.[3,4] Thus, protecting cellular components from oxidative damage and protecting overall health.

Artemisia annua plant, known as sweet wormwood, has been used for treating fever and malaria.[5] Beyond its antimalarial properties, recent studies have highlighted the plant's rich phytochemical composition and its potential antioxidant and anti-inflammatory activities.[6]

These bioactive properties make the plant a potential therapeutic agent in cancer therapy and oxidative stress-related conditions.[7] Investigating the whole plant extract rather than isolated compounds allows for a synergistic evaluation of its therapeutic effects, potentially offering more potent and broad-spectrum bioactivities.[6,7] This study aims to evaluate the cytotoxic and antioxidant properties of *Artemisia annua* whole plant.

2. MATERIALS AND METHODS

2.1 Plant collection and identification: The whole part of the plant was collected from ABU Zaria for five days, verified and authenticated (*Artemisia annua* ABU 0275) at the herbarium Botany section of the Department of Biological Science Ahmadu Bello University Zaria, Kaduna State, Nigeria.

2.2 Sample Treatment: The whole plant was washed to remove dirt, rinsed and air-dried, ground, and sieved. The powdered sample was weighed and stored in a clean polythene bags at room temperature.

2.3 Extraction: Cold extraction was done using the maceration method. A portion of (500g) of the powdered sample was soaked continuously with 2000ml of n-hexane, ethyl acetate, and methanol, respectively, allowed to stand for seven (7) days at room temperature, then decanted and filtered with 20cm filter paper. The filtrate was concentrated using a rotary evaporator to get the crude extract, while the residue was dried and soaked with ethyl acetate as well as methanol.

2.4 Collection: *Artemia salina* shrimp eggs were collected for cytotoxicity test from a standard laboratory abroad (cell- culture laboratory, United Kingdom) for BSLT.

2.5 Brine Shrimp Lethality Test (BSLT) Assays Procedure
Brine shrimp (Artemia salina) eggs were hatched in seawater for 48 hours to obtain larvae. Extracts (0.2 g) were dissolved in 2 ml solvent of extraction, and concentrations of 1000, 100, and 10 µg/ ml were prepared in triplicates with controls. Ten larvae were introduced into each vial, and survival was recorded after 24 hours. LC_{50} values were calculated using Finney probit analysis software. The extracts were labelled in the order n-hexane (001LN), ethyl acetate (002LN), and methanol (003LN).

2.6 Antioxidant Assay
Radical scavenging assay was done using DPPH assay, ABTS assay, and Metal chelating assay with the crude extracts, and the scavenging activity was expressed as percentage inhibition, using the standards BHA, ascorbic acid and α-tocopherol. The following concentration were done from 0.25, 0.5,1 and 1.5 mg/ml.[8]

3. RESULTS AND DISCUSSION

3.1 Results

3.1.1 Cytotoxicity Results Using BSLT

LC50 values on n-hexane, ethyl acetate and methanol extracts are shown below as 81.27, 67.42 and 51.19, respectively, in Table 1. This indicates the toxicity of the extract against brine-shrimp larvae.

Table 1: Results of Brine-Shrimp Lethality Test (BSLT) of *A. annua* Whole Plant.

CRUDE EXTRACTS	SOLVENT OF EXTRACTION	LC_{50} (U/L)
001LN	n-Hexane	81.27 (139.06-455.34)
002LN	Ethyl Acetate	67.42 (42.16-518.18)
003LN	Methanol	51.59 (42.36-379.34)

LC_{50}< 1000µg/cm^3 = Toxic, LC_{50}>1000µg/cm^3 =Not Toxic *High/Low 95% Confidence Interval

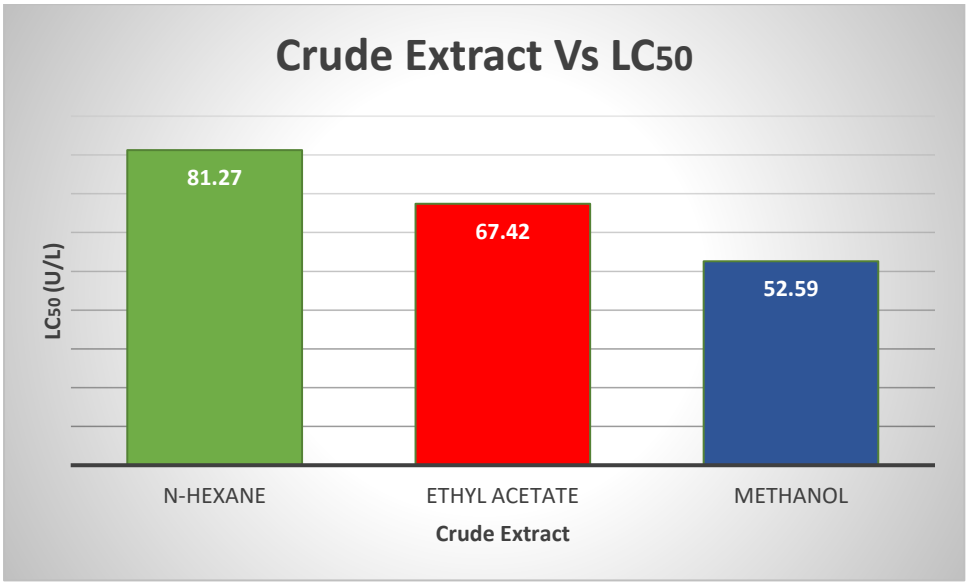

Figure 1: A bar Chart showing the LC_{50} of Artemisia annua whole plant extract.

3.2 Antioxidant Assay

These result shows the in-vitro lab-based tests used to evaluate the crude extract's ability to combat oxidative stress.

Table 2: Percentage (%) Inhibition of Crude Extracts and Standards against Assay type

This table shows the radical scavenging activity at the highest concentration, at 1.5 mg/ml

Extracts Type	Assay Type	Highest % @1.5mg/ml
Hexane	DPPH	73.3%
	ABTS	85.1%
	Metal Chelation	87.3%
Ethyl Acetate	DPPH	83.0%
	ABTS	851%
	Metal Chelation	87.3%
Methanol	DPPH	83.3%
	ABTS	89.1%
	Metal Chelation	88.3%
	Control	
Standard		Max % Inhibition (at 1.5 mg/mL)
BHA		81.2%
Ascorbic Acid		78.3%
α-Tocopherol		69.7%

DPPH (1,1-diphenyl-2-picrylhydrazyl), ABTS (2,2'-azinobis-(3-ethylbenzothiazoline-6-sulfonic acid) and Metal Chelation were used with the extracts.

Standards Used: BHA, Ascorbic Acid, α-Tocopherol.

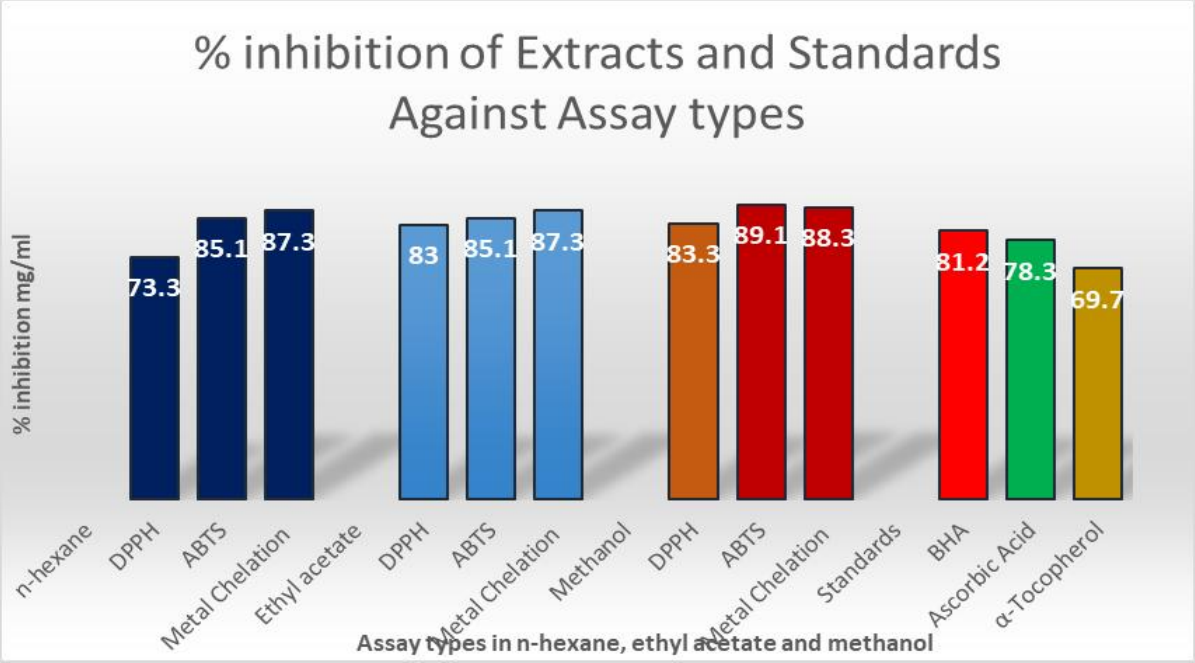

Figure 2: A bar chart showing the Percentage (%) Inhibition of Crude Extracts and Standard against Assay types.

3.2 Discussion

From figure 1, methanol extract has the lowest LC_{50} value (U/L) of (51.59), having the highest potency activity, followed by ethyl acetate extract (67.42) and n-hexane extract (81.27). indicating that methanol has the highest concentration of cytotoxicity bioactive compounds compared to n-hexane and ethyl acetate. No prior study has reported the cytotoxicity of *Artemisia annua* whole plant using Brine shrimp lethality test (BSLT).

From figure 2, the antioxidant assay using radical scavenging test shows that the extracts showed strong activity to compare the standards, with methanol extract exhibiting the highest scavenging activity in DPPH, ABTS and metal chelating scavenging assay followed by ethyl acetate and n-hexane. Thus, it can be said that methanol crude extract possesses good activity due to better extraction of polar antioxidants such as phenols and flavonoids being a polar solvent.[9]

4. CONCLUSION

This study evaluated the cytotoxic effects and antioxidant activity of three extracts from whole plant. These findings highlight methanol extract's superior activity compared to n-hexane and ethyl acetate extracts. This study confirms the cytotoxic potential of *A. annua* and suggest that the plant extracts, especially methanol and ethyl acetate fractions, possess strong antioxidant potential and may serve as an effective natural alternative to synthetic antioxidants. This study establishes a strong foundation for further investigation into isolation and characterization of active compounds from the crude extracts.

ACKNOWLEDGEMENT

My profound appreciation goes to the American Chemical Society (ACS) for this invaluable opportunity, and to the editorial committee for their dedication and support throughout this process. I am equally grateful to the Department of Chemistry, University of Abuja, for providing the essential facilities that contributed to the success of this research. My deepest thanks go especially to my supervisor for her exceptional guidance, commitment, and unwavering support in bringing this work to fruition.

CONFLICT OF INTERESTS

The authors declare no conflict of interests.

REFERENCES

(1) Iqbal, S; Younas, U; Chan, K; Zia-Ul-Haq, M; Ismail, M. Chemical composition of *Artemisia annua L*. leaves and antioxidant potential of extracts as a function of extraction solvents. Molecules. 2012. 17(5), 6020-32.
(2) Ekor, M. The growing use of herbal medicines: Issues relating to adverse reactions and challenges in monitoring safety. Front Pharmacology. 2014, 4, 177.
(3) Mohamed, S; Mohamed, M. I. Antioxidants and Phytochemical Profiles in medicinal plants: Unravelling molecular mechanisms. Scholars international Journal of Biochemistry. 2024, 7(7), 106-117.
(4) Newman, D. J., Cragg, G. M. Natural products as sources of new drugs from 1981 to 2014. Journal of Natural Products. 2016, 79(3), 629–661.
(5) Septembre-Malaterre, A; Lalarizo Rakoto, M; Marodon, C; Bedoui, Y; Nakab, J; Simon, E; Hoarau, L; Savriama, S; Strasberg, D; Guiraud, P; Selambarom, J; Gasque, P. *Artemisia annua*, a Traditional Plant Brought to Light. International Jorunal Molecular Sciences. 2020, 21(14), 4986.
(6) Swamikannu, B; Umapathy, V. R; Natarajan, P. M; Nandini, M. S, Queency, S; Vimalarani, V; Rajinikanth, S. Unlocking the Therapeutic Benefits of Artemisia Annua: A Comprehensive Overview of its Medicinal Properties. Journal of Pharmacy and Bioallied Sciences. 2024, (5), S4248-S4253.
(7) Singh, V., Kaur, G. Unlocking the therapeutic benefits of *Artemisia annua*: A comprehensive overview of its medicinal properties. Journal of Pharmacy and Bioallied Sciences. 2024,16(5), 69–76.
(8) Nachiketa, B; Archna, S; Ashwani, K. Radical Scavenging and Antioxidant Potential of Nuts and Leaves Extracts of *Semecarpus anacardium (L.).* American Journal of Plant Sciences. 2013, 4(8),1679-1683.
(9) Skowyra, M; Maria, G; Sergovia, F; Almajao, P. Antioxidant properties of *Artemisia annua* Extracts in Model food emulsions. Antioxidant (Basels). 2014, 3(1), 116-128.

ISBN: 978-978-68-0485-9 DOI: https://doi.org/10.55455/acsnigeria.1.2.38-43

Synthesis of Aluminium Metal-Organic Frameworks for the Removal of Emerging Pollutants from Aqueous Solution: Kinetics and Thermodynamics

Samuel Emmanuel Egga, Mohammed Ibrahim, Saraya Akuben Yakubu, Joshua Agbu Samuel, Eunice Kaze Ajang, Ismail Busari Adebayo, and Aisha Abdulkarim Lawal
Department of Chemistry, Faculty of Natural Sciences, University of Jos, P.M.B. 2084 Jos, Plateau State, Nigeria.
Corresponding Author's email: emmanuels@unijos.edu.ng, samegga13@gmail.com

ABSTRACT

Serious environmental and human health problems caused by emerging pollutants have attracted worldwide concern and recently, metal–organic frameworks (MOFs) with high porosity have drawn global attention for their effects on the adsorption efficiency for the removal of emerging pollutants from the environment. In this study, aluminium based metal-organic frameworks (MIL-53) were synthesized by the hydrothermal method. The synthesized MOFs were characterized using Fourier transform infrared spectroscopy (FT-IR), X-ray diffraction (XRD), scanning electron microscopy (SEM), and Brunauer-Emmett-Teller (BET) surface analysis and used as suitable adsorbent to remove Amoxicillin, Bromophenol blue, and Methyl red from simulated aqueous solutions. The influences of different parameters such as adsorbent dosage, contact time, initial ion concentration, and temperature were investigated and the results indicated that the adsorption process followed pseudo-second order. Five well-known models including Langmuir, Freudlich, Temkin, Reddlich-Peterson, and Jossen's 3P were employed to correlate the experimental data obtained from the batch adsorption experiments and the thermodynamic studies show that the adsorption of the pollutants on the synthesized MOFs is spontaneous and feasible. Consequently, MOFs-53 with a high adsorption performance has potential applications for the removal of emerging contaminants from wastewater. In line with the Millennium developments and Sustainable Goals MDGs/SDGs Vision 2030, the findings seek to address a crucial component of environmental protection and public health by unveiling the development of cheap, effective, and sustainable adsorbent materials for tailored scale more efficient water filtration and purification technology.
KEYWORDS: MOFs, Adsorption isotherms, Emerging pollutants, Thermodynamic studies

1. INTRODUCTION

Modern society presently characterized with rapid growth, industrialization, urbanization and several anthropogenic activities in the quest to comfort life has consequently increased the release of several groups of pollutants into water bodies, endangering aquatic ecosystems and public health.[1] These set of pollutants are known as emerging pollutants which includes textile waste, industrial chemicals, pharmaceuticals, personal care items, agricultural chemicals and other generated domestic waste substances which have currently drawn increasing attention because of their potential threat to the physiological anatomy of living organisms even at low concentrations due to their persistence, and bioaccumulativecharacteristics.[2] The inefficiency of conventional water treatment techniques to effectively eliminate these contaminants makes the innovation of sophisticated and more potent remediation technologies necessary such as the (MOFs) adsorbent a considerable option for sustainable development.[3]

Reports in recent years have seen a significant increase of interest in metal-organic frameworks (MOFs), which is conceived as a family of porous crystalline materials made of metal ions or clusters coupled to organic ligands characterized to be employed for use in several environmental remediation applications. They are promising options for the adsorption of different pollutants from aqueous solutions due to their large surface area, adjustable porosity, and chemical adaptability.[4,5]Aluminium-based MOFs are particularly well-suited for industrial water treatment applications because of their cost-effectiveness, non-toxicity, as well as thermal and chemical stability.[6,7]

The synthesis and design of aluminium metal-organic frameworks and their usage in eliminating amoxicillin, bromophenol blue, and methyl red from aqueous solutions are the main topics of this investigation. To gain a better understanding of the mechanisms behind the interaction between MIL-53(Al) and the targeted contaminants, special attention is paid to examining the adsorption kinetics and thermodynamic characteristics. This research work is in correlation with the global millennium and sustainable development goals.

2. MATERIALS AND METHODS

2.1. Materials. Terephthalic acid (%), aluminium nitrate nonahydrate, N, N-dimethylformamide (DMF), Bromophenol blue, Methyl red, Methanol, and 2-Propanol were purchased from Sigma Aldrich. Amoxicillin was provided by Eurolink Nigeria Ltd., Jos-Nigeria. All reagents used were of analytical grade.

2.2. Preparation of Al-MOFs. A modified version of a previously reported process[8,9] was used to synthesize Al-based MOFs under hydrothermal conditions. In 70 mL of a solution (30 mL DMF: 20 mL 2-propanol: 20 mL distilled water), precisely 1.21g of teraphthalic acid was added to it. An aluminium nitrate nonahydrate of 1.53 g was then dissolved in the solution of terephthalic acid, DMF, propanol, and distilled water. After 30 minutes of agitating, the mixture was transferred to a Teflon-lined stainless autoclave reactor and heated to 130 °C for four hours. Methanol was used to filter and wash the crystal product for five days. The remnant traces of contaminants from the mixture were evaporated by activating MIL-53(Al) for72 hours at 130 °C.

2.3. Characterization. The synthesized Al-MOFs were characterized using FT-IR, XRD, BET, and SEM.

2.4. Simulation of the Stock Solution of the Contaminants

2.4.1. Preparation of Amoxicillin (AM), Bromophenol Blue (BB), and Methyl Red (MR)Stock Solutions. Amoxicillin, Bromophenol blue, and Methyl red stock solutions of 250 mg/L using distilled water and the required standard concentrations were obtained by serial dilution of the stock solution.

2.5. Batch Adsorption Experimental Methods. Sorption tests were carried out to investigate the adsorption behavior of the Al-based MOFs. A comparative study was performed to estimate and evaluate the adsorption capacity and kinetic model for removing AM, BB, and MR from the water. This method allowed the accurate estimation of the rate at which pollutants were adhered to the surface of the porous materials. During the entire set of experiments, a range of parameters were examined to analyze their effect on the adsorption process. Among the parameters were initial ion concentration (50 to 250 mg/L), adsorbent doses (0.15 to 0.75 g/L), contact time (30 to 150 minutes), and temperature (30 to 70 °C). Each mixture was then agitated at 3000 rpm for 30 minutes using a centrifuge. The solution mixture was then filtered and the adsorption extent of AM, BB, and MR were determined using UV-Vis spectrophotometer at wavelengths of 272, 590, and530 nm, respectively. The amount and percentage of ion adsorbed were calculated for each experiment using the equations adopted in previous studies reported (Rafatullah et al.,).[10]

3. RESULTS AND DISCUSSION

3.1. Characterization. FT-IR spectra of MIL-53(Al) adsorbent and after adsorbing the pollutants are shown in Figure 1. The substantial reduction in the peak between 600 and 1500 cm^{-1} after adsorption could be as a result of the pollutants adhered to the surface and filling the pores of the MOFs[11].Figure 2 shows the MIL-53's XRD patterns. The steep peak indicates that the MOFs are crystalline while Figure 3 shows that the pore size distribution was 2.1 nm, indicating it is a nanoparticle as determined by BET. Figure 4 as well, shows the SEM image at 100 µm which described the structure of MOFs-53 to be crystalline having high porosity and large surface area.

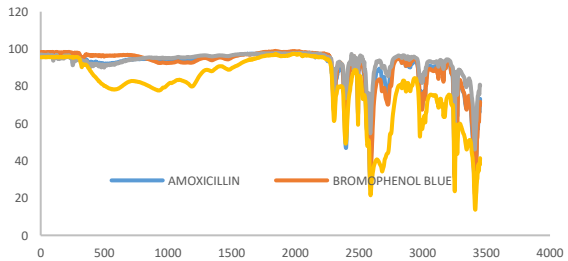

Figure 1. FT-IR Spectra of MIL-53(Al)

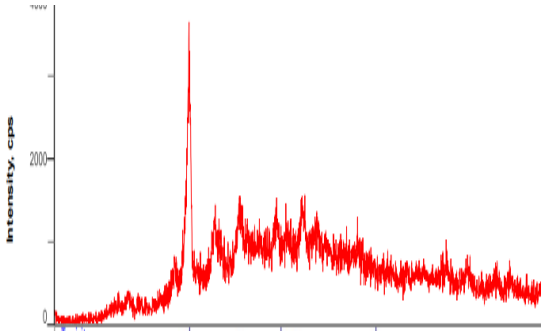

Figure 2. XRD of MIL-53(Al)

ISBN: 978-978-68-0485-9 DOI: https://doi.org/10.55455/acsnigeria.1.2.38-43

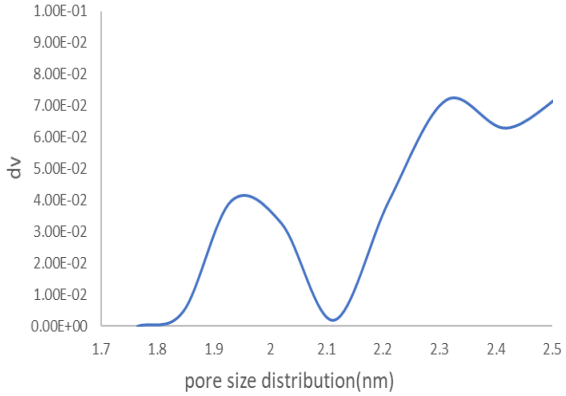

Figure 3. BET of MIL-53(Al)

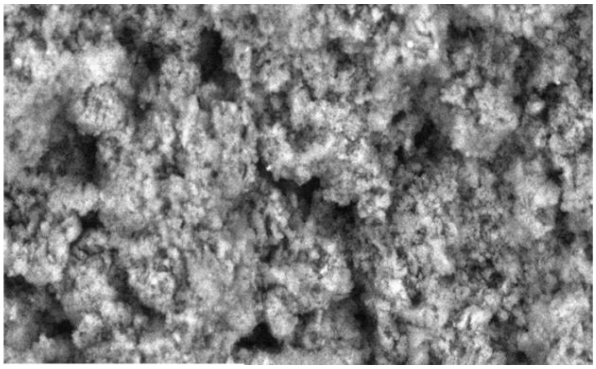

Figure 4. SEM image of MIL-53(Al) at 100 μm

3.2. Batch Adsorption Studies. It was deduced from Table 1, that the removal rate of AM, BB, and MR decreases with an increase in the starting ion concentration. At larger concentrations, the adsorbent active sites become saturated, which results in a decrease in percentage removal. As seen in Table 2, the adsorption capacity further increased as the adsorbent dosage increased from 0.15 to 0.75 g which suggested that more sites became available for holding and engulfing the contaminants in the water. Table 3 also, shows how temperature affects the pollutants' ability to be adsorbed. Consequently, at 30 °C, a rapid adsorption of contaminates by the MOFs was observed which suggests that these contaminants are most effectively removed at a relatively low temperature and the highest and optimal removal of the contaminants at the ideal contact time of 150 minutes, with a small deviation in the case of methyl red, is depicted in Table 4 together with the observed removal in percentage at various timing ranges.

3.3. Adsorption Isotherms. Adsorption isotherms are used to explain how the adsorbent and adsorbate are in equilibrium. The equilibrium adsorption data were evaluated using Freundlich, Langmuir, Jossen's 3P, Reddlich-Peterson, and Temkin isotherm models and the predicted values are presented in Table 5.

Table 1. Effect of Initial Ion Concentration

Conc. (mg/L)	Percentage Removal		
	AM	BB	MR
20	97.967	95.818	75.450
40	96.967	81.273	73.294
40	95.622	74.455	69.960
80	95.300	63.545	67.607
100	94.744	57.409	65.450

Table 2. Effect of Adsorbent Dosage

Dosage (g)	Percentage Removal		
	AM	BB	MR
0.15	90.967	76.045	82.313
0,30	91.522	79.455	79.568
0.45	93.967	80.591	77.607
0.60	94.633	84.455	73.294
0.75	95.411	85.591	69.176

Table 3. Effect of Temperature

Temp. (K)	Percentage Removal		
	AM	BB	MR
303	94.189	85.136	84.078
313	93.633	81.045	77.019
323	93.967	79.227	73.098
333	93.522	73.318	70.745
343	93.189	71.955	68.196

Table 4. Effect of Contact Time

Time (mins)	Percentage Removal		
	AM	BB	MR
30	92.744	95.364	75.450
60	94.189	95.819	73.294
90	92.077	96.045	69.960
120	93.189	96.273	67.607
150	94.522	96.727	65.450

ISBN: 978-978-68-0485-9 DOI: https://doi.org/10.55455/acsnigeria.1.2.38-43

3.4. Adsorption Kinetics. The Pseudo second-order model[12,13]was used to evaluate the mechanisms controlling the process of the contaminant adsorption from the aqueous solution, such as chemical reaction, mass transfer, and diffusion control. Table 6 shows the results of the model's evaluation for the plotted experimental data which depicted a correlation coefficient (R^2) of 1.000, 0.911, and 0.999 for AM, BB, and MR, respectively, hence these results demonstrated excellent fit and linearity.

Table 5. Isotherm Parameters

Isotherms	Parameters	Values		
		AM	BB	MR
Freundlich	R^2	0.979	0.854	0.989
	n	-29.325	-4.985	10.245
	K_F (L/g)	7.093	0.996	11.400
Langmuir	R^2	0.952	0.855	0.996
	Qmax (mg/g)	19.194	0.413	2.149
	B (L/mg)	0.122	-4.101	-5.267
Temkin	R^2	0.879	0.904	0.990
	K_T (Lg^{-1})	1.260	-5.045	0.002
	b ($Jmol^{-1}$)	9876.940	-19551.270	-2721.816
Reddlich-Peterson	ß	1.061	1.201	1.1000
	A	7.563	2.463	11.473
	R^2	1.000	0.995	1.000
Jossen's 3P	F	-0.222	-0.098	-0.646
	H	0.001	0.404	0.015
	R^2	0.985	0.942	0.992

Table 6. Pseudo-Second-Order Kinetic Parameters

Equation	Parameters	Values		
		AM	BB	MR
Pseudo- second- order	q_e(mg/g) cal.	0.178	0.444	2.348
	K_2	6.450	-0.191	-0.061
	R^2	1.000	0.911	0.999

Table 7. Thermodynamic Parameters

T(K)	ΔG(kJ/mol)			ΔH (J/mol)			ΔS (J/mol.K)			R^2		
	AM	BB	MR	AM	BB	MR	AM	BB	MR	AM	BB	MR
303	- 6.343	-6.949	-5.838	472.131	357.739	194.480	22.495	24.115	19.910	0.953	0.949	0.992
313	-6.568	-7.190	-6.037									
323	-6.793	-7.431	-6.236									
333	-7.018	-7.672	-6.435									
343	-7.243	-7.913	-6.634									

3.5. Thermodynamic Studies. The thermodynamic studies revealed temperature affects the contaminant adsorption processes in two ways; The first one is that an increase in temperature leads to a higher diffusion rate of the adsorbent and secondly, the adsorption capacity at equilibrium is also influenced by temperature which is in agreement with previous reported similar studies.[14] The Gibbs and Van't Hoff plots were used to evaluate the free energy (ΔG) where heats of adsorption (ΔH) and changes in the system entropy (ΔS), determine the viability of the adsorption process, and the

parameters are presented in Table 7.The observations of negative values of ΔG show that the process is feasible and spontaneous. Furthermore, the endothermic nature of the adsorption process was emphasized by the positive values of ΔH AM (472.131 J/mol), BB, (357.739 J/mol), and MR (194.480 J/mol) respectively). The degree of randomness at the MOFs or adsorbate solution interface is improved by the rate of pollutants' adsorption on MIL-53(Al), as indicated by the positive values of ΔS for AM (22.49 J/K), BB (24.115 J/K), and MR (19.91 J/K) respectively.[15]

CONCLUSION

Al-MOFs was synthesized and designed by mixing different solvents and the characterization results revealed the material as crystalline, Porous with good pore sizes and stable to both physical and chemical conditions. The results of its high rate of absorption and removal of Amoxicillin, Bromophenol blue, and Methyl red from the simulated aqueous solution also demonstrated the efficiency of these MOFs with high adsorbing capacity to remove these three pollutants significantly in water. The optimal conditions that favor Amoxicillin, Bromophenol blue, and Methyl red adsorption and removal from water were as follows: adsorbent dosage (0.75, 0.75, and 0.15 g), contact time (150, 150, and 30 mins), initial ion concentration (20 mg/L), and temperature (30 ° C) respectively. It was observed also, that the process was entirely endothermic, practicable, and spontaneous. Therefore, Al-based (MOFs) can be highly considered and used as an efficient adsorbent for wastewater treatment in real-world applications.

ACKNOWLEDGEMENTS

The authors acknowledge and appreciate Eurolink Nigeria Ltd., Jos, Plateau State for supporting this research with some valuable chemicals.

CONFLICT OF INTERESTS

The authors declare no conflict of interests.

REFERENCES

1. Bashir, I., Lone, F. A., Bhat, R. A., Mir, S. A., Dar, Z. A., Dar, S. A. Concerns and Threats of Contamination on Aquatic Ecosystems. *Bioremediation and Biotechnology*: Sustainable Approaches to Pollution Degradation, **2020**, 1-26.
2. Thakur, S., Chandra, A., Kumar, V., Bharti, S. Environmental Pollutants: EndocrineDisruptors/Pesticides/Reactive Dyes and Inorganic Toxic Compounds Metals, Radionuclides, and Metalloids and Their Impact on the Ecosystem. *In Biotechnology for Environmental Sustainability,* **2025**, (pp. 55-100). Singapore: Springer Nature Singapore.
3. Saravanan, A., Kumar, P. S., Jeevanantham, S., Karishma, S., Tajsabreen, B., Yaashikaa, P. R., Reshma, B. Effective Water/Wastewater Treatment Methodologies for Toxic Pollutants Removal: Processes and Applications Towards Sustainable Development. *Chemosphere,* **2021**,280, 130595.
4. Cai, G., Yan, P., Zhang, L., Zhou, H. C., Jiang, H. L. (2021). Metal–Organic Framework-Based Hierarchically Porous Materials: Synthesis and Applications. *Chemical Reviews,* **2021** 121(20), 12278-12326.
5. Sun, Q., Qin, L., Lai, C., Liu, S., Chen, W., Xu, F., Ye, H. Constructing Functional Metal-Organic Frameworks by Ligand Design for Environmental Applications. *Journal of Hazardous Materials,* **2023**, 447, 130848.
6. Rambau, K. M. A. *Metal Organic Frameworks from Unconventional Metal Feedstock for Energy Storage Applications,* **2021**(Doctoral dissertation, University of Pretoria (South Africa).
7. Singh, N., Dhillon, A., Kumar, D. Metal-Organic Frameworks for Adsorption of Fluoride for Groundwater Treatment. *Groundwater for Sustainable Development,* **2023**, 23, 100967.
8. Chen, X. Y., Vinh-Thang, H., Rodrigue, D., Kaliaguine, S. Amine-Functionalized MIL-53 Metal–Organic Framework in Polyimide Mixed Matrix Membranes for CO_2/CH_4Separation. *Industrial & Engineering Chemistry Research***2012**,51(19), 6895-6906.
9. Angı, D. *Adsorption Kinetics of Methane Reformer Off-Gases on Aluminum Based Metal-Organic Frameworks***2017**(Master's thesis, Izmir Institute of Technology (Turkey)).

10. Rafatullah, M. M. R. Y., Sulaiman, O., Hashim, R., Ahmad, A. Adsorption of Copper (II), Chromium (III), Nickel (II) and Lead (II) Ions from Aqueous Solutions by Meranti Sawdust. *Journal of Hazardous Materials,* **2009**, 170(2-3), 969-977.
11. Abuzalat,O., Wong, D.,Elsayed. M.A. Nano-porous Composites of Activated Carbon-Metal Organic Frameworks (Fe-BDC@AC) for the Rapid Removal of Cr (VI): Synthesis, Adsorption, and Kinetics Studies. *Journal of Organometallic Polymers and Meterials,* **2022**,*32:1924-1934.*
12. Ahmed, M.B., Zhou, J.L, Ngo, H.H., Guo, W., Chen, M. Progress in the Preparation and Application of Modified Biochar for Improved Contaminant Removal from Water and Wastewater. *Bioresource Technology,* **2016**, 214: 836-851.
13. Simonin, J.P. On the Comparison of Pseudo-First Order and Pseudo Second Order Rate Laws in Modeling of Adsorption Kinetics. *Chemical Engineering Journal*, **2016**, 300, 254-263.
14. Pathak, P., Sharma, S. Sorption Isotherms, Kinetics, and Thermodynamics of Contaminants in Indian Soils. *Journal of Environmental Engineering,* **2018**, 144(10), 04018109.
15. Mittal, A., Mittal, J., Malviya, A., Kaur, D., Gupta, V.K. Adsorption of Hazardous Crystal Violet from Wastewater by Waste Material. *Journal of Colloid and Interface Science,* **2010**, 343: 463-473.

ISBN: 978-978-68-0485-9
http://acsnigeria.org/publications/proceedings

Determination of the level of pesticide residues in irrigation soil from Akko, Gombe State, Nigeria

Mohammad Bashir Sulaiman[1*], Aliyu Fadawa Tijjani[2], Abdullahi Muhammad Gimba[3]
[1]Department of Chemistry, Northwest University Sokoto, Sokoto State, Nigeria
[2]Department of Science Laboratory Technology, Federal Polytechnic of Oil and Gas, Bonny Island, Nigeria
[3]Department of Science Laboratory Technology, Gombe State Polytechnic Bajoga, Gombe State, Nigeria
Corresponding Author's email: sulaiman.mbashir@nwus.edu.ng; sulaimanmbashir35@gmail.com

ABSTRACT

This study determined pesticide residues levels in irrigation soil from Akko, Gombe State, Nigeria. A total of 54 soil samples were collected from three different irrigation farmlands, and the pesticide residues were extracted and analyzed using Agilent GC 7890B, coupled with MSD 5977A. The mean concentration of dichlorvos in the soil samples ranged from 0.00 - 0.089 mg·kg^{-1}, while the concentrations of dimethoate, lindane, aldrin, cypermethrin, and pyrazophos were below the detectable limit in all the studied samples. Paraquat dichloride ranged from 0.00 - 0.084 mg·kg^{-1}, while chlorpyrifos ranged from 0.00 - 0.079 mg·kg^{-1}, and p,p'-DDT ranged from 0.078 - 0.098 mg·kg^{-1}, while heptachlor concentration ranged from 0.00 - 0.086 mg·kg^{-1} in the soil samples. The levels of cyhalothrin ranged from 0.00 - 0.095 mg·kg^{-1}, dieldrin ranged from 0.00 - 0.085 mg·kg^{-1}, while that of endrin ranged from 0.00 - 0.097 mg·kg^{-1}. The concentrations of endosulfan ranged from 0.00 - 0.106 mg·kg^{-1}. This considerable level of these pesticide residues may accumulate in food crops through the uptake of soil and have a negative impact on human health. However, monitoring and continuous stringent regulations should be imposed with regard to the usage of pesticides in soil and foodstuff for public health protection.

KEYWORDS: Determination, irrigation, pesticide residues, soil.

1. INTRODUCTION

Pesticides are substances commonly used in modern agricultural practices to protect crops from various pests and diseases.[1-3] Many farmers use pesticides in order to increase yield and to protect their farms from diseases. However, after pesticide application, residues often remain in the soil and crops even after harvest, eventually entering the food chain.[4,5] Pesticides are toxic to humans both acute and chronic health effects depending on the quantity and types of exposure.[6] Conversely, the use of pesticides has significantly contributed to the increase in global food production over the past several decades.[7]

Globally, approximately 3 million tons of pesticides are used each year, representing a market value of US$40 billion.[8] In the European Union, nearly 500 substances are approved for pesticide use, with annual sales averaging 374,000 tons between 2011 and 2016.[9] Although pesticides enhance agricultural productivity and play a crucial economic role, their excessive use has raised significant environmental and public health concerns.[10] The widespread issue of diffuse agrochemical pollution has emerged as a significant threat to soil health[11], potentially undermining multiple United Nations Sustainable Development Goals related to the soil environment.[12,13]

Soil contamination poses significant threats to soil functions, biodiversity, and food safety, while also facilitating the off-site spread of pollutants through wind and water erosion. This dispersal can disrupt sink ecosystems and create additional exposure pathways for humans and non-target organisms to harmful contaminants.[13,14] Despite the significant impacts of soil contamination, EU regulations do not require monitoring pesticide residues in soil, in contrast to the mandatory water monitoring established by the Water Framework Directive.[7] There is a lack of extensive international studies on pesticide residues in soil, as existing research typically analyzes only individual pesticides or a small group of them.[7,15,16]

Several studies have characterized the occurrence of both currently used and banned pesticides in soils at national or regional levels.[17-22] Effective control of pesticide levels in food can only be achieved through systematic residue monitoring. In recent years, increased surveillance efforts have been implemented, emphasizing proper pesticide application rates and regulatory adherence.[23-25] Despite the public health risks, the usage of these pesticides is increasing, and they are used for both agricultural and non-agricultural purposes in Nigeria.[5] Hence, this study to investigate the level of pesticide residues in irrigation soil from Akko, Gombe State, Nigeria.

2. MATERIALS AND METHODS

2.1 Study area

The Akko Local Government Area is one of the eleven local governments in Gombe State. Akko is located between the latitudes of 10.97320° E and the longitudes of 10.28899° N of the equator. The area falls within the northern Guinea savanna zone of the Akko, Gombe State. Akko covers a total area of 2,627 km² (1,014 sq mi), with approximate population of 337,853.[26] The area receives an average annual rainfall of approximately 600 mm, which is sufficient for a single farming season. The annual rainfall pattern is erratic at the beginning of the rainy season, starting in April and intensifying as the season advances, raising the average from 600 to 1000 mm. The temperature as high as 41°C and the as low as 16°C. The generally high temperatures and low humidity favor high rates of evapotranspiration, leading to net water deficiencies. Akko L.G.A. is in the interior Savanna woodland, which can sustain large-scale livestock farming, as well as the cultivation of agricultural products like onions, spinach, tomatoes, rice, groundnuts, yams, cassava, and maize. The study area was selected due to of dry farming activities.

2.2 Soil sample collection

Soil samples were collected from three farms (labelled Farm A, Farm B, and Farm C) using a nested sub-sampling approach. Each farm contains six sub-farms; from each sub-farm three soil cores were taken at a depth of 0–20 cm, yielding 18 samples per farm (3 samples × 6 sub-farms = 18). All 18 samples from each farm were composited into a single representative sample for that farm (i.e., one composite for Farm A, one for Farm B, and one for Farm C). Samples were labelled sequentially as A, B, and C corresponding to the three farms. The samples were all label and transported to laboratory for analysis.

2.3 Reagent

Reagents/Solvents: n-hexane and dichloromethane (HPLC grade). Copper powder and concentrated sulfuric acid were obtained from Loba Chemie India.

2.4 Sample Extraction

Five grams of the sample was weighed into a 50 mL centrifuge tube, and 30 mL aliquots of the extraction solvent consisting of a mixture of n-hexane/dichloromethane (1/1, v/v) were added and shaken for 15 min (using a universal shaker, IKA Werke). After 15 minutes, the sample mixture was ultrasonically extracted at 25°C for 20 min. The mixture was centrifuged at 8,000 rpm for 8 minutes, and the resulting supernatant was transferred into a separate container. The extraction process was repeated twice, after which all extracts were combined and concentrated using a rotary evaporator under mild vacuum until dryness. The residue was dissolved in 40 mL of n-hexane and analyzed using GC system: Agilent 7890A GC (Agilent Technologies)

2.5 Sample Clean up

Five grams of copper was added to the dissolved sample mixture, shaken for 5 min, and centrifuged at 8000 rpm for 5 min. The supernatant was collected, 3 mL of concentrated H_2SO_4 was added, and the mixture was vortex for 1 min.The mixture was again centrifuged at 2,000 rpm for 5 minutes, and the resulting supernatant was collected and treated with 1 mL of concentrated sulfuric acid. Vortex-mixed again for 1 min, and then centrifuged at 2000 r/min for 5 min. The supernatant solvent was dried by a rotary evaporator, and the residue was reconstituted with 1 mL n-hexane and then vortex-mixed.

2.6 Instrumental Analysis

A 1 µL aliquot of the reconstituted sample was injected into a gas chromatograph (Agilent 7890B GC coupled with a 5977A MSD) for analysis, using helium as the carrier gas. The column temperature program was set at 150 °C for 1 min, ramp at 25°C /min to 230 °C, hold for 2 min; and ramp at 20°C /min to 240 °C, hold for 1 min; ramp at 20 °C /min to 260 °C, and hold for 5 min; ramp at 3°C /min to 280 °C, and hold for 5 min; ramp at 2°C /min to 285 °C, and hold for 10 min. The injection port temperature and transfer line were set at 240 °C and 250 °C, respectively. The injection was made in the splitless mode with purge on after 0.75 min. [27]

2.7 Preparation of Calibration Standards

Working standard solutions were prepared by diluting the stock solutions to 10 µg/mL in ethyl acetate. Appropriate aliquots were taken and further diluted with ethyl acetate to give a series of calibration standard solutions with concentrations of 10, 20, 50, 75, and 100 ng/mL. Extracted calibration

standards were prepared by spiking blank water samples (1 L) with the working standard solution prior to extraction to give concentrations of 10 ng/L, 20 ng/L, 10, 20, 50, 75, and 100 ng/L. After extraction and reconstitution (1 L to 1 mL), concentrations of these equate to of 0, 20, 50, 75, and 100 ng/L.[28]

2.8 Method of Data Analysis

The residues were analyzed using a Shimadzu gas chromatograph (GC-2010), equipped with 63Ni, an electron capture detector that allows the detection of contaminants even at trace concentrations. The GC conditions and detector response were adjusted to match the relative retention time and response. The capillary column was coated with ZB5 (30 m x 0.25 mm, 0.25 µm film thickness). Sample preparation, extraction, cleanup, and analysis were performed according to the procedure.[29]

3. RESULTS AND DISCUSSION

3.1 Pesticide residues Percentage in the soil samples

The percentage of pesticide residues is presented in Figure 1. The percentage level of dichlorvos in the soil samples was in the range of 27.50% and 34.85% in farms B and C, respectively, while the percentage level of paraquat dichloride in the soil was 12.90% in farm A and below the detectable limit in farms B and C. The levels of chlorpyrifos in the soils were in the order of 24.38% and 32.78% in farms B and C, whereas they were below detectable in farm A. The p,p'-DDT distribution in the studied soils was 15.05%, 24.07%, and 32.36% in farms A, B, and C, respectively. The heptachlor in the soil wass in the order of 13.21% in farm A, below detectable in farms B and C, while that of cyhalothrin had the following percentages in the same order: 14.59%, and dieldrin sulphate distribution in the studied soils was 13.05% and 24.07% in farms A and B, respectively. The percentage level of endrin in the soils was 14.90% in farm A and below the detectable limit in farms B and C, whereas that of endosulfan was 16.28% in similar orders.

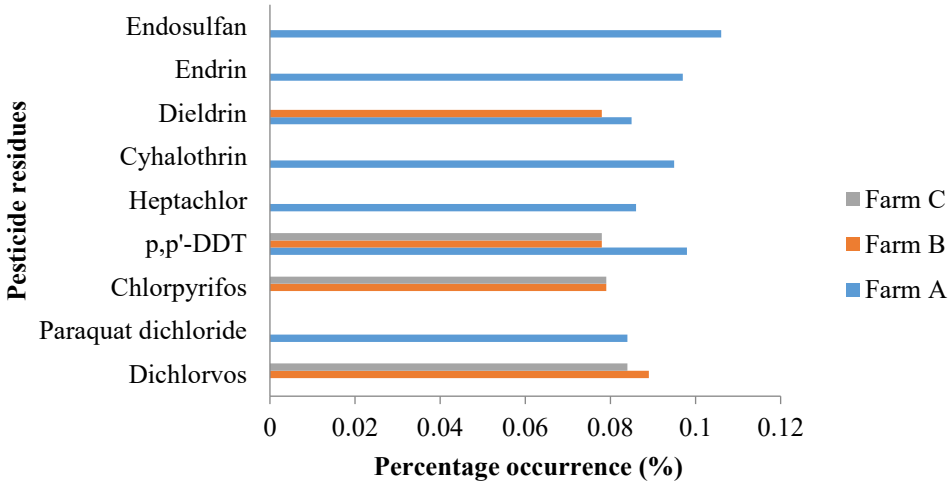

Figure 1: Percentage (%) of pesticide residues in the soil samples

3.2 Levels of pesticide residues in soil samples

The pesticide levels in the soil samples are presented in Table 1. The mean concentration of dichlorvos in the soil samples ranged from 0.00 to 0.089 mg·kg^{-1}, and the concentrations of dimethoate, lindane, aldrin, cypermethrin, and pyrazophos in the samples were below the detectable limit. Paraquat dichloride concentration was 0.084 mg kg^{-1} in farm A and was below the detectable limit in farms B and C. Chlorpyrifos concentration in the samples ranged from 0.00 to 0.079 mg·kg^{-1}, and concentrations of p,p'-DDT in the samples ranged from 0.078 to 0.098 mg·kg^{-1}, while heptachlor concentration ranged from 0.00 to 0.086 mg·kg^{-1} in the samples. The levels of cyhalothrin in the samples ranged from 0.00 to 0.095 mg·kg^{-1}, the dieldrin ranged from 0.00 to 0.085 mg·kg^{-1} in the sampled soils, while that of endrin ranged from 0.00 to 0.097 mg·kg^{-1}. The endosulfan concentrations in the samples ranged from 0.00 to 0.106 mg·kg^{-1}. Han et al. also reported that the content of chlorpyrifos, 7.2 - 77.2 µg/kg, was below the value of 0.079 mg kg^{-1} obtained in this study[31]. The level

of p,p'-DDT obtained in this study was above (4.01 µg/kg) that reported in soils from the farms of Kumasi, Ghana.[30] and 34.0 reported from the soils of China.[31]

The level of cyhalothrin was higher than that reported by Han et al.[31] but lower than that the cypermethrin reported by Han et al.[31]. Vincent et al. reported the detection of aldrin in soil 1.20 µg/kg, which is higher than the values obtained in this study.[30] In a Thailand project of food webs in rice paddies, a high level of aldrin was also detected in rice soils (28.6 µg/kg), [32] while dieldrin values were reported as 1.5-3.9 µg/kg by Han et al., which were below the values of 0.078-0.085 mg·kg^{-1} in this study.[31] Moreover, this study showed that the levels of pesticide residues in the studied soils were higher than those in early reported studies conducted in other parts of the world.[22-34] This could be due to unawareness and misuse of the use of OCP pesticides in Nigeria.[7]

Table 1: Levels of pesticide residues in soil (mg kg^{-1}) samples

S/No		Farm A	Farm B	Farm C
1	Dichlorvos	BDL	0.089±0.105	0.084±0.098
2	Dimethoate	BDL	BDL	BDL
3	Paraquat dichloride	0.084±0.105	BDL	BDL
4	Lindane	BDL	BDL	BDL
5	Chlorpyrifos	BDL	0.079±0.078	0.079±0.088
6	p,p'-DDT	0.098±0.089	0.078±0.098	0.078±0.100
7	Aldrin	BDL	BDL	BDL
8	Heptachlor	0.086±0.099	BDL	BDL
9	Cyhalothrin	0.095±0110	BDL	BDL
10	Cypermethrin	BDL	BDL	BDL
11	Pyrazophos	BDL	BDL	BDL
12	Dieldrin	0.085±0.110	0.078±0.101	BDL
13	Endrin	0.097±0.974	BDL	BDL
14	Endosulfan	0.106±0.0970	BDL	BDL

BDL= below detectable limit

4. CONCLUSION

The present study was conducted to determine pesticide residues levels in the irrigation soil of Kunnuwal, Akko Local Government Area Gombe State, Nigeria. Generally, the pesticide residue concentrations in the various soils have been recorded at a reasonable concentration. Hence, the need for regular monitoring of pesticide residues should be encouraged, since an increase in misuse of pesticides for agricultural produce is still ongoing in Nigeria. Based on the findings of this study, the following recommendations for further action and studies are suggested: the present work critically focused on the pesticide residue assessment of irrigation soil in the study area; the results, therefore, suggest the need for further studies on agricultural produce to help in understanding the chemical form and behavior of the pesticide residues; there is a need to develop an environmental monitoring and management program for pesticide residues in Nigeria.

CONFLICT OF INTERESTS

The authors declare no conflict of interests.

REFERENCES

(1) Guler, G.O.; Cakmak Y.S.; Dagli Z.; Aktumsek, A.; Ozparlak, H. Organo-chlorine pesticide residues in wheat from Konya region, Turkey. *Food Chem Toxicol*. **2010**, *4*, 1218-1221.
(2) Ahoudi, H.; Gnandi, K.; Tanouayi, G.; Ouro-sama, K.; Yorke, J.C.; Creppy, E.E. and Moesch, C. Assessment of pesticides residues contents in the vegetables cultivated in urban area of

Lome (southern Togo) and their risks on public health and the environment, Togo. *Int J Biol Chem Sci*. **2018**, *12*, 2172-2185.
(3) Maigari, A.U.; Sulaiman, M.B.; Buhari, M.; Abdullahi, A.O. Pesticide residues in selected vegetables from Gombe markets, Gombe State, Nigeria: assessing the health impact. *Ife J Sci*. **2021**, *23(1),* 77-87.
(4) Ononamadu, C.J.; Barau, M.M.; Salawu, K.; Ihegboro, G.O.; Owolarafe, T.A.; Lawal, A.T.; Oshobu, M.L.; Unah, P.E. Screening of selected vegetables from Wudil, Farmlands in Kano State, Nigeria for organophosphorus and organochlorine pesticide residues. *J Environ Occup Sci*. **2019**, *82*, 20-25.
(5) Sulaiman, M.B.; Maigari A.U.; Ihedioha, J.N.; Lawal, S.R.; Gimba A.M.; Shuhaibu, A.B. Levels and health risk assessment of organochlorine pesticide residues in vegetables from Yamaltu area in Gombe, Nigeria. *French-Ukraine Journal of Chemistry.* **2021**, *9(1),* 19-30.
(6) Ahmad, M.F.; Ahmad, F.A.; Alsayegh, A.A.; Zeyaullah, M.; AlShahrani, A.M.; Muzammil K.; Saati, A.A.; Wahab, S.; Elbendary, E.Y.; Kambal, N.; Abdelrahman, M.H.; Hussain, S. Pesticides impacts on human health and the environment with their mechanisms of action and possible countermeasures. *Heliyon*, **2024**, *10(7)*, e29128.
(7) Silva, V.; Mol, H.G.J.; Zomer, P.; Tienstra, M.; Ritsema, C.J.; Geissen, V. Pesticide residues in European agricultural soils – A hidden reality unfolded. Science of *The Total Environment.* **2019**, *653*, 1532-1545. https://doi.org/10.1016/j.scitotenv.2018.10.441.
(8) Pimentel, D. Pesticides and Pest Control. In: Peshin, R.; Dhawan, A.K. (eds) Integrated Pest Management: Innovation-Development Process. *Springer*, *Dordrecht*. **2009**. Doi; 10.1007/978-1-4020-8992-3_3
(9) EC (2018) EU pesticides database - active substances. http://ec.europa.eu/food/plant/pesticides/eu-pesticides-database/public/?event=activesubstance.selection&language=EN. (Last access May) 2018.
(10) Zhou, W.; Li, M.; Achal, V. A comprehensive review on environmental and human health impacts of chemical pesticide usage. *Emerging Contaminants.* **2025**, *11*, 1,100410.
(11) Stolte, J.; Tesfai, M.; Oygarden, L.; Kvaerno, S.; Keizer, J.; Verheijen, F.; Panagos, P.; Ballabio, C.; Hessel, R. Soil threats in Europe: status, methods, drivers and effects on ecosystem services: deliverable 2.1 RECARE project. (98673 ed.) (JRC Technical reports). *European Commission DG Joint Research Centre*. **2016**. doi.org/10.2788/488054.
(12) Keesstra, S. D.; Bouma, J.; Wallinga, J.; Tittonell, P.; Smith, P.; Cerdà, A.; Montanarella, L.; Quinton, J. N.; Pachepsky, Y.; van der Putten, W. H.; Bardgett, R. D.; Moolenaar, S.; Mol, G.; Jansen, B.; Fresco, L.O. The significance of soils and soil science towards realization of the United Nations Sustainable Development Goals, *Soil.* **2016**, *2*, 111-128. Doi; 10.5194/soil-2-111-2016.
(13) Pérez, P.A.; Eugenio, N.P. Status of local soil contamination in Europe: Revision of the indicator "Progress in the management Contaminated Sites in Europe, EUR 29124 EN, Publications Office of the European Union, Luxembourg, **2018**, ISBN 978-92-79-80072-6, Doi:10.2760/093804, JRC107508.
(14) FAO and ITPS. Global Assessment of the Impact of Plant Protection Products on Soil Functions and Soil Ecosystems FAO, Rome. **2017**, 40 pp
(15) Covaci, A.; Manirakiza, P.; Schepens, P. Persistent Organochlorine Pollutants in Soils from Belgium, Italy, Greece, and Romania. *Bull. Environ. Contam. Toxicol.* **2002**, *68*, 97-103. Doi: 10.1007/s00128-001-0224-6
(16) Růzicková, P.; Klánová, J.; Cupr, P.; Lammel, G.; Holoubek, I. An assessment of air-soil exchange of polychlorinated biphenyls and organochlorine pesticides across central and southern Europe. *Environ Sci Technol.* **2008**, *42(1),* 179-85.
(17) Orton, T.G.; Saby, N.P.A.; Arrouays, D.; Jolivet, C.C.; Villanneau, E.J.; Marchant, B.P. et al. Spatial distribution of Lindane concentration in topsoil across France *Sci. Total Environ.* **2013**, *443*, 338-350.
(18) Masia, A.; Vasquez, K.; Campo, J.; Pico, Y. Assessment of two extraction methods to determine pesticides in soils, sediments and sludges. Application to the Turia River Basin *J. Chromatogr. A.* **2015**, *1378*, 19-31.
(19) Pose-Juan, E. Sanchez-Martin, M.J. Andrades, M.S. Rodriguez-Cruz, M.S. Herrero-Hernandez E. Pesticide residues in vineyard soils from Spain: spatial and temporal distributions. *Sci. Total Environ*. **2015**, *514*, 351-358.

(20) Qu, C.K.; Albanese, S.; Chen, W.; Lima, A.; Doherty, A.L.; Piccolo, A. et al. The status of organochlorine pesticide contamination in the soils of the Campanian Plain, southern Italy, and correlations with soil properties and cancer risk Environ. *Pollut*. **2016**, *216*, 500-511.
(21) Chiaia-Hernández A.C.; Keller, A.; Waechter, D.; Steinlin, C.; Camenzuli, L.; Hollender J., et al. Long-term persistence of pesticides and tps in archived agricultural soil samples and comparison with pesticide application. *Environ. Sci. Technol.* **2017**, *51*, 10642-10651.
(22) Ockleford, C.; Adriaanse, P.; Berny, P. Brock, T. Duquesne, S. Grilli, S. et al. Scientific opinion addressing the state of the science on risk assessment of plant protection products for in-soil organisms. *EFSA J*. **2017**, *15*.
(23) FRN. Federal Republic of Nigeria, Official Gazette, Legal Notice on publication of the details of the Breakdown of the National and State Provisional total, 2006 Census. The Federal Republic of Nigeria Official Gazette, Government Notice No. 21, Lagos. **2007**, *94*, 1-26.
(24) Martin R.; Samuel F. et al. Interventions to reduce pesticide exposure from the agricultural sector in Africa: a workshop report. *Int. J. Environ. Res. Public Health.* **2022**,*19,* 8973.
(25) Beyuo, J.; Sackey, L.N.A.; Yeboah, C. et al. The implications of pesticide residue in food crops on human health: a critical review. *Discov Agric.* **2024**, *2*, 123.
(26) Wondimu, K.T.; Geletu, A.K.; Kedir, W.M. Recent developments in monitoring of organophosphorus pesticides in food samples. *Journal of Agriculture and Food Research*. **2025**,*19*, 101709.
(27) Liangliang, T.; Dongmei, H.; Yongfu, S.; Feng, H.; Yuan, W.; Hongli, Y.; Huijuan, Y. Method for the Analysis of 7 Indictor Polychlorinated Biphenyls (PCBs) and 13 Organochlorine Pesticide Residues in Sediment by Gas Chromatography (GC). *Earth Environ. Sci.* **2019**, *237*, 022053.
(28) Indrajit, S.; Samir, V. Environmental Analysis, Analysisof Pesticide esticide residues in drinking water as per bureau of indian standards using the agilent 7000 gc/ms/ms with pesticides analyzer; Solutions for Your Analytical Business Markets and Applications Programs. EU: Agilent Technologies, Inc. **2006**.
(29) Jona, T.; Yargeau, V. Multiresidue method for the fast and efficient analysis of current-use pesticides in streambed sediments using pressurized liquid extraction. *Science of the Total Environment*. **2024**, *906*, 167703.
(30) Vincent, K.B.; Nathaniel, O.B.; Lawrence, S.B.; Samuel, A. Human Risk Assessment of Organochlorine Pesticide Residues in Vegetables from Kumasi, Ghana. *J Chem.* **2018**. Doi: 10.1155/2018/3269065.
(31) Han, Y.; Mo, R.; Yuan, X.; Zhong, D.; Tang, F.; Ye, C; Liu, Y. Pesticide residues in nut-planted soils of China and their relationship between nut/soil. *Chemosphere*. **2017**. Doi:10.1016/j.chemosphere.2017.03.138.
(32) Chaiyarat, R.; Sookjam, C.; Eiam-Ampai, K. Organochlorine pesticide levels in the food web in rice paddies of Bueng Boraphet wetland, Thailand. *Environ Monit Assess*. **2015**, *187,* 230-240.

ISBN: 978-978-68-0485-9 http://acsnigeria.org/publications/proceedings

Assessment of the Quality Parameters of Edible Refined and Cold Pressed Vegetable Oil Sold at Katako Market in Jos, Plateau State

Juliet Dingtsen Dodo., Deborah Samson Madaki., and John Sunday Salami
Department of Chemistry, Faculty of Natural Sciences, University of Jos. Jos. Nigeria
Corresponding Author's Email: dodojuliet1969@gmail.com

ABSTRACT

The quality parameters of edible refined and cold pressed vegetable oil sold at Katako market in Jos were assessed. Two samples of refined made from soya and two samples of cold pressed made from groundnut were purchase. The analysis adopted the standard analytical methods from the 16th edition of Association of Official Analytical Chemist (AOAC, 2016). Physicochemical parameters tested was colour, odour, density, smoke point, moisture content, acid value, iodine value, peroxide value and saponification value. Toxic elements like cadmium, lead, arsenic and chromium were determine using Atomic Absorption Spectroscopy, digested with a mixture of nitric acid/hydrogen peroxide in a ratio of 5:1 Results indicates that, density 0.84±0.02-0.88±0.03 g/cm^3, 0.86 g/cm^3, moisture content 0.21-0.52,0.21±0.03-0.32±0.01%, smoke point 220±0.01-234±0.02, 224±0.05-234±0.02^{o}C, acid value 0.81±0.20-0.87±0.09, 0.91±0.30-1.03±0.13 mgKOH/g ,iodine value 5.71±0.89- 30.14±2.24, 1.59±0.45-7.74±0.13 I_2/100g, peroxide value 1.40±0.28-2.30±0.14, 3.15±0.21-4.30±0.28 meqO_2/kg, saponification value 180±1.41-189±1.41, 190±2.83-194±1.41mgKOH/g, cadmium 0.19±0.00, 0.38±0.00-0.57±0.01 mg/kg lead 0.29±0.01, 0.29±0.01 mg/kg, arsenic BDL-1.10±0.00 , 1.85±0.00-3.34±0.00 mg/kg, for the refined and cold pressed oils respectively. Chromium was below detectable limit of the instrument. Moisture content of the oils was higher than the recommended value of 0.20 %, acid value was higher than 0.6 mg, cadmium, lead as well as arsenic were all higher than the permissible limit set by FAO/WHO (CODEX Alimentarius) values. These oils are probably affected by unfavourable storage conditions, though they are of good quality and suitable for consumption, but the cold pressed vegetable oil had better quality parameters compared to the refined oil using the FAO/WHO (CODEX Alimentarius) standard values.

KEYWORDS: Quality parameters, Edible oil, Cold pressed, Refined, Katako Market.

1. INTRODUCTION

Oil (Oleum in latin) can be defined as a wide range of flammable substances which are either be a liquid or solid (fat) at room temperature or 25^{o}C [1]. Oils produced by plants are known as vegetable oil. Vegetable oils are important to man as a source of nutrient (fat in the human diet) and industrial raw materials[1]. Cooking oils and oils that are part of other foods can be oxidized in a more standing and a higher temperature[2]. The quality of oil is determined by several parameters such as peroxide number, acid number, iodine number[3]. Cold pressed oils are unrefined, with greater nutritional properties, but oxidizes faster at lower temperatures than refined oils[4]. The methods of extraction make all the difference in the quality and flavour of oil. The process of cold pressed extraction does not involve excess application of heat or chemical solvents, the oils obtained from this method retain their original flavour, taste, aroma, and nutritional value. Meanwhile, regular refined oils are extracted by using high temperatures and treated with chemical solvents which degrades their flavour, taste, and nutritional composition[5].

Edible vegetable oils are a group of fats derived from either seeds, nuts, cereal grains or fruits[6]. Not all these vegetable oils can be edible and also exist as liquid oils at ambient temperatures, but this research work report is centered on edible vegetable oils which are liquid at room temperatures.

If the extraction is done by a solvent, is it called refined oil, because the solvent allows to produce a standardized oil by modifying its fatty acids[4]. The polyunsaturated fatty acids content in cold pressed oil is high and this makes them unsuitable for frying as the temperature degrades its quality, flavor and aroma. Cold pressed oils are relatively nontoxic and has a large safety margin (>5000 mg/kg)[7]. It has become important to assess the quality parameters of edible refined and cold pressed vegetable oil to ascertain their safety levels for consumers especially those sold in Katako Market.

2. MATERIALS AND METHODS

2.1 Sample Collection

One litre each of the vegetable oils were bought randomly at Katako Market, stored at room temperature and transported to the Department of Chemistry laboratory of the University of Jos for analysis.

2.2 Determination of Colour, Odour, Density, Moisture content of Cold pressed and refined edible vegetable oils sold at Katako Market.
The colour was determined according to the methods described by [8]

2.3 Determination of smoke point of cold pressed and refined edible vegetable oils sold at Katako Market.
The oil was heated in a boiling tube clamped to a thermometer. The temperature was read out at the point where smoke was visibly seen rising from the oil in the boiling tube. The temperature was observed for 15 seconds and the range of the temperature within that period was recorded.

2.4 Determination of Physico-chemical properties of cold pressed and refined edible vegetable oils sold at Katako Market.
Acid value was determined by titrimetric method according to [9].
About 1.0 g of each oil was weighed and dissolved with 50 cm^3 of ethanol in a conical flask. Two drops of phenolphthalein indicator were added and titrated to pink end point with 0.1 M potassium hydroxide solution (KOH). Acid value was calculated according to the following Equation

$$\text{Acid value} = \frac{56.1 \times V \times C}{m}$$

Where 56.1 is equivalent weight of KOH, V is the volume in cm^3 of standard volumetric KOH solution used, C is the exact concentration of KOH solution used (0.1 M); m is the mass in grams

2.5 Saponification value (SV)
This was carried out using the method described by[10]. Two grams of the oil sample was added to a flask with 30 cm^3 of ethanolic potassium hydroxide solution, attached to a reflux condenser heated on a water bath for 1 hour.After the sample had cooled, 1cm^3 of phenolphthalein indicator was added and titrated with 0.5M hydrochloric acid until a pink endpoint was reached. A blank determination was also carried out. Saponification value was calculated using equation:

$$\text{Saponification Value} = \frac{(a - b) \times M \times 56.1}{\text{sample wght } (g)}$$

Where: a = sample titrate value M = molarity of the HCl b = blank titrate value 56.1 = molecular weight of KOH

2.6 Determination of the Levels of Heavy Metals in cold pressed and refined edible vegetable oils sold at Katako Market.
Digestion was carried out by adding 10cm^3 of nitric acid to 1 gram of each sample, followed by 2cm^3 of hydrogen peroxide and heated till a clear solution was obtained. The resulting solution was made up to 50cm^3 and transferred into a plastic bottle. The presence of Lead, Chromium, Cadmium and Arsenic were determined using Atomic Absorption Spectroscopy.

3. RESULTS AND DISCUSSION

3.1 Results
Table 1 present the physical properties of cold press and refined vegetable oils sold at Katako market. The refined soya oil has high moisture content and may be susceptible to rancidity.

Table 1: Physical Parameters of cold pressed and refined vegetable oil sold at Katako market.

Physical properties	Samples				
	RA (soya)	RB (soya)	CA (G/nut)	CB (G/nut)	WHO/FAO (CODEX) Standard
Colour	Amber yellow	Amber yellow	Orange red	Orange red	Nil
Odour	Odourless	Odourless	Nut-like aroma	Nut-like aroma	Neutral
Density (g/cm^3)	0.84	0.88	0.86	0.86	0.914 –0.925
Moisture content (%)	0.52	0.44	0.21	0.32	0.20
Smoke Point (ºC)	230 – 232	220 – 225	230 – 234	224 – 228	230 – 240

Key: RA=Refined vegetable oil A, **RB**=Refined vegetable oil B, CA = cold pressed vegetable oil A CB=cold pressed vegetable oil B

Table 2: Chemical parameters of cold pressed and refined edible vegetable oil sold at Katako market.

Samples of oil	Acid values mgKOH/g	Iodine values I_2/100g	Peroxide values meqO_2/kg	Saponification values mgKOH/g
RA	0.87±0.09	30.14±2.24	2.30±0.14	180±1.41
RB	0.81±0.20	5.71±0.89	1.40±028	189±1.41
CA	0.91±0.30	1.59±0.45	3.15±0.21	190±2.83
CB	1.03±0.13	7.74±6.88	4.30±0.28	194±1.41
WHO/FAO (CODEX) Standard	a (0.6mg/0.4mg)	b (124 – 139/77 – 107)	10	c (189 – 195/ 187 – 196)

Key: RA=Refined vegetable oil A, **RB**=Refined vegetable oil B, CA = cold pressed vegetable oil A CB=cold pressed vegetable oil B

Table 3: Concentration level of Heavy metals in cold pressed and refined edible vegetable oil sold at Katako market.

Sample	Elements (mg/kg)			
	Cd	Pb	As	Cr
RA	0.19±0.00	0.29±0.00	1.10±0.00	BDL
RB	0.19±0.00	0.29±0.01	BDL	BDL
CA	0.57±0.01	0.29±0.01	1.85±0.00	BDL
CB	0.38±0.00	0.29±0.01	3.34±0.00	BDL
WHO/FAO (CODEX) Standard	0.05	0.10	0.10	0.003

Key:
RA = Refined vegetable oil A, **RB =** Refined vegetable oil B, **CA =** Cold pressed vegetable oil A, **CB =** Cold pressed vegetable oil B, **BDL=** Below detectable limit

3.2 Discussion

The physical properties of cold pressed and refined edible oil such as colour, odour, density, moisture content and smoke point are shown in Table 1. Sample RB had the highest density while RA had the lowest. Sample RA contains the highest moisture content and CA had the lowest. Sample CA had the highest range of smoke point temperature while RB had the lowest. Densities of vegetable oil varies with type and temperature. The densities of samples RA, RB were in the range of 0.84- 0.86 which agrees with the works of [6]. All samples were within the acceptable range of 0.914–0.925 g/cm^3 recommended by by WHO/CODEX.

When moisture content ranges from 0.05 to 0.30 in edible oils, it shows that rancidity likely to occur. The maximum allowed moisture content in edible oils is 0.20%[11]. Lower moisture content indicates a longer shelf life of edible vegetable oil. The moisture content for samples RA, RB, CA, and CB are 0.52%, 0.44%, 0.21%, and 0.32%, respectively. All samples are within an acceptable range, except sample RA (refined soya oil).

Smoke Point is the temperature at which fat begins to breakdown and oxidize according to [12]. For optimal taste and to maintain their nutritional value, oil should not be used above its smoke point in frying. The oil with high smoke points is best for cooking, sample CA (cold pressed G/nut oil) had the highest smoke point while sample RB had the lowest smoke point in this research. These are comparable to the results obtained by[12]. All samples are within the standard range according to WHO/CODEX.

Acid value is use as a quality control parameter for oils and fats. Higher acid value and free fatty acid content is an indication of a low-quality oil. Sample CA had the lowest acid value while RA had the highest which are comparable to results obtained by [13]. The WHO/FAO (CODEX) standard is 0.6. All samples studied were within the respective standards set by WHO/CODEX as seen in Table 2.

The Iodine value measures the degree of unsaturation of a particular vegetable oil. It measures the amount of iodine absorbed by 100 parts of weight of the sample. Studies have shown that oils with a high degree of unsaturation, the higher will be the iodine value, likewise the greater the possibility of the vegetable oil to become rancid or to get oxidize [14]. Oils with high iodine value have more of the

unsaturated fatty acids that are prone to degradation reactions such as auto oxidation or polymerization. Standards value for soya oil are (124–139) and groundnut oil (77–107) as provided by WHO/FAO. Only sample RA is within the range for soya oil, while all others are below the recommended values.
Peroxide value is the common indicator of oxidation and rancidity of lipids. Peroxides are formed from the oxidation of triglycerides in the oil with high moisture content. Oil samples having peroxide values less than 10meq/kg is safe for human consumption, but oil samples having peroxide value less than 4meq/kg are considered to be fresh and healthy[12]. The WHO/FAO (CODEX) standard is 10 meqO_2/kg. All samples meet the standard.
Saponification value is the amount of KOH required to saponify one gram of fat. Higher saponification value indicates lower fatty acids average length and this will mean lighter molecular weight of the triglycerides in oils and vice versa. The standards for soya oil (189–195) and groundnut oil (187–196) are provided by WHO/FAO. All samples meet the respective standards.
Heavy metals cannot be degraded or destroyed. As trace elements, some heavy metals like copper, selenium, zinc are essential for the metabolism of the human body. However, at higher concentrations they can lead to poisoning. Sample RB had the least concentration of heavy metals over sample CB. Heavy metals tend to bioaccumulation, causing an increase in their concentration in a biological organism over time. This is in comparison to the substance concentration in the environment. High exposure of heavy metals can cause obstruction in the functions of the lungs, which can lead to lung cancer, cause skin irritation and ulceration. While long-term exposure can lead to kidney and liver damage, circulatory and nerve tissue damage, degenerative, inflammatory and neoplastic damage to the skin, respiratory system, blood, lymphatic system, nervous system as well as the reproductive systems. Heavy metals can accumulate in aquatic animals, which can add to the danger of eating fish. All samples had value within the standard set by WHO/CODEX, with all below the limit like in lead, cadmium while arsenic, chromium was below detectable limit of the instrument as seen in Table 3.

4. CONCLUSION

The quality of edible refined and cold pressed vegetable oil sold at Katako market in terms of physicochemical parameters indicate a consistent trend in density, smoke point, iodine values, peroxides and saponification values with the FAO/WHO standards. The refined soya is likely to go rancid within a short period of storage because it has the highest moisture content. The cold pressed groundnut oil is the best for frying because it has the highest smoke point value, lowest acid and free fatty acid content depicting a high-quality oil. All samples are considered fresh and healthy based on their peroxide values. Both oil samples can be saponified. From the results obtained in this study, it can be concluded that the cold pressed vegetable oil had parameters are statistically significant to the FAO/WHO values compared to the refined vegetable oil. Cold pressed oil is better in quality compared to refined vegetable oil. The consumption of cold pressed vegetable oil recommended in preference to that of refined vegetable oils.

CONFLICT OF INTERESTS

The authors declare no conflict of interests.

REFERENCES

(1). Yang, R.; Zhang, L.; Li, P.; Yu, L.; Mao, J.; Wang, X.; Zhang, Q. A review of chemical composition and nutritional properties of minor vegetable oils in China. *Trends in Food Science & Technology,* 2018, *74,* 26–32.

(2). Gharby, S.; Asbbane, A.; Nid Ahmed, M.; Gagour, J.; Hallouch, O.; Oubannin, S.; Bijla, L.; Goh, K. W.; Bouyahya, A.; Ibourki, M. Vegetable oil oxidation: Mechanisms, impacts on quality, and approaches to enhance shelf life. *Food Chemistry:* 2025*, 10*(28), 102541.

(3) . Geng, L.; Zhou, W.; Qu, X.; Sa, R.; Liang, J.; Wang, X.; Sun, M. Iodine values, peroxide values and acid values of Bohai algae oil compared with other oils during the cooking. *Heliyon*, 2023, *9*(4), e15088.

(4) .Gorica, P.; Vezirka, J.; Vesna, A. K.; Elena, S. Differences in chemical parameters of cold pressed and refined cooking oil. *Macedonian Journal of Animal Science,* 2016, *6*(1), 47–50.

(5) . Cravotto, C.; Claux, O.; Bartier, M.; Fabiano-Tixier, S.; Tabasso, S. Leading edge technologies and perspectives in industrial oilseed extraction. *Molecules,* 2023, *28*(16), 5973.

(6). Iloamaeke, I. M.; Unoka, E. C.; Ikezuagu, B. C.; Simon, C. J. Quality assessment of selected brands of vegetable oil sold at Relief Market Onitsha, Anambra State of Nigeria. *International Journal of Research and Innovation in Applied Science,* 2024, *9*(5), 317–327.

(7). Ait, A. S,; Ait, E. D.; Aksoylu, Ö. Z.; Günç E. P.; Khettal, B. Acute and 28-day repeated dose toxicity evaluations of cold pressed Pinus halepensis Mill. seed oil in mice and rats. Regul Toxicol Pharmacol. 2022 Jul;132:105191. doi: 10.1016/j.yrtph.2022.105191. Epub 2022 May 22. PMID: 35613671.

(8). Association of Analytical Chemists International. *Official methods of analysis of AOAC International* (22nd ed.), 2023, AOAC International.

(9).Pearson, D. (1981) The Chemical Analysis of Food. Churchill Livingstone, Edinburgh, 504-530.

(10).Gebeyehu, H. R.; Gebreyes, B. G. Physico-chemical and fatty acid composition determination of canola varieties cultivated in Ethiopian agro-ecology. *International Journal of Novel Research in Life Sciences,*2019, *6*(6), 41–51. http://www.noveltyjournals.com

(11). Negash, Y. A.; Amare, D. E.; Bitew, B. D.; & Dagne, H. Assessment of quality of edible vegetable oils accessed in Gondar City, Northwest Ethiopia. *BMC Research Notes*, 2019, *12*, 793.

(12). Pardeshi, S. Assessment on the quality of some edible cooking oils sold in local market using AV, PV, smoke point, flash point and fire point. *Food Analyst*, DPHL, 2020, 7(10). 1 - 7.

(13).Ichu, C.; Nwakanma, H. Comparative Study of the Physicochemical Characterization and Quality of Edible Vegetable Oils. *International Journal of Research in Informative Science Application & Techniques (IJRISAT)*, 2019, 3(2), 1-9.

(14).Ronald, S. K., & Ronald, S. P. (1991). *Composition and analysis of foods* (9th ed., pp. 507–544). Longman.

ISBN: 978-978-68-0485-9 DOI: https://doi.org/10.55455/acsnigeria.1.2.55-58

Walnut Shell: An Effective Treatment for Cassava Wastewater

Oluwayemi Olanike Onawumi[1,2]*, Olubunmi Abiola Adewusi,[3] Temitope Chris Alagbada[1], Praise Mojisola Olaniyi[1], Kaothar Adeola Ibrahim[1], Aisha Adebimpe Bakare[1] and Ayomide Deborah Ogundare[1]

[1]Department of Pure and Applied Chemistry, Ladoke Akintola University of Technology, P.M.B. 4000, Ogbomoso, Oyo State, Nigeria

[2]Department of Chemistry, University of Ilorin, Ilorin, Kwara State.

Department of Chemistry, Lagos State University, Ojo, Lagos State

Corresponding Author's Email: ooeonawumi@lautech.edu.ng

ABSTRACT

Cassava wastewater, a byproduct of cassava processing, poses significant environmental challenges due to its high levels of organic compounds, cyanogenic glycosides, and other pollutants. This study focuses on investigating the feasibility of using walnut shell-based activated carbon as an eco-friendly and cost-effective adsorbent for removing contaminants from cassava effluents.Walnut shells were processed into activated carbon through activation and carbonization using orthophosphoric acid as the activating agent. The prepared activated carbon was then used in a column setup where the cassava wastewater was passed through the column to allow for the adsorption of contaminants. Heavy metals, COD, sulphates, nitrates, and pH analysis were carried out before and after treatment to assess the adsorbent's effectiveness. The results showed that the concentration of Cyanide reduced from 3.91 ± 0.10 mg/L to 1.91 ± 0.15 mg/L. Chromium reduced from 0.07 ± 0.01 mg/L to 0.03 ± 0.01 mg/L, Lead reduced from 11.25 ± 0.31 mg/L to 0.97 ± 0.06 mg/L, while cadmium and manganese were completely removed from the effluent. A slight change was observed in the COD level. Sulphate levels decreased from 677.00 ± 4.00 mg/L to 178.48 ± 0.54 mg/L, while nitrate concentrations dropped from 54.40 ± 0.40 mg/L to 21.27 ± 0.78 mg/L. The findings in this study affirmed that walnut shell-based activated carbon is an effective adsorbent for the treatment of cassava wastewater.

KEYWORDS: Contaminants, Adsorption, Pollutants, Effluent, Cassava.

1. INTRODUCTION

Cassava (Manihot esculenta) is one of the most important crops in many tropical and subtropical regions, with its processing being a significant source of economic activity.Although cassava plays a significant role in both the food and industrial sectors, its processing into starch involves procedures that generate substantial amounts of waste. The primary by-product of this process is cassava-washing water, also known as manipueira.[1]However, this effluent contains high levels of organic pollutants, suspended solids, and cyanogenic compounds, all of which are harmful to the environment. Research indicates that cassava factory effluent contains high biochemical oxygen demand (BOD) and chemical oxygen demand (COD), leading to oxygen depletion in water bodies.[2]If not properly managed, the discharge of this effluent into the environment can lead to severe pollution issues. This is primarily due to its high organic content and the presence of cyanide, a toxic substance harmful to most aerobic organisms, produced through the hydrolysis of cyanogenic glycosides naturally found in cassava tubers.[3]This effluent can cause environmental pollution, water contamination, and aquatic ecosystem disruption among others.

Chemical treatments, such as coagulation and precipitation, may help remove some contaminants but require costly chemicals and infrastructure that may be unavailable or unaffordable in rural areas where cassava processing is most common. Biological treatments, while capable of degrading organic matter, are not always effective at breaking down cyanogenic compounds, leaving hazardous toxins in the water. Furthermore, physical treatments, such as filtration and sedimentation, do not fully address the removal of dissolved organic and toxic compounds, thus limiting their overall effectiveness.[4]

There is a growing need for sustainable and environmentally friendly alternatives that make use of natural waste products. Among the various techniques employed for the removal of chemical contaminants from the environment such as electrochemical reactions, membrane separation, anaerobic and aerobic biodegradation, and advanced oxidation processes, adsorption stands out as one of the most widely adopted methods. Its widespread application can be attributed to several advantages, including low energy requirements, environmental friendliness, high adsorption capacity, favorable surface morphology, and reusability.[5-6]Walnut shells, a byproduct of walnut processing, have attracted attention due to their high lignocellulosic content and excellent adsorption properties. They

are widely available, low-cost, and offer a greener solution for wastewater treatment,[7] which is an indication of a good precursor for the adsorptive treatment of cassava wastewater.
The purpose of this study is to explore the potential of walnut shells as a natural adsorbent for the treatment and purification of wastewater originating from cassava processing plants, with the objective of minimizing the concentration of organic pollutants and cyanogenic compounds in the resulting effluent.

2. MATERIALS AND METHODS

2.1 Chemicals used and sample collection.

The chemicals employed for this study includes: Dilute Hydrochloric (HCl) acid, Orthophosphoric acid. The chemicals are analytical grade. Walnut shell were collected from Sabo market, Ogbomoso, Oyo state, Nigeria. The cassava wastewater was collected at Aranda, Ogbomoso.

2.2 Pre-treatment and chemical activation of walnut shell-based activated carbon

Walnut shells were washed with distilled water, air-dried, ground, and sieved before being stored for adsorption studies. For activation, 300 g of sieved shell was mixed with 0.3 M orthophosphoric acid and heated with continuous stirring until fully absorbed. The mixture was cooled, then carbonized at 200 °C for 6 hours. The carbonized product was washed to neutrality with distilled water and oven-dried at 105 °C. The resulting activated carbon was stored in an air-tight container for further use.

2.3 Analysis of Raw Cassava Effluent

Physicochemical parameters determination

The biological oxygen demand determination of the Cassava wastewater in mg/L was carried out using standard methods described in the guide manualAPHA[8]. The dissolved oxygen content was determined before and after incubation. Sample incubation was for 5 days at 20ºC in a BOD bottle, and physicochemical determination of the Cassava wastewater was calculated after the incubation period. The chemical oxygen demand was carried out using a Liebig condenser with a 300 mm jacket.

Elemental analysis

The mineral content of the water samples was determined using wet digestion methods as described by Aremu *et al*.[9] The process involved accurately measuring a specific amount of the sample and subjecting it to wet digestion to break down the organic matrix and release the minerals into a solution. Approximately 100 mL of the water sample was measured and placed into a clean, dry digestion flask. To the digestion flask, 10 mL of concentrated nitric acid (HNO_3) was added. This acid is a strong oxidizing agent that facilitates the breakdown of organic matter. The flasks were then placed on a hot plate or in a digestion block, and the temperature was gradually increased to approximately 150 °C. The samples were heated until the solution became clear, indicating complete digestion. After digestion, the samples were allowed to cool to room temperature. The clear digest was then diluted to 50 mL with deionized water. The concentrations of Lead, cadmium, mercury chromium and magnesium in the digested samples were determined using a flame photometer (Model 405, Corning UK).Sulphate test was performed gravimetrically and compared with spectrophotometer analysis. Nitrate and cyanide tests were performed volumetrically, and spectrophotometric analysis was done.[10]

2.4 Experimental Procedure

Cassava wastewater was treated using a column process setup of beds filled with walnut shell-derived activated carbon, chosen for its simplicity, efficiency, and capacity for large volumes. Wastewater was pumped through the column at a controlled flow rate, enabling effective contact and adsorption of organic pollutants, heavy metals, and cyanogenic compounds. Contact time was optimized to maximize adsorption. Samples were collected periodically to monitor pollutant concentrations and analyze changes in physicochemical properties, including COD, BOD, hydrogen cyanide, and heavy metals. Treatment efficiency was assessed based on the percentage removal of these contaminants, demonstrating the effectiveness of walnut shell-based activated carbon.

3. RESULTS AND DISCUSSION

The pH of a water sample is a crucial parameter that affects its overall chemical balance and influences the behavior of various pollutants and treatment efficacy.[11]For the raw water sample (RWS), the pH was 4.50±0.50, which is acidic as shown in Table 1. After treatment with walnut shell, the pH slightly reduced to 4.10±0.24. Although this change is minimal, it suggests that walnut shells do not significantly alter the pH. In general, pH can be affected by adsorbents, particularly those that release acidic or basic components.[12] However, walnut shells, being a natural organic adsorbent, are primarily neutral in their

impact on pH levels. Literature shows that organic adsorbents, like walnut shells, have little to no significant effect on the pH, as they lack strong acidic or basic groups that could drastically change the solution's hydrogen ion concentration.[7]

Table 1: Result of physicochemical parameters and metal ion analysis on the samples

Parameters and Metal ions present	RWS	TWS	Standard (WHO) (mg/L)	EU Standard (mg/L)
pH	4.50±0.50	4.10±0.24	-	-
COD (mg/L)	212.80±0.27	162.45±0.50	< 10	-
Cadmium (mg/L)	0.03±0.01	-	0.003	0.005
Chromium (mg/L)	0.07±0.01	0.03±0.01	0.05	0.05
Manganese(mg/L)	0.04±0.01	-	0.5	0.05
Lead (mg/L)	11.25±0.31	0.97±0.06	0.01	0.01
Sulphate (mg/L)	677.00±4.00	178.48±0.54	500	250
Nitrate (mg/L)	54.40±0.40	21.27±0.78	50	50
Cyanide (mg/L)	3.91±0.10	1.91±0.15	0.07	0.05

The COD is an indicator of the organic pollutant load in wastewater. It decreased from 212.80±0.27 mg/L in the raw wastewater sample (RWS) to 162.45±0.50mg/L in the treated wastewater sample (TWS) as presented in Table 1. This reduction demonstrates the adsorbent's ability to remove organic contaminants. However, the COD value remained well above the World Health Organization (WHO) permissible limit of <10 mg/L for drinking water.[13] This suggests that while walnut shell activated carbon reduces the organic load, additional treatment steps are necessary to meet stringent standards.

Heavy metal concentrations,particularly cadmium, chromium, manganese, lead, and cyanide, exceed permissible limits in several cases. Cyanide, a highly toxic compound linked to industrial waste, was present in the raw effluent at a concentration of 3.91 ± 0.10 mg/L, which is significantly above safe levels. Treatment with walnut shell reduced this concentration by nearly 50% to 1.91 ± 0.15 mg/L. Cadmium (0.03 ± 0.01 mg/L) was completely removed after treatment, addressing concerns over its bioaccumulative and long-term health effects.[14] Lead levels decreased from 0.05 ± 0.01 mg/L to 0.01 ± 0.01 mg/L, highlighting walnut shell's strong potential for lead removal. Chromium was reduced from 0.07 ± 0.01 mg/L to 0.03 ± 0.01 mg/L, indicating partial adsorption, likely dependent on the chromium species present. Manganese, initially at 0.04 ± 0.01 mg/L, was fully eliminated, improving water quality. Sulphate concentration dropped from 677.00 ± 4.00 mg/L to 178.48 ± 0.54 mg/L, and nitrate levels decreased from 54.40 ± 0.40 mg/L to 21.27 ± 0.78 mg/L—a 60% reduction—demonstrating walnut shell's efficacy in mitigating various inorganic pollutants.

4. CONCLUSION

This study investigated the effectiveness of walnut shell-based activated carbon in the treatment of cassava wastewater. The results demonstrate that walnut shell-activated carbon is capable of reducing the levels of several key pollutants, including sulphate,nitrate and cyanide. The walnut shell effectively reduced heavy metals to safer levels. Cadmium and manganese were completely removed from the water, chromium was reduced from 0.07 ± 0.01 mg/L to 0.03 ± 0.01 mg/L, and lead decreased from 11.25 ± 0.31 mg/L to 0.97 ± 0.06 mg/L. These results indicate a strong adsorption affinity of walnut shells for heavy metals, making it suitable for applications where metal contamination is a concern.

CONFLICT OF INTERESTS

The authors declare no conflict of interests.

REFERENCES

(1) dos Santos, J. D.; Veit, M. T.; Juchen, P. T.; da Cunha Gonçalves, G.; Palacio, S. M.; Fagundes-Klen, M. Use of different coagulants for cassava processing wastewater treatment. *Journal of Environmental Chemical Engineering*, **2018,** *6* (2), 1821-1827.

(2) Oghenejoboh, K. M. Effects of cassava wastewater on the quality of receiving water body intended for fish farming. *British Journal of Applied Science and Technology*, **2015,** *6* (2), 164-171.

(3) Olaniyan, S. A.; Hussein, J. B.; Oke, M. O.; Akinwande, B. A.; Workneh, T. S.; Ayodele, M.; Adeyemi, I. A. Assessment of the physicochemical characteristics of by-products of cassava processing and their effects on biodiversity. *Environmental Monitoring and Assessment*, **2025,** *197* (5), 1-19.
(4) Danish, M.; Ahmad, M. "Use of agricultural waste for wastewater treatment: A review," *Environmental Science and Pollution Research*, **2018,** *25* (36), 35925-35935.
(5) Saleh, I. A.; Zouari, N.; Al-Ghouti, M. A. Removal of pesticides from water and wastewater: Chemical, physical and biological treatment approaches. *Environmental Technology & Innovation*, **2020,** *19*, https://doi.org/10.1016/j.eti.2020.101026.
(6) Bello, O. S.; Alagbada, T. C.; Alao, O. C.; Olatunde, A. M. Sequestering a non-steroidal anti-inflammatory drug using modified orange peels. *Applied Water Science*, **2020,** *10* (7), 1-11.
(7) Albatrni, H.; Qiblawey, H.; Al-Marri, M. J. Walnut shell-based adsorbents: A review study on preparation, mechanism, and application. *Journal of Water Process Engineering*, **2022,** 45, https://doi.org/10.1016/j.jwpe.2021.102527
(8) American Public Health Association. *Standard Methods for the Examination of Water and Wastewater*, 19th ed.; American Public Health Association: New York, 1995; 1193 pp.
(9) Aremu, M. O.; Oko, O. J.; Andrew, C. Ground water and river quality assessment for some heavy metals and physicochemical parameters in Wukari town, Taraba State, Nigeria. *International Journal of Sciences*, **2017,** *6* (5), 73-80.
(10) Mousavi, S. R.; Balali-Mood, M.; Riahi-Zanjani, B.; Sadeghi, M. Determination of cyanide and nitrate concentrations in drinking, irrigation, and wastewaters. *Journal of Research in Medical Sciences: The Official Journal of Isfahan University of Medical Sciences*, **2013,** *18* (1), 65-68.
(11) Saravanan, A.; Kumar, P. S.; Jeevanantham, S.; Karishma, S.; Tajsabreen, B.; Yaashikaa, P. R.; Reshma, B. Effective water/wastewater treatment methodologies for toxic pollutants removal: Processes and applications towards sustainable development. *Chemosphere*, **2021,** *280*, doi.org/10.1016/j.chemosphere.2021.130595.
(12) Islam, M. A.; Morton, D. W.; Johnson, B. B.; Angove, M. J. Adsorption of humic and fulvic acids onto a range of adsorbents in aqueous systems, and their effect on the adsorption of other species: A review. *Separation and Purification Technology*, **2020,** *247*, https://doi.org/10.1016/j.seppur.2020.116949.
(13) World Health Organization. *Progress on Drinking Water, Sanitation and Hygiene: 2017 Update and SDG Baselines*; World Health Organization: Geneva, 2017; pp 1–116.
(14) Genchi, G.; Sinicropi, M. S.; Lauria, G.; Carocci, A.; Catalano, A. The effects of cadmium toxicity. *International journal of environmental research and public health*, **2020,** *17* (11), 3782. https://doi.org/10.3390/ijerph17113782

ISBN: 978-978-68-0485-9
http://acsnigeria.org/publications/proceedings

Structure-Based Drug Discovery of Soursop (*Annona muricata*) Bioactive Compounds: Anticancer Efficacy through Quantum Chemical Calculations, Molecular Docking, and ADMET Studies with 7SA9 and 4ZFI Proteins

Humphrey Sam Samuel[1, 2, 5*], Joseph Dennis [2], Deborah Alahira[3], Bulus Bako[1, 2], Augustine Michael Abakpa[2], Emmanuel Edet Etim[1, 2] and John Paul Shinggu[1, 2 4]

[1]Computational Astrochemistry and Bio-Simulation Research Group, Federal University Wukari, Wukari, Taraba State, Nigeria.

[2]Department of Chemical Sciences, Federal University Wukari, Wukari, Taraba State, Nigeria.

[3]Department of Food Science and Technology, Federal University Wukari, Wukari, Taraba State, Nigeria.

[4]Department of Chemistry and Biochemistry, University of South Carolina, Columbia, SC, 29208 United States

[5]Department of Chemistry, Emory University, Atlanta, Georgia, 30322 United States

Corresponding Author's Email: humphreysedeke@gmail.com

ABSTRACT

The ongoing quest for less harmful and more effective anticancer drugs has prompted scientists to look at natural substances made from plants. The bioactive substances Annonacin, Quercetin, Coreximine, and Kaempferol from Soursop (*Annona muricata*) and their possible anticancer effects are the main subjects of this investigation. To anticipate the interactions and binding affinities of these compounds with cancer-related proteins, Human MUC16 SEA5 Domain (7SA9) and Mouse Double Minute 2 (4ZFI), we used molecular docking experiments in conjunction with a structure-based drug discovery strategy. Furthermore, ADMET (Absorption, Distribution, Metabolism, Excretion, and Toxicity) and density functional theory (DFT) calculations were carried out. According to the ADMET results, annonacin poses toxicity hazards while coreximine is the safest. Although they need to be optimized for solubility and toxicity reduction, quercetin and kaempferol exhibit intermediate potential. Quercetin has the greatest binding interactions (hydrogen bonds, π-stacking, and electrostatic contacts) according to the DFT findings. In contrast, Annonacin and Kaempferol have weaker, less specific interactions, while Coreximine has a high affinity but hydrophobic-driven binding to 4ZFI. According to the research, *Annona muricata* has bioactive chemicals that could be used to create novel cancer medications.

KEYWORDS: Molecular-Docking; Anti-cancer; Soursop; Pharmacokinetics; Natural Compounds

1. INTRODUCTION

Cancer continues to be a major cause of death worldwide, indicating the urgent need for less harmful and more effective treatment options. [1, 2] The potential of natural plant-based chemicals in cancer treatment has drawn a lot of attention because of their varied bioactive qualities and comparatively reduced toxicity when compared to manufactured medications.[3] Although soursop is well-known for its antidiabetic, analgesic, and anti-inflammatory activities, it has recently drawn attention from scientists due to possible anticancer effects.[4, 5] According to preclinical research, gallic, chlorogenic, 4-hydroxybenzoic, protocatechuic, syringic and ellagic acids, epicatechin, lutein, tocotrienol, tocopherols, annonacin, kaempferol, coreximine, and quercetin are among the bioactive components found in soursop but annonacin, kaempferol, coreximine, and quercetin that have demonstrated the most promise.[6] The biological significance of the 7SA9 and 4ZFI proteins to cancer pathways and their potential as therapeutic targets for drug development led to their selection as the study's main targets.[7] The majority of prior research on soursop has been on its many therapeutic uses, with multiple studies examining its antidiabetic, analgesic, and anti-inflammatory qualities.[8] However, most studies have focused on in vitro and in vivo experiments without a detailed computational investigation of the molecular interactions between bioactive compounds and target proteins.[9] The novelty lies on employing quantum chemical calculations to analyse the electronic properties of these compounds, molecular docking to predict their binding affinities with 7SA9 and 4ZFI proteins, and ADMET studies to evaluate their drug-likeness and pharmacokinetic properties.

2. COMPUTATIONAL DETAILS

2.0 Computational Details

2.1 Molecular Docking Simulation

To examine the interactions between bioactive chemicals from Soursop and the 7SA9 and 4ZFI proteins, this study used the AutoDock tool to perform molecular docking simulations. The required PDB and PDBQT formats of the four bioactive chemicals and proteins were created using Auto dock Tools.[10] Biovia Discovery Studio 2021 was used to visualize the docking results, enabling a thorough examination of the interactions and binding affinities between the target proteins and the bioactive chemicals.

2.2 Quantum Chemical Studies and ADMET Studies

The B3LYP functional and the 6-311* (d, p) basis sets were selected for their balance of computing cost, efficiency, and accuracy in the widely used density functional theory (DFT). Gauss view 6.0, a molecular modelling program, was used to create the initial molecular structures using databases. The most stable conformations were then found by optimizing the geometry. The Gaussian 09 software package was used for all DFT calculations, and solvent effects were only taken into account when employing the Polarizable Continuum Model (PCM), when it was required to replicate physiological conditions.[11] Computational tools such as SwissADME (http://www.swissadme.ch/index.php) and pkCSM (https://biosig.lab.uq.edu.au/pkcsm/prediction) were utilized to predict drug-likeness and bioavailability of the compounds. [12, 13]

3. RESULTS AND DISCUSSION

3.1 Molecular Docking Interactions

3.1.1 Annonacin

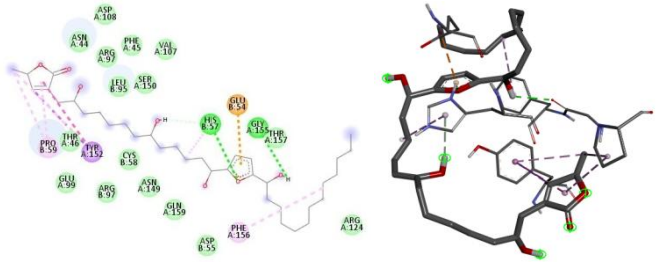

Figure 1: Protein-Ligand Interactions between Annonacin and 7SA9

The varying bond lengths underscore the flexibility and adaptability of these hydrophobic interactions, shaping the overall Bond Types as shown in **Figure 1.**

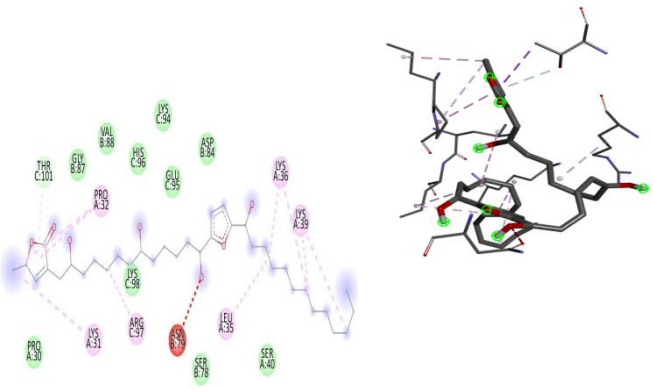

Figure 2: Protein-Ligand Interactions between Annonacin and 4ZFI

The different bond lengths highlight the hydrophobic interaction's plasticity and flexibility, forming the overall Bond Types as seen in **Figure 2.**

3.1.2 Quercetin

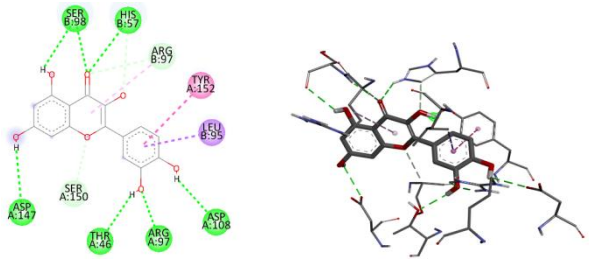

Figure 3: Protein-Ligand Interactions between Quercetin and 7SA9 protein

Conventional hydrogen bond as shown in **Figure 3** is observed with ARG97, ARG97, HIS57, SER98, THR46, ASP108, SER98, and ASP147 featuring a precise and directional interaction characterized by a bond length of 3.07406 Å, 1.99628 Å, 2.80662 Å, 2.38993 Å, 2.33035 Å, 2.82918 Å, 2.67892 Å, and 2.96446 Å, respectively

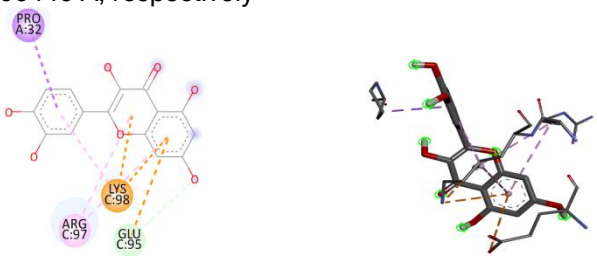

Figure 4: Protein-Ligand Interactions between Quercetin and 4ZFI protein

3.1.3 Kaempferol

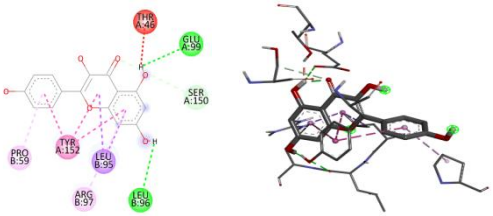

Figure 5: Protein-Ligand Interactions between Kaempferol and 7SA9 protein

As shown in **Figure 5,** distinctive conventional hydrogen bond is observed with GLU99, GLU99, and LEU96, featuring a precise and directional interaction characterized by a bond length of 2.69720 Å, 1.80097 Å, and 2.98426 Å, respectively.

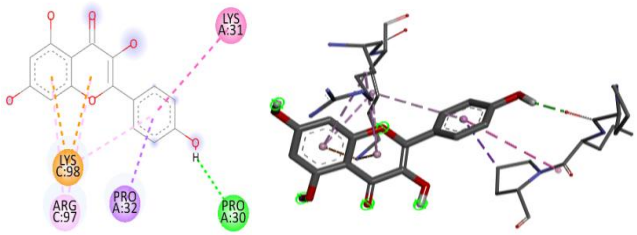

Figure 6: Protein-Ligand Interactions between Kaempferol and 4ZFI protein

Π-sigma interactions with PRO32 with bond lengths of 3.49863 Å, respectively, emphasize the involvement of aromatic systems in stabilizing the binding complex, providing additional anchoring points that reinforce the structural integrity of the binding site, as shown in **Figure 6.**

3.1.4 Coreximine

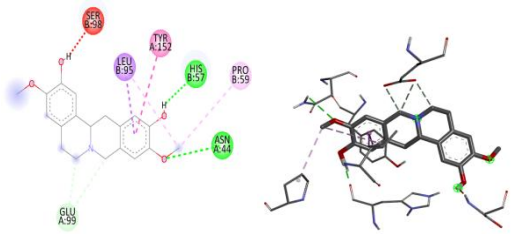

Figure 7: Protein-Ligand Interactions between Coreximine and 7SA9 protein

The π-π stacked interaction indicates a parallel arrangement of aromatic rings between TYR152 with a bond length of 4.55928 Å, and the bond length shows a relatively weak interaction as shown in **Figure 7.**

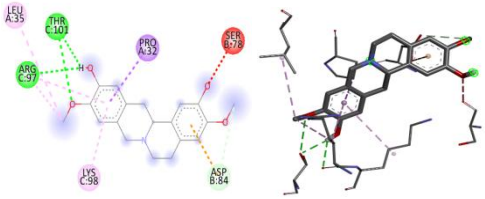

Figure 8: Protein-Ligand Interactions between Coreximine and 4ZFI protein
The hierarchy of binding strength—quercetin > kaempferol > annonacin > coreximine highlights quercetin's superior potential, though kaempferol's balanced profile warrants further exploration.

Table 1: Molecular Docking Results of Bioactive Compounds

Parameter	Annonacin	Quercetin	Kaempferol	Coreximine
Binding Affinity (kcal/mol)				
7SA9	-7.40	-6.50	-5.30	-8.80
4ZFI	-5.20	-4.90	-4.10	-9.60
Key Hydrogen Bonds				
7SA9	HIS57 (2.56 Å)	ARG97 (1.99 Å)	GLU99 (1.80 Å)	ASN44 (2.94 Å)
4ZFI	THR101 (3.88 Å)	LYS98 (3.85 Å)	PRO30 (2.04 Å)	THR101 (2.27 Å)
Key Hydrophobic Interactions				
7SA9	π-Alkyl (TYR152)	π-π Stacked (TYR152)	π-Sigma (LEU95)	π-π Stacked (TYR152)
4ZFI	Alkyl (LEU35)	π-Alkyl (ARG97)	π-Alkyl (ARG97)	π -Alkyl (ARG97)
Electrostatic Interactions				
7SA9	π-Anion (GLU54)	π-Cation (LYS98)	–	–
4ZFI	–	π-Anion (GLU95)	π-Cation (LYS98)	π -Anion (ASP84)

When comparing the tested drugs' binding affinities to two cancer-related protein targets (7SA9 and 4ZFI), the docking results show notable differences. Coreximine was the most promising choice for additional research since it showed the greatest binding to both proteins (-8.80 kcal/mol with 7SA9 and -9.60 kcal/mol with 4ZFI). While annonacin showed a moderate but constant affinity for both targets (-5.20 to -7.40 kcal/mol), quercetin demonstrated selective effectiveness against 7SA9 (-6.50 kcal/mol) but lesser binding to 4ZFI (-4.90 kcal/mol). Between -4.10 and -5.30 kcal/mol, kaempferol showed the weakest interactions of all the substances studied.

3.2 Results of Quantum Chemical Calculations

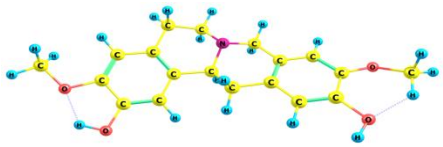

Figure 9: Optimized Geometry of Coreximine

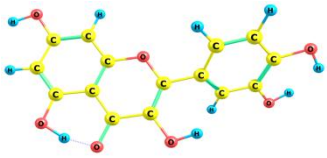

Figure 10: Optimized Geometry of Quercetin

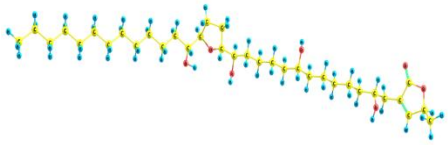

Figure 11: Optimized Geometry of Annonacin

Figure 12: Optimized Geometry of Kaempferol

Table 2: Quantum chemical parameters for Coreximine, Annonacin, Kaempferol, and Quercetin

Parameter	Coreximine	Quercetin	Annonacin	Kaempferol
Zero Point Energy (kcal/mol)	248.127	148.287	715.387	141.350
Polarizability (A.U)	150.561	150.294	211.242	216.534
Dipole Moment (Debye)	2.871	4.926	2.589	4.974
Enthalpy of Formation (Kcal/mol)	261.813	160.144	745.768	152.519
Free Energy (kcal/mol)	216.780	119.246	653.715	113.448
Entropy (kcal/mol)	0.151	0.137	0.309	0.131

T**able 2** shows some quantum chemical parameters for Coreximine, Quercetin, Annonacin, and Kaempferol, and the optimized structures can be seen in **Figure, 9, 10, 11, and 12,** respectively, offering insights into their stability, reactivity, and potential anticancer properties. A molecule's zero-point energy, or ZPE, is its lowest energy state. With the largest ZPE and hence higher reactivity, annonacin may be better able to disrupt the functions of cancer cells. Quercetin may be the least reactive, as seen by its lowest ZPE value, which is followed by intermediate values for coreximine and kaempferol. When targeting cancer cells, high reactivity can be useful, but stability must be balanced. Since annonacin has the highest ZPE (715.387 kcal/mol), it is more reactive due to its higher intrinsic energy.

Table 3: HOMO-LUMO Energies of Coreximine, Annonacin, Kaempferol and Quercetin

Molecule	HOMO Energy(ev)	LUMO Energy(ev)	Energy Difference ΔE (ev)
Coreximine	-3.0923	2.7726	5.8649
Annonacin	-8.1578	6.5297	14.6875
Kaempferol	-6.0434	-2.0420	4.0014
Quercetin	-3.0434	0.6134	3.6568

Quercetin and Kaempferol demonstrate particularly favourable electronic profiles for anticancer activity, as evidenced by their relatively small HOMO-LUMO gaps (3.6568 eV and 4.0014 eV, respectively). The exceptionally large HOMO-LUMO gap of Annonacin (14.6875 eV), as shown in **Table 3** suggests high kinetic stability but potentially limited reactivity.

3.3 ADMET Results

In addition, quercetin and kaempferol exhibit reduced toxicity risks and neither hepatotoxicity nor mutagenicity (AMES−), in comparison with annonacin, which causes drug-induced liver injury (DILI+++). They also improve their safety profiles due to their balanced CYP450 interactions, which show moderate inhibition without significant interference. Both chemicals have substantial potential for drug-induced liver damage, according to their toxicity profiles, and quercetin also exhibits AMES toxicity. The most promising candidate from an ADMET standpoint is coreximine, as shown by the comparison of these four molecules in Table 4.

Table 4: ADMET Profiles of Potential Anticancer Compounds

Parameter	Annonacin	Coreximine	Kaempferol	Quercetin
Molecular Weight (g/mol)	568.250 (High)	327.150 (Moderate)	286.050 (Low)	302.040 (Low)
logP	4.506 (High lipophilicity)	2.155 (Moderate)	2.656 (Moderate)	2.155 (Moderate)
Logs	-2.067 (Low solubility)	-3.624 (Very low)	-3.624 (Very low)	-3.671 (Very low)
TPSA (Å²)	120.360	62.160	111.130	131.360
Rotatable Bonds	14 (Flexible)	2 (Rigid)	1 (Very rigid)	1 (Very rigid)
Permeability (Caco-2/MDCK)	Poor	Poor (P-gp substrate)	Poor	Poor
Plasma Protein Binding (PPB)	>100% (Very high)	82.251% (Moderate)	97.861% (High)	95.496% (High)
BBB Penetration	--	+++ (High)	--	--
CYP Inhibition	CYP1A2, 2C9, 2D6, 3A4	None	CYP1A2, 2C9	CYP1A2, 2C9
Major Toxicity Concerns	Hepatotoxicity, Mutagenicity, Carcinogenicity	Skin sensitization (++)	DILI (+++), Skin sensitization (++)	DILI (+++), AMES toxicity (+), Skin sensitization (+++)
Drug-Likeness	Fails some rules	Compliant (QED = 0.888)	Compliant	Compliant (with alerts)

4. CONCLUSION

This study has demonstrated the strong anticancer potential of the bioactive compounds, including Annonacin, Quercetin, Coreximine, and Kaempferol, that are present in soursop (*Annona muricata*). When it came to creating many hydrogen bonds (e.g., with ARG97: 1.99 Å), π-stacking, and metal chelation, coreximine was the most effective binder to target proteins (7SA9 and 4ZFI). Kaempferol showed balanced interactions but a lower affinity than quercetin, whereas coreximine had the lowest binding, and annonacin depended on hydrophobic contacts. Additional *Annona muricata* ingredients should be screened for in future investigations, and cell-based and animal studies should be used to experimentally validate the anticipated action and development of optimized formulations to enhance bioavailability and target specificity.

CONFLICT OF INTERESTS

The authors declare no conflict of interests.

REFERENCES

(1) Weth, F. R.; Hoggarth, G. B.; Weth, A. F.; Paterson, E.; White, M. P.; Tan, S. T; & Gray, C. Unlocking hidden potential: advancements, approaches, and obstacles in repurposing drugs for cancer therapy. British J. Cancer. 2024, 130(5), 703-715.

(2) Boshuizen, J.; Peeper, D. S. Rational cancer treatment combinations: an urgent clinical need. Mol. cell, 2020, 78(6), 1002-1018.

(3) Dehelean, C. A.; Marcovici, I.; Soica, C.; Mioc, M.; Coricovac, D., Iurciuc, S.; & Pinzaru, I. Plant-derived anticancer compounds as new perspectives in drug discovery and alternative therapy. Mol. 2021, 26(4), 1109.

(4) Santos, I. L.; Rodrigues, A. M; Amante, E. R.; & Silva, L. H. Soursop (*Annona muricata*) properties and perspectives for integral valorization. Foods, 2023, 12(7), 1448.

(5) Abdul Wahab, S. M.; Jantan, I.; Haque, M. A.; Arshad, L. Exploring the leaves of *Annona muricata* L. as a source of potential anti-inflammatory and anticancer agents. Frontiers in pharm. 2018, 9, 344514.

(6) Ilango, S.; Sahoo, D. K.; Paital, B.; Kathirvel, K.; Gabriel, J. I.; Subramaniam, K.; Nirmaladevi, R. A review on *Annona muricata* and its anticancer activity. Cancers, 14(18), 4539.

(7) Bio Smart Notes. Biological significance of proteins. *Bio Smart Notes*. 2025, https://biosmartnotes.com/biological-significance-of-proteins/

(8) Coria-Téllez, A. V.; Montalvo-Gónzalez, E.; Yahia, E. M.; Obledo-Vázquez, E. N. *Annona muricata*: A comprehensive review on its traditional medicinal uses, phytochemicals, pharmacological activities, mechanisms of action and toxicity. Arabian J. chem, 2018, 11(5), 662-691.

(9) Lin, J.; Sahakian, D. C.; De Morais, S. M.; Xu, J. J.; Polzer, R. J.; Winter, S. M. The role of absorption, distribution, metabolism, excretion and toxicity in drug discovery. *Current topics in medicinal chemistry*, 2003, *3*(10), 1125-1154.

(10) Trott, O.; & Olson, A. J. AutoDock Vina: improving the speed and accuracy of docking with a new scoring function, efficient optimization, and multithreading. J. com. Chem. 2010, 31(2), 455-461.

(11) Wang, Y.; Cheng, X.; Yang, X.; & Yang, X. DFT study of solvent effects for some organic molecules using a polarizable continuum model. J. solution chem. 2006, 35, 869-878.

(12) Riviere, J. E. Absorption, distribution, metabolism, and elimination. Veterinary pharmacology and therapeutics, 2009, 9.

(13) Daina, A.; Michielin, O.; Zoete, V. SwissADME: a free web tool to evaluate pharmacokinetics, drug-likeness and medicinal chemistry friendliness of small molecules. Sci. reports, 2021, 7(1), 42717

ISBN: 978-978-68-0485-9 http://acsnigeria.org/publications/proceedings

Environmental Impact of Trace Metals and Total Petroleum Hydrocarbon (TPH) in the Okrika Stretch of Bonny River: A Seasonal Variation Study

[*1]Ugo Nweke-Maraizu, [2]Bulus Bako, [2,3]Humphrey Sam Samuel, and [2]Emmanuel Edet Etim

[1]Department of Chemistry, Rivers State University, Nkpolu-Oroworukwo, Port Harcourt, Nigeria
[2]Department of Chemical Sciences, Federal University Wukari, Nigeria
[3]Department of Chemistry, Emory University, Atlanta, Georgia, 30322 United States
Corresponding Author's email: nwekemaraizuugo@gmail.com

ABSTRACT

The accumulation of TPH and effect of metal contamination in aquatic environments has direct consequences to man and to the ecosystem which tends to bioaccumulate in the food chain. This study investigates the seasonal variations in trace metal and TPH levels in the Okrika section of the Bonny River's water and sediment, assessing their potential environmental impact. Water and sediment samples were collected during the dry and wet seasons and analyzed for trace metals and TPH using standard analytical techniques. The result shows the values recorded for zinc in water at all the sites, and the wastewater/effluent was found to be below the DPR/FMENV allowable limit of 1 mg/L. Significant seasonal fluctuation was observed ($p < 0.05$). Zinc levels in all monitoring sites, including the sediment effluent sample, were found to be far below the USEPA regulatory limit of 121 mg/kg. This implies that the creeks sediment is not contaminated by zinc at present. There was no significant seasonal variation ($p < 0.05$). Results revealed notable seasonal fluctuations, with higher concentrations of trace metals and TPH observed in various seasons likely due to reduced dilution and increased anthropogenic inputs. The findings highlight the need for continuous environmental monitoring, regulatory enforcement, and remediation efforts to mitigate pollution in the Bonny River.

KEYWORDS: Environment, pollution, Bonny River, Dry season, heavy metals.

1. INTRODUCTION

Urbanization and industrialization have had a detrimental impact on Bonny River over time. The toxicity, persistence, and bioaccumulation of heavy metals in sediments make them one of the most dangerous environmental contaminants.[1] In order to detect and manage metal pollution in estuaries, sediment analyses offer certain advantages over surface water. This is because the rate at which the concentration of metals in sediment changes is slower than that of water. The capacity of sediment to retain, absorb, and release a various range of pollutants, such as nutrients and heavy metals, over a long duration makes it a perfect archive. The Bonny River, which flows through the center of Nigeria's Niger Delta, is essential to the local inhabitants' economic and ecological well-being. As an aquatic ecosystem, the Okrika portion is the most significant and complex of its many components. This ecosystem's state is intimately related to the physical and the surface water's chemical properties.[2] The Bonny River's Okrika portion experiences separate rainy and dry seasons, each with its own set of natural characteristics. Water quality and, by consequently, the aquatic ecosystems health can be greatly impacted by these seasonal variations.[3] The study aims to evaluate the environmental impact of Total Petroleum Hydrocarbon (TPH) and trace metals in the Okrika Stretch of Bonny River.

2. MATERIALS AND METHODS

2.1 Study area and sample location

The research was carried out in Okrika Local Government Area, situated in Rivers State, Nigeria. Okrika, positioned within the Niger Delta region, is a wetland about 56km upstream from the Bight of Benin is the Bonny River. The sampling point include PREW, EKC, OKC, KOC and the control site, located in Ogoloma Creek, remains unaffected by Ekerekana creeks' activities, jetty, and oil bunkering.

2.2 Collecting Samples

2.2.1 Collecting of surface water samples

The samples were collected using pre-washed 1-liter plastic containers. 2mL of Nitric acid that had been concentrated was added to each surface water sample. During BOD sample collection, care was taken to avoid air entrapment, and bottles were wrapped in dark polyethylene bags, and to get rid of light, they were incubated for five days, preventing potential algae-induced DO production. The

tetraoxosulphate (VI) acid was used to acidify the COD samples and DO measurements were conducted in situ in the field.

2.2.2 Collection of sediment samples

At low tide, sediment samples were gathered with the aid of Eckmann grab sampler.[4] The samples were taken to the laboratory in pre-acid rinsed polyethene bags and stored by freezing. Sediment samples for total petroleum hydrocarbons were kept in a plain clear glass bottles previously washed to avoid contamination at 4°C in an ice pack and transported to the laboratory.

2.3 Determination of trace metal ions in water

For digestion, 100mL of each water sample were put into a conical flask. In a fume hood, 5 mL of HNO_3 was added to the sample. After gradually heating the samples, they were evaporated to the smallest volume (about 20 mL) on a hot plate. 5mL of strong nitric acid were added to the conical flasks after they had cooled. A light-colored, transparent solution indicated that digestion was complete, therefore heating was continued and strong nitric acid was added as needed. After that, the filtrate was brought up to mark in a 100 ml volumetric flask. A Buck Scientific model 200A Atomic Absorption Spectrometer (AAS) with an air acetylene flame was used to measure the absorbance of the sample extract solution in comparison to the reference solutions. The preconcentrated sample extracts were also used to determine the principal cations. A 250 mL standard flask was filled with a serially diluted mixed standard solution that contained 1 mg of the metal ion in 1 mL of the stock solution made by pipetting the proper amounts of commercially purchased stock solutions (BDH chemicals). A Buck Scientific model 200A Atomic Absorption Spectrometer (AAS) with an air-acetylene flame was used to measure the amounts of each metal ion in comparison to the standards solution. As previously mentioned, the concentrations of metals, including the main cations, in wastewater and effluent were measured.

2.4 Determination of trace metal ions in sediments

To analyze for trace metals, sediment samples were ground up, allowed to air dry at room temperature, and then sieved through a 0.5 mm sieve. A 100 mL conical flask was filled with one gram of the sieved sediment samples, which were weighed using a high precision weighing scale. For digestion, 1g of the weighted sediment sample was put into a 100mL conical flask. In a fume hood, 10mL of a 1:1 mixture of hydrogen peroxide and HNO_3 were applied to the sample. On a hot plate, it was cooked to 950C. 3mL of hydrogen peroxide and two more mL of water were added, covered, and heated until the effervescence stopped. After letting it cool, Whatman No. 1 filter paper was used to filter it into a 50 mL volumetric flask, and additional distilled water was added to make up the difference. A Buck Scientific model 200A Spectrophotometer fitted with an air-acetylene flame (AAS) was used to measure the amounts of heavy metals.

3. RESULTS AND DISCUSSION

The concentrations of selected trace metals in water samples collected from different locations within the Okrika region of the Bonny River during the dry season are presented in Table 1

Table 1: During the dry season, mean levels of trace metals (mg/l) in the Okrika region of the Bonny River

Metal	DPR	WHO	CSOC	PREW	EKC	OKC	KOC
Iron (mg/l)	1	0.3	1.659±0.257	2.170±0.052	1.620±0.164	1.226±0.079	2.232±0.083
Zinc (mg/l)	1	3.0	0.071±0.00	0.071±0.00	0.071±0.00	0.071±0.00	0.071±0.00
Nickel (mg/l)	0.015	0.02	0.395±0.031	0.071±0.002	0.056±0.0065	0.228±0.031	0.245±0.032
Lead (mg/l)	0.01	0.01	0.071±0.012	0.035±0.012	0.037±0.0055	0.023±0.003	0.072±0.003
Copper (mg/l)	0.01	0.5	0.044±0.009	0.025±0.006	0.026±0.00308	0.122±0.017	0.049±0.0033

Table 2: During the wet season, mean trace metal levels (mg/l) in water of the Okrika region of Bonny River in wet season

Metal	DPR	WHO	CSOC	PREW	EKC	OKC	KOC
Zinc (mg/l)	1	3.0	0.071±0.045	0.0705±0.0027	0.071±0.045	0.037±0.0032	0.071±0.045
Iron (mg/l)	1	0.3	1.178±0.095	2.9156±0.155	2.916±0.098	2.274±0.072	2.155±0.015
Nickel (mg/l)	0.015	0.02	0.221±0.006	0.0705±0.0031	0.071±0.003	0.037±0.011	0.159±0.043
Lead (mg/l)	0.01	0.01	0.038±0.015	0.012±0.001	0.012±0.004	0.023±0.0021	0.071±0.004
Copper (mg/l)	0.01	0.5	0.027±0.004	0.020±0.001	0.033±0.006	0.037±0.002	0.036±0.005

DPR: Department of Petroleum Resources. WHO: World Health Organization. CSOC: Control Station Ogoloma creek PREW: Port Harcourt Refinery effluent/waste water outfall. EKC: Ekerekana creek. OKC: Okochiri creek. KOC: Kalio/Okpoka creek.

Tables 1 and 2 above show the findings of the trace metal analysis of the surface water of the Okrika section of the Bonny River. While the range in the wet season was between 0.037±0.003 and 0.071±0.045 mg/L, with 0.0705±0.0027 mg/L found in the effluent/waste water sample and 0.071±0.045 mg/L found in the control location, zinc recorded the same mean concentration of 0.071 mg/l in all sampled locations during the dry season, including the effluent samples and the control location. The average iron concentration during the dry season was between 1.226±0.079 and 2.232±0.083 mg/l; location 3 (KOC) had the highest concentration, while location 2 (OKC) had the lowest; effluent/wastewater had 2.170±0.052 mg/L, while the control location had 1.781±0.419 mg/L.
During the wet season, it varied between 2.155±0.015 and 2.916±0.098 mg/L; site 1 (EKC) had the greatest value, while location 3 (KOC) had the lowest. The effluent/wastewater sample had a concentration of 2.916±0.155 mg/L, while the control location had a concentration of 1.178±0.095 mg/L. During the dry season, the mean nickel concentrations varied between 0.056 ± 0.0065 and 0.245 ± 0.032 mg/L. The values at site 1 (EKC) and location 3 (KOC) were the lowest and highest, respectively. The wastewater/effluent sample had a concentration of 0.071 ± 0.002 mg/L, while the control site had a concentration of 0.199 ± 0.140 mg/L. The concentration varied between 0.037±0.011 and 0.159±0.043 mg/L over the rainy season. The highest value was observed at location 3 (KOC), while the lowest value was observed at location 2 (OKC). Specifically, 0.071±0.003 mg/L was obtained in the effluent/wastewater sample, and 0.221±0.006 mg/L was obtained in the control location.

Table 3: Average levels of TPH and trace metals (mg/kg) in the sediments of the Bonny River's Okrika portion during the dry season

Parameter	FMENV	CSOC	PREW	EKC	OKC	KOC
TPH (mg/kg)	50-5000	65.652±1.61	1689.00±19.85	866.867±7.83	1846.500±28.76	84.668±6.4
Calcium (mg/kg)	N/A	2.117±0.046	16.373±0.386	4.405±0.243	5.354±0.372	1.645±0.03
Magnesium (mg/kg)	N/A	3.288±0.226	5.406±0.363	3.529±0.172	5.163±0.102	4.158±0.07
Sodium (mg/kg)	N/A	65.976±2.161	5.175±0.111	34.504±1.333	64.401±2.627	64.288±3.3
Potassium (mg/kg)	N/A	24.138±1.317	2.283±0.316	3.344±0.376	7.466±3.061	19.231±1.0
Zinc (mg/kg)	N/A	2.235±0.080	3.154±1.636	1.265±0.013	0.394±0.079	0.214±0.01
Iron (mg/kg)	N/A	80.389±1.592	77.113±32.100	55.892±12.716	92.764±8.474	83.830±4.9
Nickel (mg/kg)	140	0.248±0.017	0.268±0.017	0.123±0.023	0.268±0.0163	0.240±0.03
Lead (mg/kg)	35	0.069±0.006	0.041±0.006	0.115±0.017	0.073±0.0037	0.042±0.00
Copper (mg/kg)	0.3	0.119±0.056	0.061±0.015	0.127±0.010	0.072±0.035	0.111±0.01

Table 4: Average levels of TPH and trace metals (mg/kg) in the sediments of the Okrika portion of the Bonny River during the rainy season

Parameters	DPR/FMENV	CSOC	PREW	EKC	OKC	KOC
TPH (mg/kg)	50-5000	73.825±24.1	1244.500±22761	67.522±18.29	690.833±9.57	70.815±6.33
Calcium (mg/kg)	N/A	2.597±0.085	11.470±0.777	3.284±0.275	4.583±0.153	2.282±0.143
Magnesium (mg/kg)	N/A	4.416±0.081	3.212±0.102	625.580±124768	5.050±0.146	4.948±0.218
Sodium (mg/kg)	N/A	73.427±2.186	6.997±0.137	30.218±1.940	50.726±6.806	75.027±6.161
Potassium (mg/kg)	N/A	11.930±0.439	1.702±0.161	410.624±68.768	2.498±0.305	13.676±0.520
Zinc (mg/kg)	N/A	1.475±0.60	1.722±0.198	0.703±0.100	0.761±0.125	1.316±0.197
Iron (mg/kg)	N/A	73.720±3.357	71.723±6.665	45.185±2.630	148.500±14.039	62.700±3.24
Nickel (mg/kg)	140	0.230±0.015	0.188±0.015	0.191±0.269	0.219±0.021	0.199±0.011
Lead (mg/kg)	35	0.033±0.003	0.049±0.004	0.075±0.005	0.045±0.006	0.042±0.004
Copper	0.3	0.0700.009	0.068±0.030	0.090±0.0036	0.040±0.003	0.081±0.003

The analytical findings of the trace metals in the sediments of the Okrika section of the Bonny River are displayed in Tables 3 and 4. During the dry season, the average calcium concentration was between 1.645±0.035 and 5.354±0.372 mg/kg; the effluent/waste water sample had 16.373±0.386 mg/kg, while the control location had 2.117±0.046 mg/kg. The effluent/waste water sample had a value of 11.470±0.777 mg/kg during the wet season, whereas the control location had 2.597±0.085 mg/kg. The range was 2.282±0.143 to 4.583±0.153 mg/kg. Between 3.529±0.172 and 5.163±0.102 mg/kg were the mean magnesium concentrations measured throughout the dry season. The effluent/waste water sample had a value of 5.406±0.363 mg/kg, whereas the control location had 3.288±0226 mg/kg. The effluent/waste water sample contained 3.212±0.102 mg/l during the wet season, whereas the control location had 4.416±0.081 mg/kg. The values varied from 4.948±0.218 to 625.580±124.768 mg/kg. During the dry season, the amount of potassium in the sediments ranged from 3.344±0.376 to 19.231±1.045 mg/kg, whereas the control location had 24.138±1.317 mg/kg and the effluent/waste water had 2.283±0.316 mg/kg. The effluent/waste water had 1.722±0.161 mg/kg during the wet season, while the control location had 11.930±0.439 mg/kg. The range was 2.498±0.305 to 410.624±68.768 mg/kg. The dry season sodium levels from the different sediments ranged from 34.504±1.333 to 64.401±2.627 mg/kg, whereas the control location had 65.976±2.161 mg/kg and the effluent/waste water had 5.175±0.111 mg/kg. The effluent/waste water had 6.997±0.137 mg/kg during the wet season, while the control location had 73.427±2.186 mg/kg. It varied between 30.218±1.940 and 75.027±6.161 mg/kg. Copper concentrations in dry-season sediment samples varied from 0.072±0.035 to 0.127±0.010 mg/kg, whereas the control location had 0.119±0.056 mg/kg and the effluent/waste water had 0.061±0.015 mg/kg. The effluent/waste water had 0.068±0.030 mg/kg during the wet season, compared to 0.070±0.009 at the control location, with a range of 0.040±0.003 to 0.090±0.0036 mg/kg. Site 1 (EKC) had the highest copper concentration during the dry and wet seasons, while site 2 (OKC) had the lowest concentration.

4. CONCLUSION

The Okrika stretch of Bonny River is an important resource for many people. The health of this ecosystem is therefore essential to the wellbeing of the communities, hence this study to determine the status of the water bodies. The results revealed that some of the trace metals (Fe, Ni, Pb and Cu) in some locations were higher than DPR/FMENV recommended standard while some locations were within the DPR/FMENV limit. Concentrations of Zn at all the sampled locations were within the DPR/FMENV permissible limit. Levels of Zn, Fe, Ni, Pb and Cu in sediment were all within the USEPA and WHO permissible limit. Further research should focus on the continuous monitoring and proactive measures to mitigate pollution and protect the aquatic environment.

CONFLICT OF INTERESTS

The authors declare no conflict of interests.

REFERENCES

(1) Omokheyeke, O; Onojake, C., M.; Sikoki, D., F. Total hydrocarbon profile and trace metal level in sediments from the upper Bonny estuary in southern Nigeria. *Bulletin of Earth Sciences of Thailand*, 2021, *8*(1), 57–68. https://ph01.tci-thaijo.org/index.php/bestjournal/article/view/246723

(2) Marcus, A. C.; Okoye, C. O. B.; & Ibeto, C. N. Environmental pollution quality assessment of the water of Bonny River and Creeks around Okrika. International Journal of Applied Environmental Sciences, 2013, 8(1), 1- 11. ISSN: 0973-6077.

(3) Nafagha-Lawal, M. O.; Ojimelukwe, A. E.; Lelei, E. K.; Uche, A. O.; Kika, P. E.; Igbiri, S.; Babatunde, B. B.; & Sikoki, F. D. Nutrients dynamics in water and sediment of the Bonny Estuary, Niger Delta, Nigeria. Environmental Monitoring and Assessment, 2022; 194(7), 510. https://doi.org/10.1007/s10661-022-10148-y

(4) APHA. Standard methods for the examination of water and wastewater, 18th Edition. American Public Health Association, American Water Works Association, Water Pollution Control Federation (APHA-AWWAWPCF). Published by the American Public Health Association, Washington. 1992.

ISBN: 978-978-68-0485-9 DOI: https://doi.org/10.55455/acsnigeria.1.2.71-75

The Cytotoxic Effects of Extracts of Different Solvents of *Lonchocarpus cyanescens'* Stem Against Triple-Negative Breast Cancer (TNBC) Cell Lines

***Adeola Olayemi Olutola, Bilkisu Adedoyin, Ahmed Umar, Fagge Khadija Ali, Jemima Simon Wakama, and Lilian Chidera Okafor.**
Applied Chemistry Research Laboratory, University of Abuja, FCT, Abuja Nigeria.
Corresponding Author's email: Olutola.pelumi@gmail.com. 08137890676

ABSTRACT

Lonchocarpus cyanescens, a plant widely used in traditional African medicine, has shown promise for cancer therapy. This study evaluates the cytotoxic effects of extracts from different solvents (n-hexane, ethyl acetate and methanol) from *L. cyanescens* against four triple-negative breast cancer cell lines (MCF7, MDA-MB-231, Hs578T, and SkBr3). Brine Shrimp Lethality Test (BSLT) was carried out as preliminary toxicity test and MTT assay for in-vitro cytotoxicity against the four TNBC cell lines respectively. In the BSLT, methanol showed the highest toxicity (LC_{50} = 51.19 µL), followed by A20E (LC_{50} = 72.26 µL) and A10N (LC_{50} = 81.27 µL), indicating that methanol highest concentration of cytotoxic bioactive compounds compared to the hexane and ethyl acetate extracts. The MTT assay further supported these findings, revealing that methanol extract had the lowest IC_{50} values: 77 µM for MCF7, 69 µM for MDA-MB-231, and 71 µM for SkBr3, making it the most potent extract. In contrast, n-hexane extract, had IC_{50} values >100 µg/mL across all cell lines, except for MDA-MB-231 where it has 97 µM while ethyl acetate exhibited moderate activity with an IC_{50} of 87 µM against MDA-MB-231 and 71 µM against Hs578T respectively. These findings confirm the cytotoxic potential of *L.C* and highlight its prospective role in TNBC therapy. This study establishes a strong foundation for additional investigations into isolation and characterizing of active compounds from the crude extracts as well as mechanistic studies to determine its mode of action against breast cancer cells.

KEYWORDS: Lonchocarpus cyanescens (L.C), Triple Negative Breast Cancer (TNBC), Cytotoxicity, MTT, BSLT.

1. INTRODUCTION

Globally, the prevalence of cancer and its associated mortality rate is still rising, particularly in undeveloped and developing nations. In Nigeria, it is constantly increasing and this may be attributed to lack of affordable healthcare for early diagnosis and treatment. Breast and prostate cancer have the highest incidence in women and men, respectively [1]. Different plant extracts contain phytochemicals that can be utilized as chemotherapeutics. These phytochemicals have demonstrated a variety of anti-tumor, anti-inflammatory, anti-oxidant, anti-cancer, and antibacterial properties [2]. Researchers have attributed the anticancer activity of medicinal plants to the presence of antioxidants [3]. TNBC is the most aggressive kind of breast cancer, accounting for about 15–25% of all occurrences. Because TNBC lacks ER, PR, and HER2 receptor expression, it is resistant to hormones and HER2-therapies, making treatment difficult [4]. *Lonchocarpus cyanescens* is part of the *Lonchocarpus* species belonging to the Fabaceae family. The plant has historically been utilized for medical purposes. In Senegal, the leaves are served as a side dish with couscous. It is believed in Ghana that L.C roots are more effective than leaves for treating skin disorders and ulcers. In Sierra Leone and Guinea-Bissau, leprosy has also been thought to be treatable using the leaves and roots of this plant. Laxatives can be made from leaves. Leaf sap is consumed in Benin to treat diarrhea and gastrointestinal problems. Women are given a decoction of leafy twigs and roots during or after childbirth, and it is also used as an aphrodisiac. Yaws are treated with ground root, and sores are treated by washing in water containing powdered root [5]. The antioxidant property of its leaf extract using bio-assay was investigated [6]. Acute ulcerous pain in rats with aqueous root extract of *L. cyanescens*, which exhibited both antiulcer and analgesic effects, justifying the folkloric claim for the health benefits of this plant was studied [7]. The anti-cancer property of the plant has not been fully investigated. Hence, the present study is aimed to investigate the cytotoxicity of the crude extracts from Nigeria *Lonchocarpus cyanescens* for breast cancer therapy.

2. MATERIALS AND METHODS

2.1 Plant Collection and Identification

The stem bark of the plant was collected at random during the morning and evening over a period of five 5days from Dumbi Zaria, Kaduna State. It was subsequently presented for verification and authentication at the Botany section of the Department of Biological Sciences, Ahmadu Bello University Zaria, Kaduna, Nigeria. A sample with identification number ABU090058 has been deposited at the herbarium section of the Department.

2.2 Sample Treatment

Freshly collected stem bark was washed to remove dirt, rinsed and air dried at a room temperature. This was pulverized using a wood milling machine, sieved, weighed and stored in clean containers at ambient temperature and stored for further utilization.

2.3 Extraction of Crude Extracts

The crude extracts of Lonchocarpus cyanescens' stem was extracted by cold maceration continuosly with n-hexane, ethyl acetate and methanol (1500ml each). A portion (500g) of the pulverized plant stems part was soaked using 1500 mL of n-hexane and allowed to stand for seven (7) days at room temperature, filtered with filter paper to get the crude extracts of Lonchocarpus cyanescens and concentrated in vaccuo. Then the residue was dried, soaked with ethyl acetate and allowed to stand for another 7 days. The same procedure was carried out for the ethyl acetate and Methanol.

2.4 Collection of Tnbc Cell Lines and Artemia Salina Shrimp Eggs.

Artemia salina shrimp eggs were collected for cytotoxicity test from standard laboratory abroad for BSLT. Four TNBC cell lines were used in the course of this study which includes: invasive ductal carcinoma (MCF7), Adenocarcinoma (MDA-MB-231), invasive ductal carcinoma (Hs578T), and Invasive ductal carcinoma (SKBr3) respectively and were collected from cell-culture laboratory, centre for Natural Product Discovery. School of Biochemical Science, Liverpool John Moones University (LJMU) Liverpool, UK.

2.5 Cytotoxicity Assay of the Crude Extracts.

2.5.1 The BSLT assay protocol

The cytotoxicity of n-hexane (A10N), Ethyl acetate (A20E) and Methanol (A30M) crude extracts, were evaluated using the Brine Shrimp Lethality assay (BSLT) [8].

2.5.2 MTT Assay of the Crude Extracts

The cell lines were trypsinized, cleaned with phosphate buffer saline (PBS), plated on 96-well plates, and incubated for 24 hours at 37°C with 5% CO_2. Various quantities of L.C. crude extracts were applied to the cells. In order to get final extract concentrations, stock solutions were diluted in culture media, with a final DMSO content of 0.1%. The identical batch of cells was subjected to each concentration in triplicate. The ability of living cells to convert the yellow dye 3-(4,5-dimethyl-2-thiazolyl)-2,5-diphenyl-2H-tetrazolium bromide (MTT) into a blue formazan product was used to measure the growth of tumor cells. Following a 24-hour incubation period, MTT solution was added to each well's medium, and the mixture was then incubated for an additional two hours. The formazan crystals formed by live cells were dissolved in iso-propanol and gently agitated after the MTT reagent was withdrawn. A plate reader was then used to measure the absorbance at 560 nm.

3. RESULTS AND DISCUSSION

3.1 Results

3.1.1 Brine–shrimp lethality test result of n-Hexane (A10N), Ethyl acetate (A20E) and Methanol (A30M) Crude extracts of *L. cyanescens*.

The LC_{50} value of n-Hexane, ethyl acetate and methanol are shown as 81.27, 72.26 and 51.19 respectively in table 1.

Table 1: LC_{50} values of n-Hexane (A10N), Ethyl acetate (A20E) and Methanol (A30M) Crude extracts of *L. cyanescens*

Conc.	**1000 µg/cm³**		**100 µg/cm³**		**10 µg/cm³**		**Control**		**LC_{50}U/L Limit**
Sample Extract	Survivor	Dead	Survivor	Dead	Survivor	Dead	Survivor	Dead	
A10N	2	28	5	25	16	14	10	0	81.27
A20E	5	25	6	24	14	16	10	0	83.79
A30M	0	30	5	25	12	18	10	0	51.19

Key: LC_{50}< 1000µg/cm³ = Toxic, LC $_{50}$ >1000µg/cm3 =Not Toxic *High/Low 95% Confidence interval.

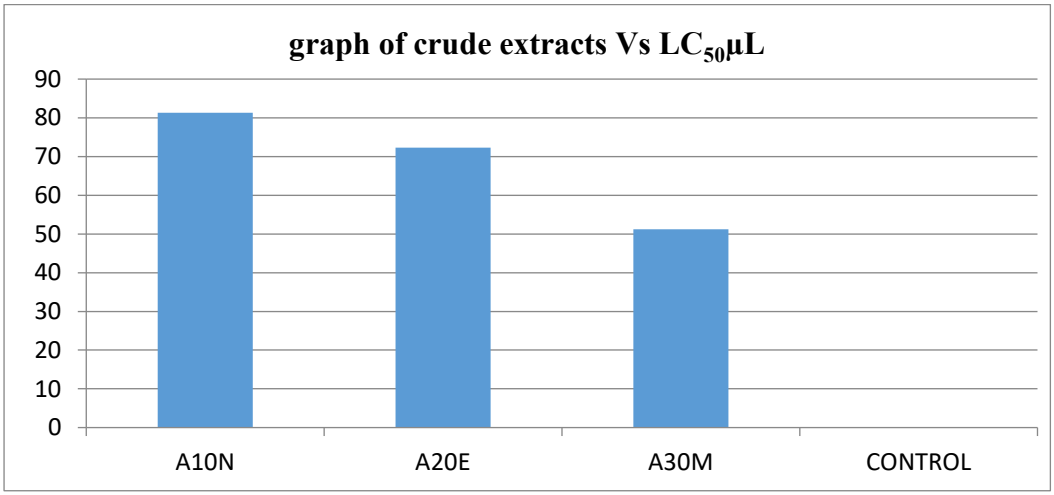

Figure 1: A Graph showing the LC_{50} values for the crude extracts of *L. cyanescens*

3.1.2 The MTT assay protocol of n-Hexane, Ethyl acetate and Methanol Crude extracts

Table 2: IC_{50} values of n-Hexane, Ethyl acetate and Methanol Crude extracts compared with the IC_{50} values of Etoposide, a standard reference.

Cell type	**A10N**	**A20E**	**A30M**	**Etoposide**
		IC_{50} values (µg/mL)		
MCF7	>100	>100	77	68
Hs578T	>100	71	98	78
SKBr3	>100	>100	>71	70
MDA-MB-231	97	87	69	68

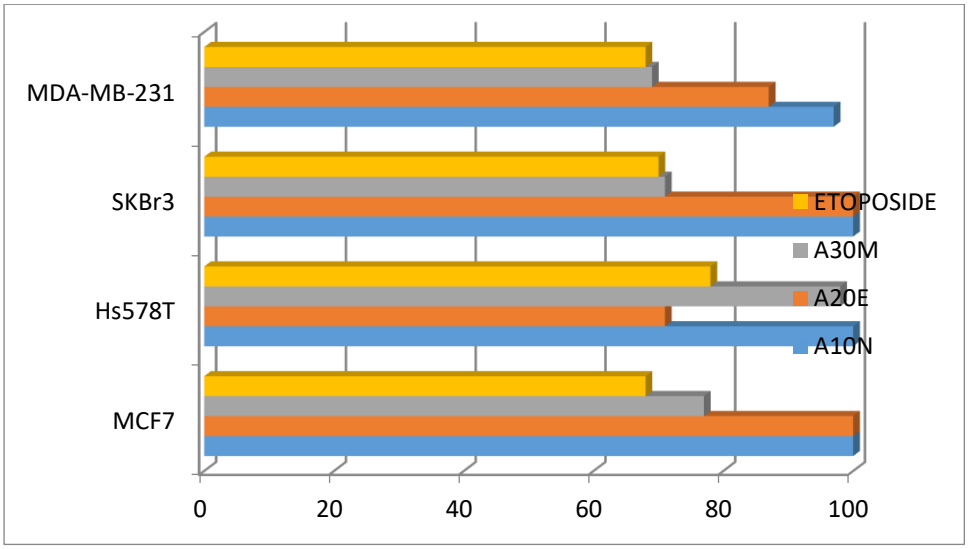

Figure 2: A bar graph showing the IC_{50} values of A10N, A20E and A30M on TNBC cell lines against the standard drug, ETOPOSIDE

3.2 Discussion

From table 1, Methanol extract has the highest (potent) activity, followed by ethyl-acetate and then n-hexane extracts, indicating that methanol had the highest concentration of cytotoxic bioactive compounds compared to the hexane and ethyl acetate extracts. Lower IC_{50} value indicates more potent inhibition. The MTT assay supported these findings, revealing that methanol extract had the lowest IC_{50} values: 77 µM for MCF7, 69 µM for MDA-MB-231, and 71µM for SkBr3, making it the most potent and effective extract in table 2. Thus, it can be said that the methanol crude extracts pose good activity (Highest activity) followed by Ethyl acetate and then the n-Hexane, however, lower than that of standard drugs Etoposide. The high cytotoxicity recorded may be partly attributed to the presence of secondary metabolite groups of tannin, saponin, terpenoid, steroid, cardiac glycoside, flavonoids and phlobatannins [9]. A compound is categorized as very toxic if it has an LC_{50} value of less than 30 ppm, is categorized as toxic if it has an LC_{50} value of 30-1000 ppm, and is categorized as non-toxic if it has an LC_{50} value above 1000 ppm [10]. No prior study has reported the cytotoxicity of *Lonchocarpus cyanescens'* stem using the Brine Shrimp Lethality Test (BSLT) and MTT assay. However, some studies have been conducted on species *lonchocarpus* and family of the plant and a few in vivo cytotoxicity studies have been conducted on *L. cyanescens* and species.

4. CONCLUSION

This study evaluated the cytotoxic effects of extracts of different solvents from *L. cyanescens'* stem against four TNBC cell lines comparing their efficacy to the standard drug, Etoposide. These findings highlight methanol extract's superior activity compared to the hexane and ethyl acetate extracts. The findings from this study provide the first BSLT- MTT based toxicity evaluation of the stem of *L. cyanscens*, demonstrating significant cytotoxic activity across all solvent extracts.
These findings confirm the cytotoxic potential of *L. cyanescens* and highlight its prospective role in TNBC therapy. This study establishes a strong foundation for further investigations into the isolation and characterization of active compounds from the crude extracts as well as mechanistic studies to determine its mode of action against breast cancer cells.

CONFLICT OF INTERESTS

The authors declare no conflict of interests.

REFERENCES

(1) López-Abente, G.; Aragonés, N.; Pérez-Gómez, B.; Pollan, M.; García-Pérez, J.; Ramis, R.; Fernández-Navarro, P. (2014). Time trends in municipal distribution patterns of cancer mortality in Spain. *BMC Cancer, 14*, 535.

(2) Obayemi, J. D.; Salifu, A. A.; Eluu, S. C.; Uzonwanne, V. O.; Jusu, S. M.; Nwazojie, C. C.; Onyekanne, C. E.; Ojelabi, O.; Panye, L.; Moore, C. M. (2020). LHRH-conjugated drugs as targeted therapeutic agents for the specific targeting and localized treatment of triple negative breast cancer. *Scientific Reports, 10*, 8212.

(3) Umadevi, M.; Kumar, K. P. S.; Bhowmik, D.; Duraivel, S. (2013). Traditionally used anticancer herbs in India. *Journal of Medicinal Plants Studies*, *1*(3), 56–74.

(4) Kreike, B.; van Kouwenhove, M.; Horlings, H.; Weigelt, B.; Peterse, H.; Bartelink, H.; Van de Vijver, M. J. (2007). Gene expression profiling and histopathological characterization of triple-negative/basal-like breast carcinomas. *Breast Cancer Research, 9*(5), 65.

(5) Iwu, M. M.; Anyanwu, B. N. (1982). Phytotherapeutic profile of Nigerian herbs. I: Anti-inflammatory and anti-arthritic agents. *Journal of Ethnopharmacology, 6*(3), 263–274.

(6) Samuel, B.; Adigun, O.; Adaramoye, O. (2014). Bioassay-guided investigation of *Lonchocarpus cyanescens* Benth leaves extracts for antioxidant activities. *Journal of Pharmacognosy and Phytotherapy*, *6*(9), 133-141.

(7) **Adeoye, A. T.; Adedapo, A. A.; Abatan, M. O. (2016).** Study on acute ulcerous pain in rats treated with aqueous root extract of *Lonchocarpus cyanescens*. *Journal of Acute Disease, 5*(6), 454–457.

(8) Fatope, M. O. (1995). Phytocompounds: Their bioassay and diversity. *Discovery and Innovation, 7*(3), 229–236.

(9) Moronkola, D. O.; Oladosu, I. A. (2013). Chemical composition of *Lonchocarpus cyanescens* Benth., (Fabaceae)—Case study of its volatile oils, and two triterpenoids. *American Journal of Plant Sciences, 4*(8), 1653–1659.

(10) Meyer, B. N.; Ferrigni, N. R.; Putnam, J. E.; Jacobsen, L. B.; Nichols, D. E.; McLaughlin, J. L. (1982). Brine shrimp: A convenient general bioassay for active plant constituents. *Journal of Medicinal Plant Research, 45*, 31–34.

ISBN: 978-978-68-0485-9 http://acsnigeria.org/publications/proceedings

In Vitro Cytotoxicity of *Lonchocarpus laxiflorus* for Breast Cancer Therapy

Fagge Khadija Ali*, Bilkisu Adedoyin, Ahmed Umar, Jamimah Simon Wakawa, and Olutola Adeola Olayemi

Applied Chemistry Research Laboratory, University of Abuja, FCT, Abuja, Nigeria.

Corresponding Author's email: Khadeejafagge4646@gmail.com Tel: 07061959125

ABSTRACT

Lonchocarpus laxiflorus, a medicinal plant native to Nigeria and West Africa, contains bioactive compounds with reported therapeutic potential. This study evaluates the in vitro cytotoxic effects of crude extracts (n-hexane, ethyl acetate, and methanol) from *L. laxiflorus* stem bark against TNBC cell lines. The Brine Shrimp Lethality Test (BSLT) was conducted to assess general toxicity, and the MTT assay was conducted on four TNBC cell lines (*MCF7, Hs578T, SkBr3, and MDAMB-231*) with etoposide as the standard drug. The BSLT results showed high cytotoxicity across all extracts, with LC_{50} values of 67.42 µg/mL (n-hexane), 61.59 µg/mL (ethyl acetate), and 51.5 µg/mL (methanol), indicating the highest toxicity in the methanol extract. Similarly, the MTT assay revealed that the methanol extract exhibited the strongest cytotoxicity against MCF7 cells (IC_{50} = 67 µM), comparable to etoposide (IC_{50} = 68 µM), suggesting potent anti-cancer activity. In contrast, ethyl acetate and n-hexane indicate toxic value, but not as high as the methanol extract, indicating lower cytotoxic effects than methanol. These results reinforce the scientific basis for the plant's traditional medicinal use and its potential application in modern breast cancer therapy and drug development.

KEYWORDS: Cytotoxicity, BSLT, MTT, TNBC, Anti-cancer agents.

1. INTRODUCTION

Cancer is a large group of interconnected diseases that arises as a result of the body's inability to control cell division, manifested by body cells dividing uncontrollably and spreading to surrounding tissues[1]. Several studies have stated that, globally, cancer ranks as the most prevalent cause of mortality. The World Health Organization defined breast cancer as a disease in which abnormal breast cells grow out of control and form tumours, which can spread throughout the body and become fatal if left unchecked and untreated and a diagnosis of triple negative breast cancer means that the three most common types of receptors known to fuel most breast cancer growth oestrogen, progesterone, and the HER-2/neu gene– are not present in the cancer tumour[2]. This has necessitated the need for the search for ways of curbing the dreadful menace of cancer. Chemotherapy, the treatment of cancer, is not without side effects, which also contribute to the severe complications associated with cancer treatment[3]. Consequently, the demand for plant-based therapeutics has grown, especially due to their affordability and accessibility in many developing countries.

Lonchocarpus laxiflorus, a Fabaceae member, is widely used in African traditional medicine. It has been employed in managing mental disorders, skin infections, jaundice, intestinal worms, and reproductive disorders across countries such as Nigeria, Benin, Kenya, and Senegal[4, 5]. Despite its widespread ethnomedicinal use, limited scientific literature exists on its cytotoxic properties. This study aims to bridge that gap by evaluating the *in vitro* cytotoxicity of its stem bark extracts against TNBC cells using the Brine Shrimp Lethality Test and MTT assay.

2. MATERIALS AND METHODS

2.1 Plant collection and identification

The plant sample stem-bark was carefully collected in the morning and evening immediately after sunset for a period of 5days from area B-Z Samaru in ABU campus, Kaduna State, and presented for verification and authentication with voucher number ABU01083 obtained at the herbarium Botany section of the Department of Biological Sciences, Ahmadu Bello University Zaria, Kaduna, Nigeria.

2.2 Sample Preparation

The freshly collected stem bark of the plant was carefully separated, air-dried at room temperature, and pulverized in the laboratory using a wood milling machine. Thereafter, the powdered sample was placed in a clean polythene bag and stored at room temperature for the experiment.

2.3 Collection of TNBC cell lines for bioassay study. (Triple Negative breast cancer)

Four cell lines were used in the analysis, which include **invasive ductal carcinoma (MCF7)**, **Adenocarcinoma (MDA-MB-231)**, **invasive ductal carcinoma (Hs578T)**, and **Invasive ductal carcinoma (SKBr3),** respectively representing different types of breast cancer cells collected from the cell-culture laboratory, Center for Natural Product Discovery. School of Biochemical Science, Liverpool. John Moores University (LJMU), Liverpool. UK.

2.4 Extraction of Crude Extracts

A weighted 500g portion of the pulverized plant samples was separately macerated using Hexane, Ethyl acetate, and methanol (100%) as solvents for seven days using 1.5L of each solvent, respectively, then decanted and filtered. Evaporated to dryness and weighed.

2.5 Cytotoxicity Assay

The Brine shrimp cytotoxicity test: The toxicity level test of the crude extracts was carried out according to[6, 7]. To ascertain their toxicity against the brine shrimps.

2.6 MTT assay protocol [3-(4.5-Dimethylthiazol-2-yl)-2-5-Diphenyltetrazolium Bromide]

The MTT assay protocol is to measure the toxicity of viable cells, and the MTT assay was carried out according to [8], with little modification from [9]. The results were evaluated against the underlisted TNBC cell lines: - MCF7 invasive ductal carcinoma, -MDAMB-231 Adenocarcinoma, - Hs578T Invasive ductal carcinoma, - SkBr3 Invasive ductal carcinoma, and Cells were treated with graded concentrations of extracts, followed by MTT incubation, solubilization of formazan crystals, and absorbance measurement at 560 nm.

2.7 Anticancer Activity

The anticancer activity of the crude extracts was carried out on triple-negative breast cancer (TNBC) cell lines to determine the anticancer activity of each of the crude extracts. This was conducted using MTT, bioassays on the TNBC cell line.

3. RESULTS AND DISCUSSION

3.1 Results

3.1.1 Brine Shrimp Lethality Test (BSLT) Results for *Lonchocarpus laxiflorus* Crude Extracts

LC_{50} of the crude extracts of *Lonchocarpus laxiflorus* stem bark of ethyl acetate, methanol, and n-hexane

CRUDE EXTRACTS	SOLVENT OF EXTRACTION	LC_{50}(µ/L)
K100	n-Hexane	67.42(43.8-515.49)
K200	Ethyl acetate	61.59(47.06-377.31)
K300	Methanol	51.5(45.49-377.99)

LC_{50}> 1000µg/cm^3 = Toxic, LC_{50}>1000µg/cm^3 =Not Toxic *High/Low 95% Confidence interval

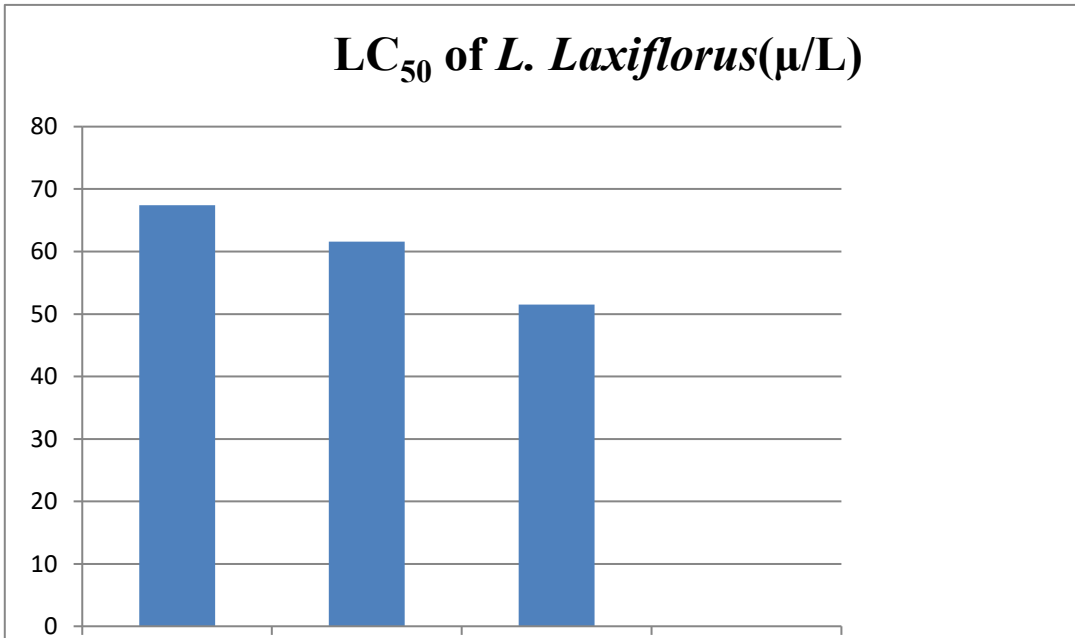

Figure 1: LC_{50} of crude extract *of L. laxiflorus* stem-bark

Table 2: IC_{50} values of the crude extract of the stem bark of *Lonchocarpus laxiflorus*

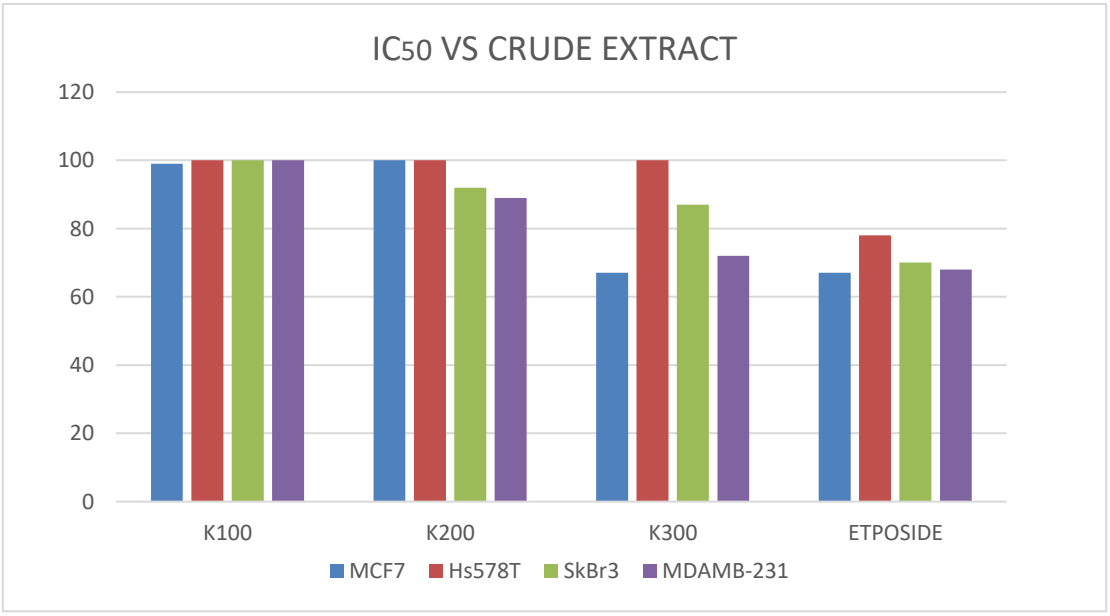

Figure 2: Graph of crude extract versus IC_{50}

3.2 Discussion

This study investigated the cytotoxicity of *Lonchocarpus laxiflorus* stem-bark extracts using both the Brine Shrimp Lethality Test (BSLT) and MTT ([3-(4.5-Dimethylthiazol-2-yl)-2,5-Diphenyltetrazolium Bromide] assay. All extracts showed significant toxicity in the BSLT, with survival rates decreasing across concentrations of 1000, 100, and 10 g/cm³. Ethyl acetate and methanol extracts caused the highest mortality (30 larvae), indicating greater toxicity compared to n-hexane. Correspondingly, the LC_{50} values were lowest for methanol (51.51 µg/mL) and ethyl acetate (61.59 µg/mL), suggesting strong cytotoxic potential. To the best of our knowledge, no prior study has reported the cytotoxicity of *Lonchocarpus laxiflorus* using the Brine Shrimp Lethality Test (BSLT). However, some studies have been conducted on the species *Lonchocarpus* and the family to which the plant belongs, and a few in vivo cytotoxicity studies have been conducted on *L. laxiflorus* and the species.

Using the MTT assay, extracts (K100, K200, K300) were tested on four breast cancer cell lines (MCF7, Hs578T, SKBr3, and MDAMB-231). K300 displayed the most potent activity, especially against MCF7 (67 µg/mL) and MDAMB-231 (72 µg/mL), closely matching the standard drug Etoposide (68 µg/mL). K100 and K200 were less effective, particularly against Hs578T, with IC_{50} values exceeding 100 µg/mL. No prior study has reported the MTT cytotoxicity of *L. laxiflorus* stem bark. This represents the first report of *L. laxiflorus* stem bark cytotoxicity using BSLT and MTT assays. The results align with previous findings from other *Lonchocarpus* species and Fabaceae members [10]. Thus, this study confirms that methanol and ethyl acetate extracts show promising anti-cancer properties. Further anticancer investigations can be done.

4. CONCLUSION

This study demonstrates that *Lonchocarpus laxiflorus* stem bark extracts possess significant *in vitro* cytotoxic activity against triple-negative breast cancer (TNBC) cell lines. Among the three solvents used, the methanol extract exhibited the highest cytotoxicity in both the Brine Shrimp Lethality Test and the MTT assay, with IC_{50} values comparable to those of the standard chemotherapeutic drug, etoposide. These findings suggest the presence of potent bioactive compounds in the methanol extract capable of inhibiting breast cancer cell proliferation. The study provides the first scientific evidence supporting the anticancer potential of *L. laxiflorus* and justifies its traditional use in herbal medicine.

ACKNOWLEDGEMENT

We thank the Center for Biotechnology Research and Development, Bayero University, Kano, Nigeria, for their service and support in the bioassay analysis of this study. The authors express their sincere gratitude to the Department of Chemistry, University of Abuja, for providing the necessary facilities and support throughout this research. We acknowledge our supervisors, mentors, Family, and colleagues.

CONFLICT OF INTERESTS

The authors declare no conflict of interest.

REFERENCES

1. World Health Organization. Symposium on Breast Cancer Awareness; WHO: Geneva, 2021.
2. American Cancer Society. Triple-Negative Breast Cancer. https://www.cancer.org/cancer/breast-cancer/about/types-of-breast-cancer/triple-negative.html (accessed 2023).
3. Avni, G. D.; Qazi, G. N.; Ganju, R. K.; El-Tamer, M.; Singh, J.; Saxena, A. K.; Bedi, Y. S.; Taneja, S. C.; Bhat, H. K. Medicinal Plants and Cancer Chemoprevention. Curr. Drug Metab. 2008, 9 (7), 581–591. https://doi.org/10.2174/138920008785821657
4. Sarkar, S.; Zaidi, S.; Chaturvedi, A. K.; Srivastava, R.; Dwivedi, P. K.; Shukla, R. Search for Herbal Medicine: Anti-Asthmatic Activity of Methanolic Extract of Curcuma longa. J. Pharmacogn. Phytochem. 2015, 3, 59–72.
5. Neuwinger, H. D. African Ethnobotany: Poisons and Drugs: Chemistry, Pharmacology, Toxicology; CRC Press: Boca Raton, FL, 1996; ISBN 978-3-8261-0077-2.
6. Fatope, M. O.; Ibrahim, H.; Takeda, Y. Screening of Higher Plants Reputed as Pesticides Using the Brine Shrimp Lethality Assay. Int. J. Pharmacogn. 1993, 31 (4), 250–254. https://doi.org/10.3109/13880209309082949
7. Oloyede, G. K.; Onocha, P. A.; Olaniran, B. B. Phytochemical, Toxicity, Antimicrobial, and Antioxidant Screening of Leaf Extracts of Peperomia pellucida from Nigeria. Adv. Environ. Biol. 2011, 5 (12), 3700–3709.
8. Mosmann, T. Rapid Colorimetric Assay for Cellular Growth and Survival: Application to Proliferation and Cytotoxicity Assays. J. Immunol. Methods 1983, 65 (1–2), 55–63. https://doi.org/10.1016/0022-1759(83)90303-4

9. van Meerloo, J.; Kaspers, G. J. L.; Cloos, J. Cell Sensitivity Assays: The MTT Assay. In Cancer Cell Culture; Cree, I. A., Ed.; Methods in Molecular Biology; Humana Press: Totowa, NJ, 2011; Vol. 731, pp 237–245. https://doi.org/10.1007/978-1-61779-080-5_20
10. Magalhães, A. F.; Santos, C. C.; Magalhães, E. G.; Nogueira, M. A. Detection of Polyhydroxyalkaloids in Lonchocarpus Extracts by GC–MS of Acetylated Derivatives. Phytochem. Anal. 2002, 13 (4), 215–221. https://doi.org/10.1002/pca.645

ISBN: 978-978-68-0485-9 DOI: https://doi.org/10.55455/acsnigeria.1.2.81-86

Antimicrobial Activity of Crude Extracts from *Lonchocarpus sericeus* Roots

Samuel Ugbedeojo Onuche[1*], Bilkisu Adedoyin[1], Hadiza Aminu Isa[2], and Ahmed Umar[1]
[1]Applied Chemistry Research Laboratory, Department of Chemistry, University of Abuja, FCT, Nigeria.
[2] Department of Chemistry, faculty of Science, Nigerian Defence Academy, Kaduna.Nigeria
Corresponding Author's email:samuelonuche479@gmail.com

ABSTRACT

Lonchocarpus sericeus is a plant genus in the legume family (Fabaceae). It is cultivated and used in folk medicine for its antitumor, antimicrobial, antiviral, antimycotic, and hepatoprotection properties. This study investigates the phytochemical composition and antimicrobial efficacy of the crude extracts of *L.sericeus*. Standard phytochemical screening methods were applied to both methanol and ethyl acetate extracts. Antimicrobial activities were assessed through inhibition zone assays, and minimum inhibitory concentration (MIC) testing against several microbial strains. The phytochemical analysis revealed the presence of alkaloids, triterpenes, cardiac glycosides, saponins, tannins, steroids, coumarins, amino acid and resins. Antimicrobial assay of the methanol extract demonstrated varying degrees of inhibition against different microbial strains, suggesting potential broad-spectrum activity. Both extracts exhibited similar MIC profiles for most bacterial strains suggesting comparable antimicrobial activity. These findings show the significant medicinal properties of *L.sericeus* and support its traditional use in treating infectious and metabolic ailments.

KEYWORDS: Antimicrobial, *Lonchocarpus sericeus,* Phytochemical.

1. INTRODUCTION

Microbial infections and antibiotic resistance pose severe threats to global health, contributing significantly to mortality rates across the world. In 2013, infections accounted for 9.2 million fatalities, constituting approximately 17% of total deaths.[1,2] The rise of antibiotic resistance has compromised the efficacy of existing antibacterial treatments.[3,4] The prevalence of microbial infections has led to the exploration of plants for potential antibiotic compounds.[5,6] Medicinal plants harbor compounds which are active that can serve as cost-effective and efficient herbal antibiotics for common bacterial illnesses. The plant *Lonchocarpussericeus* which falls under the family of fabacea has been explored traditionally to treat several illnesses. In Nigeria, the leaves are employed for broad-spectrum healing while the bark is exploited for management of body pains, arthritis, rheumatism, cutaneous and subcutaneous parasitic infection, malnutrition, debility, paralysis and convulsions. The roots are notably employed for the treatment of leprosy. The fruit and seeds are used as insect repellants and arachnicides.[7]

A decoction or infusion of the plant leaves is used for gastrointestinal and hepatic disorders and for alleviation of malaria. It is also used in folk medicine for its antitumoral, antimicrobial, antiviral, antimycotic, choleretic-cholagog, hepatoprotector properties. The plant is also consumed as a diuretic and a tonic to maintain wellness. The leaves, the bark and roots of this plant are being employed as an anti-inflammatory, antimicrobial and anticancer plant.[8] This study evaluates the phytochemical constituents and antimicrobial efficacy of ethyl acetate and methanolic extracts of *L. sericeus* roots against selected microbial strains using both the disk diffusion method and MIC assays.

2. MATERIALS AND METHODS

2.1 Plant identification and collection

Roots samples of *L. sericeus* were collected from Saye village in Zaria, Kaduna State, and was authenticated and verified at the Botany division of the Department of Biological Sciences, Ahmadu Bello University Zaria, Kaduna, Nigeria with the identification number; ABU01085.

2.2 Sample Treatment for Extraction

The root samples were carefully cleaned, dried, and pulverized using wood milling machine. The powdered sample was weighed and stored in a polythene bag at room temperature.

2.3 Extraction of Crude Extracts

Cold maceration was employed to obtain the plant extracts. 100g of the pulverized root sample was immersed in 500 ml of ethyl acetate for 72 hours at room temperature, followed by filtration and

evaporation at 78°C using a rotary evaporator. The same procedure was repeated using methanol as the solvent.

2.4 Phytochemical Screenings for Crude Extracts

Both ethyl acetate and methanol extracts underwent qualitative phytochemical tests using established procedures.[9,10]

2.5 Antimicrobial Assay Procedure

Sample Preparation: Concentrations of 1.0 mg/cm^3, 0.5 mg/ cm^3 and 0.25 mg/ cm^{3}were prepared for each extracts by dissolving 0.49 mg, 0.98 mg and 1.96 mg of each extract in 2cm^{3}of the respective solvents of extraction. The solution of the extracts was prepared by dissolving 0.49 mg, 0.98 mg and 1.96 mg of extracts in 2 cm^3 of hexane to give an approximate concentration of 0.25, 0.5 and 1.0 mg/cm^3 respectively. The solvent of extraction was used as control only. Test solutions were individually prepared in triplicates. The same method was employed using Cyprofloxacin, Gentamycin and Amoxacillin which were used as standard drugs.

2.6 Test of Minimum Inhibitory Concentration (MIC)/Minimum Bactericidal Concentration (MBC)

The MIC and MBC of the extract were assessed using the micro dilution agar technique. The extracts underwent serial dilution in sterile distilled water, resulting in a decreasing concentration range from 160 to 1.25 mg/cm³ across nine (9) labeled sterile tubes (1 through 9). Wells were created in Mueller Hinton agar (MHA) plates, solidified after insertion, using a sterile cork borer with an 8 mm diameter. 100 µL was aseptically added of each dilution to the wells in triplicate and a standardized inoculum (1.5 X 108 CFU/cm³) of the microbial isolate was introduced. 100 µL of methanol was added to the wells to serve as a control. All test plates were then incubated at 37°C and observed for growth after 24 hours. The lowest concentration of an extract displaying a distinct zone of inhibition was considered as the MIC. The MBC was determined using a 100 µL aliquot from the tube containing the MIC was placed on an MHA plate and spread. After another 24 hours of incubation at 37°C, examination of the plates were carried out for bacterial growth to identify the extract concentration required to eliminate 99.9% of bacterial isolates.

3. RESULTS AND DISCUSSION

3.1 Result

3.1.1 Phytochemical Analysis

Phytochemical screening analysis of the crude extracts of ethyl-acetate and methanol showed the appearance of various secondary metabolites constituents present in the plant as shown in Table 1

Table 1: Results of Phytochemical screenings of ethyl acetate and methanolic crude extracts of *L. sericeus*

Phytocompounds	Ethyl acetate Extract	Methanol Extract
Alkaloids	+	+
Triterpenes	+	+
Cardiac glycosides	+	+
Saponins	+	+
Condensed tannins	+	+
Steroids	+	+
Quinones	-	-
Anthraquinones	-	-
Tannins	+	+
Coumarins	+	+
Amino Acid	+	+
Resins	+	+

Key: (+) = present, (-) = absent

3.1.2 Antimicrobial test

Analysis of methanol extract of *Lonchocarpussericeus* antimicrobial zone inhibition is presented in table 2 below.

Table 2: Results of crude extracts of *L. sericeus*antimicrobial zone inhibition

Microbial strain	Concentration (x10^2 µg/ml)			
	4	5	6	7
Staphylococcus aureus	3.3	9	11.7	21.7
Streptococcus pneumonia	2.3	4.7	9	15
Salmonella typhi	6.3	10.7	15.3	22
Corynbacteriumulcerans	-	-	-	-
Escherichia coli	5	9.7	16.3	28
Pseudomonas aeruginosa	7.3	14.7	22.3	30
B.cereus	8.6	12.3	17	24.7
Trichophyton rulorrum	4	7.3	11.7	16
Aspergillus niger	8	12.3	17.3	27.7
Candida ablican	4.7	8.7	14	22.7
Control	-	-	-	-

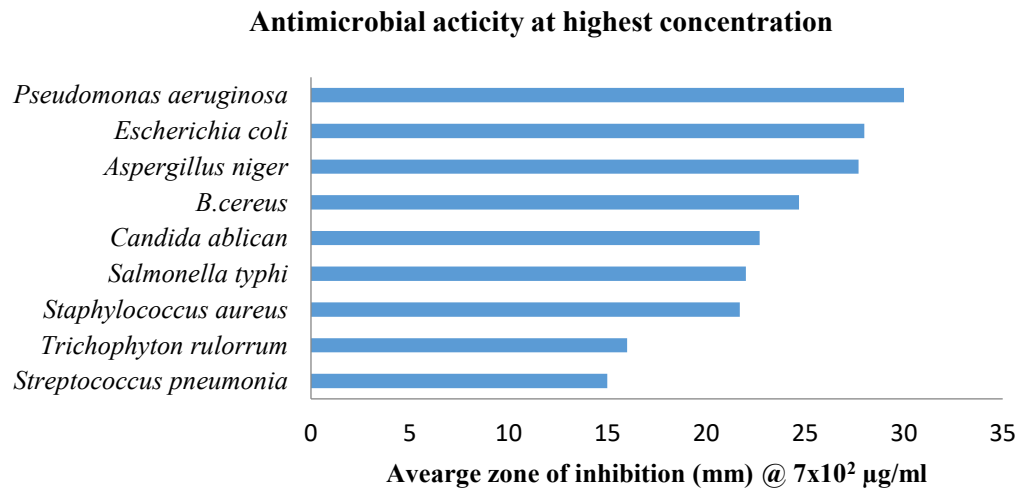

Figure 1: Methanol extract antimicrobial inhibition at highest concentration

3.1.3 Minimum Inhibitory Concentration

The result of MIC of the crude extracts of *Lonchocarpussericeus*Table 3

Table 3: Result of minimum inhibitory concentration of the crude extracts of *L. sericeus*

Bacterial strains	Ciprofloxacin	Ethyl acetate	Methanol
Staphylococcus aureus	0:648×10^{-3}	1.52	1.69
Streptococcus pneumonia	0:648×10^{-3}	6.49	6.49
Salmonella typhi	0:648×10^{-3}	6.49	6.49
B. cerues	0:648×10^{-3}	3.04	3.37
Pseudomonas aeruginosa	0:041×10^{-3}	6.10	6.75
Escherichia coli	0:041×10^{-3}	6.1	6.75
Trichophyton rulorrum	0:648×10^{-3}	3.10	4.75
Aspergillus niger	0:648×10^{-3}	3.10	5.75
Candida ablican	0:648×10^{-3}	6.10	6.75

The MICs of the crude extractson different bacterial strains. β= MIC value (6.250)

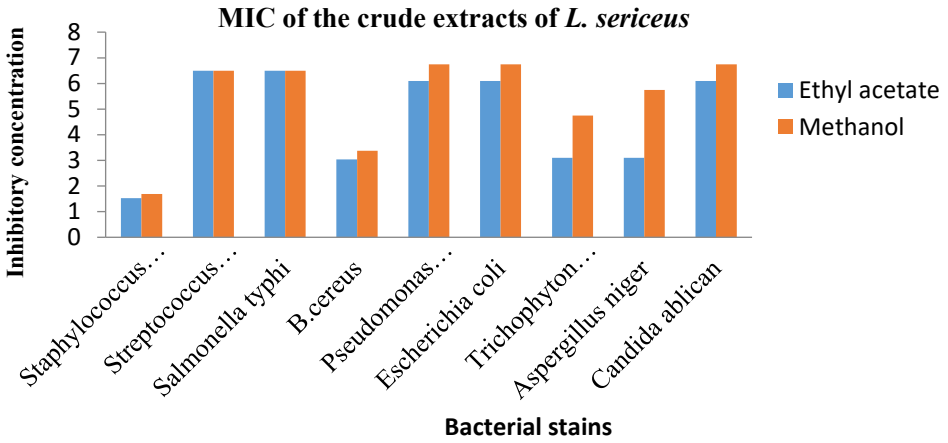

Figure 2:MIC of the crude extracts of *L. sericeus*

3.2 Discussion

Phytochemical screening result showed encompassing alkaloids, steriods, triterpenes, saponins, cardiac glycosides, tannins (both condensed and hydrolysable), coumarins, amino acid, and resins, in both ethyl acetate and methanolic extracts. Notably, quinones and anthraquinones were absent in both extracts (Table 1). The antimicrobial efficacy of the methanolic extract was determined through inhibition zone measurements and MIC determination. The inhibition zones increased with higher concentrations of the extract. *Pseudomonas aeruginosa and Escherichia coli* exhibited the largest inhibition zones (up to 31 mm), indicating strong susceptibility. *Corynebacterium ulcerans* showed no response at any concentration (Table 2). MIC testing showed that *Staphylococcus aureus* was the most susceptible strain to the ethyl acetate extract (MIC = 1.52 mg/ml). Both extracts had MICs between 3.04–6.75 mg/ml for most strains, while ciprofloxacin showed superior activity at nanogram levels (Table 3).

The presence of phytochemicals in the roots of *L. sericeus* makes it advantageous to humans since these compounds have exhibited potent medicinal activities including analgesic, anticancer, bactericidal, wound healing, hepatoprotective, anti-inflammatory and antioxidant properties.[7] Compounds such as alkaloids, tannins, and saponins have been noted for their ability to disrupt microbial membranes or inhibit enzyme systems.[11,12] Alkaloids are also recognized as one of the classes of therapeutically active plant substances. Pure, isolated, and synthetic derivatives are quite useful as basic medicinal agents because of their analgesic, anti-nociceptive, antioxidant and intestinal anti-inflammatory activities.[7] Flavonoids are quite renowned for their anti-oxidant, hepatoprotective and anti-cancer potentials.[13] Also flavonoids are notable for their anti-inflammatory and allergic effect coupled with their gastric mucus production.[14] The antimicrobial screening of *L. sericeus* crude extracts revealed promising inhibitory effects against a spectrum of bacterial and fungal pathogens. The results demonstrated a dose-dependent increase in inhibition zones, and varying minimum inhibitory concentration (MIC) values, consistent with patterns observed in medicinal plant research.[11,15] Ciprofloxacin, used as the reference drug, exhibited superior potency, with MIC values spanning from 0.041×10^{-3} to 0.648×10^{-3} mg/ml, aligning with its known efficacy in nanogram concentrations.[16,17] In contrast, the MICs of both ethyl acetate and methanolic extracts of *L. sericeus* ranged from 1.52 to 6.75 mg/ml, typical for crude plant preparations. While less potent than ciprofloxacin, the extracts demonstrated broad-spectrum activity, particularly in strains such as *Staphylococcus aureus*, *Bacillus cereus, Escherichia coli,* and *Pseudomonas aeruginosa*. The Gram-positive organisms, particularly *S. aureus and B. cereus,* showed strong susceptibility to the extracts, with inhibition zones of up to 25 mm and MICs as low as 1.52 mg/ml. This finding is consistent with previous research indicating that Gram-positive bacteria are generally more vulnerable to plant extracts, due to their simple peptidoglycan-rich cell wall, which facilitates better permeability of bioactive compounds.[12,11] Substantial inhibition was observed against Gram-negative species such as *E. coli* and *P. aeruginosa*, known to be resistant due to their outer lipopolysaccharide membrane.[18] Zones of inhibition reached 30–31 mm, with MICs around 6.10–6.75 mg/ml. This shows that *L. sericeus* contain non-polar phytochemicals, such as flavonoids or terpenoids, capable of disrupting bacterial membranes.[19] The extracts also demonstrated moderate antifungal activity, with *Trichophyton rulorrum* and *Aspergillus niger* exhibiting inhibition zones of 15–28 mm and MICs

between 3.10 and 5.75 mg/ml. Fungal organisms are typically more resilient due to their complex chitinous cell walls, however these findings indicate that the extracts may possess broad antifungal compounds, in line with literature on plant secondary metabolites such as phenolics and saponins.[20]

4. CONCLUSION

The integrated phytochemical and antimicrobial evaluation of *Lonchocarpussericeus* roots reveals that the plant contains a diverse array of bioactive compounds that contribute its significant antimicrobial activity and this supports its traditional medicinal use and suggests potential as a natural antimicrobial agent, especially against Gram-positive bacteria and select fungal species. Further studies should focus on phytochemical characterization, synergy with antibiotics, and mechanistic assays to explore its full therapeutic potential.

CONFLICT OF INTERESTS

The authors declare no conflict of interests.

REFERENCES

(1) WHO G. WHO methods and data sources for global burden of disease estimates 2000–2011. Geneva: Department of Health Statistics and Information Systems; **2013**.

(2) Gupta M, Sharma R, Kumar A. Comparative potential of simvastatin, Rosuvastatin and Fluvastatin against bacterial infection: an in silico and in vitro study. Orient Pharm Exp Med. **2019**:1–17. https://doi.org/10.1007/ s13596-019-00359-z.

(3) WHO. Antimicrobial resistance: Global report on surveillance, vol. 2014. Geneva: WHO; **2014**.

(4) Baym M.; Stone L.K.; Kishony R. Multidrug evolutionary strategies to reverse antibiotic resistance. *Science.* **2016**;351(6268):aad3292.

(5) Burapadaja S.; Bunchoo A. Antimicrobial activity of tannins from Terminaliacitrina. *Planta Medica.* **1995**;61:365–366.

(6) Adenisa S.K.; Idowu O.; Ogundaini A.O.; Oladimeji H.; Olugbade T A.; Onawunmi G O.; Pais M. Antimicrobial constituents of the leaves of *Acalyphawilkesiana* and *Acalyphahispida*. *Phytother Res.* **2000**;14:371–374.

(7) Uwemedimo E.; Johnbull O.; Okenwa U. Phytochemical, anti-inflammatory and analgesic properties of stembark extract and fractions of Lonchocarpussericeus Poir.(Papilionaceae) in albino mice. *Avicenna J Phytomed.* **2020**:10(6):584–593

(8) Addotey J.N.; Amoo I. The Use Of Flavonoids AsA Marker For Standardization OfLonchocarpusSericeus; *World Journal Of Pharmacy And Pharmaceutical Sciences;* **2016**:5(4);55-74 DOI: 10.20959/wjpps20164-6346.

(9) Trease, G. E.; Evans, W. C. Trease and Evan's Textbook of Pharmacognosy. 13th Edition. *Cambridge University Press*, London. **1989**:546.

(10) William P.J.; Douglas A.K. Extraction of plant secondary metabolites. *PubMed;*doi: **2012**:10.1007/978-1-61779-624-1_13.

(11) Cowan, M. M. Plant products as antimicrobial agents. Clinical Microbiology Reviews. **1999**:12(4), 564–582.

(12) Doughari, J. H.; Human, .S.; Benade, S. Antimicrobial activity of Lanneaacida against some selected microorganisms. African Journal of Biotechnology. **2007**:6(24), 2897–2900.

(13) Kumar S.; Pandey A.K. Chemistry and Biological Activities of Flavonoids: An Overview. Sci Worl J. **2013** doi: 10.1155/2013/162750.

(14) Pan M.H, Lai CS, Ho CT. Anti-inflammatory activity of natural dietary flavonoids. *Food Function.* **2010**;1:15–31.

(15) Eloff, J. N. A sensitive and quick microplate method to determine the minimal inhibitory concentration of plant extracts for bacteria. *Planta Medica.**1998**:64*(8), 711–713.

(16) Hooper, D. C., & Jacoby, G. A. Mechanisms of drug resistance: Quinolone resistance. *Annals of the New York Academy of Sciences.* **2015**:1354*(1), 12–31.*

(17) Clinical and Laboratory Standards Institute (CLSI**).** *Performance Standards for Antimicrobial Susceptibility Testing* (31st ed.). CLSI supplement M100. Clinical and Laboratory Standards Institute. **2021**

(18) Nikaido, H. Molecular basis of bacterial outer membrane permeability revisited. Microbiology and Molecular Biology Reviews. **2003**: 67(4), 593–656.
(19) Shai, L. J.; McGaw, L. J.; Aderogba, M. A.; Mdee, L. K.; Eloff, J. N. In vitro antimicrobial activity of extracts from selected South African medicinal plants. *BMC Complementary and Alternative Medicine.* **2008***:8*(1), 27.
(20) Oyetayo, V. O.; Akinmoladun, F. O.; Ojo, A. S**.** Antifungal activities of two tropical medicinal plants. *Research Journal of Medicinal Plants.* **2009***:3*(3), 100–107.

ISBN: 978-978-68-0485-9 DOI: https://doi.org/10.55455/acsnigeria.1.2.87-91

Virtual Screening of Chitosan Derivatives as Potential Inhibitors against *Cassava Linamarase*

Adetoun Akitoye[a], Oluwafemi Aina[b], Akinkunmi Bamigboye[a], Sulyman Ibrahim[c], Isaac Akinbulu[a], and Wesley Okiei[a]

a) University of Lagos, Akoka, Lagos b) Dept of Bioscience, Trinity University, Yaba Lagos Nigeria c) Department of Industrial Chemistry, University of Ilorin, Ilorin

Corresponding Author's email: aakitoye@unilag.edu.ng

ABSTRACT

Linamarase is a key enzyme involved in the hydrolysis of linamarin, a cyanogenic glycoside present in cassava. Its inhibition is crucial for reducing the release of hydrogen cyanide, a toxic chemical of concern in cassava. In this study, the inhibitory potential of chitosan derivatives against linamarase was evaluated. The binding interaction of linamarase-linamarin complex was first established, followed by virtual screening of chitosan derivatives, which were ranked based on their binding energies and interactions with active site residues. Chitosan derivatives, including N-(carboxymethylidene) chitosan,N-(2-chloro-6-fluorobenzyl) chitosan, N-maleoyl-chitosan, octyl-chitosan, sulfoethyl chitosan, and sulfobutyl chitosan, among others, exhibited the high affinities for linamarase compared with that of the typical linamarase-linamarin interaction. Sulfobutyl chitosan particularly demonstrated the strongest inhibitory potential due to its ability to form stable interactions with key amino acid residues present in linamarase's active site (such as Glu464, Glu406, and Gln193). These findings identify promising candidates for linamarase inactivation from the top performers, offering a potential strategy for cyanide detoxification in cassava, which could significantly enhance the crop's acceptance, shelf life, marketability, and economic value across Nigeria and Africa, thereby promoting food security (SDG 2).

KEYWORDS: Molecular docking, Chitosan derivatives, Cyanide Detoxification, Enzyme inactivation, Food Security.

1. INTRODUCTION

β-glucosidase (EC 3.2.1.21) is a class of glycoside hydrolases (GH) that catalyse the hydrolysis of various glycosides and oligosaccharides.[1] The similarity of amino sequence of β-glucosidases allow for their grouping into families. Cassava (Manihot esculenta) and maize (Zea mays) belong to the GH 1 family with similar amino acid sequence and reactivity.[2] Therefore, β-glucosidase of cassava, linamarase, is structurally similar to that of maize, DIMBOAGlc-hydrolase.

Linamarase, naturally occurring in the cell wall of cassava, catalyses cyanogenic glycosides linamarin and lotaustralin into glucose and acetone cyanohydrin, the latter, which is further broken down into cyanide and acetone.[3] During cassava harvest, contact occurs between the cassava tissues and external elements, which inevitably leads to the wounding of its cell wall, subsequently activating the catalysis of linamarin and lotaustralin by linamarase, thus releasing hydrogen cyanide, a toxic chemical to cassava.[4]

In this study, the inhibitory potential of chitosan derivatives is evaluated against the linamarase enzyme. This is in order to identify the most suitable candidate for linamarase inactivation for limiting or inhibiting cyanide production in cassava.

2. METHODOLOGY

2.1 Ligands and protein preparation

Previously reported chitosan derivatives (85 3D (SDF files) were downloaded from PubChem database (pubchem.ncbi.nlm.nih.gov). The 3D structures were energy-minimized using the MMF94 force field, and then converted to Protein Data Bank Partial Charge and Atom Type (PDBQT) format by Open Babel software.[5] Linamarin was also prepared and saved in pdbqt format, following the same process, the ligand file names were computed in a text file, while linamarase was prepared using AutoDock Tool, sequentially removing water molecules and heteroatoms, while polar hydrogens and Koleman charges were added and then saved in pdbqt format.

2.2 Structure-based virtual screening

The binding site of the linamarase enzyme was assigned on AutoDock Tools by setting the grid box, which corresponds to the active site as reported by,[6] and validated by POcket-CAvity Search

Application (POCASA).[7] Thereafter, virtual screening was carried out using AutoDock Vina automated by a Perl Strawberry script. An exhaustiveness of 8 and a number of modes of 10 was set to ensure that different poses of ligands are explored. Consequently, the interaction of each ligand (specifically chitosan derivatives) with the linamarase enzyme were evaluated and ranked based on their binding energies and interactions with active site residues.

3. RESULTS AND DISCUSSION

3.1 Active site determination

POCASA was used to determine the binding pockets of linamarase with a probe radius of 2 Å and a grid size of 1 Å.[7] POCASA unveiled three binding pockets, which were ranked by the volume and volume-depth (VD) value. The volume of a binding pocket depicts the free space available for small molecules to occupy, whereas VD evaluates the potential of a binding pocket to be functional by taking into account its depth. From the three pockets unveiled, 680, 322, and 95, the highest ranked pocket recorded a volume of 1133 Å, and a VD value of 4571 Å (Figure 1a). Comparatively, pocket 680 depicted a volume at least 40 times larger and VD value at least 53 times larger than both pockets 322 and 95, proving pocket 680 as the most likely binding site. Many proteins form pockets when they fold, allowing small molecules to fit in them; these pockets can serve as active sites. The active site of a protein gives more information about its function and structure. Czjzek et al[6]. previously reported the active site of linamarase, showing its opening around loops A, B, C, and D. Glu 406, a nucleophilic part of the catalytic machinery, is located at the bottom of the active site and binds to beta-D-glucopyranose (Figure 1). Czjzek et al[6] also showed that the aglycone-binding pocket contains Phe 198, Phe 205, Phe 466, and Trp 378, which validates the findings from this study.

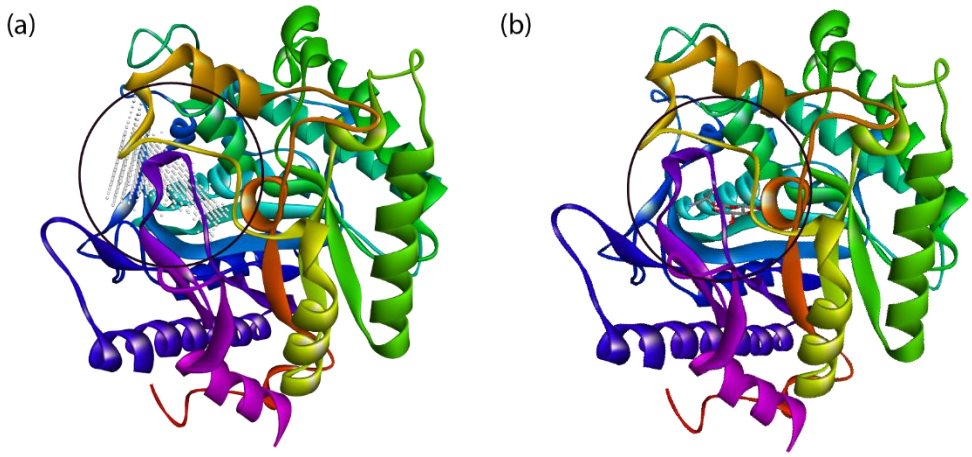

Figure 1: (a) The predicted binding pocket of linamarase, predicted by POCASA (b) Binding site of linamarin with linamarase.

3.2 Structure-based virtual screening

Further to energy minimization of the chitosan derivatives to be analyzed, the eighty-five (85) compounds were screened by docking them at the binding pocket 680 predicted by POCASA.[6] Of the eighty-five chitosan derivatives evaluated, seventy (70) demonstrated a higher binding affinity referenced against linamarin (-7.299 kcal mol^{-1}) (Figure. 2).

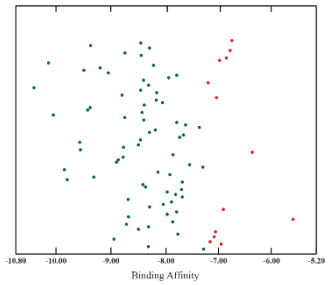

Figure 2: Scatter plot of 85 chitosan derivatives analyzed, showing 70 ligands (≥ -7.746 kcal mol^{-1}) benchmarked against linamarin

Upon further evaluation, chitosan derivatives with close differences from the binding energy of linamarin were screened out, leaving a set of 26 chitosan derivatives that were top performers among all the chitosan derivatives analyzed (Table 1). These chitosan derivatives consistently showed high binding affinities (≥ -7.746 kcal mol^{-1}) across the structure-based virtual screening platform employed. Structure-based virtual screening (SBVS) is a computational strategy used to evaluate how a collection of molecules bind to a target protein by docking them into the 3D structure of the protein.[8] The goal of SBVS is to funnel down a large library of molecules to a smaller list within a short time before performing *in silico* and *in vitro* analysis, which are often much more complex, time-consuming, and expensive. From the virtual screening carried out, a PDB (Protein Data Bank) file was generated, which showed the interaction between each chitosan derivative and the protein, and the type of bond formed between the amino acids

Table 1: Binding affinity of the top 26 chitosan derivatives.

PubChem CID	Chemical name	Binding affinity (kcal mol^{-1})
129721275	N-(2-chloro-6-fluorobenzyl)chitosan	-10.46
129674979	N-(carboxymethylidene)chitosan	-10.19
129830721	N-(3-nitro-4-aminobenzoyl)chitosan	-10.1
132280892	N-(2-thienylmethyl)chitosan	-9.893
135121658	N-(2-azidoethyl)chitosan	-9.84
129853204	N-adamantylethyl-chitosan	-9.608
129865140	N-(2-hydroxybenzyl)chitosan	-9.595
129682035	N-(hydroxypropyl)chitosan	-9.529
129826896	N-(2-(2-pyridyl)ethyl)chitosan	-9.46
129821432	N-(phenylacetyl)chitosan	-9.412
71306969	Carboxymethyl chitosan	-9.406
135121652	N-maleoyl-chitosan	-9.228
129689767	N-succinyl-chitosan	-9.075
129689767	Carboxymethylchitosan	-8.969
169435702	Dimethylethyl amino-chitosan	-8.7
129887062	Carboxy-chitosan	-8.476
129880215	N-sulfo-chitosan	-8.407
129721847	N-methylcarboxy-chitosan	-8.325
129867891	Chitosan oligosaccharide	-8.308
129856284	N-(2-sulfoethyl)chitosan	-8.183
129844296	Chitosan-6-mercaptonicotinic acid	-8.053
129652128	Sulfobutyl-chitosan	-7.979
164186159	Octyl-chitosan	-7.746

Subsequently, further analysis was carried out to understand the amino acid interaction between each of the top performing chitosan derivatives matched against the amino acid interaction between the linamarin-linamarase ensemble. Figure 3 shows the most similar interactions achieved by some of the ligands.

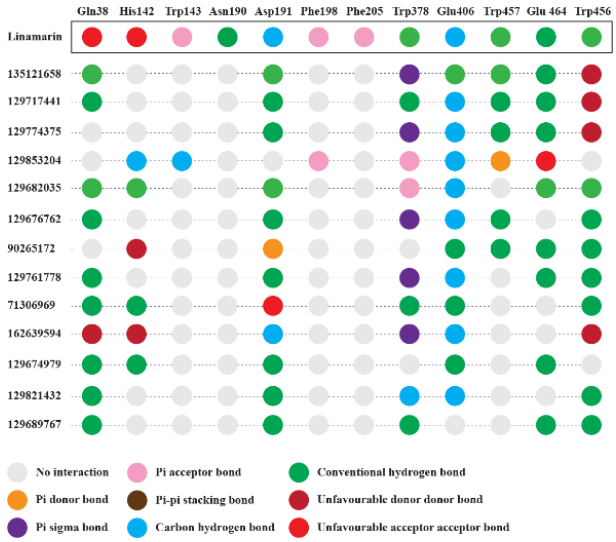

Figure 3: Amino acid interaction of top perming chitosan derivatives

Thirteen (13) of the 26 chitosan derivatives had a C-H bond with at least four of the amino acids linamarin interacts with, validating their strong and potent binding affinities.

4. CONCLUSION

The inhibition of linamarase is crucial for detoxifying cyanide in cassava, a major tropical crop with great potential to address food insecurity. This study successfully evaluated the inhibitory potential of eighty-five chitosan derivatives against cassava linanmarase. Of the eighty-five chitosan derivatives evaluated, seventy (70) demonstrated higher binding affinities than linamarin-linamarase interaction. These were further screened to twenty-six, of which thirteen (13) of these demonstrated strong and similar interactions with salient amino acids involved in the linamarin-linamarase interaction. This validates these chitosan derivatives as potential candidates for inhibiting the cyanogenic activity caused by the hydrolysis of linamarin.

CONFLICT OF INTERESTS

The authors declare no conflict of interests.

REFERENCES

(1) Sengupta, S.; Datta, M.; Datta, S. β-Glucosidase: Structure, function and industrial applications. In *Glycoside hydrolases*; Academic Press, 2023; pp 97–120.

(2) Paul, L.; Shadrack, D. M.; Mudogo, C. N.; Mtei, K. M.; Machunda, R. L.; Ntie-Kang, F. Structural Characterization of Cassava Linamarase-Linamarin Enzyme Complex: An Integrated Computational Approach. *J. Biomol. Struct. Dyn.* **2022**, *40* (19), 9270–9278.

(3) Nnebe, N. Thermostability of cassava linamarase. (M.Sc. thesis, McGill University, Canada, 2015.

(4) Paul, L.; Mudogo, C. N.; Mtei, K. M.; Machunda, R. L.; Ntie-Kang, F. A Computer- Based Approach for Developing Linamarase Inhibitory Agents. *Phys. Sci. Rev.* **2020**, *5* (7), 20190098.

(5) Kwofie, S. K.; Broni, E.; Yunus, F. U.; Nsoh, J.; Adoboe, D.; Miller, W. A., III; Wilson, M. D. Molecular Docking Simulation Studies Identifies Potential Natural Product Derived-Antiwolbachial Compounds as Filaricides against Onchocerciasis. *Biomedicines* **2021**, *9* (11), 1682.

(6) Czjzek, M.; Cicek, M.; Zamboni, V.; Bevan, D. R.; Henrissat, B.; Esen, A. The Mechanism of Substrate (Aglycone) Specificity in β-Glucosidases Is Revealed by Crystal Structures of Mutant Maize β-Glucosidase-DIMBOA,-DIMBOAGlc, and-Dhurrin Complexes. *Proc. Natl. Acad. Sci.* **2000**, *97* (25), 13555–13560.

(7) Yu, J.; Zhou, Y.; Tanaka, I.; Yao, M. ROLL: A New Algorithm for the Detection of Protein Pockets and Cavities with a Rolling Probe Sphere. *Bioinformatics* **2010**, *26* (1), 46–52.

(8) Li, Q.; Shah, S. Structure-Based Virtual Screening. In *Protein bioinformatics: From protein modifications and networks to proteomics*; 2017; pp 111–124.

ISBN: 978-978-68-0485-9 DOI: https://doi.org/10.55455/acsnigeria.1.2.92-97

Screening of Ethyl Acetate Fraction of *Ocimum gratissimum* Leaf Methanol Extract for Antioxidant Potentials and Alpha-Amylase and Alpha-Glucosidase Inhibitors

Tajudeen Afolayan Lawal[1]* and Qazeem Oyeniyi Sholadoye[2]
[1]*Department of Biochemistry and Forensic Science, Nigeria Police Academy, Wudil, Kano, Nigeria
[2]Department of Chemistry, Nigeria Police Academy, Wudil, Kano, Nigeria
Corresponding Author's email: lawalat40@gmail.com

ABSTRACT

Type 2 diabetes mellitus (T2DM) is a global health challenge characterised by impaired carbohydrate metabolism and oxidative stress, necessitating safer plant-based therapeutic alternatives. This study evaluated the antidiabetic and antioxidant potential of the ethyl acetate fraction of *Ocimum gratissimum* leaf extract (EAFOGL) using *in vitro* and *in silico* approaches. Enzyme inhibition assays revealed that EAFOGL moderately suppressed α-amylase and α-glucosidase activities, with IC_{50} values of 87.17 ± 5.20 and 49.84 ± 6.72 µg/mL, respectively, relative to acarbose (52.12 ± 2.74 and 40.94 ± 3.44 µg/mL). Antioxidant evaluations demonstrated radical scavenging and metal chelating activities with IC_{50} values of 90.32 ± 9.91 and 98.58 ± 13.29 µg/mL, respectively, which were lower than standard antioxidants but still significant. LC-MS profiling identified five predominant compounds, namely laricresinol, nitrendipine, eupatilin, 6,7-dimethoxy-2-(1-piperazinyl)-4-quinazolinamine, and N-succinoyl anthranilic acid. Molecular docking indicated strong binding affinities of these phytochemicals for α-amylase, α-glucosidase, and the Keap1 protein, with nitrendipine showing notable interactions with α-amylase (−6.91 kcal/mol) and Keap1 (−6.54 kcal/mol), and laricresinol binding effectively to α-glucosidase (−6.98 kcal/mol). Key interactions involved hydrogen bonding and hydrophobic contact with catalytic residues such as His305 and Arg416. In conclusion, EAFOGL exhibited promising dual antidiabetic and antioxidant properties, supporting its potential use in mitigating hyperglycaemia and oxidative stress associated with T2DM. Further in vivo studies and mechanistic investigations are recommended to validate its therapeutic efficacy and establish its safety profile.

KEYWORDS: *Ocimum gratissimum*; Enzyme inhibition; Antioxidant; Molecular docking; Diabetes

1. INTRODUCTION

The increasing global rates of type 2 diabetes mellitus (T2DM) represent a significant public health issue. Characterised by persistent high blood sugar and insulin resistance, T2DM can result in complications such as heart, kidney, and nerve damage. A common treatment approach involves targeting digestive enzymes like α-amylase and α-glucosidase, which facilitate carbohydrate breakdown and glucose absorption, thereby reducing blood sugar spikes after meals.[1,2] Oxidative stress also plays a critical role in T2DM by disrupting insulin signalling and damaging pancreatic β-cells through excessive reactive oxygen species (ROS).[3,4] Consequently, there is an increasing demand for natural substances with antioxidant and enzyme-inhibiting properties.[5] *Ocimum gratissimum* L., known as African basil, has traditional uses in managing diabetes and inflammation.[6] Although crude extracts demonstrate potent bioactivity, investigating the mechanisms of its ethyl acetate fraction offers valuable research opportunities.[7] While acarbose, a synthetic enzyme inhibitor, is effective clinically, it often causes gastrointestinal side effects, leading to growing interest in plant-based alternatives with fewer adverse effects.[8] Redox-modulating capacity is evaluated using antioxidant tests like DPPH and metal chelation assays.[9,10] Phytochemicals in complex extracts are identified via LC-MS, and molecular docking models illustrate how these compounds interact with targets such as α-amylase, α-glucosidase, and Keap1.[12] This study examines the antidiabetic and antioxidant effects of EAEOGL, identifies its phytochemicals through LC-MS, and investigates molecular interactions with key proteins using computer-aided docking analyses.

2. MATERIALS AND METHODS

2.1 Collection, Extraction, and Fractionation of Plants

Fresh leaves of *Ocimum gratissimum* from Bayero University, Nigeria, were authenticated (Voucher No. BUKHAN00306). The leaves were air-dried and ground into a powder, then extracted with 80% methanol (1:10 w/v) via maceration for 72 hours, followed by filtration. The filtrate was concentrated at 40 °C under reduced pressure. The crude extract was partitioned into *n*-hexane, chloroform, ethyl acetate, and *n*-butanol fractions. Based on bioactivity results, the EAFOGL was chosen for further analysis.[7,13]

2.2 Enzyme Inhibition Assays

The inhibitory activity of α-amylase was measured using the DNSA method.[8] Briefly, 250 µL of EAFOGL was mixed with phosphate buffer (pH 6.9) and α-amylase, then incubated before adding a starch solution. After incubation, the DNSA reagent was added, the mixture was boiled, and the absorbance was read at 540 nm. Acarbose served as the positive control. IC_{50} values were calculated using nonlinear regression analysis.[14] To assess α-glucosidase inhibition, 50 µL of EAFOGL was incubated with α-glucosidase in phosphate buffer at 37 °C, then pNPG was added.[15] The reaction was stopped with sodium carbonate, and absorbance was measured at 405 nm, with acarbose as the standard.[16,17]

2.3 Antioxidant Assays

The DPPH assay consisted of mixing 0.1 mM DPPH with different concentrations of EAFOGL.[18] After incubating in the dark for 30 minutes, absorbance was measured at 517 nm, using ascorbic acid as the standard. To evaluate metal chelation, $FeCl_2$ and the ferrozine reagent were used, and the absorbance was recorded at 562 nm, with EDTA serving as the reference standard.[19]

2.4 LC-MS Analysis

Phytochemical profiling was carried out via LC-MS using reverse-phase C18 chromatography in negative ion mode.[11] Mass spectra were matched with MassBank database entries to identify constituents based on m/z values and retention times.

2.5 Molecular Docking Studies

In silico docking of LC-MS-identified compounds was done against α-amylase (PDB: 1HNY), α-glucosidase (4J5T), and Keap1 (4L7B) using MOE 2019.01 software.[20,21] Ligands were sketched with ChemDraw and optimised using MMFF94 in Avogadro.[22] Docking interactions were visualised using Discovery Studio Visualizer (version 10).[23]

2.6 Statistical Analysis

All experiments were performed in triplicate, and the results are shown as the mean ± standard deviation (SD). Statistical analysis was conducted using a one-way ANOVA followed by Tukey's post hoc test with GraphPad Prism version 9.5.1. A significance threshold of $p < 0.05$ was set.

3. RESULTS AND DISCUSSION

3.1 Enzyme Inhibitory Activity of EAFOGL

The EAFOGL exhibited a dose-dependent inhibitory effect on both α-amylase and α-glucosidase enzymes. The recorded IC50 values were 87.17 ± 5.20 µg/mL for α-amylase and 49.84 ± 6.72 µg/mL for α-glucosidase. In comparison, acarbose exhibited IC_{50} values of 52.12 ± 2.74 µg/mL for α-amylase and 40.94 ± 3.44 µg/mL for α-glucosidase (**Figure 1**). Although EAFOGL was found to be less effective than acarbose, the results suggest a moderate level of enzyme inhibition, indicating that it possesses bioactive compounds with potential antidiabetic properties.[15]

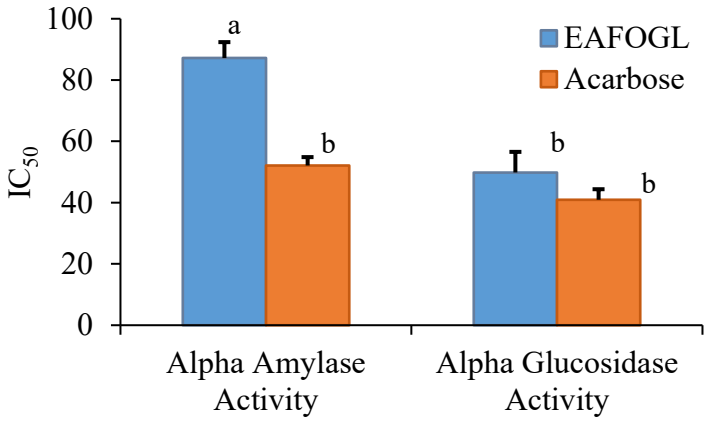

Figure 1: The inhibitory impact of EAFOGL on α-amylase and α-glucosidase.
Note: Bars marked with different letters indicate a statistically significant difference (α=0.05); bars sharing the same letter do not show a significant difference.

3.2 Antioxidant Activity of EAFOGL

EAFOGL showed notable antioxidant activity in both assays. It had IC_{50} values of 90.32 ± 9.91 µg/mL for DPPH scavenging and 98.58 ± 13.29 µg/mL for metal chelation, compared to ascorbic acid (59.07 ± 5.99 µg/mL) and EDTA (70.11 ± 9.34 µg/mL) (**Figure 2**). Though less potent than the standards, the results highlight EAFOGL's capacity to neutralise free radicals and chelate metal ions.[9,10]

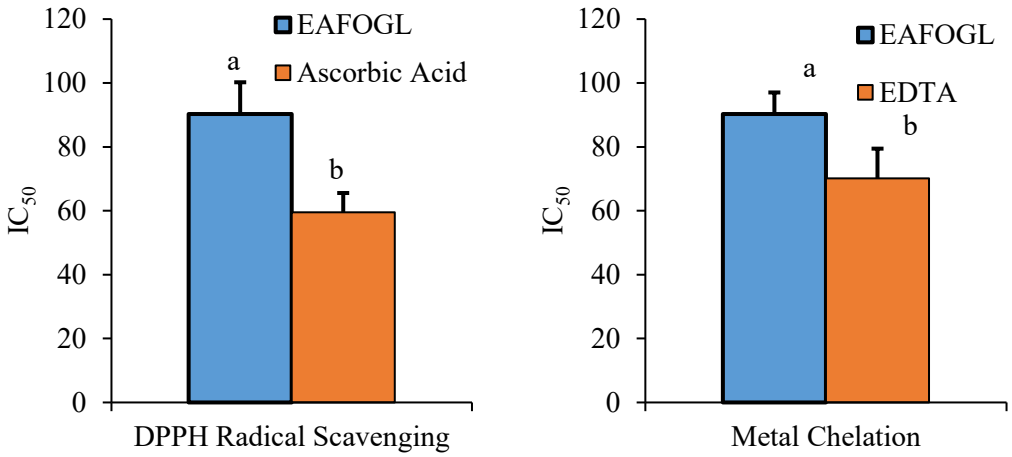

Figure 2: Scavenging Activity against DPPH Radicals and Metal Chelating Ability of EAFOGL
Note: Bars designated with different letters signify statistically significant differences (α = 0.05), whereas bars sharing the same letter indicate no significant differences.

3.3 LC-MS Identification of Bioactive Compounds

LC-MS analysis of EAFOGL tentatively identified five compounds: lariciresinol, nitrendipine, eupatilin, 6,7-dimethoxy-2-(1-piperazinyl)-4-quinazolinamine, and N-succinoyl anthranilic acid (**Table 1, Figure 3**). Identification was based on m/z values and retention times matched against the MassBank database.[11]

Table 1: Result of LC-MS analysis of OGEAF showing MZ (negative mode)

Retention time	Base peak (m/z)	Actual mass	Tentative compound
1.980	359.496	360.496	Lariciresinol
8.475	359.155	360.155	Nitrendipin
10.405	343.893	344.893	Euoatilin
2.605	288.335	289.335	6,7-Dimethoxy-2-(1-piperazinyl)-4-quinazolinamine
6.546	235.684	236.684	N-succinoyl anthranilic acid

NB: Compounds obtained from https://massbank.eu/MassBank/Result.jsp, using MZ in negative mode

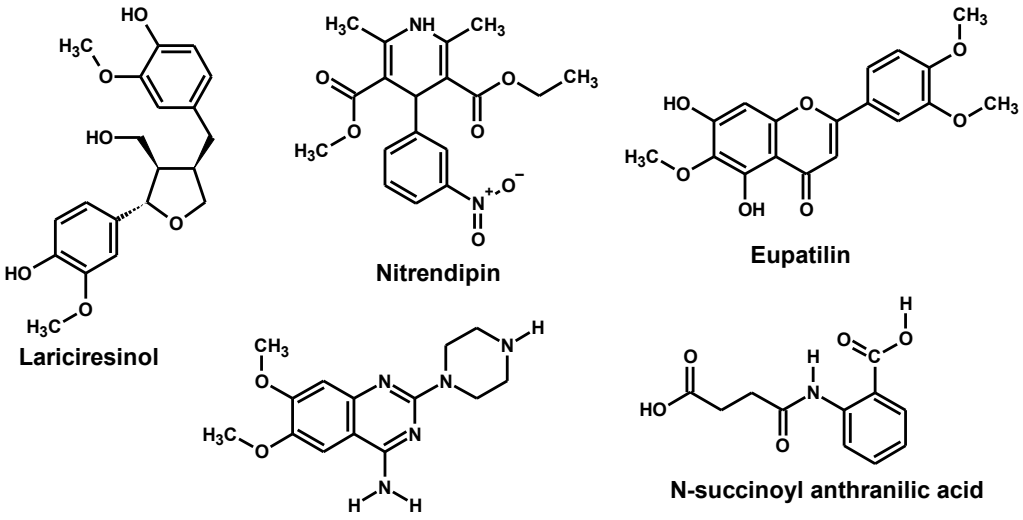

Figure 3: Structures of the Identified Compounds from LC-MS Analysis

3.4 Molecular Docking Analysis

In silico docking analysis demonstrated that nitrendipine and lariciresinol exhibited favourable binding affinities with α-amylase (-6.91 kcal/mol), α-glucosidase (-6.98 kcal/mol), and Keap1 (-6.54 kcal/mol) (**Table 2**). Although slightly weaker than acarbose (-8.63 and -6.53 kcal/mol), the results suggest potential interactions with key antidiabetic and antioxidant targets.[12,16,19]

Table 2: Molecular docking scores of alpha-amylase, alpha-glucosidase, and Keap1 with the ligands

Ligands	α-Amylase	α-Glucosidase	Keap1
6,7-Dimethoxy-2-(1-piperazinyl)-4-quinazolinamine	-5.8232	-6.4801	-5.7186
Eupatilin	-6.4671	-6.40771	-6.2851
Lariciresinol	-6.7305	**-6.9770**	-5.9911
N-succinoyl anthranilic acid	-5.8070	-6.3553	-5.0126
Nitrendipine	**-6.9058**	-6.0953	**-6.5437**
Acarbose*	-8.6252	-6.5282	-
Bardoxolone methyl**	-	-	-6.5186

* Standard control ligand for alpha amylase and alpha-glucosidase proteins
** Standard control ligand for Keap1 protein

The docking uncovered important interactions, including hydrogen bonds, π–π stacking, salt bridges, and hydrophobic interactions. Notably, nitrendipine bound to α-amylase via His305, Arg195, and Glu233, residues also targeted by acarbose.[16]

4. CONCLUSION

EAFOGL demonstrated moderate α-glucosidase and α-amylase inhibition, alongside significant antioxidant activity. LC-MS and molecular docking identified compounds, particularly lariciresinol, nitrendipine, and eupatilin, as likely contributors. The findings suggest EAFOGL may exert dual antidiabetic and antioxidant effects through enzyme inhibition and Nrf2 pathway activation, warranting further pharmacological validation.

CONFLICT OF INTERESTS

The authors declare no conflict of interest.

REFERENCES

(1) International Diabetes Federation. Type 2 Diabetes. https://idf.org/about-diabetes/types-of-diabetes/type-2/ (accessed July 2025).
(2) World Health Organisation. Diabetes Fact Sheet. https://www.who.int/en/news-room/fact-sheets/detail/diabetes (accessed July 2024).
(3) Kasai, S.; Kokubu, D.; Mizukami, H.; Itoh, K. Mitochondrial Reactive Oxygen Species, Insulin Resistance, and Nrf2-Mediated Oxidative Stress Response. Biomolecules 2023, 13 (10), 1544. https://doi.org/10.3390/biom13101544.
(4) Clemente-Suárez, V. J.; Martín-Rodríguez, A.; Beltrán-Velasco, A. I.; Ramos-Campo, D. J.; Tornero-Aguilera, J. F. Functional and Therapeutic Roles of Plant-Derived Antioxidants in Type 2 Diabetes Mellitus. Antioxidants 2025, 14 (6), 725. https://doi.org/10.3390/antiox14060725.
(5) Shirkhan, F.; Mirdamadi, S.; Mirzaei, M.; Akbari Adergani, B.; Nasoohi, N. In Vitro Investigation of Antidiabetic and Antioxidant Properties of Major Prebiotics and Plant-Based Dietary Fibers. J. Diabetes Metab. Disord. 2025, 24 (1), 105. https://doi.org/10.1007/s40200-025-01610-y.
(6) Ogunyemi, O. M.; Adeyeye, E. O.; Macaulay, O. S.; Shonibare, A. O.; Lawal, T. A. Machine Learning-Based QSAR and Molecular Modeling Identify Promising PTP1B Modulators from *Ocimum gratissimum*. Mol. Divers. 2025. https://doi.org/10.1007/s11030-025-11255-x.
(7) Bose, N.; Pal, T. K. Variation of Antioxidant Properties of *Ocimum gratissimum* Leaves with Extraction Methods. Int. J. Front. Life Sci. Res. 2025, 8 (1), 20–29. https://doi.org/10.53294/ijflsr.2025.8.1.0022.
(8) Ali, H.; Houghton, P. J.; Soumyanath, A. α-Amylase Inhibitory Activity of Some Malaysian Plants Used to Treat Diabetes; J. Ethnopharmacol. 2006, 107 (3), 449–455. https://doi.org/10.1016/j.jep.2006.04.004.
(9) Gulcin, İ.; Alwasel, S. H. Metal Ions and Chelators in Antioxidant Assays. Processes 2022, 10 (1), 132. https://doi.org/10.3390/pr10010132.
(10) Gulcin, İ.; Alwasel, S. H. DPPH Radical Scavenging Assay. Processes 2023, 11 (8), 2248. https://doi.org/10.3390/pr11082248.
(11) Etsassala, N. G. E. R.; Badmus, J. A.; Marnewick, J. L.; Egieyeh, S.; Iwuoha, E. I.; Nchu, F.; Hussein, A. A. Antioxidant and Enzyme Inhibitory Properties of Salvia aurita Extracts. Antioxidants 2020, 9 (11), 1149. https://doi.org/10.3390/antiox9111149.
(12) Magaji, Y.; Abdullahi, Z.; Haroun, A. A.; Abdulazeez, M. T.; Okolo, A. A. Structure-Based Docking of Secondary Metabolites Against Diabetes-Related Enzymes. J. Appl. Life Sci. Int. 2022, 25 (3), 40–50. https://doi.org/10.9734/jalsi/2022/v25i330294.
(13) Dev-Sharma, A.; Kaur, I.; Angish, S.; Kumari, K.; Pathania, A.; Sharma, D. Biotechnologia 2022, 103 (2), 131–142. https://doi.org/10.5114/bta.2022.116206.
(14) Motulsky, H.; Christopoulos, A. Fitting Models to Biological Data; Oxford University Press: Oxford, 2004.
(15) Lawal, T. A. Screening of Aqueous Extract of Persea americana Seeds for Alpha-Glucosidase Inhibitors. Biochem. Res. Int. 2022, Article ID 3492203. https://doi.org/10.1155/2022/3492203.
(16) Lawal, T. A.; Sholadoye, Q. O.; Ononamadu, C. J.; Musa, B.; Akinjoko, V. O.; Segba, D. E. Evaluation of Antioxidant and Antidiabetic Properties of Ethyl Acetate Fraction from Anacardium occidentale Leaves, In Vitro and In Silico. Acta Pharma Rep. 2024, 3 (2), 23. https://doi.org/10.51470/APR.2024.03.02.23.
(17) Chiasson, J. L.; Josse, R. G.; Gomis, R.; Hanefeld, M.; Karasik, A.; Laakso, M. Acarbose Treatment and the Risk of Cardiovascular Disease and Hypertension in Patients with Impaired Glucose Tolerance: The STOP-NIDDM Trial. JAMA 2003, 290 (4), 486–494. https://doi.org/10.1001/jama.290.4.486.
(18) Ceriello, A.; Motz, E. Is Oxidative Stress the Pathogenic Mechanism Underlying Insulin Resistance, Diabetes, and Cardiovascular Disease? The Common Soil Hypothesis Revisited. Arterioscler. Thromb. Vasc. Biol. 2004, 24 (5), 816–823. https://doi.org/10.1161/01.ATV.0000122852.22604.78.
(19) Dinis, T. C. P.; Madeira, V. M. C.; Almeida, L. M. Action of Phenolic Derivatives as Inhibitors of Membrane Lipid Peroxidation and as Peroxyl Radical Scavengers. Arch. Biochem. Biophys. 1994, 315 (1), 161–169. https://doi.org/10.1006/abbi.1994.1485.
(20) Tonelli, C.; Chio, I. I. C.; Tuveson, D. A. Transcriptional Regulation by Nrf2. Antioxid. Redox Signal. 2018, 29 (17), 1727–1745. https://doi.org/10.1089/ars.2017.7342.
(21) Chemical Computing Group. MOE (Molecular Operating Environment), Version 2019.01; Chemical Computing Group ULC: Montreal, Canada, 2019. https://www.chemcomp.com.

(22) Hanwell, M. D.; Curtis, D. E.; Lonie, D. C.; Vandermeersch, T.; Zurek, E.; Hutchison, G. R. Avogadro: An Advanced Semantic Chemical Editor, Visualization, and Analysis Platform. J. Cheminform. 2012, 4, 17. https://doi.org/10.1186/1758-2946-4-17.
(23) BIOVIA. Discovery Studio Visualizer, Version 20.1.0.19295; Dassault Systèmes, 2020. https://discover.3ds.com/discovery-studio-visualizer-download.

ISBN: 978-978-68-0485-9 DOI: https://doi.org/10.55455/acsnigeria.1.2.98-101

Chemical Composition Analysis of Essential Oil from the Leaves of *Heliotropium angiospermum*

Peter Ugbeno Omenka[1*], Bilkisu Adedoyin[1], Samuel Ugbedeojo Onuche[1], Hadiza Aminu Isah[2], and Ahmed Umar[1]

[1]Applied Chemistry Research Laboratory, University of Abuja Nigeria.
[2] Department of Chemistry, Nigeria Defense Academy. Kaduna Nigeria
Corresponding Author's email:peterugbeno289@gmail.com

ABSTRACT

Helitropium Angiospermum commonly called scorpion's tail is an herbaceous annual or short lived perennial plant in the family ofBoraginaceae. It is used in traditional medicine for gastrointestinal disorders, inflammation and in some cases, used for cancer-related diseases. This study investigates the chemical composition of essential oil from the leaves of *H. angiospermum*. Gas chromatography-mass spectrometry (GC-MS) analysis was employed to identify andquantify the constituents present in the oil. At least 20 chemical constituents were identified, including hydrocarbons, esters, cyclic siloxanes, unsaturated compounds, fatty acid derivatives, and other compounds. The percentage composition of these constituents varied, with tridecane, 9-octadecene, and cycloheptasiloxane being themost abundant. The presence of diverse chemical constituents suggests that the oil possesses a complex profile with potential implications for its fragrance, therapeutic properties, and other characteristics.

KEYWORDS: *Helitropium angiospermum*, Essential oil, chemical constituents, Octadecene, Tridecane

1. INTRODUCTION

Aromatic plants have a long history of use in traditional medicine due to their preservative and medicinal properties (digestive, diuretic, expectorant andsedative), in foods to impart flavor and aroma, and as antioxidants and antibacterial agents.[1] Several medicinal properties of aromatic plants are found in their essential oils and are related to their composition.[2] Essential oils are plant secondary metabolites characterized by a strong odor and are natural multicomponent systems consisting mainly ofterpenes and volatile hydrocarbons. The chemical profiles of essential oil products differ not only in the number of molecules but also in the stereochemical species obtained.[3] Harvests can vary inquality, quantity and composition depending on climate, soil composition, plant species, age and plant cycle stage.[4,5] Essential oils and their individual volatile components are important compounds for biomedical or pharmaceutical purposes due to their antiseptic and medicinal properties.[2] Some essential oils exhibit specific therapeutic properties that can prevent or even treat certain organ dysfunctions or systemic disorders.[6,7] *Heliotropium angiospermum* commonly known as scorpion's tail is an herbaceous annual or short lived perennial plant in the family of Boraginaceae. It grows about 1 meter tall, with hispid (hairy) stems, alternate lanceolate leaves, and distinctive scorpoid cymes of small white flowers, giving rise to its name.[8] It is used as a traditional remedy for gastrointestinal disorders. A tea made from its leaves is administered to treat colitis, dysentery and diarrhea.[9] The most common application of the plant involves the treatment of inflammatory skin conditions, generalized inflammation, and in some cases, used for cancer-related symptoms.[10] This study therefore seeks to investigate the chemical composition of the essential oil from the leaves of *H. angiospermum.*

2. MATERIALS AND METHODS

2.1 Sample Collection

The leaves of *Heliotropium angiospermum* were collected at the Botanical Garden of Ahmadu Bello University, Zaria, Kaduna State and was authenticated and verified at the Botany division of the Department of Biological Sciences, Ahmadu Bello University Zaria, Kaduna, Nigeria with the identification number; ABU02768.

2.2 Extraction of essential oils

The essential oil was extracted from the fresh leaves of *Heliotropium angiospermum* successively using hydro distillation in a Clevenger-type apparatus for 6 hours, following standard protocol.[11] 2.1kg of the sample was extracted for the first cycle. The distillate, containing the volatile oil, was collected in the apparatus's receiver arm, where it was dissolved in analytical-grade n-hexane. The oil-hexane mixture was then transferred to sample bottles. To preserve the volatile oil, it was stored in sealed

glass vials at 4^{0}C under refrigeration. The experiment was repeated for the second and third cycle using the same amount of fresh sample in each case.

2.3 GC-MS Analysis of the Essential Oil

GC-MS analysis of the oil extract was carried out on an Agilent Technology 7890A GC system coupled to a 5975 VLSMD Mass Spectrometer with aninjector 7683B series device. An Agilent (9091) 413:325 0C column (30 m x320 Nm x 25) was used with helium as carrier gas at a flow rate of3.3245cm3/min. The GC oven was initially programmed at 500^{0}C (hold for 1 min) and finally 3000^{0}C (hold for 5 minutes) at a rate of 8^{0}C/minute while the trial temperature was 37.25^{0}C. For MS, electron impact ionization was achievedwith ionization energy of 70ev. The column heater was set at 250^{0}C while the pressure was 10.143 psi with an average velocity of 66.45 cm/sec andhold–up time of 0.7525 minute was recorded. The oil was diluted with n-hexane and 2µl of diluted sample was injected automatically in the split less mode. Identification of the constituent compounds peaks was made by the Chem-Office software along with the MS-library. The individual constituentswere identified by their retention times identical to the compounds knownfrom the literature data and also by comparing their spectra with those storedin the NIST0.8/Database.

3. RESULTS AND DISCUSSION

3.1 Results

The various chemical constituents present in the essential of *Helitropium angiospermum* leaves are shown in Table 1

Table 1: Essential oil constituents of *H. angiospermum* leaves

S/N	Chemical Constituents	Total percentage constituents (%)	Retention time (mins)
1	Tridecane	3.60	15.006
2	1-Heneicosyl formate	1.06	16.351
3	Decane	2.35	11.579
4	Cyclooctane	1.03	11.722
5	4-Tetradecene, (E)	2.04	16.73
6	3-methyl-decane	3.06	16.803
7	Cycloheptasiloxane	3.66	18.068
8	9-Octadecene	6.28	19.012
9	Cycloeicosane	2.22	23.252
10	11-Octadecenoic acid	3.00	25.28
11	Methyl stearate	2.11	25.678
12	Cyclononasiloxane	1.30	27.332
13	Bis(2-ethylhexyl)phthalate	1.18	29.271
14	Heptasiloxane	1.98	29.323
15	Cannabinol	2.78	29.666
16	Trimethylsilyl ether	2.52	31.795
17	4-Tetradecane	2.04	16.803
18	Cyclopentane	1.14	16.940
19	Heptylcyclohexane	1.50	17.47
20	2,3-Dimercaptobutane-1,4-diol	1.53	19.555

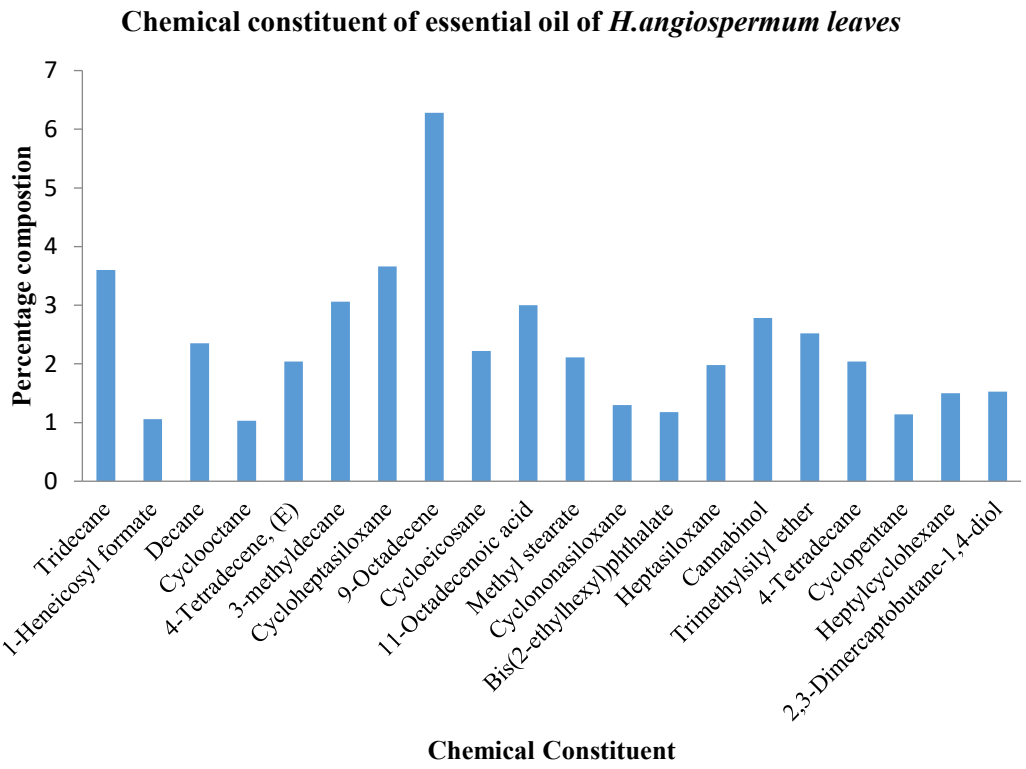

Figure 1: Chemical constituent of essential oil of *H.angiospermum* leaves

3.2 Discussion

GC-MS analysis identified 20 chemical constituents in the essential oil of *Heliotropium angiospermum* leaves, representing a mixture of hydrocarbons, fatty acid derivatives, siloxanes, esters and potentially bioactive compounds. The most abundant constituents were 9-Octadecene (6.28%), Cycloheptasiloxane (3.66%), Tridecane (3.60%), 3-Methyl-decane (3.06%), and 11-Octadecenoic acid (3.00%). These results indicate chemically diverse oil with multiple potential uses.[3] Hydrocarbons like Tridecane and 9-Octadecene contribute to the oil's hydrophobic character and may exhibit insecticidal properties.[3] Fatty acids such as 11-Octadecenoic acid and Methyl stearate are known for their emollient and anti-inflammatory effects.[12] Siloxanes like Cycloheptasiloxane and Cyclononasiloxane are typically attributed to lab contamination, though their detection is not uncommon in GC-MS analysis of natural products.[13] Cannabinol, if present naturally, may suggest anti-inflammatory and neuroprotective effects.[14] The detection of Bis(2-ethylhexyl)phthalate is likely due to laboratory contamination and has known endocrine-disrupting effects.[15] The presence of 2,3-Dimercaptobutane-1,4-diol suggests possible antioxidant or metal-chelating potential.[16]

Essential oils from other *Heliotropium* species, such as *H.indicum*, have shown high levels of phytol, hexadecanoic acid, and terpenoids.[17] In contrast, *H. angiospermum* appears to lack classical terpenoids but contains a variety of alkanes, alkenes and siloxanes, suggesting a distinct chemotype or possible environmental influence on secondary metabolism.
The chemical profile suggests the oil may be usefulin antimicrobial, cosmetic, and possibly therapeutic products.

4. CONCLUSION

GC-MS results confirm a complex chemical composition with promising biological and industrial relevance. The unusual presence of certain compounds like Cannabinol requires further verification. Future research should focus on isolation of active components, and bioactivity testing.

CONFLICT OF INTERESTS

The authors declare no conflict of interests.

REFERENCES

(1) Freitas I.R. and M.G. Cattelan. Antimicrobial and antioxidant properties ofessential oils in food systems—an overview. In: Microbial Contamination andFood Degradation. **2018**

(2) Raut J.S. and S.M. Karuppayil. A status review on the medicinal properties of essential oils. Industrial Crops and Products; **2014**;62:250–264. doi: 10.1016/j. indcrop.2014.05.055.

(3) Bakkali F.; S. Averbeck, D. Averbeck and M. Idaomar. Biological effects of essential oils – A review. *Food and Food Chem Toxicol*; **2008**;46(2):446-75.

(4) Angioni, A., Barra, A., Coroneo, V., Dessi, S., Cabras, P. Chemical composition,seasonal variability, and antifungal activity of Lavandulastoechas L. ssp.stoechas essential oils from stem/leaves and flowers*. J. Agric. Food Chem*. **2006**;54, 4364–4370.

(5) Masotti, V.; Juteau, F.; Bessie`re, J.M.; Viano, J.; Seasonal and phonological variations of the essential oil from the narrow endemic species Artemisiamolinieri and its biological activities*. J. Agric. Food Chem.* **2003**;51, 7115–7121

(6) Buchbauer G. and R. Bohusch.Biological activities of essential oils an update. In:Handbook of Essential Oils: Science, Technology, and Applications. Edit.,BaşerKHCaB, G., **2016**;281–307, CRC Press, Boca Raton, USA.

(7) Asif M., A.H.S. Yehya, S.S. Dahham, S.K. Mohamed,A. Shafaei, M.O. Ezzat *et al*., Establishment of in vitro and in vivo anti-colon cancer efficacy of essentialoils containing oleo-gum resin extract of Mesuaferrea*. Biomedicine & Pharmacotherapy*, **2019**;109, 1620–1629.

(8) NPOST (Native plant society of Texas). *Heliotropium angiospermum* (scorpion-tail heliotrope). Retrieved fromwww.npsot.org/posts/native-plant/heliotropium-angiospermum. **2022**

(9) Backyard nature. Scorpion-Tail Heliotrope: *Heliotropium angiospermum.* Retrieved from www.backyardnature.net/yucatan/heliotro.htm. **2016.**

(10) VillafanaRizo, Y., Garcia Rodriguez, D., Alvarez Gonzalez, .A., & Paz Pena. Traditional knowledge about the use of medicinal plants in santiago de cuba: the case of *Heliotropium angiospermum* murray. *Cuban Journal of Medicinal Plants*, **2024**;13(1), 45-53.

(11) British Pharmacopoeia Commission*.British Pharmacopoeia* (Vol. II). Her Majesty's Stationery Office. **1980**

(12) Tse-Hung H.; Pei-Wen W.; Shih-Chun Y.; Wei-Ling C.; Jia-You F. Cosmetic and therapeutic applications of fish oil's fatty acids on the skin. *Marine Drugs*, **2018** ;16(8):256.doi: 10.3390/md16080256.

(13) Santos, M. R.; Alviano C.S.; Alviano D.S.; Muricy G. Siloxane derivatives in GC-MS: Artifact or constituent? Chromatographia, **2007**;66, 195–200.

(14) Pertwee, R. G. Cannabinoid pharmacology: the first 66 years. *British Journal of Pharmacology*, **2006**;147(S1), S163–S171.

(15) Hauser, R.; Calafat, A. M. Phthalates and human health. Occupational and Environmental Medicine, **2005**;62(11), 806–818.

(16) Forman, H. J.; Zhang H.; Rinna A. Glutathione: overview of its protective roles, measurement, and biosynthesis. *Molecular Aspects of Medicine,* **2009**;30(1-2), 1-12.

(17) Kumar, A.; Ilavarasan R.; Jayachandran T.; Deecaraman M.; *et al*. Phytochemical investigation and GC-MS analysis of *Heliotropiumindicum L*. *International Journal of Pharmaceutical Sciences Review and Research*, **2014**;25(2), 146-150.

ISBN: 978-978-68-0485-9 DOI: https://doi.org/10.55455/acsnigeria.1.2.102-108

Biological and Catalytic Activity of Biosynthesized Iron Nanoparticles (FeNPs) using Aqueous Extract from the Bark of *Antiaris toxicaria*

Thomas Ndidi Asiwe, Atim Sunday Johnson, Idongesit Bassey Anweting and Simon Nzikahyel
Department of Chemistry, University of Uyo, P.M.B 1017, Uyo, Nigeria
Corresponding Author's email: michealasiwe@gmail.com

ABSTRACT

Iron nanoparticles (FeNPs) were synthesized using *Antiaris toxicaria* bark extract as a reducing and stabilizing agent. The FeNPs were analyzed with UV-visible spectroscopy (UV-Vis), Fourier Transform Infrared Spectroscopy (FTIR), X-ray Powder Diffraction (XRD), scanning electron microscopy (SEM), Transmission Electron Microscopy (TEM) and Energy dispersive spectroscopy (EDS). The extract quickly reduced Fe^{2+} to Fe^{0}, forming FeNPs (1–100 nm) with a face-centered cubic structure, confirmed by XRD. UV-Vis showed a surface plasmon resonance peak at 308 nm. FTIR peaks at 3296.3 cm^{-1} (O–H group), 2165.78 cm^{-1} (CH_2 stretching), and 1631.5 cm^{-1} (C=O group) indicated the extract's role in FeNPs formation. The FeNPs showed strong antimicrobial activity, with a 30 mm inhibition zone against *Candida albicans* at 250 mg/mL, and high catalytic activity in degrading brilliant green dye.

KEYWORDS: Iron nanoparticles, *Antiaris toxicaria*, characterization, plant extract, brilliant green.

1. INTRODUCTION

Nanoparticles (NPs), which measure 10^{-9}, exhibit properties very different from bulk materials due to their minute size and increased surface area [1]. They are categorized into two broad groups: organic nanoparticles, which includes fullerenes, and inorganic nanoparticles, including metals like iron and silver or metal oxides such as titanium dioxide [2,3]. As their size decreases, surface area-to-volume ratio increases, making them more chemically reactive. Through chemical modification, nanoparticles are stabilized in suspension, preventing agglomeration and enabling the usage in areas like cancer therapy, water treatment and biosensing [4]. Iron nanoparticles (FeNPs) are especially noteworthy for their strong magnetic behavior and reactivity, which make them useful in drug delivery, antimicrobial treatments, and pollutant degradation [5,4,6]. A sustainable way to produce such particles is green synthesis, that employs extract of plants, microbes, or algae as reducing and stabilizing agents. This method is not only cost-effective but also avoids toxic byproducts. Plant-derived compounds like flavonoids as well as phenols, in particular, play an important role in forming and stabilizing nanoparticles [7].

One promising source is *Antiaris toxicaria*, a tree native to Nigeria and Kenya. The tree bark is found of bioactive molecules like flavonoids, tannins and cardiac glycosides and has traditionally been employed in traditional medicine to relieve chest pain and support mental health [8]. While many other plants have been investigated for producing iron nanoparticles with antimicrobial or environmental-remediation properties, the bark of *A. toxicaria* remains underexplored. This study therefore investigates its use in fabricating FeNPs, characterizing them with UV–Vis, FTIR, XRD, TEM, SEM, and EDS, and evaluating its antimicrobial and catalytic activities. This study not only contributes to green nanotechnology but also highlights an overlooked natural resource with potential medical and environmental applications.

2. MATERIALS AND METHODS

2.1. Materials

Iron (II) chloride tetrahydrate ($FeCl_2.4H_2O$) (97.0%, SureChem), brilliant green (BG) (99.5%, JHD), and hydrogen peroxide (H_2O_2) (99.5%, JHD) were used, all analytical grade. Deionized water was used throughout. *Antiaris toxicaria* bark was collected from Ibiono, Akwa Ibom, Nigeria.

2.2. Extract Preparation

Bark of *A. toxicaria* was rinsed with tap and deionized water, cut and air-dried. Thirty grams (30 g) of powdered bark was boiled in 300 mL deionized water at 80°C for 30 minutes, cooled, and filtered through Whatman No. 1 paper to achieve the extract for nanoparticles synthesis.

2.3. Nanoparticle Synthesis

A modified method [9], 0.099 g $FeCl_2{\cdot}4H_2O$ was dissolved in 250 mL deionized water making a 0.001 M solution, heated at 60°C for 60 mins with stirring. 5 mL of the extract was mixed with 5 mL

precursor solution, stirred until the colour changed from light brown to black, indicating FeNPs formation. The nanoparticles were filtered, washed, oven-dried at 70°C for 2 hours, and stored sealed.

2.4. Characterization

The synthesized nanoparticles were analyzed using UV-Vis spectroscopy (Shimadzu UV-1800, 200–800 nm), FTIR (Perkin Elmer 1750) for functional groups, SEM (JEOL JSM-6610LV) with EDS for elemental composition, TEM (JEOL JEM-2100F, 200 kV) for size and morphology, and XRD (Rigaku Ultima IV, 4–90° 2θ) for crystallinity. Catalytic activity was evaluated with a Unicam Helios spectrophotometer.

2.5. Antimicrobial Activity

The extract and synthesized NPs were tested against *Salmonella* sp., *Staphylococcus aureus*, *Candida albicans*, *Pseudomonas aeruginosa*, and *Aspergillus flavus*. All the organisms were gotten from Department of Microbiology, University of Uyo. Using agar well diffusion, isolates were diluted (10^3 for Gram-positive/fungi, 10^5 for Gram-negative), standardized to 0.5 McFarland (OD 0.008–0.1 at 600 nm), and 0.1 mL spread on Mueller-Hinton agar. 5 mm wells received 0.2 mL extract and FeNPs (150–250 mg/mL). Controls were chloramphenicol (25 mg/mL) and nystatin (40 mg/mL). Bacteria were incubated at 37°C for 24 hours, fungi at 28°C for 72 hours, and inhibition zones measured. MIC was determined by diluting samples, inoculating microbes, and noting the concentration at its lowest preventing growth after 24 to 48 hours.

2.6 Dye Reduction

Catalytic activity was tested by mixing 6 mL 0.1 mM BG with 4 mL 8 mM H_2O_2, measuring absorbance for 10 minutes. Another test combined 6 mL BG, 2 mL FeNP solution, and 2 mL H_2O_2, tracking absorbance with Genesys 50 UV-Vis spectrophotometer.

3. RESULTS AND DISCUSSION

3.1. UV-visible spectroscopy

A colour change of the solution from light brown to black within 60 mins, indicating FeNPs formation. This colour change is likely as a result of surface plasmon resonance (SPR) excitation in FeNPs, driven by the extract's phenolic compounds and Bioactive compounds which reduce iron ions into nanoparticles. UV-Vis spectroscopy confirmed FeNPs synthesis, showing a peak absorbance value at 308 nm (Figure 1), typical of iron's SPR in the ultraviolet region, consistent with reported absorbance at 289 to 320 nm in similar studies [10,11,12].

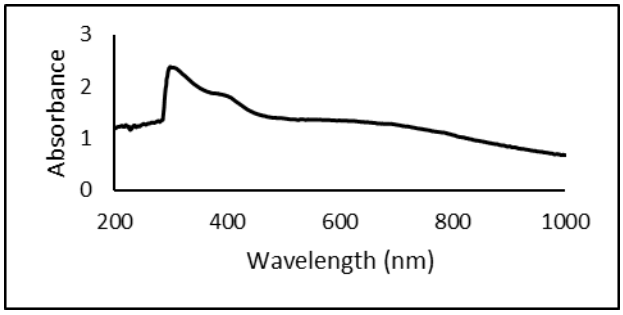

Figure 1. UV- visible spectrum of FeNPs **Source:** Field data

3.2. Energy Dispersive Spectroscopy (EDS) Analysis

The EDS analysis of the synthesized FeNPs, presented iron, oxygen, carbon, and silicon in their percentage composition (Figure 2). These extra elements likely result from the metabolites in the *A. toxicaria* extract employed in the synthesis. Similar results were noted [13] in their study of silver nanoparticles made with *Citrus reticulata* peel extract, where additional elements were also attributed to the plant's bioactive molecules.

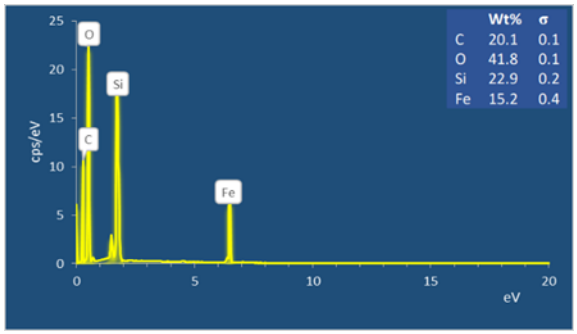

Figure 2. EDS of FeNPs **Source:** Field data

3.3. Fourier Transform-Infrared Radiation (FT-IR) Analysis

In FTIR spectra (Figure 3a for extract, 3b for FeNPs) showed peak shifts with $FeCl_2 \cdot 4H_2O$ to 425.92, 1631.5, 2165.8, and 3296.3 cm^{-1}. The extract's peak at 422.29 cm^{-1} moved to 425.92 cm^{-1}, indicating an O–Fe–O network and ring-opening. A band at 1635.41 cm^{-1} showed C=C stretching in aromatic rings, while 2165.8 cm^{-1} indicated CH_2 as well as C-H alkane groups. O–H stretching in carboxylic acids shifted from 3325.35 cm^{-1} to 3296.3 cm^{-1}, and peaks 402.66, 413.97, and 467.28 cm^{-1} also shifted, suggesting ring-opening. Proteins and flavonoids likely reduced Fe^{2+} to Fe^0 and capped the FeNPs, with flavonoids as primary reducing agents.

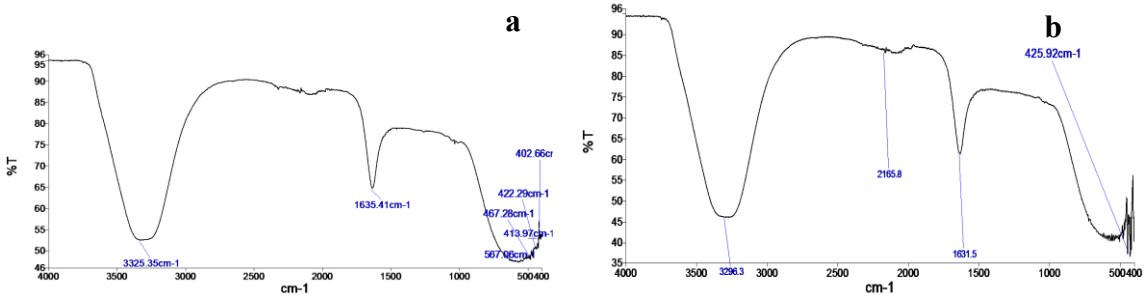

Figure 3. FT-IR spectrum of (a) bark *A. toxicaria* extract and (b) FeNPs **Source:** Field data

3.4. SEM and TEM Analysis

SEM images of the iron nanoparticles (FeNPs), revealed in Figure 4, reveal spherical particles with noticeable clustering, indicating some agglomeration. TEM images (Figure 5) confirm that the FeNPs are mostly spherical, well-dispersed, and homogeneous, though some have irregular shapes. Particle sizes, ranging up to 100 nm aligning with previous studies [14,15]

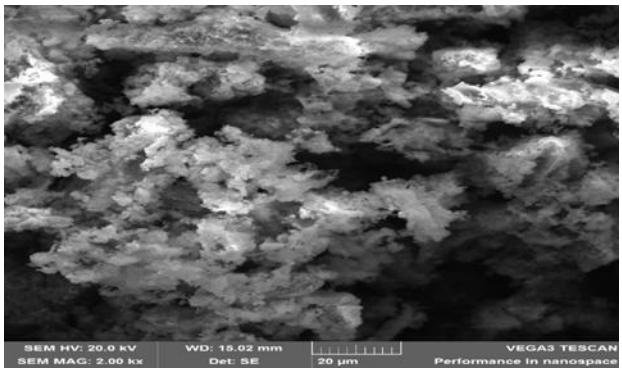

Figure 4. SEM image of FeNPs **Source:** Field data

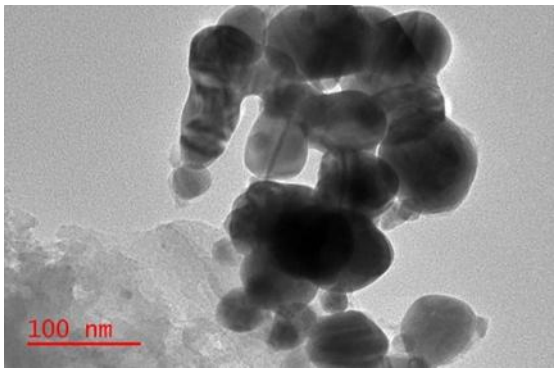

Figure 5. TEM image of FeNPs **Source:** Field data

3.5. X-ray Diffraction

The XRD pattern presents sharp peaks confirming the crystalline nature of the biosynthesized iron nanoparticles (FeNPs). Four distinct peaks at 2θ angles of 33.97°, 44.68°, 47.58°, and 57.4° match the (111), (200), (300), and (330) planes (Figure 6), indicating a face-centered cubic (fcc) structure for iron, consistent with prior studies [16,17]. These results verify the successful green synthesis and high purity of the FeNPs.

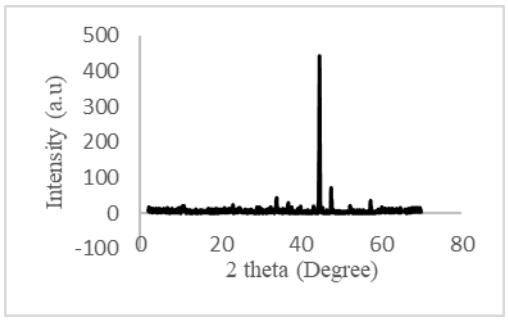

Figure 6. XRD pattern of FeNPs **Source:** Field data

3.6. Antimicrobial Studies

The bark extract of *A. toxicaria* and its iron nanoparticles (FeNPs) were tested for antimicrobial effects by measuring inhibition zones. Tables 1 present the antibacterial and antifungal activities at various concentrations. At 250 mg/mL, the extract inhibited *Staphylococcus aureus, Salmonella sp., Pseudomonas aeruginosa, Candida albicans,* and *Aspergillus flavus* with zones of 22 mm, 27 mm, 20 mm, 21 mm, and 24 mm, respectively. FeNPs showed zones of 28 mm, 23 mm, 20 mm, 30 mm, and 16 mm, respectively. Higher concentrations of both extract and FeNPs increased antimicrobial activity. The standard drug chloramphenicol showed stronger inhibition against bacteria (38 mm, 24 mm, 40 mm for *S. aureus, Salmonella sp.,* and *P. aeruginosa*), while nystatin inhibited *C. albicans (33 mm) and A. flavus* (15 mm). Figure 7 shows the minimum inhibitory concentration (MIC) for both extract and FeNPs, with *S. aureus, C. albicans,* and *A. flavus* showing an MIC of 50 mg/mL. The results are consistent with reports from similar study [18] suggesting that both the extract and FeNPs effectively inhibit microbial growth, likely due to the extract's bioactive compounds and the nanoparticles' large surface area, which may disrupt bacterial cell membranes, increasing permeability and causing cell death.

Table 1: Antimicrobial activity with inhibition zones at different concentration of the bark extract of *A. toxicaria* and FeNPs against test organisms.

Microorganism	Zones of Inhibition (mm) Concentration (mg/mL)						Standard
	A. toxicaria			FeNPs			Chloramphenicol/ Nystatin
	250	200	150	250	200	150	25/40
Stahylococcus aureus	22	19	15	28	22	17	38

Salmonella sp	27	24	20	23	18	15	24
Pseudomonas aeruginosa	20	16	12	20	16	12	40
Candida albicans	21	16	13	30	26	22	33
Aspergillus flavus	24	18	14	16	12	9	15

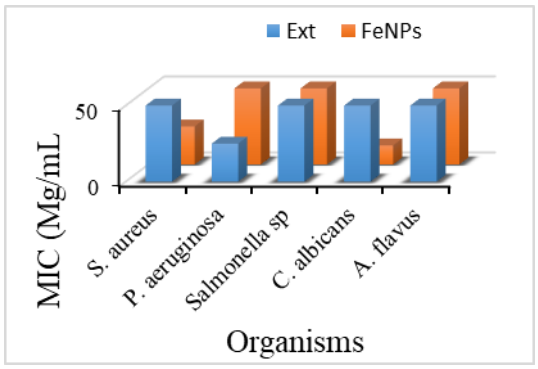

Figure 7. MIC of *A. toxicaria* extract and FeNPs **Source:** Field data

3.7. Catalytic activity of iron nanoparticles

Pure BG dye, with a λmax of 625 nm, changed from deep green to colorless over 10-minute intervals, indicating degradation (Figure 8). FeNPs facilitated this by acting as a redox catalyst, transferring electrons between hydrogen peroxide and BG. The absorption spectrum showed decreasing BG peaks and increasing FeNP peaks over time, with the dye's absorbance nearing baseline. UV spectra revealed an FeNP SPR band after 10 minutes (Figure 8a). Without FeNPs, H_2O_2 degraded BG slowly, with minimal absorbance reduction (Figure 8b). With FeNPs, absorbance dropped significantly, showing faster degradation. A plot of Log (At - A∞) versus time (Figure 9) indicated pseudo-first-order kinetics for BG degradation, given excess H_2O_2. The rate constant for H_2O_2 alone was 0.023 min^{-1}, while FeNPs increased it to 0.226 min^{-1}, demonstrating superior catalytic efficiency as similar report was reported [19]

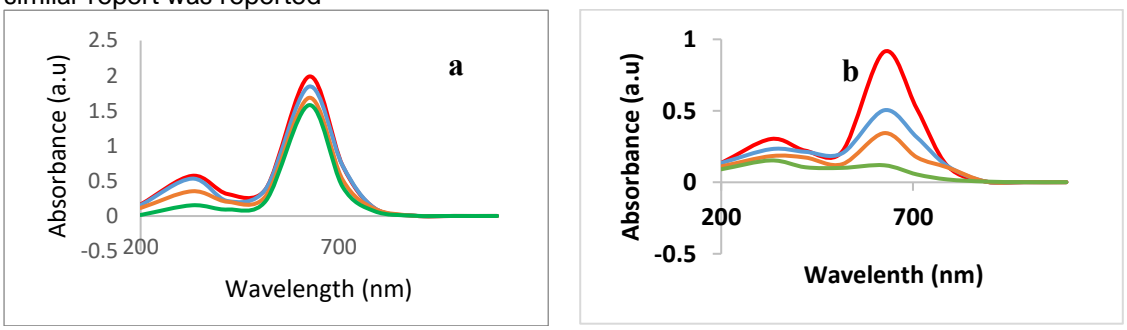

Figure 8. Reduction of BG dye with of H_2O_2 and (a) absence of FeNPs (b) presence of FeNPs **Source: Field data**

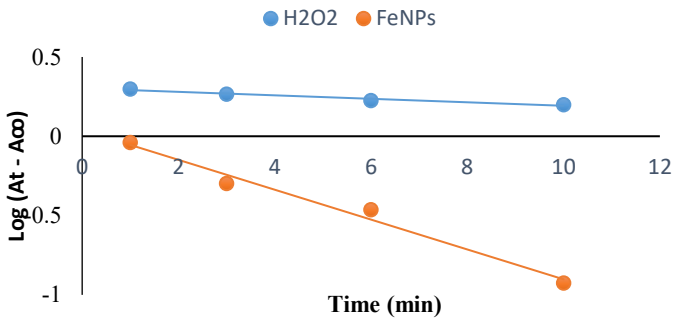

Figure 9. Plots for the degradation reaction of BG by H_2O_2 and FeNPs
Source: Field data

4. CONCLUSION

Iron nanoparticles were successfully synthesized using *A. toxicaria* bark extract, which served as both a reducing and stabilizing agent. The particles (1–100 nm) formed a stable cubic structure and showed strong antimicrobial activity, with a 30 mm inhibition zone against *Candida albicans*. They also degraded Brilliant Green dye effectively, highlighting their promise for both infection control and environmental cleanup. Further research is needed to fully explore their potential.

ACKNOWLEDGEMENTS

We wish to sincerely appreciate the financial assistance granted us by the Tertiary Education Trust Fund (TETFUND) through the Management of the University of Uyo, Uyo for this research.

CONFLICT OF INTERESTS

The authors declare no conflict of interests.

REFERENCES

(1) Khan, I.; Saeed, K.; Khan, I. Nanoparticles: Properties, Applications and Toxicities. *Arab. J. Chem.* **2019**, *12* (7), 908–931.

(2) Johnson, A.; Uwa, P. Eco-Friendly Synthesis of Iron Nanoparticles Using *Uvaria chamae*: Characterisation and Biological Activity. *Inorg. Nano-Met. Chem.* **2019**, 49 (12), 431–442.

(3) Ituen, E.; Ekemini, E.; Yuanhua, L.; Singh, A. Green Synthesis of *Citrus reticulata* Peels Extract Silver Nanoparticles and Characterisation of Structural, Biocide and Anticorrosion Properties. *J. Mol. Struct.* **2020**, *1207*, 127819.

(4) Abdellatif, A. A. H.; Alturki, H. N. H.; Tawfeek, H. M. Different Cellulosic Polymers for Synthesising Silver Nanoparticles with Antioxidant and Antibacterial Activities. *Sci. Rep.* **2021**, *11* (1), 84.

(5) Sandhu, Z. A.; Raza, M. A.; Alqurashi, A.; Sajid, S.; Ashraf, S.; Imtiaz, K.; Latif, M. Advances in the Optimization of Fe Nanoparticles: Unlocking Antifungal Properties for Biomedical Applications. *Pharmaceutics* **2024**, *16* (5), 645.

(6) Hariharan, K.; Patel, P.; Mehta, T. Surface Modifications of Gold Nanoparticles: Stabilization and Recent Applications in Cancer Therapy. *Pharm. Dev. Technol.* **2022**, *27* (6), 665–683.

(7) Santhosh, P. B.; Genova, J.; Chamati, H. Green Synthesis of Gold Nanoparticles: An Eco-Friendly Approach. *Chemistry* **2022**, *4* (2), 345–369.

(8) Umdale, S.; Mirgal, A.; Gaikwad, N. Phytoconstituents, Medicinal Uses and Conservation of Upastree (*Antiaris toxicaria* Lesch). In Biodiversity and Genetic Improvement of Medicinal and Aromatic Plants II; Springer Nature Switzerland: *Cham*, **2025**; pp 269–284.

(9) Asiwe, T. N.; Anweting, I. B.; Johnson, A. S.; Simon, N.; Shaibu, S. E. Eco-Friendly Synthesis and Characterization of Silver and Zinc Nanoparticles Using Aqueous Extract from the Bark of *Antiaris toxicaria*. *Commun. Phys. Sci.* **2024**, *12* (1), 149–161.

(10) Khan, Y.; Sadia, H.; Ali Shah, S. Z.; Khan, M. N.; Shah, A. A.; Ullah, N.; Khan, M. I. Classification, Synthetic, and Characterization Approaches to Nanoparticles, and Their Applications in Various Fields of Nanotechnology: A Review. *Catalysts* **2022**, *12* (11), 1386.

(11) Subiono, T.; Tavip, M. A. Qualitative and Quantitative Phytochemicals of Leaves, Bark and Roots of *Antiaris toxicaria* Lesch., a Promising Natural Medicinal Plant and Source of Pesticides. *Plant Sci. Today* **2023**, *10* (1), 5–10.

(12) Alsailawi, H. A.; Mudhafar, M.; Hanan, A. H.; Ayat, S. S.; Dhahi, S. J.; Ruaa, K. M.; Raheem, H. A. Phytochemical Screening and Antibacterial Activities of *Antiaris toxicaria* Stem, *Polyalthia rumphii* Leaves and *Polyalthia bullata* Stem Extracts. *AIP Conf. Proc.* **2023**, *2845* (1), AIP Publishing, September.

(13) Rizwan, M.; Shoukat, A.; Ayub, A.; Razzaq, B.; Tahir, M. B. Types and Classification of Nanomaterials. In Nanomaterials: Synthesis, Characterization, Hazards and Safety; *Elsevier*, 2021; pp 31-54

(14) Aderolu, H. A.; Aboaba, O. O.; Aderolu, A. Z.; Abdulwahab, K. O.; Suliman, A. A.; Emmanuel, U. C. Biological Synthesis of Copper Nanoparticles and Its Antimicrobial Potential on Selected Bacteria Food-Borne Pathogens. *Ife J. Sci.* 2021, 23 (1), 11–21.

(15) Borah, R.; Ag, K. R.; Minja, A. C.; Verbruggen, S. W. A Review on Self-Assembly of Colloidal Nanoparticles into Clusters, Patterns, and Films: Emerging Synthesis Techniques and Applications. *Small Methods* **2023**, 7 (6), 2201536.

(16) Sreelekha, E.; George, B.; Shyam, A.; Sajina, N.; Mathew, B. A Comparative Study on the Synthesis, Characterisation, and Antioxidant Activity of Green and Chemically Synthesised Silver Nanoparticles. *BioNanoScience* **2021**, *11*, 489–496.

ISBN: 978-978-68-0485-9 DOI: https://doi.org/10.55455/acsnigeria.1.2.109-113

AI-Integrated Chemistry Solutions for Sustainable Plastic Waste Management

[a]Enebi Estella Jasper, [b]Oteiva Mokie Frank, [c]Jude Chinedu Onwuka, and [d]Adeiza Jesse Omeiza

[a] Department of Chemical Sciences, Dennis Osadebay University, Asaba, Delta State.
[b] QAQC Department, INDORAMA-Eleme Petrochemicals Ltd, Port-Harcourt, Rivers State.
[c]Department of Science Lab. Tech, Federal University of Lafia, Nasarawa State.
[d] Department of Chemistry, Federal University of Lafia, Nasarawa State.
Corresponding Author's email: enebi.jasper@dou.edu.ng

ABSTRACT

One of the biggest environmental problems of the 21st century is plastic pollution. In order to handle the increasing amounts of plastic waste, traditional recycling and waste management techniques are frequently ineffective and insufficient. Artificial Intelligence (AI) has recently become an essential tool for enhancing recycling effectiveness, managing plastic waste, and creating sustainable plastic substitutes. With an emphasis on AI-enhanced recycling procedures, the expansion of recycling technologies, and the creation of biodegradable plastic substitutes, this paper examines the current status of AI-driven chemistry solutions in plastic waste management. The practical uses of AI in this field are highlighted by real-world case studies, which further illustrate how AI has the potential to completely transform the plastic waste management sector.

KEYWORDS: Plastic pollution, Artificial Intelligence (AI), Recycling, Sustainable, Biodegradable

1. INTRODUCTION

Plastics have a significant impact on modern life due to their durability, affordability, and versatility. However, for most of these same reasons, they have become recalcitrant and environmentally persistent. Globally, over 450 million tonnes of plastic are produced annually, with less than ten percent being effectively recycled.[1] The rest is either incinerated, dumped in landfills, or spills into the environment, where it continues to persist, contaminating soil and water, threatening aquatic life, obstructing drainage, affecting human health, and causing a host of other negative consequences. Incineration and photodegradation of these plastics release toxic fumes into the air, with degradation products traveling along the food chain, contributing to bioaccumulation in humans and resulting in a variety of health issues, including cancer.[2]

Conventional recycling methods, such as mechanical and chemical recycling, are inadequate and have a number of drawbacks.[3] For instance, sorting errors and high operational costs characterize mechanical recycling, which is the most common method.[5] Mechanical sorting also often renders sorted plastics non-recyclable.[5] Chemical recycling methods, on the other hand, which offer an alternative by breaking plastics down to monomers through pyrolysis, polymerization, and solvolysis, usually require a lot of energy and are not economical on a small scale.[6] Additionally, it produces secondary waste that could be harmful to the environment. It is based on the drawbacks of these conventional methods that artificial intelligence (AI), is being explored as a sustainable method for addressing plastic pollution more effectively. There is a global need for innovative solutions to the problem of plastic pollution, especially as increasing production and use continue to outweigh recycling and upscaling, thereby translating into a steady increase in plastic waste.

Artificial Intelligence (AI), with its ability to recognize patterns and make data-driven decisions, offers promising avenues for improving plastic waste management. When integrated with chemistry, AI can accelerate the design of sustainable materials, optimize degradation pathways, and transform recycling and policy systems. This review highlights the emerging integration of Artificial Intelligence (AI) with chemistry in tackling the global challenge of plastic pollution. Unlike conventional recycling-focused discussions, it further emphasizes AI-driven innovations in sustainable material design, optimization of plastic degradation pathways, and improvements in stages of waste management. It aims to provide a comprehensive synthesis of recent advances, identify knowledge gaps, and outline potential directions for future research. The scope encompasses AI applications in plastic detection, sorting, recycling, biodegradation, and sustainable alternatives, providing an all-encompassing view of how AI and chemistry can transform global strategies for mitigating plastic pollution.

2. THE CHEMISTRY OF PLASTIC WASTE

Plastic waste originates from synthetic polymers that are primarily derived from petrochemicals. Common examples, such as polyethylene (PE), polystyrene (PS), polypropylene (PP), and polyvinyl chloride(PVC) (Fig. 1), among others, are designed to be durable, hydrophobic, and chemically inert, which makes it difficult for them to degrade naturally.[7] When disposed of into the environment, these wastes are fragmented under UV radiation and mechanical stress, forming micro-and nanoplastics which retain the properties of the parent polymer.

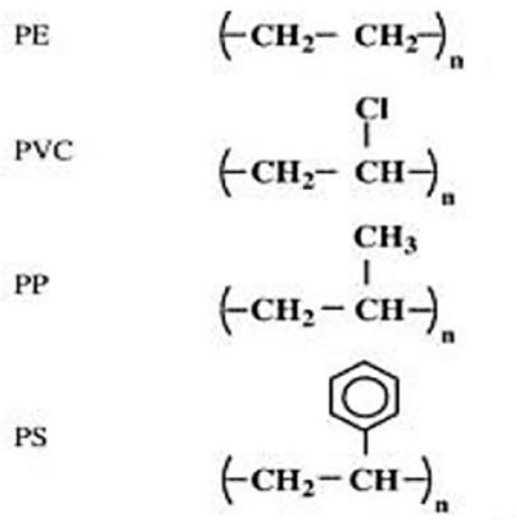

Fig 1: Common petrochemical-derived plastics (synthetic polymers) showing their repeating structural units

These fragments persist in the ecosystem for several years, constituting a nuisance. Understanding the chemistry of plastic waste is crucial for determining its risks and for developing effective mitigation strategies to address plastic pollution. With advances in data analytics and computational chemistry, AI is being harnessed to transform the sorting, recycling, and redesigning of plastic waste for a sustainable future.

3. APPLICATIONS OF AI IN PLASTIC WASTE MANAGEMENT

AI provides powerful tools for addressing inefficiencies in the plastic waste lifecycle. Innovative AI-driven applications have been incorporated into critical stages of plastic pollution management, including sorting, recycling, and redesign. In sorting, AI-enabled robotic systems equipped with computer vision and sensor technologies have significantly improved the accuracy and speed of plastic classification. These systems analyze differences in color, composition, and shape in real time. AI-enabled robotic systems, such as those developed by AMP Robotics in the United States, use computer vision and deep learning to identify and sort different plastic types with high precision. The AMP Cortex system outperforms human workers by using deep learning to identify and sort up to 80 items per minute with over 95% accuracy.[8] A Finnish company, ZenRobotics, also uses AI-driven sorting to distinguish various polymer types using near-infrared spectroscopy (NIR), enhancing material recovery rates.[9] Systems like TOMRA's GAINnext™ combine hyperspectral imaging and convolutional neural networks (CNNs) to distinguish between polymers such as polyethylene terephthalate (PET) and high-density polyethylene (HDPE), facilitating more effective separation and cleaner recycling streams.[10] This level of sorting precision is vital for chemical recycling processes, where contamination can significantly hinder material recovery.

In the domain of recycling, AI has helped to optimize reaction processes such as pyrolysis and depolymerization by adjusting factors that influence these processes, thus resulting in improved yield and energy efficiency. For instance, AI models can dynamically control reactor conditions and simulate reaction mechanisms to maximize depolymerization output for plastics like PET and polystyrene.[11] Catalysts have also been designed using machine learning (ML) to predict structure-reactivity relationships in mixed polymer streams for deconstructing and upcycling plastic waste.[12] Notably, AI–

guided computational modelingusing ML was instrumental in engineering hydrolases to depolymerise polyethylene terephthalate (PET). This research by Lu *et al*.[13] overcomes the challenge of recycling multicolored mixed PET products. Samsara Eco, an Australian climate technology company, has also developed enzyme-based recycling methods that are capable of breaking down nylon 6 and PET for unlimited reuse, offering a potential breakthrough in circular plastics.[14] Likewise, BASF's ChemCycling project utilizes AI-driven simulations to optimize the chemical recycling of mixed plastic waste, ensuring high yield and minimal byproducts.[15]

Concerning the redesign of sustainable plastics, AI is driving transformation by streamlining the discovery and optimization of environmentally friendly plastics. Through powerful simulations and predictive modeling, AI facilitates the design of materials such as polyhydroxyalkanoates (PHAs), polylactic acid (PLA), and other biodegradable nanocomposites tailored for durability and end-of-life degradation[16,17]. Collaboration between government, academia, and industry has been central to accelerating these innovations. In the United States, the BOTTLE (Bio-Optimized Technologies to keep Thermoplastics out of Landfills and the Environment) Consortium, launched by the U.S. Department of Energy, exemplifies public-private partnerships that leverage AI in plastic redesign. Using machine learning, robotics, and enzyme modeling, BOTTLE designs innovative plastics that are easier to recycle, thereby promoting circularity and material recovery.[18] Industries such as Danimer Scientific use AI-guided fermentation analytics to boost microbial production of polyhydroxylalkanoates (PHAs)—bioplastics derived from renewable feedstocks such as canola oil.[19] These redesign innovations, driven by AI, highlight a clear pathway toward closed-loop plastic economies.

5. CHALLENGES, LIMITATIONS, AND ETHICAL CONSIDERATIONS

Despite being a promising tool, AI's application to plastic waste management faces a lot of drawbacks, one of which is a lack of high-quality datasets on polymer behavior and properties. Model interpretability is another challenge, as many AI systems function as "black boxes," making predictions without offering precise justifications. This makes regulatory approval more difficult and diminishes stakeholder trust.[20] Furthermore, its use in low-income countries is limited by the poor distribution of technological infrastructure and a lower level of AI literacy.[21,22] Ethical concerns such as the risk of displacing human workers through automation, biases in training data, and the environmental costs of AI itself, particularly the energy demands of large-scale deep learning models, need to be taken into consideration.

6. CONCLUSION AND FUTURE DIRECTIONS

Plastic waste pollution presents one of the most persistent environmental crises of our time, threatening ecosystems, human health, and the sustainability of global development. Traditional waste management approaches have proven insufficient in mitigating the scale and complexity of plastic pollution. However, the integration of Artificial Intelligence and chemistry holds immense promise for transforming plastic waste from an environmental burden into a resource for innovation. By enabling smarter material design, real-time waste tracking, and optimized recycling processes, AI enhances the capabilities of chemistry in addressing one of the most pressing sustainability challenges of our time. However, realizing this potential requires addressing data, infrastructure, and ethical constraints through inclusive and interdisciplinary collaboration. With sustained investment and coordinated action, AI-integrated chemistry can catalyze a shift toward a more circular and sustainable plastics economy.

CONFLICT OF INTERESTS

The authors declare no conflict of interest.

REFERENCES

(1) UNEP. *Turning off the Tap: How the World Can End Plastic Pollution and Create a Circular Economy*; United Nations Environment Programme, **2023**. https://www.unep.org

(2) Carbery, M.; O'Connor, W.; Thavamani, P. Trophic transfer of microplastics and mixed contaminants in the marine food web and implications for human health. *Environ. Int.* **2018,** *115*, 400–409. https://doi.org/10.1016/j.envint.2018.03.007

(3) Siddiqua, A.; Hahladakis, J.N.; Al-Attiya, W.A.K. An overview of the environmental pollution and health effects associated with waste landfilling and open dumping. *Environ. Sci. Pollut. Res.* **2022,** *29*, 58514–58536.

(4) Van Camp, N.; Lase, I.S.; De Meester, S.; Hoozée, S.; Ragaert, K. Exposing the pitfalls of plastics mechanical recycling through cost calculation. *Waste Manag.* **2024**. https://doi.org/10.1016/j.wasman.2024.08.017

(5) Ragaert, K.; Delva, L.; Van Geem, K. Mechanical and chemical recycling of solid plastic waste. *Waste Manag.* **2017**, *69*, 24–58. https://doi.org/10.1016/j.wasman.2017.07.044

(6) Harasymchuk, I.; Kočí, V.; Vitvarová, M. Chemical recycling: comprehensive overview of methods and technologies. *Int. J. Sustain. Eng.* **2024**, *17* (1), 124–148. https://doi.org/10.1080/19397038.2024.2409162

(7) Saxena, N.; Srivastava, N.; Ibrahim, A.S.; Kumar, R. Chemistry in plastic recycling: Breaking down polymers. In *Waste Management for Smart Cities*; Jain, P., Yadav, S.K., Priyadarshini, I., Eds.; Springer: Singapore, **2025**; pp 67–80. https://doi.org/10.1007/978-981-97-8253-6_3

(8) Waste Today. AMP releases Cortex C robotics system. *Waste Today Magazine*; May 2, **2023**. https://www.wastetodaymagazine.com/news/amp-releases-cortex-c-robotics-system/

(9) ZenRobotics. *ZenRobotics Launches Fourth Generation of Waste Sorting Robots*; February 12, **2023**.https://www.terex.com/zenrobotics/about-us/news/zenrobotics-launch-fourth-generation-of-waste-sorting-robots

(10) TOMRA. *GAINnext™ – Deep Learning in Waste Sorting*; TOMRA, **2023**. https://www.tomra.com/en/waste-metal-recycling

(11) Ramesh, S.; Gupta, V.; Basak, S. AI-enhanced plastic pyrolysis: Optimizing process parameters for efficiency and yield. *J. Clean. Prod.* **2023**, *397*, 136718. https://doi.org/10.1016/j.jclepro.2023.136718

(12) Fang, Y.; Wen, Y.; Dai, L.; Wang, C.-H.; You, S.; Li, W. Artificial intelligence in plastic recycling and conversion: A review. *Resour. Conserv. Recycl.* **2025**, 15, 108090. https://doi.org/10.1016/j.resconrec.2024.108090

(13) Lu, H.; Diaz, D.J.; Czarnecki, N.J.; et al. Machine learning-aided engineering of hydrolases for PET depolymerization. *Nature* 2022, *604*, 662–667. https://doi.org/10.1038/s41586-022-04599-z

(14) Samsara Eco. *Samsara Eco Breaks New Ground in Solving the Plastics Crisis*; February 15, **2024**.https://www.samsaraeco.eco/news/samsara-eco-breaks-new-ground-in-solving-the-plastics-crisis

(15) BASF. *BASF Launches ChemCycling in the United States*; Press release, February 21, **2024**. https://www.basf.com/us/en/media/news-releases/2024/02/basf-launches-chemcycling-in-the-united-states-.html

(16) Chen, T.; Pang, Z.; He, S.; et al. Machine intelligence-accelerated discovery of all-natural plastic substitutes. *Nat. Nanotechnol.* **2024**, *19*, 782–791. https://doi.org/10.1038/s41565-024-01635-z

(17) Kuenneth, C.; Lalonde, J.; Marrone, B.L.; Iverson, C.N.; Ramprasad, R.; Pilania, G. *Commun. Mater.* 2022, *3*, 96. https://doi.org/10.1038/s43246-022-00319-2

(18) U.S. Department of Energy. *BOTTLE: Bio-Optimized Technologies to Keep Thermoplastics out of Landfills and the Environment*; **2023**. https://www.energy.gov/eere/bioenergy/bottle-bio-optimized-technologies-keep-thermoplastics-out-landfills-and-environment

(19) Danimer Scientific. *PHA: Beginning of Life*; Danimer Scientific, **2025**. https://danimerscientific.com/pha-beginning-of-life

(20) Mittelstadt, B.D.; Allo, P.; Taddeo, M.; Wachter, S.; Floridi, L. The ethics of algorithms: Mapping the debate. *Big Data Soc.* **2016**, *3* (2). https://doi.org/10.1177/2053951716679679

(21) Solaja, O.M. Harnessing Artificial Intelligence for Human Rights Protection: Advancing Sustainable Plastic Waste Recycling in Nigeria. *J. Public Adm. Finance Law* **2024**, *31*, 433–449.

(22) Metz, C.E.; Balogun, O.A. Role of AI in reducing global plastics use: Predictive analytics for global sustainability. *Glob. J. Eng. Technol. Adv.* **2024**, *21* (2), 57–69.

ISBN: 978-978-68-0485-9 DOI: https://doi.org/10.55455/acsnigeria.1.2.114-126

Eco-friendly Algal-Based Zinc Oxide Nanoparticles for Corrosion Protection of Steel in Acidic Media

Omotola Michael Fayomi[1*], Sonter Camillus Iorumbur[1], James Asamu Akande[2], Idirisu Jibril Limangba[3], and Moses Saviour Iorungwa[1]
[1]Department of Chemistry, Joseph Sarwuan Tarka University, Makurdi.
[2]Department of Chemistry and Biochemistry, Caleb University, Imota Lagos.
[3]Department of Chemistry, Baze University, Abuja.
Corresponding Author's email: omotolafayomi@gmail.com

ABSTRACT

Adding corrosion inhibitor in corrosive medium is one of the effective methods to solve the corrosion of steel materials. Nanomaterials, particularly zinc oxide nanoparticles (ZnO-NPs), have emerged as promising corrosion inhibitor due to their high surface area, reactivity and biocompatibility. The research is based on green synthesis of zinc oxide nanoparticles using *Oedogonium species* aqueous extract, followed by the evaluation of corrosion inhibition on mild steel in 0.5 M HCl aqueous solution. The green synthesized metal oxide nanoparticles were characterized by Scanning Electron Microscopy-Energy-Dispersive X-ray spectroscopy (SEM-EDX), Fourier Transform Infrared Spectroscopy (FT-IR), UV-spectroscopy and powder x-ray diffractometer (PXRD). The formation of zinc oxide nanoparticles was confirmed by the presence of an absorption peak between 410 and 420 nm using UV–visible spectrophotometer. SEM image revealed the average particle size of 15 nm. Elemental component in the nano-particles were determined by EDX and crystallographic structure was monitored by PXRD. Weight loss method was used and revealed a maximum inhibition efficiency of 81% at 0.2g/L, by exposing mild steel samples to corrosive environments in the presence and absence of nanomaterial, the weight loss was calculated over time to determine the effectiveness of the protective layer.

KEYWORDS: Inhibition Efficiency, *Oedogonium sp.*, PXRD, Zinc oxide NPs, weight loss, and Hydrochloric acid

1. INTRODUCTION

Nanotechnology brings together science and engineering to work with materials at incredibly small scales—usually between 1 and 100 nanometers [1]. One area where nanotechnology shows promise is in addressing corrosion, a persistent issue for industries that rely on mild steel. This metal is popular in construction, automotive, and chemical processing due to its strength and low cost, but it doesn't hold up well in acidic environments—such as those found in cleaning processes, pickling, or oil well acid treatments [2].Recent advancements in nanotechnology have opened new avenues for corrosion protection, particularly through the development of high-performance coatings, self-healing materials, and nanoalloys. For example, nanocoatings have proven effective in shielding steel pipelines from harsh, corrosive environments by enhancing surface durability [3]. Zinc oxide nanoparticles (ZnO NPs) have gained considerable attention as effective corrosion inhibitors, largely due to their high surface area, chemical reactivity, and biocompatibility [4]. Among metal oxide nanoparticles (MO-NPs), ZnO stands out for its multifunctional protective mechanisms. One of the primary modes of protection involves the formation of a compact, adherent layer on the metal surface, serving as a physical barrier that limits exposure to corrosive agents like moisture, oxygen, and chloride ions [5]. Their electrocatalytic properties can further inhibit cathodic reactions by restricting oxygen diffusion, while hydrophobic coatings derived from these materials help reduce water ingress—an essential factor in corrosion prevention [6]. Due to these multifunctional attributes, ZnO NPs coatings are widely utilized in industries where corrosion resistance is critical. The nanoparticles' ability to form dense, uniform layers enhances both the durability and protective capability of coatings, while their photocatalytic behaviour supports broader applications in self-cleaning materials, pollution control, and solar energy systems [7]. Despite their effectiveness, conventional methods for synthesizing nanoparticles—such as laser ablation [8] and thermal decomposition [9] —are often costly, energy-intensive, and carry environmental and safety concerns. As a result, there has been a growing shift toward more sustainable and affordable synthesis techniques over the past decade. Among these, biosynthesis has emerged as a particularly promising alternative. This method relies on naturally derived biological materials, including plant extracts [10], algae [11], fungi [12], and yeast [13], to reduce metal salts and facilitate nanoparticle formation.

Green algae have gained attention as an effective and sustainable source for synthesizing zinc oxide nanoparticles (ZnO NPs), owing to their abundance of bioactive compounds such as phenols, flavonoids, and proteins. These natural components play a key role in reducing and stabilizing metal precursors during nanoparticle formation. Unlike traditional synthesis methods—such as sol-gel [14] and chemical vapour deposition [15] —which tend to be costly, resource-heavy, and environmentally harmful the green synthesis route offers a cleaner, more energy-efficient alternative. Recent studies have shown that ZnO NPs synthesized from algae species like *Sargassum muticum* possess strong corrosion-inhibiting properties, particularly in acidic conditions. Their nanoscale size and high surface area enable better interaction with corrosive agents enhancing their ability to protect metal surfaces [16].

Meanwhile, the earlier studies demonstrated that green algae extracts alone can effectively inhibit corrosion in acidic media—achieving up to 93% protection on austenitic steel with only 100 ppm [17] and 91% on mild steel at 1M HCl concentrations [18] —there had been little investigation into combining these natural inhibitors with the superior physicochemical properties of nanoparticles. Emerging studies have now confirmed that ZnO nanoparticles synthesized using green algae like *Ulva fasciata* and *Cladophora glomerata* not only retain the eco-friendly characteristics of the plant extract but also significantly enhance the corrosion inhibition of mild steel in acidic environments [19,20]. These biogenically synthesized nanoparticles exhibit high surface area, reactivity, and uniformity—traits that allow them to adsorb effectively onto metal surfaces and form protective barriers. Their integration with algal compounds enhances their stability and performance, offering a dual benefit of sustainability and efficiency in corrosion prevention. This study aims to evaluate the corrosion inhibition performance of zinc oxide nanoparticles (ZnO-NPs) synthesized using the green alga *Oedogonium species* as a natural capping and stabilizing agent. The ZnO-NPs were characterized using standard analytical techniques, and their effectiveness in preventing mild steel corrosion in 0.5 M HCl was assessed through the weight loss method. The goal is to develop a sustainable, eco-friendly alternative to traditional corrosion inhibitors.

2. MATERIALS AND METHODS

2.1. Materials

Zinc nitrate hexahydrate ($Zn(NO_3)_2{\cdot}6H_2O$), sodium hydroxide (NaOH), ethanol 99.9% of analytical grade (Molychem products) were obtained from a commercial dealer and used without any additional reagents. All the glassware was washed with deionized water and oven dried. The green algae, *Oedogonium sp.* were freshly collected from River Benue, Makurdi Nigeria, and were identified in the Department of Botany of Joseph Sarwuan University, Makurdi, Nigeria. The deionized water was used for all the homogenization process.

2.2 Preparation of crude extract

The Green Algae, *Oedogonium sp.*, after collection were severally washed to remove dirt, air-dried for days, pulverized, sieved and stored in an airtight container. For extract preparation 24 g fine powder of *Oedogonium sp.*, was added into 400 mL deionized water. Then it was heated at 60°C for 1 hour. The obtain extract was filtered using filter paper (Whatman no. 1) and stored at 4°C for further use [21].

2.3. Synthesis of ZnO Nanoparticles

The solution of ($Zn(NO_3)_2{\cdot}6H_2O$) was prepared in deionized water. For the preparation of zinc oxide NPs, the flask containing zinc nitrate (11.9g, 0.2M) in 320 mL was reacted with 80 mL of the aqueous *Oedogonium sp.* (algae) Extract the addition of 2M NaOH and stirred using a magnetic stirrer heated at 70°C and stirring was nonstop until a homogenous mixture of the solution was attained. The colour changes from brown solution to pale green paste solution. The product was centrifuged and dried in the oven at 75°C for 48 hours. The particles with brown color obtained were calcined at 500°C for 2 hours in a muffle furnace to give white zinc oxide nanoparticles [22].

2.4 Characterization of Algal-mediated ZnO NPs

The biosynthesized zinc oxide (ZnO) nanoparticles were characterized using UV–Vis, FTIR, XRD, and SEM techniques. UV–Vis spectra were recorded on a JENWAY 6405 spectrophotometer within 200–600 nm to confirm nanoparticle formation. FTIR analysis using an Agilent 630 Cary spectrometer

identified functional groups involved in nanoparticle reduction and stabilization, with spectra obtained from KBr pellets (4% w/w) in the 400–4000 cm^{-1} range.

XRD patterns were collected using a Rigaku Miniflex 600 diffractometer (Cu Kα, λ = 1.5406 Å, 40 kV, 30 mA) to determine crystallinity, lattice parameters, and grain size. Surface morphology and particle distribution were examined with a Phenom ProX SEM, revealing particle structure, porosity, and aggregation behavior of the ZnO nanoparticles.

2.5 Weight Loss Measurement

The corrosion inhibition performance of ZnO nanoparticles on mild steel in 0.5 M HCl solution was evaluated using a gravimetric method, adapted from standard procedures commonly used in corrosion studies [23]. Mild steel coupons were initially cleaned, dried and weighed before being immersed in hydrochloric acid solutions with and without varying concentrations of ZnO nanoparticles at 303 K for a duration of 3 hours. After immersion, the samples were rinsed thoroughly with distilled water and acetone, dried and reweighed to determine the mass loss. All experiments were conducted in triplicate to ensure accuracy and the average values were used to calculate the corrosion rate (C_R), inhibition efficiency (IE %) and surface coverage (θ) were calculated using equations (1), (2), and (3) respectively

$$\text{Corrosion rate } (g/h/cm^2) = \frac{\Delta w}{At} \quad (1)$$

where Δw is the weight loss in milligrams of the coupons before and after in immersion(g), A is the surface area of the metal coupon in (cm^2), t is the period of immersion in hours.

$$\text{Inhibition efficiency (IE \%)} = \left(\frac{W_0 - W_1}{W_0}\right) \times 100 \quad (2)$$

$$\text{Surface Coverage } (\theta) = \left(\frac{W_0 - W_1}{W_0}\right) \quad (3)$$

where W_0 and W_1 represent the weight losses of the steel in the absence and presence of the ZnO nanoparticles, respectively.

The procedure was repeated at temperature values of 303, 313, 323 and 333K.

2.6 Determination of Activation Energy (E_a)

The plot of log C_R against I/T in equation 4 give a slope (5) from which the activation energy E_a was estimated. The Arrhenius equation described the relationship between the corrosion rate (C_R) and temperature (T) [24].

$$logCR = \frac{-E_a}{2.303RT} + \log y \quad (4)$$

$$\text{Slope} = \frac{-E_a}{2.303R} \quad (5)$$

E_a is the activation energy, R is the gas constant, T is the temperature in Kelvin and y is the exponential factor.

2.7 Determination of Enthalpy and Entropy Change

The enthalpy change (ΔH) and entropy change (ΔS) were calculated using the transition state theory. An alternative of the transition theory is the Arrhenius Equation.

$$C_R = \frac{RT}{Nh}\ exp^{\left(\frac{\Delta S}{R}\right)}\ exp^{\left(-\frac{\Delta H}{R}\right)} \quad (6)$$

The linear form of the above equation is

$$Log\frac{CR}{T} = log\frac{R}{Nh} + log\left\{exp\left(\frac{\Delta S}{R}\right)\right\} + log\left[exp\left(-\frac{\Delta H}{RT}\right)\right] \quad (7)$$

Since $Log\ e^x = \frac{x}{ln10}$, equation 7 becomes

$$Log\frac{CR}{T} = log\frac{R}{Nh} + \left(\frac{\Delta S}{ln10}\right) + \left(\frac{-\Delta H}{2.303R}\right) \quad (8)$$

$$Log\frac{CR}{T} = \frac{-\Delta H}{2.303R}\left({}^{1}/_{T}\right) + log\frac{R}{Nh} + \left(\frac{\Delta S}{2.303}\right) \quad (9)$$

Where h, is the plank constant, N is the Avogadro's number ΔS is the entropy change and ΔH is the enthalpy change. The change in enthalpy ΔH and entropy change ΔS were evaluated from the plot of $Log\frac{CR}{T}$ against ${}^{1}/_{T}$.

2.7.1 Adsorption isotherm and adsorption constant

The nature of corrosion inhibition has been deduced in terms of the adsorption characteristics of the inhibitor on how the nanoparticles adsorb on the metal surface. The adsorption isotherm model that best describes the adsorption of Zinc oxide nanoparticles on mild steel in 0.5 M HCl solution was obtained by fitting the concentration and the degree of surface coverage of the inhibitor θ into the various adsorption isotherm models. These isotherms include Langmuir, Freundlich and Tempkin were expressed in their linear form as:

The Langmuir adsorption isotherm model;

$$\frac{C}{\theta} = \frac{1}{K_{ads}} + C \quad (10)$$

Freundlich adsorption isotherm model:

$$\log \theta = \log (K_f) + n\log C \quad (11)$$

Tempkin adsorption isotherm model;

$$\theta = lnC + K_{ads} \quad (12)$$

2.7.2 Determination of adsorption thermodynamics parameters

The expression for Gibb's free energy change of adsorption ΔG_{ads} presented in Equation 9 was used to investigate the feasibility and the nature of the adsorption.

$$\Delta G_{ads} = -RTln(55.5K_{ads}) \quad (13)$$

K_{ads} is the adsorption equilibrium constant obtained from the isotherm and the number 55.5 is the molar concentration of water in solution.

3. RESULTS AND DISCUSSION

3.1 UV/Visible Analysis of ZnO nanoparticles

The UV–Vis spectrum (Figure 1) confirmed the successful biosynthesis of ZnO nanoparticles using *Oedogonium sp.* extract. The extract exhibited a strong band near 232 nm, associated with phytochemicals acting as reducing and stabilizing agents. After synthesis, a distinct peak at ~300 nm appeared, characteristic of ZnO nanoparticles and their excitonic transitions [25]. The absence of this ZnO-specific peak in the pure extract and its appearance in the product clearly demonstrate the role of algal biomolecules in nanoparticle formation.

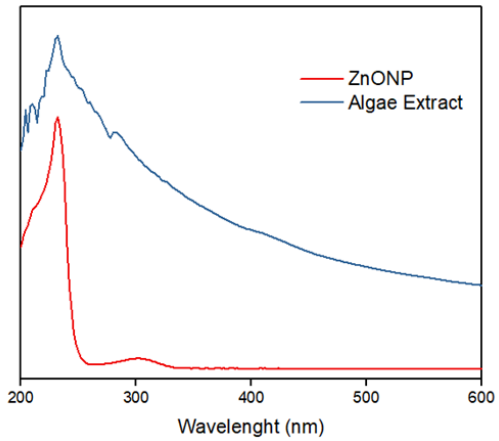

Figure 1: UV-Visible Analysis of ZnO Nanoparticles and the Algae Extract

3.2 Fourier Transform Infra-red (FT-IR) analysis of ZnO nanoparticle:

FTIR analysis was performed to identify the functional groups involved in ZnO nanoparticle formation [26]. As shown in Figure 2, the broad absorption band around 3420–3510 cm^{-1} corresponds to O–H stretching vibrations from surface-adsorbed water or hydroxyl groups, indicating hydrogen bonding with phytochemicals used during green synthesis [27]. Peaks observed below 1000 cm^{-1} are characteristic of Zn–O bond vibrations within the nanoparticle matrix [28]. These features confirm the presence of phytochemical functional groups and the successful formation of Zn–O linkages, which enhance the nanoparticles' surface reactivity and catalytic potential.

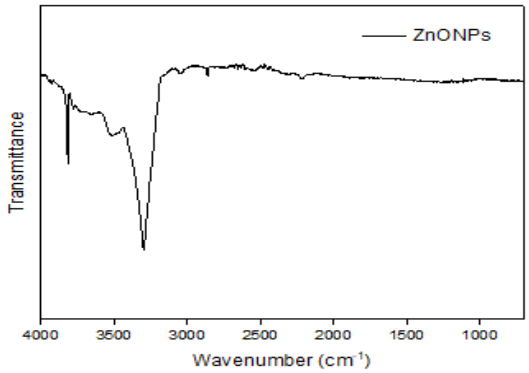

Figure 2: Fourier transform infrared spectrometer (FTIR) Analysis of ZnO Nanoparticles

3.3 Scanning Electron Microscopy (SEM) Analysis of *ZnO Nanoparticles*

Scanning Electron Microscopy (SEM) was used to examine the morphology of the synthesized ZnO nanoparticles (Figure 3). The images revealed rod-shaped structures with well-defined pores, confirming effective nanoparticle formation on the nanocomposite surface. These open pores suggest strong electrostatic interactions between the *Oedogonium sp.* extract and ZnO, supporting their potential effectiveness in corrosion inhibition.

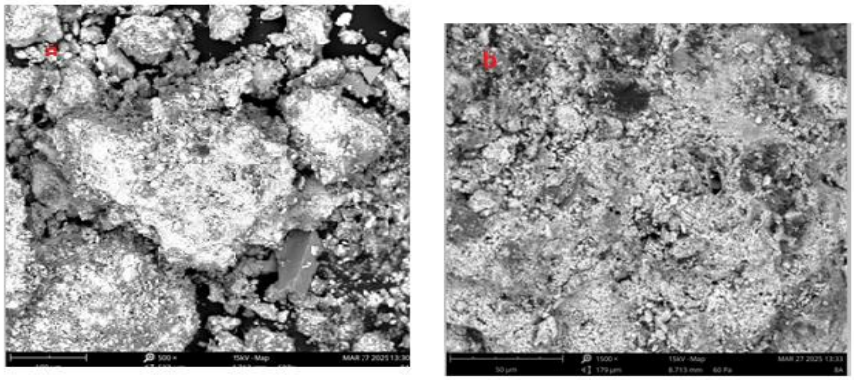

Figure 3: SEM images of Zinc Oxide Nanoparticles derived from *Oedogonium sp.* Extract (a) 5 µm (b) 1 µm

3.4 Energy Dispersive X-Ray Spectroscopy (EDX) analysis

The EDX spectrum (Figure 4) confirmed the formation of pure ZnO nanoparticles, showing dominant Zn Kα/Kβ and O Kα peaks with near-stoichiometric ratios. The absence of major impurity peaks indicates high purity, while a minor carbon signal likely originates from residual biomolecules or carbon tape [29]. Atomic composition revealed Zn (58.24–85.03 wt.%), with small amounts of C (7.07%) and N (3.14%) from algal metabolites acting as capping agents. These results verify the successful green synthesis of ZnO nanoparticles with high compositional purity, supporting their suitability for corrosion inhibition and other applications such as photocatalysis and biomedicine [30,31].

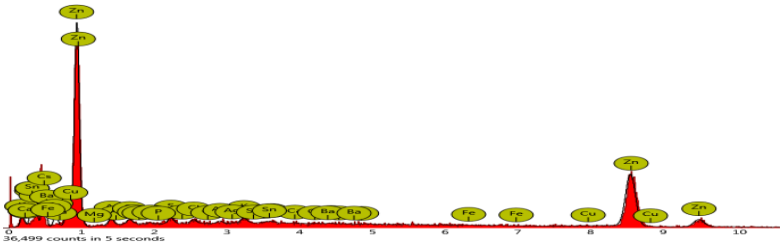

Figure 4: EDX of the Zinc Oxide Nanoparticles

3.5 X-ray diffraction (XRD) Analysis of ZnO Nanoparticle

Figure 5 displays the X-ray diffraction (XRD) spectrum of ZnO nanoparticles. It possesses a high level of crystallinity, illustrated by sharp and intense diffraction peaks. The diffractogram presents major peaks at 2 theta angles of the crystal planes (100), (002), (101), (102), (110), (103), (112), and (201) that correspond to the JCPDS card no. 04-008-8199 and can be used to specify the hexagonal wurtzite structure of ZnO [32]. These peaks are very clear, the highest peak occurring at $2\theta = 36.25^0$ is due to the (101) plane, a typical characteristic of a pure and crystalline nanoparticle of Zn-O [33]. No additional peaks are present, which proves that no secondary phases or impurities present; this indicate phase-pure Zn-O nanocrystals had been created successfully [34].

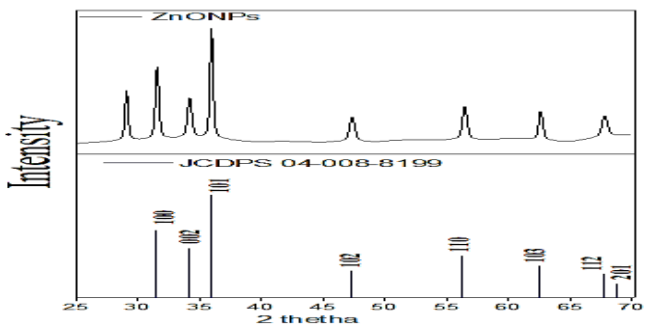

Figure 5: X-ray Diffraction (XRD) pattern of ZnO nanoparticles.

Table 1: Weight Loss (g) of Mild Steel at various concentrations of Algal-mediated Zinc oxide Nanoparticles at different Time Intervals

ZnO NPs conc. (g/L)	**Weight Loss (g)**			
	6 h	24 h	48 h	72 h
Blank	0.137	0.140	0.145	0.148
0.05	0.094	0.084	0.098	0.087
0.10	0.072	0.064	0.076	0.060
0.15	0.058	0.049	0.054	0.042
0.20	0.034	0.023	0.032	0.028

Table 2: Inhibition efficiency of various concentration of Algal-mediated Zinc oxide Nanoparticles at different Time Intervals

ZnO NPs conc. (g/L)	Inhibition Efficiency (%)			
	6 h	24 h	48 h	72 h
0.05	31	40	32	41
0.10	48	54	50	60
0.15	58	65	63	72
0.20	75	80	78	81

The experimental findings (Tables 1–8) confirm that algal-mediated ZnO nanoparticles act as efficient corrosion inhibitors through composition-, time-, and adsorption-dependent mechanisms. Weight loss analysis revealed a clear dose-dependent protection, where increased ZnO concentration reduced mass loss (e.g., 0.15 g/L: 0.042 g vs. 0.20 g/L: 0.028 g after 72 h). Optimal inhibition efficiency, reaching up to 92% in acidic media, was achieved at 0.1 wt% ZnO [35]. The nanoparticles form a protective, chemisorbed layer on the steel surface, blocking active corrosion sites and enhancing adhesion through algal biomolecules. This eco-friendly approach demonstrates superior, sustainable corrosion resistance compared to conventional synthetic inhibitors.

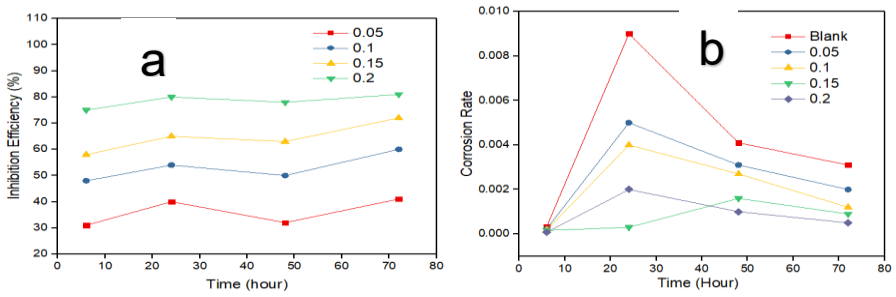

Figure 6: Effect of ZnO-NPs concentrations in 0.5 M HCl at 6 to 72 hours on the (a).inhibitory efficiency (b) corrosion rate

Table 3: Corrosion Rates of Mild Steel at different Time Immersions of Various Algal-mediated Zinc oxide Nanoparticles Concentrations

ZnO NPs conc. (g/L)	**Corrosion rate (g/h/cm²)**			
	6 h	24 h	48 h	72 h
Blank	$3.3x10^{-4}$	$9.0x10^{-3}$	$4.1x10^{-3}$	$3.1\ x10^{-3}$
0.05	$2.3\ x10^{-4}$	$5.0x10^{-3}$	$3.1x10^{-3}$	$2.0\ x10^{-3}$
0.10	$1.8\ x10^{-4}$	$4.0x10^{-3}$	$2.7x10^{-3}$	$1.2x10^{-3}$
0.15	$1.6\ x10^{-4}$	$3.0x10^{-3}$	$1.6x10^{-3}$	$9.0x10^{-4}$
0.20	$8.0\ x10^{-5}$	$2.0x10^{-3}$	$1.0x10^{-3}$	$5.0x10^{-4}$

Table 4: Weight Loss (g) of Mild Steel at various concentrations of Algal-mediated Zinc oxide Nanoparticles at different temperatures

ZnO NPs conc. (g/L)	Weight Loss (g)			
	303 K	313 K	323 K	333 K
Blank	0.138	0.136	0.139	0.141
0.05	0.098	0.098	0.097	0.099
0.10	0.073	0.073	0.059	0.077
0.15	0.059	0.054	0.048	0.056
0.20	0.037	0.037	0.027	0.029

Table 5: Inhibition efficiency of Mild Steel at various concentrations of Algal-mediated Zinc oxide Nanoparticles at different temperatures

ZnO NPs conc. (g/L)	Inhibition efficiency (%)			
	303 K	313 K	323 K	333 K
0.05	29	28	30	30
0.10	47	46	50	45
0.15	57	60	66	60
0.20	73	73	81	80

Algal capping agents such as polysaccharides and proteins promote uniform adsorption of ZnO nanoparticles on steel, forming a protective barrier that blocks active sites and restricts acid diffusion. The concentration-dependent behavior follows the Langmuir isotherm, indicating monolayer adsorption where surface coverage increases with nanoparticle concentration. ZnO NPs inhibit both anodic and cathodic reactions, while at higher temperatures, chemisorption dominates through stable Zn^{2+}–alginate complexes bound to steel heteroatoms (O, N). The rise in inhibition efficiency (IE%) with temperature suggests covalent bonding between algal-functionalized ZnO NPs and steel, consistent with the El-Awady kinetic-thermodynamic model of enhanced inhibitor–metal interactions.

Table 6: Corrosion rates of Mild Steel at various concentration of Algal-mediated Zinc oxide Nanoparticles at different temperature

ZnO NPs conc. (g/L)	Corrosion rate (g/h/cm^2)			
	303 K	313 K	323 K	333 K
Blank	1.06×10^{-3}	1.05×10^{-3}	1.07×10^{-3}	1.08×10^{-3}
0.05	8.3×10^{-4}	8.3×10^{-4}	8.2×10^{-4}	6.64×10^{-4}
0.10	5.3×10^{-4}	5.3×10^{-4}	5.0×10^{-4}	5.6×10^{-4}
0.15	4.4×10^{-4}	4.0×10^{-4}	3.6×10^{-4}	4.2×10^{-4}
0.20	2.5×10^{-4}	2.5×10^{-4}	1.9×10^{-4}	2.0×10^{-4}

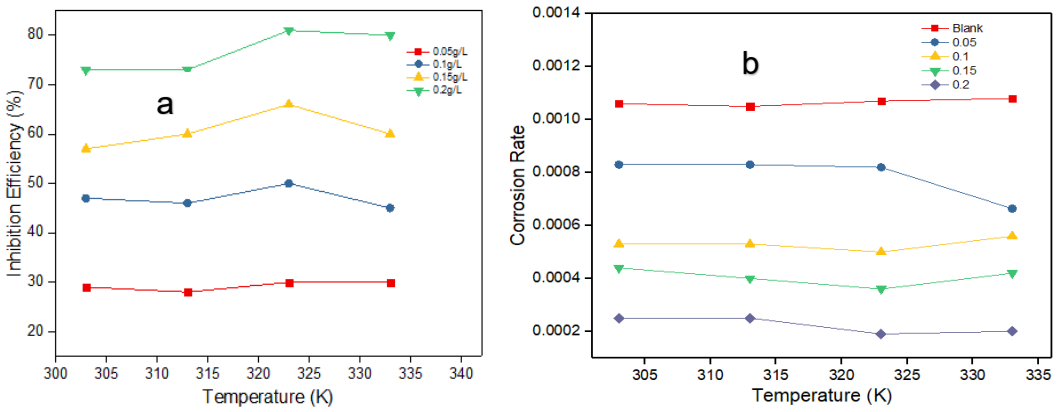

Figure 7: Effect of ZnONPs concentrations in 0.5 M HCl at 303 to 333 K on the (a) inhibitory efficiency (b) corrosion rate

Table 7: Thermodynamic Parameters for the Adsorption of ZnO Nanoparticles on Mild Steel in 0.5 M HCl

ZnONPs (g/L)	E_a (KJ/mol)	ΔH (KJ/mol)	ΔS (J/mol/K)
Blank	0.618	-2.021	-289.543
0.05	5.604	-8.244	-311.696
0.10	0.824	-1.801	-294.655
0.15	-2.183	-4.823	-311.696
0.20	-7.935	-10.578	-329.503

Table 8: Surface Coverage (θ) of ZnO Nanoparticles on Mild Steel at Various Temperatures

ZnO NPs conc.	Surface Coverage (θ)			
(g/L)	303 K	313 K	323 K	333 K
0.05	0.29	0.28	0.30	0.30
0.10	0.47	0.46	0.50	0.45
0.15	0.57	0.60	0.66	0.60
0.20	0.73	0.73	0.81	0.80

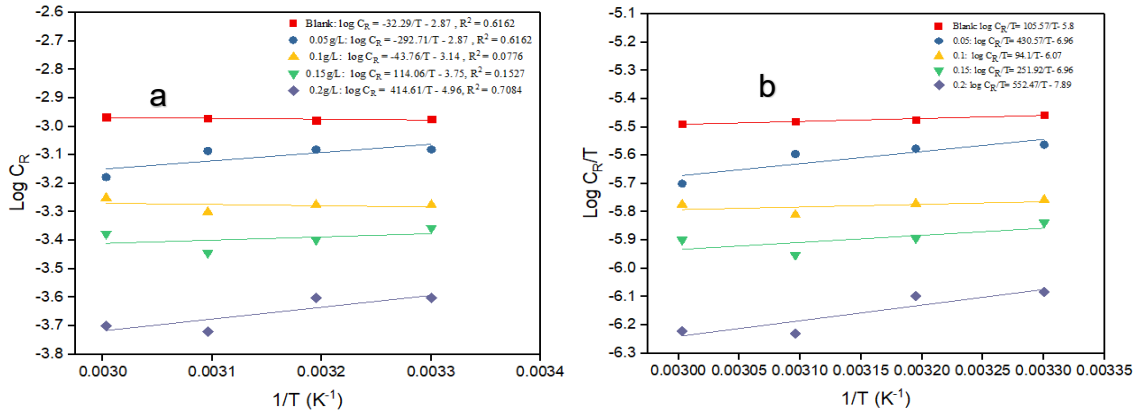

Figure 8: Plots for Determination of Enthalpy and Entropy Change

The thermodynamic results (Table 7) indicate that the adsorption of algal-mediated ZnO nanoparticles on mild steel in 0.5 M HCl is spontaneous and exothermic, as shown by negative activation energy (E_a) and enthalpy change (ΔH). Corrosion rates consistently decreased with increasing ZnO nanoparticle concentration due to thermally stable Zn–alginate complexes that blocked active corrosion sites. A slight rise in corrosion at 333 K suggests minor desorption caused by thermal motion [36]. The transition from positive (+0.62 kJ/mol) to negative Ea values indicates a shift from physical to chemisorption through covalent bonding between algal phenolic groups and iron atoms (Sophie and Antony, 2019). Surface coverage analysis ($R^2 > 0.98$) confirmed monolayer adsorption following the Langmuir model, with the strongest adsorption at 323 K and negative $\Delta G_a d_s$ values confirming spontaneity. Langmuir isotherm best described the adsorption process, while Freundlich and Temkin showed secondary fits. The high $K_a d_s$ (6.5–7.0 M^{-1}) across temperatures further supports strong, stable binding between ZnO NPs and the steel surface [4].

Table 9: Langmuir Isotherm data

Temperature (K)	Intercept	Slope	R^2	K_{ads} (M^{-1})	ΔG_{ads} (kJ/mol)
303K	0.142	0.710	0.989	7.042	-15.035
313K	0.150	0.637	0.989	6.667	-15.388
323K	0.143	0.537	0.987	6.993	-16.008
333K	0.153	0.556	0.933	6.535	-16.317

Table 10: Freundlich Isotherm data

Temperature (K)	Intercept	Slope	R^2	K_f (M^{-1})	ΔG_{ads} (kJ/mol)
303K	0.566	0.426	0.438	1.766	-11.551
313K	0.569	0.429	0.428	1.757	-11.919
323K	0.713	0.148	0.853	1.402	-11.694
333K	0.688	0.146	0.829	1.453	-12.154

Table 11: Tempkin Isotherm data

Temperature	Intercept	Slope	R^2	K	ΔG_{ads} (kJ/mol)
303K	1.179	0.302	0.969	49.599	-0.019
313K	1.219	0.318	0.935	46.216	-0.018
323K	1.361	0.362	0.882	42.934	-0.019
333K	1.293	0.343	0.832	43.366	-0.019

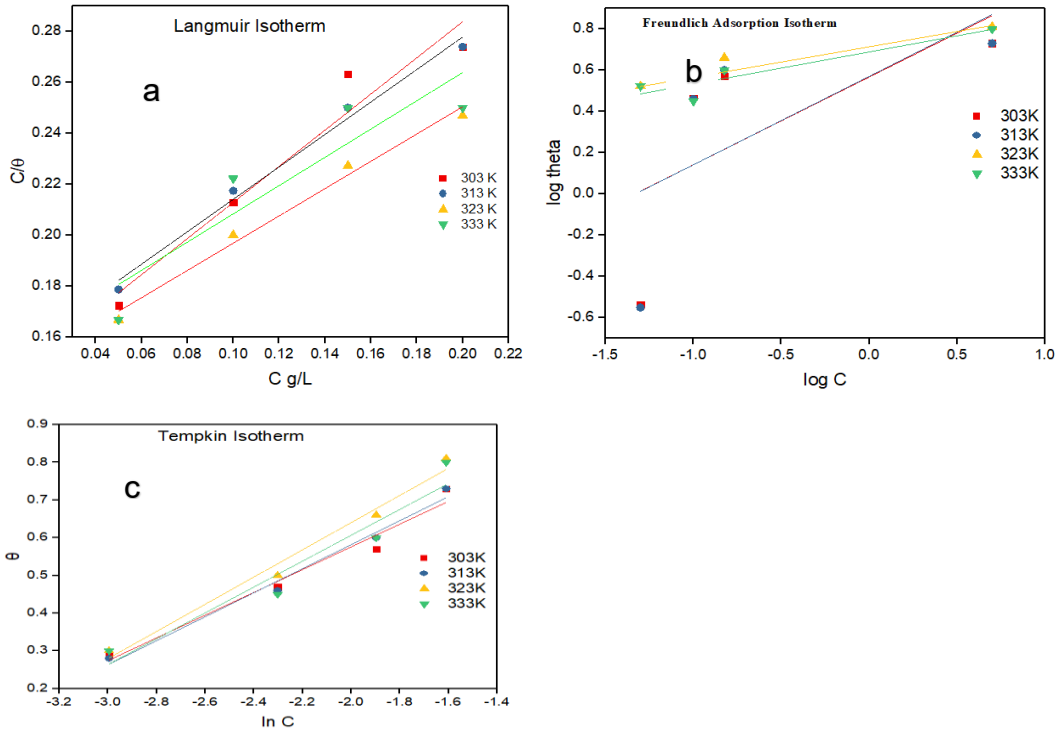

Figure 9: Adsorption isotherms of Algal-mediated ZnO-NPs on the surface of mild steel: (a) Langmuir (b) Freundlich (c) Tempkin

4. CONCLUSION

This study confirms that zinc oxide nanoparticles (ZnO-NPs) can be sustainably synthesized from zinc nitrate hexahydrate using *Oedogonium sp.* extract as a natural reducing and stabilizing agent. Characterization by UV–Vis, FTIR, SEM-EDX, and XRD verified successful nanoparticle formation. Corrosion studies showed that algal-mediated ZnO-NPs effectively protected mild steel in 0.5 M HCl, with inhibition efficiency rising from 73% at 303 K to nearly 80% at 333 K. Adsorption increased with immersion time and followed the Langmuir isotherm, indicating monolayer coverage. Thermodynamic parameters (ΔG°ads, ΔH°ads, ΔS°ads) revealed a spontaneous, exothermic process driven by both chemisorption—via heteroatoms with lone electron pairs—and physisorption through electrostatic attraction. These results highlight green-synthesized ZnO-NPs as promising, eco-friendly corrosion.

CONFLICT OF INTERESTS

The authors declare no conflict of interests.

REFERENCES

(1) Khan, I.; Saeed, K.; Khan, I. Nanoparticles: Properties, applications and toxicities. *Arab. J. Chem.* **2019**, 12, 908–931.

(2) Verma, C.; Olasunkanmi, L. O.; Quadri, T. W.; Sherif, E. S. M.; Ebenso, E. E. Gravimetric, Electrochemical, Surface Morphology, DFT, and Monte Carlo Simulation Studies on Three N-Substituted 2-Aminopyridine Derivatives as Corrosion Inhibitors of Mild Steel in Acidic Medium. *J. Phys. Chem. C* **2018,** 122, 11870–11882.

(3) Shwetha, K.; Praveen, B. M.; Devendra, B. K. A review on corrosion inhibitors: Types, mechanisms, electrochemical analysis, corrosion rate and efficiency of corrosion inhibitors on mild steel in an acidic environment. *Results in Surfaces and Interfaces* **2024**, 16, 100258.

(4) Elebo, A.; Sani, U.; Ekwumemgbo, P. A.; Ajibola, V. O. Green Synthesis and Zinc-Oxide Nanoparticles for Corrosion Inhibition and Modeling Corrosion Inhibition of Mild Steel in HCl Solutions. *Biosens. Nanotheranostics* **2024,** 3, 1-17.

(5) Azmi, H. N. S.; Alam, M. Exploring the Anti-Corrosion, Photocatalytic, and Adsorptive Functionalities of Biogenically Synthesized Zinc Oxide Nanoparticles. *Inorganics* **2024**, 12, 199.

(6) Sampath, S.; Madhavan, Y.; Muralidharan, M.; Sunderam, V.; Lawrance, A.V.; Muthupandian, S. A review on algal mediated synthesis of metal and metal oxide nanoparticles and their emerging biomedical potential. *J. Biotechnol.* **2022**, 360, 92–109.

(7) Gao, H., Li, Q., Dai, Y., Luo, F.; Zhang, H. X. High efficiency corrosion inhibitor 8-hydroxyquinoline and its synergistic effect with sodium dodecylbenzenesulphonate on AZ91D magnesium alloy. *Corros. Sci.* **2010**, 52, 1603–1609.

(8) Amendola, V.; Amans, D.; Ishikawa, Y.; Koshizaki, N.; Scirè, S.; Compagnini, G.; Reichenberger, S.; Barcikowski, S.Room-Temperature Laser Synthesis in Liquid of Oxide, Metal-Oxide Core-Shells, and Doped Oxide Nanoparticles. *Chem. - A Eur. J.* **2020,** 26, 9206–9242.

(9) Patil, S. S.; Kamble, V. S.; Patil, D. K.; Pawara, J. M. Synthesis of Metal Oxide Nanoparticles by Thermal Decomposition of a Ni(II) Complex and its Antimicrobial Activity. *Malaysian J. Chem.* **2022,** 24, 125–131.

(10) Fayomi, O. M., Olajide, O. O.; Emmanuel, S. A. Anti-Plasmodial Activity of Iron Oxide Nanoparticles Derived from Moringa Oleifera Stem Bark and Root Extracts. *FUAM J. Pure Appl. Sci.* **2025,** 5, 10–22.

(11) Bhuyar, P.; Rahim, Mohd H. A.; Sundararaju, S.; Ramaraj, R.; Maniam, G. P.; Govindan, N. Synthesis of silver nanoparticles using marine macroalgae *Padina sp*. and its antibacterial activity towards pathogenic bacteria. *Beni-Suef Univ. J. Basic Appl. Sci.* **2020,** 9, 1-15.

(12) Saitoh, N.; Fujimori, R.; Yoshimura, T.; Tanaka, H.; Kondoh, A.; Nomura, T.; Konishi, Y. Microbial recovery of palladium by baker's yeast through bioreductive deposition and biosorption. *Hydrometallurgy* **2020,** 196, 105413.

(13) Das, M.; Saxena, N.; Dwivedi, P. Emerging trends of nanoparticles application in food technology: Safety paradigms. *Nanotoxicology* **2009,** 3(1) 10-18.

(14) Itodo, A. U., Itodo, O. M., Iornumbe, E. & Fayomi, O. M. Progress in Chemical and Biochemical Research Sorptive chelation of metals by inorganic functionalized organic WOx – EDA nanowires : adsorbent characterization and isotherm studies. *Prog. Chem. Biochem. Res.* **2019,** 1, 50–59.

(15) Zhou, X. Q.; Hayat, Zakir; Zhang, Dong-Dong; Li, Meng-Yao; Hu, Si; Wu, Qiong; Cao, Y. F.; Yuan, Y. Zinc Oxide Nanoparticles: Synthesis, Characterization, Modification, and Applications in Food and Agriculture. *Processes* **2023,** 11, 1193.

(16) Sadek, R.F.; Farrag, H. A.; Abdelsalam, S. M; Keiralla, Z. M.H.; Raafat, A. I.; Araby, E. A powerful nanocomposite polymer prepared from metal oxide nanoparticles synthesized Via brown algae as anti-corrosion and anti-biofilm. *Front. Mater.* **2019,** 6, 140.

(17) Verma, D. K.; Khan, F. Green approach to corrosion inhibition of mild steel in hydrochloric acid

medium using extract of spirogyra algae. *Green Chem. Lett. Rev.* **2016,** 9, 52–60.

(18) Almanza, E., Del C. G.; Pua, L.; Pineda, Y.; Rozo, W.; Marquez, M.; Fonseca, A. Eco-friendly Chlorella vulgaris extracts for corrosion protection of steel in acidic environments. *Heliyon* **2024,** 10, e39717.

(19) Abdulwahid, K. E.; Dwaish, A. S.; Dakhil, O. A. Green synthesis and characterization of zinc oxide nanoparticles from Cladophora glomerata and its antifungal activity against some fungal isolates. *Plant Arch.* **2019,** 19, 3527–3532.

(20) Balasubramanian, R.; Ravi, S. Green Synthesised Zinc Oxide Nanoparticles from Ulva Fasciata Algae Extract for Antibacterial and Supercapacitor Application. *Int. J. Membr. Sci. Technol.* **2023,** 10, 3089–3099.

(21) Fayomi, O. M.; Olasan, J. O.; Aguoru, C. U.; Anjorin, T. S.; Sule, A. M. Effect of Biosynthesized ZnO Nanoparticles Derived From Jatropha Tajonensis on the Yield of Bambara Groundnut (Vigna Substerranean L.). *African J. Agric. Allied Sci.* **2024,** 4, 192–214.

(22) Fayomi, O. M.; Olasan, J. O.; Aguoru, C. U.; Terhemba, M. S. Growth and Yield Responses of Soybean (Glycine Max L.) to Zinc Oxide (ZnO) Nanoparticles Foliar Application. *Biotechnol. Acta* **2024,** 17, 56–66.

(23) Fayomi, O. M.; Chahul, H. F.; Ike, D. C.; Ndukwe, G. I.; Phoebe, I. M. Thermodynamic and Adsorption Study of the Corrosion Inhibition of Mild Steel by Aframomum chrysanthum Extract in 0.1 M Hydrochloric Acid Solution. *Asian J. Appl. Chem. Res.* **2021,** 8, 64–73.

(24) Mohammedali, D. R.; Salman, H. I.; Bahjat, M. N.; Abood, E. S. Synthesis of new Corrosion Inhibitor from Nano-Polymer and study its adsorption on carbon steel at different Temperatures. *Egypt. J. Chem.* **2022,** 65, 691–705.

(25) Halanayake, K. D.; Kalutharage, N. K.; Hewage, J. W. Microencapsulation of biosynthesized zinc oxide nanoparticles (ZnO-NPs) using Plumeria leaf extract and kinetic studies in the release of ZnO-NPs from microcapsules. *SN Appl. Sci.* **2021,** 3, 1–12.

(26) Pasieczna-Patkowska, S.; Cichy, M.; Flieger, J. Application of Fourier Transform Infrared (FTIR) Spectroscopy in Characterization of Green Synthesized Nanoparticles. *Molecules* **2025,** 30, 684.

(27) Alharbi, F. N., Abaker, Z. M. & Makawi, S. Z. A. Phytochemical Substances — Mediated Synthesis of Zinc Oxide. *Inorganics* **2023,** 11, 328.

(28) Jayachandran, A., Aswathy, T. R. & Achuthsankar, N. S. Green synthesis and characterization of zinc oxide nanoparticles using *Cayratia pedata* leaf extract. *Biochem. Biophys. Reports* **2021,** 26, 100995.

(29) Kaur, H. *et al.* Green synthesis of ZnO nanoparticles using E. cardamomum and zinc nitrate precursor: a dual-functional material for water purification and antibacterial applications. *RSC Adv.* **2025,** 15, 16742–16765.

(30) Chaudhary, R.; Nawaz, K.; Khan, A. K.; Hano, C.; Abbasi, B. H.; Anjum, S. An overview of the algae-mediated biosynthesis of nanoparticles and their biomedical applications. *Biomolecules* **10**, 1–35 (2020).

(31) Mohammadi, A.; Hashemi, N.; Ghassabzadeh, M.; Sharafi, A.; Yazdinezhad, A.; Danafar, H. Green synthesis and toxicological evaluation of zinc oxide nanoparticles utilizing Punica granatum fruit Peel extract: an eco-friendly approach. *Sci. Rep.* **2025,** 15, 20853.

(32) Ramike, M. P.; Ndungu, P. G.; Mamo, M. A. Exploration of the Different Dimensions of Wurtzite ZnO Structure Nanomaterials as Gas Sensors at Room Temperature. *Nanomaterials* **2023,** 13, 2810.

(33) Chand, P.; Gaur, A.; Kumar, A. Structural and optical properties of ZnO nanoparticles synthesized at different pH values. *J. Alloys Compd.* **2012,** 539, 174–178.

(34) Kahouli, M.; Barhoumi, A.; Bouzid, A.; Al-Hajry A.; Guermazi, S. Structural and optical

properties of ZnO nanoparticles prepared by direct precipitation method. *Superlattices Microstruct.* **2015,** 85, 7–23.

(35) Alprol, A. E.; Mansour, A. T.; El-Beltagi, H. S.; Ashour, M. Algal Extracts for Green Synthesis of Zinc Oxide Nanoparticles: Promising Approach for Algae Bioremediation. *Materials (Basel).* **2023,** 16, 2819.

(36) Kamburova, K.; Boshkova, N.; Radeva, T.; Boshkov, N. Smart Zinc-Based Coatings with Chitosan–Alginate Nanocontainers Loaded with ZnO and Caffeine for Corrosion Protection of Mild Steel. *Metals (Basel).* **2025,** 15, 65.

(37) Sophie, P. L.; Antony, N. Kinetic, Thermodynamic and Adsorption Isotherm Analysis for the Corrosion Inhibition of Carbon Steel in Aqueous Media by Lippia Nodiflora. *J. Emerg. Technol. Innov. Res.* **2019,** 6, 217–229.

ACS Chapter Nigeria
Book of Proceedings
15th Annual Symposium
ISBN: 978-978-68-0485-9 DOI: https://doi.org/10.55455/acsnigeria.1.2.127-133

Integrating AI into Environmental Chemistry: Predicting and Preventing Toxicity in Chemical Products

***Ayodeji Oluwole Adegun[1], Thompson Akinyele Akinnifesi[2], Morayo Omotunde Adejumo[1], Adejumoke Moriliat Hashimi[3], Gregory Olufemi Adewuyi[1], Kayode Adeniyi Aseperi[4], and Barker James[5]**

[1]Department of Chemistry, University of Ibadan, Ibadan, Nigeria
[2]Department of Chemical Sciences, Adekunle Ajasin University, Nigeria
[3]Department of Chemical Sciences, Olabisi Onabanjo University, Nigeria
[4]Centre for Process Innovation, North East England, UK
[5]School of Life Sciences, Pharmacy and Chemistry, Kingston University, London, UK
Corresponding Author's email: ayodeji2k15@gmail.com

ABSTRACT

This review critically examines the current state of AI in environmental chemistry, highlighting both its potential and limitations in predicting and preventing toxicity in chemical products. Integrating Artificial Intelligence (AI) into environmental chemistry for predicting and preventing toxicity in chemical products is an emerging field that promises to revolutionize toxicological assessments and sustainable chemical design. AI techniques, particularly machine learning (ML) and deep learning (DL), offer the potential to predict the toxicity of chemical substances rapidly, reducing reliance on traditional experimental methods that are often time-consuming, expensive, and ethically problematic. By utilizing large datasets on chemical properties, molecular structures, and biological effects, AI models can forecast the environmental and health impacts of chemicals at an early stage, enabling more efficient risk assessments. However, there are several critical challenges and limitations to consider. The accuracy of AI predictions is dependent on the availability of high-quality, comprehensive data, which is often lacking, especially for new or untested chemicals. Furthermore, the interpretability of AI models remains a significant issue, as many models function as "black boxes," making it difficult to understand the rationale behind their predictions. This lack of transparency may hinder trust in AI-driven decision-making. Additionally, AI tools may lead to biases if the data is incomplete. Despite these challenges, AI presents opportunities for the design of greener chemicals by optimizing molecular structures to reduce environmental harm and enhance biodegradability. However, integrating AI into environmental chemistry requires careful consideration of ethical, legal, and regulatory frameworks to ensure the responsible use of technology.

KEYWORDS: Artificial Intelligence; toxicity prediction, machine learning; sustainable chemical design; data quality and interpretability.

1. INTRODUCTION

The proliferation of industrial chemicals in modern society has generated unprecedented challenges in assessing environmental and human health risks[1].Traditionally, toxicity evaluations have depended on in vivo and in vitro methods, which, despite being informative, are time consuming, expensive, and ethically contentious due to animal testing[2]. With the rise of green chemistry principles and sustainability initiatives, there is a pressing demand for faster, more predictive, and less invasive toxicity assessment strategies[3]. Artificial Intelligence (AI) has rapidly emerged as a transformative tool across multiple scientific disciplines, including drug discovery, materials science, and climate modeling [4]. In environmental chemistry, AI particularly machine learning (ML) and deep learning (DL) have demonstrated immense potential in predicting chemical toxicity by recognizing hidden patterns in large datasets of molecular and toxicological information[5]. By doing so, AI offers opportunities to shift toxicity testing from a reactive to a predictive framework, allowing safer product design and proactive regulation[6].

This review provides a concise discussion of AI applications in environmental chemistry. It focuses on predictive toxicology, exposure modeling, and sustainable design, while critically evaluating challenges such as data scarcity, black-box algorithms, algorithmic bias, and regulatory hurdles. By critically evaluating these aspects, the paper highlights how AI can reshape the future of environmental risk assessment and support the global transition toward sustainable chemical management.

2. ARTIFICIAL INTELLIGENCE APPROACHES IN ENVIRONMENTAL CHEMISTRY

AI comprises computational methods designed to mimic human cognition and decision-making. Among its subsets, ML enables systems to learn patterns from data, while DL employs multilayered artificial neural networks to capture complex nonlinear relationships[7].Machine Learning methods commonly used in environmental toxicology include: Support Vector Machines (SSVMs) for classification tasks such as mutagenicity prediction[8].Random Forests (RFs) for acute toxicity and bioaccumulation risk modeling[9].Artificial Neural Networks (ANNs) for non-linear relationships between molecular descriptors and toxicological endpoints[10].Deep Learning architectures, such as Convolutional Neural Networks (CNNs) and Recurrent Neural Networks (RNNs), are increasingly applied to large-scale datasets (e.g., omics data, chemical images) for predicting multi-endpoint toxicity with higher accuracy Table 1 summarizes some commonly used tools for predicting toxicity of chemical products[11].

Table 1: Tools for Predicting Toxicity

Tool / Approach	Main Technique	Common Application	References
ToxCast	Large-scale screening	Identifying how thousands of chemicals interact with biological systems.	4,6,7,9
QSAR Models	Statistical methods	Estimating toxicity of chemicals in water and soil based on structure activity patterns.	5,10
DeepTox	Pattern recognition	Detecting hormone-like (endocrine) activity in industrial and consumer products.	4,5.11
Read-Across	Comparison approach	Inferring toxicity of new substances by comparing them to well-known chemicals.	6,7,10

3. APPLICATIONS OF AI IN TOXICITY PREDICTION

Artificial intelligence (AI) has emerged as a powerful tool for predicting chemical toxicity, offering significant improvements over conventional in vitro and in vivo testing. Traditional methods are often costly, time consuming, and ethically challenging due to reliance on animal studies.

AI-based models, particularly machine learning (ML) and deep learning (DL), enable rapid screening of large chemical libraries to identify potential hazards before extensive laboratory experiments are conducted.

3.1 Predictive Toxicology

Recent advances in artificial intelligence (AI) have greatly enhanced predictive toxicology by moving beyond traditional QSAR models toward more sophisticated deep learning and transformer-based approaches[1,2]. Models such as ChemBERTa and MolBERT leverage natural language processing techniques to learn chemical representations directly from molecular sequences, providing superior accuracy for endpoints such as mutagenicity, carcinogenicity, and endocrine disruption[3]. These models outperform conventional machine learning methods, especially when applied to diverse datasets of environmental pollutants[4]. In addition, AI has been increasingly applied to emerging contaminants such as pharmaceuticals, legacy pesticides, per- and polyfluoroalkyl substances (PFAS), and microplastics, which often lack extensive experimental toxicity data[5,6]. By combining molecular descriptors with omics datasets, modern deep learning frameworks have demonstrated high predictive power for mixture toxicity, a critical issue given that real-world exposures usually involve chemical cocktails rather than isolated compounds [7,8].

3.2 Risk and Exposure Assessment

AI applications in environmental chemistry extend beyond toxicity prediction to risk and exposure assessment, where the focus is on chemical fate, transport, and bioaccumulation[10].

Machine learning models have been integrated with hydrological and climate data to forecast how pollutants disperse in air, soil, and aquatic systems under changing environmental conditions[9].

Recent studies highlighted the use of graph neural networks (GNNs) to model interactions within soil-water systems, enabling more accurate predictions of pesticide runoff and heavy metal leaching compared with regression-based models[12]. Table 2 presents types of toxicological effects that can be predicted with AI. Similarly, AI-driven exposure models are now incorporating climate change variables such as rainfall intensity and temperature fluctuations, offering more realistic simulations of pollutants mobility in vulnerable ecosystems[13].

Table 2. Types of Toxicological Effects Predicted

Toxic Effect	Approach Used	Example Application	References
Acute Toxicity	Statistical analysis	Estimating lethal dose (LD50) for pesticides or industrial solvents	1,7
Mutagenicity	Data classification	Predicting whether a chemical may damage DNA (e.g., Ames test outcomes)	3,5
Carcinogenicity	Pattern recognition	Long-term predictions of cancer-causing potential in industrial chemicals	2,7
Endocrine Disruption	Biological modeling	Identifying substances that may mimic or block hormones in humans or wildlife	2,6

The computational workflow used to predict the toxicity of chemical compounds based on their molecular features (Fig.1) begins with the chemical structure, which represents the unique arrangement of atoms, bonds, and functional groups that determine the physicochemical and biological properties of a compound[14]. Every molecule has a distinct structure, and this structural information forms the foundation for toxicity prediction[15].

The chemical structure is then converted into molecular descriptors and fingerprints. Descriptors are numerical values that quantify specific properties of the molecule, such as molecular weight, polarity, hydrophobicity, and the number of hydrogen bond donors or acceptors[16]. Fingerprints, on the other hand, are simplified digital representations that capture the presence or absence of structural features or functional groups.Together, these descriptors and fingerprints transform the chemical structure into a mathematical format suitable for computational analysis[17].

Finally, this processed information is used to predict toxicity through computational models, often based on machine learning or quantitative structure-activity relationship (QSAR) methods. The skull-and-crossbones symbol displayed on the computer screen in the figure represents the outcome of such predictive modeling, where a compound can be flagged as toxic or non-toxic[18]. This approach provides a rapid, cost-effective, and ethical alternative to traditional laboratory and animal testing, making it highly valuable in drug discovery, environmental safety assessments, and regulatory toxicology.

Figure 1: Relationship between chemical structure and toxicity

Risk and Exposure Assessment

Beyond toxicity, AI facilitates risk assessment by simulating environmental fate, transport, and bioaccumulation of chemicals[18].

Models can predict biodegradation rates, aid persistence classification, bioaccumulation in aquatic food webs, improving ecological impact assessments[8-9], chemical transport in soil and water systems as well as enabling proactive remediation planning[19]. The AI-based workflow for toxicity prediction (Fig. 2), highlights the interconnected stages involved in assessing the potential hazards of chemical compounds[3,5,8]. The process begins with chemical compounds, which serve as the input data for toxicity studies. These compounds undergo data collection, where critical information such as chemical properties, molecular structures, and biological activity data is compiled from experimental databases and computational sources[10-11]. The collected data is then used in the stage of AI model development, which employs machine learning and deep learning approaches to identify patterns and build predictive models[12].

These models enable toxicity prediction, which involves classifying chemicals based on potential toxic effects and conducting risk assessments to evaluate environmental and human health impacts[8,10]. Predictions from AI tools can inform further chemical testing, database expansion, and safer chemical design[20]. This cyclical workflow underscores the integration of data science with environmental chemistry to create faster, cost-effective, and ethically sustainable alternatives to traditional toxicity testing [2,5,7,10,13].

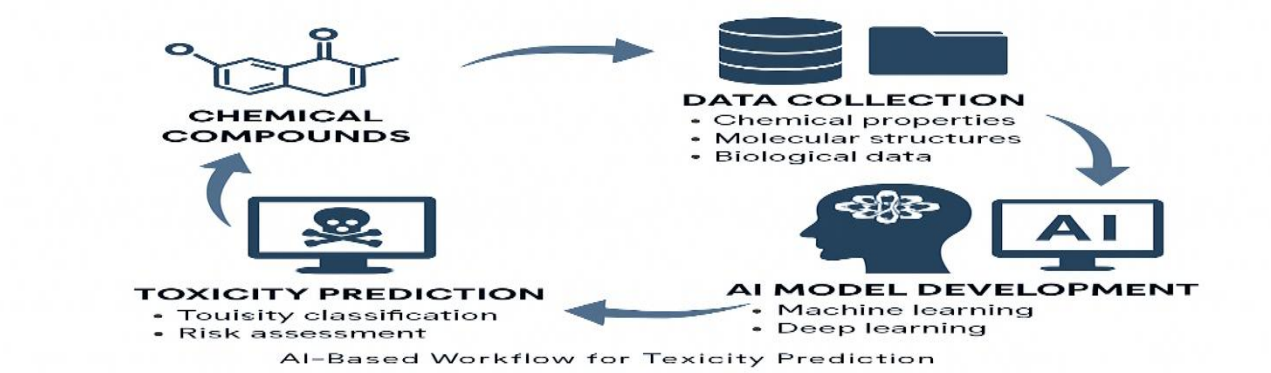

Figure 2: AI-Based Workflow for Toxicity Prediction

3.3 Greener Chemical Design

AI contributes to sustainable chemistry by guiding the design of safer alternatives: Generative models can propose novel molecules with reduced toxicity profiles[2,6,9-10]. Multi-objective optimization balances functionality, stability, and biodegradability[3,5]. Case studies show AI-driven design of flame retardants with minimized endocrine activity[14]. Beyond risk assessment, AI is transforming the design of greener and safer chemicals. Generative models such as variational autoencoders (VAEs) and generative adversarial networks (GANs) are now being applied to propose novel molecules with optimized properties[3,9]. These models allow researchers to balance multiple objectives-such as stability, biodegradability, and reduced toxicity within a single framework, greatly accelerating the development of sustainable alternatives[5]. For example, recent case studies have demonstrated the use of AI-guided molecular optimization to design flame retardants with minimized endocrine-disrupting potential and surfactants with improved biodegradability profiles[13]. Multi-objective optimization frameworks further allow chemists to reduce environmental persistence while maintaining functionality, an essential consideration in green chemistry[11]. The integration of AI in sustainable chemical design not only speeds up discovery but also aligns with regulatory pressures to reduce hazardous substances in consumer products, industrial processes, and environmental applications[14,16].

The comparative accuracy of four machine learning algorithms used for predictive modelling is illustrated in Fig.3. The vertical axis represents accuracy in percentage, ranging from 0% to 100%, while the horizontal axis lists the algorithms: Decision Tree, Random Forest, Support Vector Machine (SVM), and Neural Network[4,7,9,17].The Decision Tree model achieves the lowest accuracy at 70%, indicating that while it provides a simple and interpretable framework, it may not capture complex patterns in the data effectively[4,7,9]. In contrast, the Random Forest model significantly improves performance, reaching 85%

accuracy[11]. This increase can be attributed to its ensemble nature, where multiple decision trees are combined to reduce overfitting and improve generalization[4,6].

The Support Vector Machine (SVM) model achieves 80% accuracy, outperforming the Decision Tree but performing slightly below Random Forest. SVM is known for its effectiveness in handling high-dimensional data and finding optimal classification boundaries, though its performance can depend heavily on parameter tuning and kernel selection[13,15]. The Neural Network model records the highest accuracy at 90%, demonstrating its superior ability to capture nonlinear relationships and complex data structures[16].

Figure 3: Comparative Accuracy of ML Models

4. CHALLENGES AND LIMITATIONS

Emerging contaminants lack toxicological data, resulting in data gaps that undermine predictive reliability[15]. Biased datasets over representing certain chemical classes can also skew predictions[3,6,9]. The most significant barriers to regulatory acceptance is the “black-box” nature of many DL models as well as ethical concerns regarding algorithmic bias and accountability[4,6,12]. Despite these advances, several challenges limit the widespread adoption of AI in environmental toxicology[21].Data availability remains the most pressing barrier: many emerging contaminants, particularly those prevalent in low- and middle-income regions, lack sufficient toxicological records to train reliable models[22].This creates blind spots in predictions, especially for underrepresented chemical classes such as nanomaterials and novel agrochemicals[23]. Another concern lies in algorithmic bias, where models trained on unbalanced datasets may overrepresent well-studied industrial compounds while neglecting region-specific pollutants such as pharmaceuticals and pesticides in African water systems[24].

5. CONCLUSION

AI can transform environmental chemistry by enabling predictive and sustainable approaches to toxicity assessment. While challenges such as data quality, interpretability, and regulatory acceptance remain, continued development of transparent models, data harmonization, and supportive policies will allow AI-driven approaches to become central in safeguarding both human health and ecosystems.

6. FUTURE PROSPECTS AND RECOMMENDATIONS

The future of AI in environmental toxicology relies on developing explainable AI to improve transparency and regulatory trust, supported by international collaboration to build harmonized, open-access datasets. Robust validation frameworks are needed to ensure models perform reliably in real-world contexts. Capacity building through interdisciplinary training and stronger partnerships among academia. industry, and regulators will be vital to translate its advances into practical tools for safeguarding human health and the environment.

ACKNOWLEDGEMENTS

The authors gratefully acknowledged the financial support of the Royal Society of Chemistry, for the award of the Researchers Development and Travel Grant (Grant number: D24-6629469040) to Ayodeji Oluwole Adegun. The fund significantly supported the execution and dissemination of this research work.

CONFLICT OF INTERESTS

The authors declare no conflict of interests.

REFERENCES

(1) Bai, C.; Wu, L.; Li, R.; Cao, Y.; He, S.; Bo, X. Machine Learning-Enabled Drug-Induced Toxicity Prediction. *Adv. Sci.* 2025, *12* (16).

(2) Guo, W.; Liu, J.; Dong, F.; Song, M.; Li, Z.; Khan, M. K. H.; Patterson, T. A.; Hong, H. Review of Machine Learning and Deep Learning Models for Toxicity Prediction. *Exp. Biol. Med.* 2023, *48* (21), 1952–1973.

(3) Kostal, J.; Brooks, B. W.; Smith, C. A.; Devineni, G. O Data, Where Art Thou? Revolutionizing Data Sharing to Advance Our Sustainability Goals through Smart Chemical Innovation. *iScience* 2022, *25* (11), 105256.

(4) Su, R.; Wu, H.; Xu, B.; Liu, X.; Wei, L. Developing a Multi-Dose Computational Model for Drug-Induced Hepatotoxicity Prediction Based on Toxicogenomics Data. *IEEE/ACM Trans. Comput. Biol. Bioinf.* 2019, *16*, 1231–1239.

(5) Tang, W.; Chen, J.; Wang, Z.; Xie, H.; Hong, H. Deep Learning for Predicting Toxicity of Chemicals: A Mini Review. *J. Environ. Sci. Health C Environ. Carcinog. Ecotoxicol. Rev.* 2018, *36* (4), 252–271.

(6) Hartung, T. ToxAIcology.The Evolving Role of AI in Predictive Toxicology and Regulatory Science. *ALTEX* 2023, *40* (4), 559–570.

(7) Hartung, T.; Kleinstreuer, N. Challenges and Opportunities for Validation of AI-Based New Approach Methodologies (NAMs) in Toxicology. *ALTEX* 2025, *42* (1), 1–16.

(8) Koutsoukas, A.; St. Amand, J.; Mishra, M.; Huan, J. Predictive Toxicology: Modeling Chemical Induced Toxicological Response Combining Circular Fingerprints with Random Forest and Support Vector Machine. *Front. Environ. Sci.* 2016, *4*, 11.

(9) Khan, A.; Gupta, S.; Gupta, S. K. Multi-Hazard Disaster Studies: Monitoring, Detection, Recovery, and Management, Based on Emerging Technologies and Optimal Techniques. *Int. J. Disaster Risk Reduct.* 2020, *47*, 101642.

(10) Hong, H.; Thakkar, S.; Chen, M.; Tong, W. Development of Decision Forest Models for Prediction of Drug-Induced Liver Injury in Humans Using a Large Set of FDA-Approved Drugs. *Sci. Rep.* 2017, *7*, 17311.

(11) Idakwo, G.; Luttrell, J.; Chen, M.; Hong, H.; Zhou, Z.; Gong, P.; Zhang, C. A Review on Machine Learning Methods for *In Silico* Toxicity Prediction. *J. Environ. Sci. Health C Environ. Carcinog. Ecotoxicol. Rev.* 2018, *36*, 169–191.

(12) Maxwell, A.; Li, R.; Yang, B.; Weng, H.; Ou, A.; Hong, H.; Zhou, Z.; Gong, P.; Zhang, C. Deep Learning Architectures for Multi-Label Classification of Intelligent Health Risk Prediction. *BMC Bioinformatics* 2017, *18*, 121.

(13) Jiang, C.; Yang, H.; Di, P.; Li, W.; Tang, Y.; Liu, G. *In Silico* Prediction of Chemical Reproductive Toxicity Using Machine Learning. *J. Appl. Toxicol.* 2019, *39*, 844-854.

(14) Minerali, E.; Foil, D. H.; Zorn, K. M.; Lane, T. R.; Ekins, S. Comparing Machine Learning Algorithms for Predicting Drug-Induced Liver Injury (DILI). *Mol. Pharmaceutics* 2020, *17*, 2628-2637.

(15) Lakshmikantha, V.; Hiriyannagowda, A.; Manjunath, A.; Patted, A.; Basavaiah, J.; Anthony, A. A. IoT-Based Smart Water Quality Monitoring System. *Glob. Transitions Proc.* 2021, *2* (2), 181-186.

(16) Karim, A.; Singh, J.; Mishra, A.; Newton, M. A. H.; Sattar, A. Toxicity Prediction by Multimodal Deep Learning. *arXiv* 2019, arXiv:1907.08333.

(17) Jovanović, G.; Bezdan, T.; Romanić, S. H.; Matek Sarić, M.; Biošić, M.; Mendaš, G.; Stojić, A.; Perišić, M. Application of the AI-Based Framework for Analyzing the Dynamics of Persistent Organic Pollutants (POPs) in Human Breast Milk. *Toxics* 2025, *13* (8), 631.

(18) Huang, X.; Chen, J.; Liu, P. Assessing Chemical Exposure Risk in Breastfeeding Infants: An Explainable Machine Learning Model for Human Milk Transfer Prediction. *Ecotoxicol. Environ. Saf.* 2025, *289*, 117707.

(19) Jovanović, G.; Herceg, R. S.; Stojić, A.; Klinčić, D.; Matek, S. M.; Grzunov, L. J.; Popović, A. Introducing Modeling Techniques in the Research of POPs in Breast Milk-A Pilot Study. *Ecotoxicol. Environ. Saf.* 2019, *172*, 341-347.

(20) Radić, N.; Perišić, M.; Jovanović, G.; Bezdan, T.; Stanišić, S.; Stanić, N.; Stojić, A. An AI-Based Framework for Characterizing the Atmospheric Fate of Air Pollutants within Diverse Environmental Settings. *Atmosphere* 2025, *16*, 231.

(21) Jovanović, G.; Perišić, M.; Bačanin, N.; Živković, M.; Stanišić, S.; Štrumberger, I.; Alimpić, F.; Stojić, A. Potential of Coupling Metaheuristics-Optimized-XGBoost and SHAP in Revealing PAHs Environmental Fate. *Toxics* 2023, *11*, 394.

(22) Mendaš, G.; Jakovljević, I.; Herceg, R. S.; Fingler, S.; Jovanović, G.; Matek, S. M.; Pehnec, G.; Popović, A.; Stanković, D. Presence of Polycyclic Aromatic Hydrocarbons and Persistent Organochlorine Pollutants in Human Milk: Evaluating Their Levels, Association with Total Antioxidant Capacity, and Risk Assessment. *Sci. Total Environ.* 2024, *931*, 172911.

(23) Janakiraman, S.; Sha, R.; Mani, N. K. Recent Advancements in Point-of-Care Detection of Contaminants and Biomarkers in Human Breast Milk: A Comprehensive Review. *Sens. Actuators Rep.* 2025, *9*, 100280.

(24) Chi, Z. H.; Goodyer, C. G.; Hales, B.; Bayen, S. Characterization of Different Contaminants and Current Knowledge for Defining Chemical Mixtures in Human Milk and Infant Health Risk Assessment from 1976 to the Present. *Food Chem. Toxicol.* 2023, *179*, 113990.

ISBN: 978-978-68-0485-9 DOI: https://doi.org/10.55455/acsnigeria.1.2.134-141

Investigation of Impacts of Gas-Fired Power Plants on Ambient Carbon Monoxide (CO) of Neighboring Communities

Olumuyiwa Oyekunle Akintola[a], Olusola Adedayo Adesina[b] and Hosea Gobak Kama[c]
[a]-Department of Chemistry, National Open University of Nigeria, Jabi, Abuja
[b]-Department of Chemical and Petroleum Engineering, Afe Babalola University, Ado-Ekiti, Nigeria
[c]-Department of Environmental Sciences, National Open University of Nigeria, Jabi, Abuja
Corresponding Author's Email: ooakintola@noun.edu.ng, akintolaoo@yahoo.com

ABSTRACT

Operation of gas power plants creates emissions of various air pollutants including carbon monoxide with associated health and environmental effects. This study investigated the ground level concentrations of carbon monoxide from units of the 4 MW Gas Power Plants of a leading utility, gas and energy company in Lagos, Nigeria. Air emissions of CO from the gas power plants at the project site were calculated using the emission factors. The AERMOD dispersion modelling tool (version 9.6.1) was used to model ground level concentrations of CO associated with air emissions from the two units of 1364 kW and 774 kW of Gas Power Plants. Three different scenarios involving the gas turbines operations were considered. Scenario 1 and 2 involved the operation of 1364 kW and 774 kW, respectively while scenario 3 involved the simultaneous operation of both gas power plants. The predicted ground level CO concentrations from the three scenarios in all locations considered were within the FMEnv's limits, though, the ambient CO at the project site in scenario 1, 2 and 3 changed by 2.31%, 1.72%, and 2.68% of limit, respectively. However, sites using gas power plants near communities may further reduced emissions of air pollutants by developing relevant control techniques with continuous monitoring of these emissions at the site. This study also provides stake holders necessary information that can help in making profitable decisions and guidelines in similar situation.

KEYWORDS: Carbon monoxide, air quality, powerplants, air pollutants emissions, AERMOD

1. INTRODUCTION

The demand for reliable and cleaner energy sources has led many countries to adopt gas-fired power plants as alternatives to coal and oil-based plants. Natural gas, primarily composed of methane (CH_4), is often perceived as a cleaner fossil fuel due to its lower carbon dioxide (CO_2) emissions upon combustion. However, one of the less discussed but significant by-products of natural gas combustion is carbon monoxide (CO), a colorless, odorless, and toxic gas. Ambient CO concentrations, especially in areas proximal to power generation stations, pose potential health risks and environmental concerns.[11] Carbon monoxide is produced due to incomplete combustion of carbon-containing fuels. When released into the atmosphere, it does not only affect human health by impairing oxygen delivery to the body's organs and tissues but also contributes to the formation of ground-level ozone and secondary pollutants.[13] While vehicular emissions have traditionally been the dominant source of CO in urban areas, stationary sources like gas-fired power plants are increasingly recognized as contributors to localized pollution hotspots.[1] A power plant or generating station is broadly any facility that houses one or more generators to produce electricity for distribution or dedicated use, and according to the U.S. Energy Information Administration (EIA), the category of utility scale power plants includes facilities with at least 1 MW of generating capacity, while smaller units are considered distributed or small scale generation.[12] Numerous studies have examined the environmental impact of power generation facilities, especially regarding their contributions to air pollution. Gulliver and Briggs demonstrated the spatial variability of air pollutants near industrial facilities and highlighted the role of meteorological conditions and terrain in pollutant dispersion.[6] Recent research has further shown that dispersion modelling tools such as AERMOD and CALPUFF provide critical insights into ground level concentrations of pollutants from energy facilities, allowing regulators to make more precise policy decisions.[15] Studies conducted in developing countries highlight that poorly maintained gas-fired plants often release CO at concentrations above recommended safety thresholds, particularly when multiple turbines are operated simultaneously.[8] Similarly, Anenberg et al. and Smith et al. emphasized that even transition fuels like natural gas which is usually considered as a cleaner alternative fuel, still contribute significantly to localized air quality degradation, with combustion resulting in emissions of CO, NO_x, and particulate matter.[2,10] In Nigeria, where energy demand is growing rapidly, Olalekan et al. reported that communities near power plants face increased risks of both acute and chronic exposure to CO.[9] Furthermore, from a public health perspective, the World Health Organization and the U.S. Environmental Protection Agency provide guidelines on acceptable exposure levels to carbon monoxide, emphasizing that

prolonged exposure even at moderate levels can lead to cardiovascular and neurological issues.[13,11] Zhang et al. demonstrated that integrating continuous emissions monitoring systems (CEMS) into plant operations significantly improves compliance and reduces exceedances in pollutant concentrations.[14] In similar manner, Li et al. explored the link between combustion efficiency and CO output in gas turbines. They found that maintenance schedules and operational practices significantly influenced emission levels, suggesting that better regulation and technological upgrades could reduce CO emissions.[7] This study reveals the importance of localized investigations into CO emissions, especially in rapidly urbanizing regions where energy demand and population density intersect, considering different scenarios, location and distance of receptors. This study essentially investigates the extent to which gas-fired power plants influence ambient carbon monoxide concentrations in neighboring communities.

2. METHODOLOGY

This study investigated the ground level concentrations of carbon monoxide from units of the 4 MW Gas Power Plants of a leading utility, gas and energy company in Lagos, Nigeria. The immediate environment given adequate attention was within 50 km radius of the site. Three different scenarios involving the gas turbines operations were considered. Scenario 1 and 2 involved the operation of 1364 kW and 774 kW, respectively while scenario 3 involved the simultaneous operation of both gas power plants, approximately 2 MW. The 1364 kW and 774 kW units of the Gas Power System operated with natural gas consumption rate of 129 scm/hr and 73 scm/hr respectively. The map of the area was generated using ARC-GIS Tool (Figure 1).

The emission rates and the exhaust vent stack parameters including height, diameter, exhaust temperature, and the exit velocity used as model input parameters were obtained from the project details and site (Table 1). The calculation of air emissions of CO from the gas power plants at the project site were calculated using the emission factors.[4] The operation is assumed to be on the natural gas and at full capacity carrying the maximum load. It was assumed that all the gas reciprocating engines use natural gas and are in continuous operations at full capacity, while considering worst case scenario. American Meteorological Society/Environmental Protection Agency Regulatory Model, AERMOD (version 9.6.1); a steady-state Gaussian plume air dispersion model based on planetary boundary layer theory was used to model ground level concentrations of CO associated with air emissions from the two units of 1364 kW and 774 kW of Gas Power Plants. AERMOD considers several meteorological parameters, primarily processed by its pre-processor AERMET, which uses input data such as wind speed, wind direction, temperature, and cloud cover to calculate essential boundary layer parameters. Meteorological data from the Lakes Environmental meteorological observations on the study area, flat terrain, map of the study area and the modelling parameter in Table 1 were used in AERMOD Software for modelling. Furthermore, for the purpose of investigating the air quality implication on health and environment, the FMEnv standard for CO 11400 μg/m^3 was used.[5] The impact on project site and receptors (R) around the site were considered including: R1(0.3 km N), R2 (0.2 km NE), R3(0.17 km NW), R4(0.23 km SW) and R5 (0.3 km SW).

Figure 1: Plant project site and neighboring receptors

Table 1: Parameters used for modelling

Gas Power Plant kW	1364	774
Air Pollutant	CO	CO
Stack Emission rate (g/s)	1.1730	0.6700
Location X(m)	484.23	466.33
Location Y(m)	538.76	536.97
Discharge Temperature(K)	744	744
Base Elevation(m)	1.00	1.00
Release Height(m)	3.65	3.20
Stack Diameter(m)	0.1	0.1
Exit Velocity(m/s)	66.2	60

3. RESULTS AND DISCUSSION

Modelling results from the three operation scenarios considered in this study are presented and discussed in this subsection. The identified impacts on the ambient air quality of the host environment were also considered.

3.1 Predicted Ground Level Concentrations of CO

In Table 2, the anticipated 24 - hour ground level concentrations of CO from 1364 KW Deutz Gas power plant at the site as investigated in scenario 1 were 3.00 – 263 μg/m^3 (Figure 2). The operation of 774 KW Deutz gas power plant resulted in 24 - hour predicted concentrations of CO in the range of 2 - 196 μg/m^3 (Figure 3). In scenario 3, where the simultaneous operations of two power plants (1364 and 774 KW) were investigated, the expected concentrations of CO were 3 – 306 μg/m^3 (Figure 4).

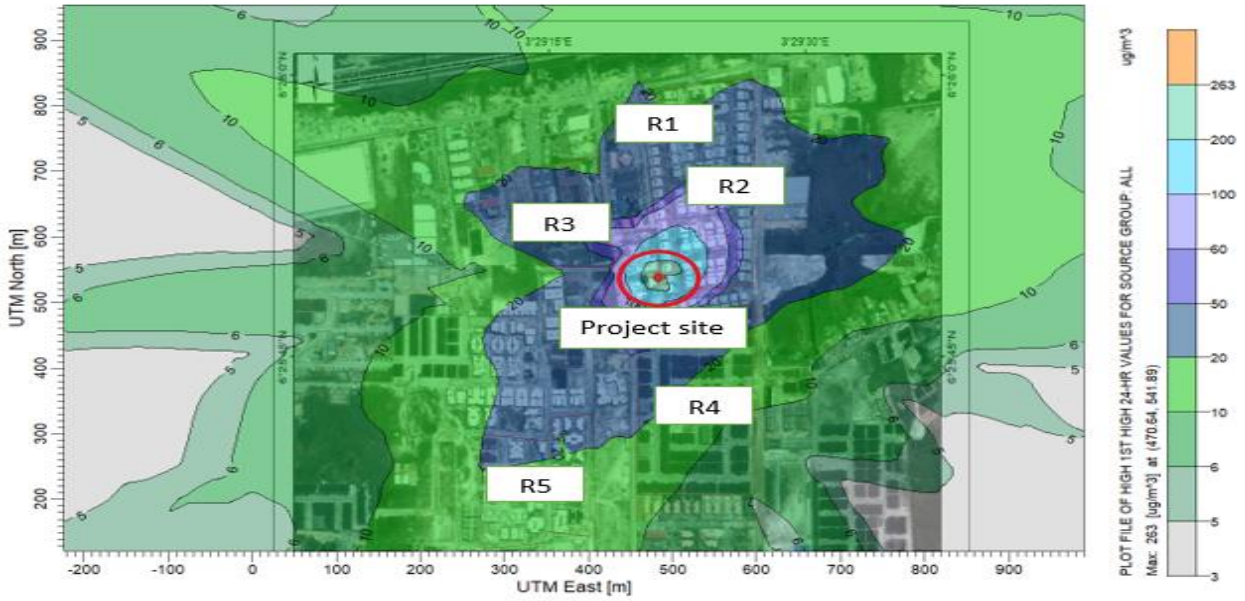

Figure 2: CO concentrations from scenario 1

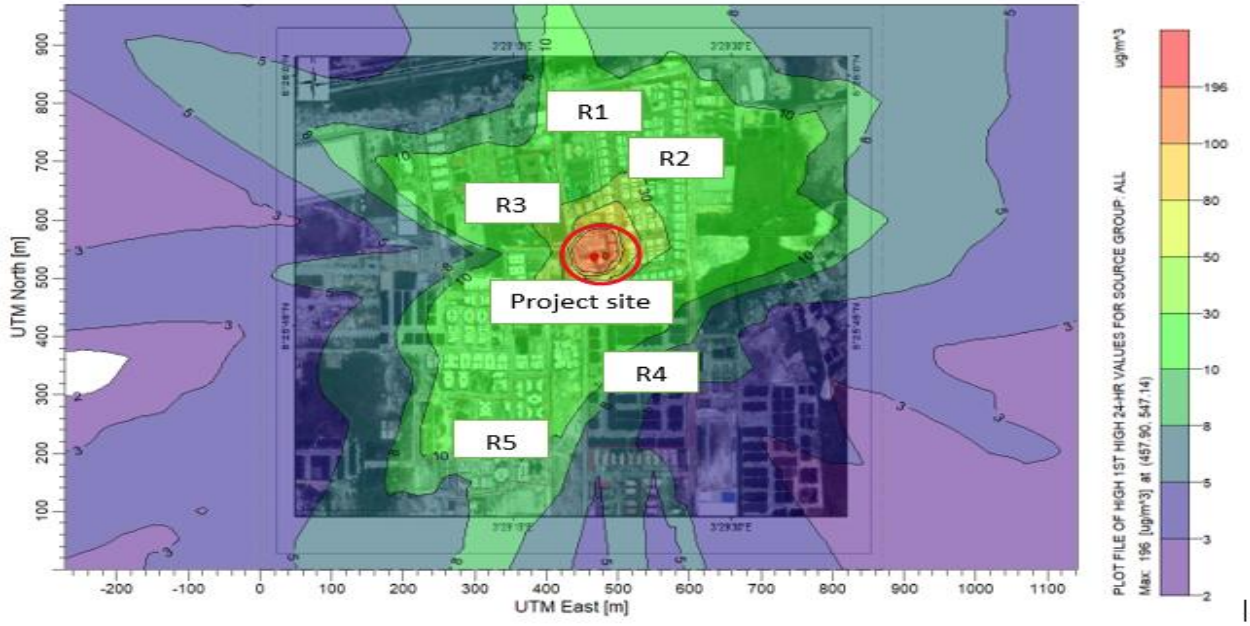

Figure 3: CO concentrations from scenario 2

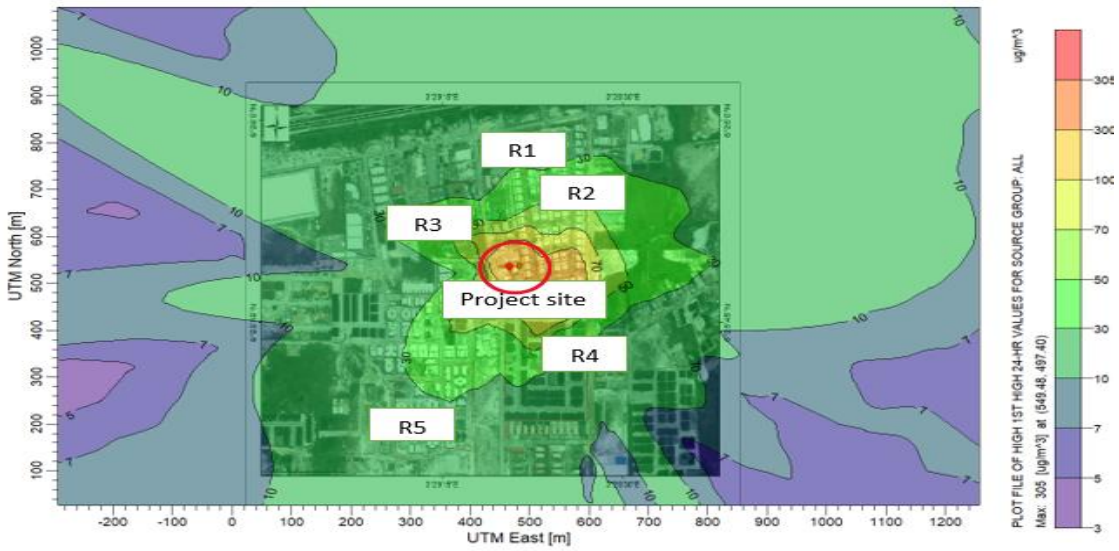

Figure 4: CO concentrations from scenario 3

3.2 Impact of Maximum Ground Level CO Concentrations on the Environment

As summarized in Table 2, considering scenario 1 - 3, the maximum 24 – hr CO concentrations from the power plants are 263.00 to 305.00 µg/m^3 at the project site, which represent 2.31 – 2.68% of FMEnv limits. In scenario 1, the investigation of 1364 kW Deutz Gas Power Plant showed that the anticipated daily CO ground level concentrations in the six (6) communities considered are 10 – 263 µg/m^3. These are 0.09 – 2.31% of FMEnV's limit. When a unit of 774 kW Deutz Gas Power Plant is operated as investigated in the scenario 2 of this study, the daily averaging period ground level concentrations of CO in the neighboring receptors are 5.00 – 196.00 µg/m^3 which are 0.04 – 1.72% of FMEnv's limit. Scenario 3 which is simultaneous operations of the two units of the gas power system (≈2 MW) will generate CO daily averaging period concentrations of 10.0 – 305.00 µg/m^3 which are 0.09 – 2.68% of limit. Figure 5 shows a graphical representation of the relationship between predicted CO concentrations at the project sites and receptors (1-5) from the source of air emission across scenario 1-3. In addition, the maximum 24-hour ground-level CO concentrations predicted for each operational scenario against the FMenv limit was illustrated in Figure 6.

Table 2: Predicted Ground Level 24 - hour ground level concentrations of CO and their implications from scenario 1-3

Location	Scenario 1		Scenario 2		Scenario 3	
	24 – Hr Maximum Predicted Concentrations (µg/m^3)	**% of Standard**	24 – Hr Maximum Predicted Concentrations (µg/m^3)	**% of Standard**	24 – Hr Maximum Predicted Concentrations (µg/m^3)	**% of Standard**
Project Site	263.00	**2.31**	196.00	**1.72**	305.00	**2.68**
R1 (0.23km N)	20.00	**0.18**	10.00	**0.09`**	50.00	**0.44**
R2(0.2km NE)	60.00	**0.53**	30.00	**0.26**	100.00	**0.88**
R3 (0.17km NW)	20.00	**0.18**	10.00	**0.09**	50.00	**0.44**
R4 (0.23km SE)	10.00	**0.09**	5.00	**0.04**	10.00	**0.09**
R5 (0.3km SW)	10.00	**0.09**	10.00	**0.09**	30.00	**0.26**

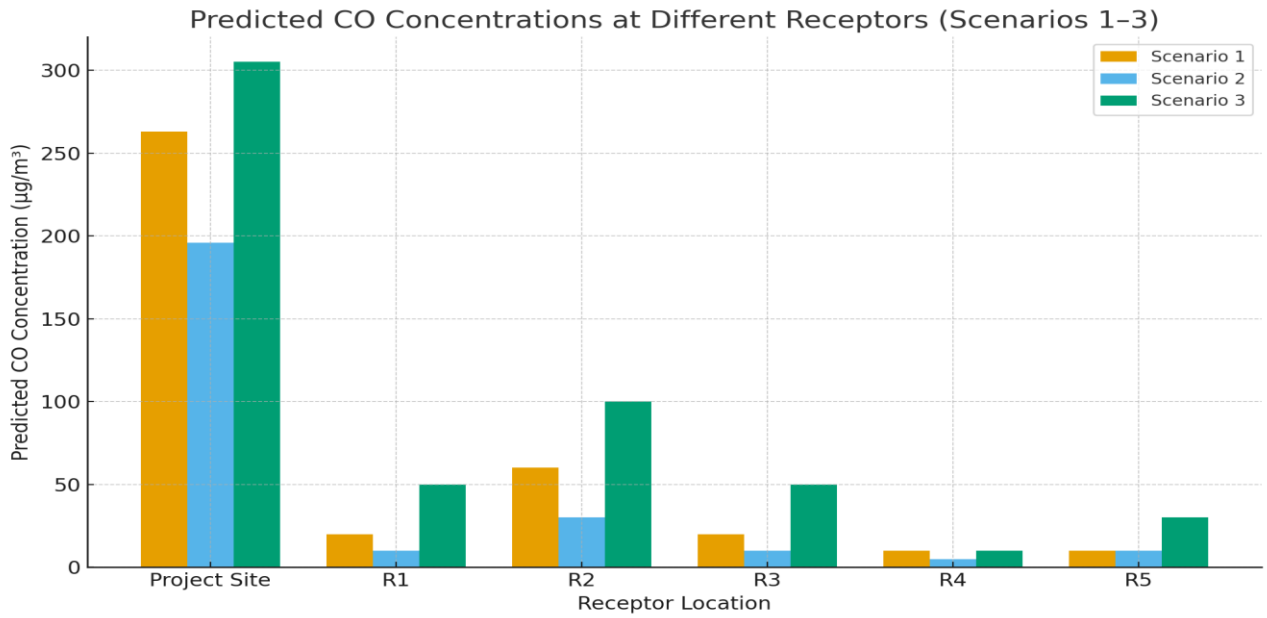

Figure 5: The predicted CO concentrations at each receptor location across Scenarios 1–3.

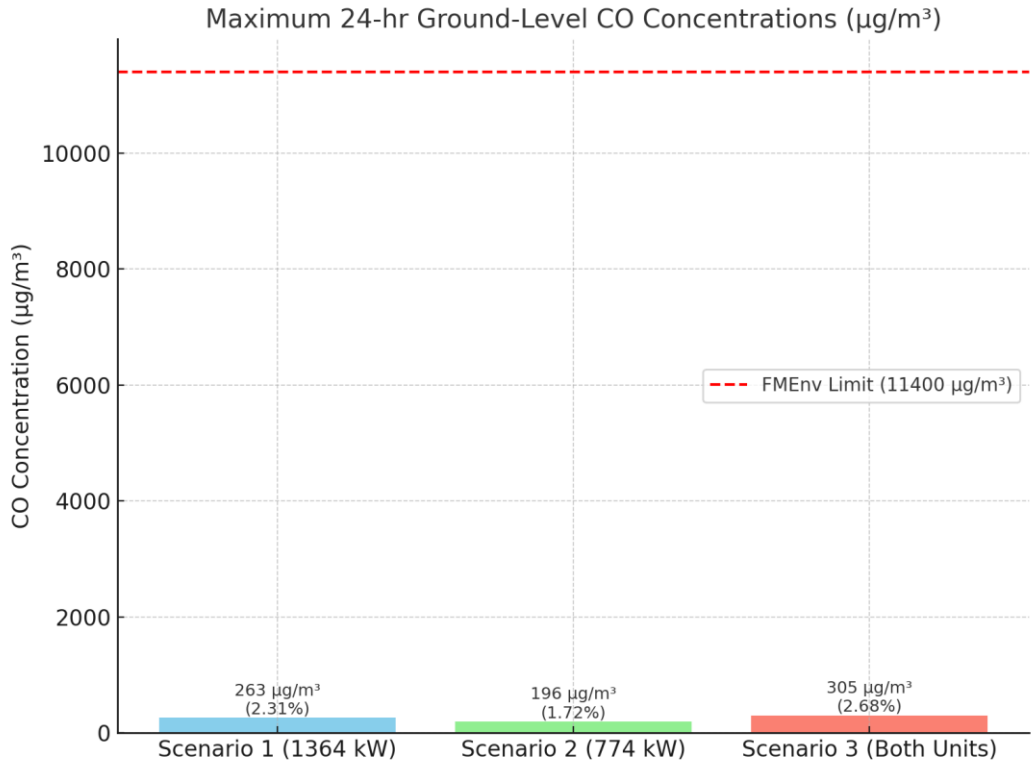

Figure 6: The maximum 24-hour ground-level CO concentrations predicted for each operational scenario

3.3 Discussion

Generally, in the three (3) scenarios and as illustrated in Figure 5, the maximum ground level concentrations of CO were recorded at the project site; 263 µg/m^3, 193 µg/m^3 and 305 µg/m^3 for scenarios 1, 2, and 3, respectively. This was followed by R2 (0.2 km NE of site) while the minimum

ground level concentrations were recorded at R4 (0.23 km SE of site) and R5 (0.3 km SW of site). Since AERMOD modelling system predicts the concentration and dispersion of contaminants downwind, that is locations in the direction of the wind from the emission source, the dispersion was influenced by the prevailing southwesterly winds in Lagos, which transported emissions predominantly north of project site, explaining higher receptor values in downwind directions.[3] These findings align with previous studies that highlight the importance of wind direction and atmospheric stability in pollutant dispersion.[6,13]

Furthermore, as illustrated in Figure 6, the predicted ground level CO concentrations across scenario 1 (1364 kW), scenario 2 (774 kW), and scenario 3 (≈ 2 MW) in all the receptors considered, that is R1 to R5, have insignificant impacts on the ambient CO. However, they affect the ambient CO at the project site by 2.31%, 1.72%, and 2.68% of limit for scenario 1, 2 and 3, respectively. These percentages are still within FMEnv limits, confirming minimal environmental impact on surrounding communities. From the results obtained in Table 2, a cumulative effect from combining scenario 1, 2 and 3 (≈ 4 MW) will still have limited impact on the ambient CO of neighboring communities

4. CONCLUSION

AERMOD tool has been used to model the ground level concentrations of CO associated with air emissions across three scenarios from different units of the 4 MW Deutz power plants in Lagos community. Location of gas power plants with capacity around 1 to 4 MW do not significantly elevate ambient CO in surrounding communities around 0.17 km away from the project site or air emission source under worst-case operating scenarios. This may be applicable to areas in the region or country with similar meteorological conditions and terrain. Regular monitoring and adoption of emission control strategies are nonetheless recommended for cumulative impact management in areas where small scale or utility gas power plants are utilised for electricity generation.

CONFLICT OF INTERESTS

The authors declare no conflict of interests.

REFERENCES

(1) Adewuyi, T. O., Akinlade, B. O., Aina, Y. A. Assessment of Air Pollutants from Gas-Fired Power Plants in Urban Areas. *Environ. Monit. Assess.* **2019,** *191* (3), 143.
(2) Anenberg, S. C., Haines, S., Wang, E., Nassikas, N., Kinney, P. L. Climate and Health Benefits of Increasing Renewable Energy Deployment in the United States. *Environ. Res. Lett.* **2020,** *15* (9), 094075.
(3) Bassett, R., Young, P. J., Blair, G. S., Samreen, F., Simm, W. The Megacity Lagos and Three Decades of Urban Heat Island Growth. *J. Appl. Meteorol. Climatol.* **2020,** *59* (12), 2041–2055.
(4) EPA. *Emission Factors and AP 42, Compilation of Air Pollutant Emission Factors*; U.S. Environmental Protection Agency: Washington, DC, 2015.*1*(3), 1-35.
(5) FEPA. *Guidelines and Standards for Environmental Pollution Control in Nigeria*; Federal Environmental Protection Agency: Lagos, 1991. 1-78
(6) Gulliver, J., Briggs, D. J. Time-Space Modeling of Journey-Time Exposure to Traffic-Related Air Pollution Using GIS. *Environ. Res.* **2011,** *111* (3), 289–294.
(7) Li, Y., Wang, J., Zhou, W. Operational Efficiency and CO Emissions in Gas Turbine Power Plants. *Energy Rep.* **2018,** *4,* 263–270.
(8) Okedere, O. B., Sonibare, J. A., Akinbami, J. F. K., Oladokun, O. Dispersion Modeling of Air Pollutants from a Gas-Fired Power Plant in Nigeria. *Atmos. Pollut. Res.* **2017,** *8* (1), 76–85.
(9) Olalekan, R. M., Afolabi, O. O., Ologunde, C. A. Air Quality and Health Impact Assessment of Industrial Emissions in Southwest Nigeria. *Int. J. Environ. Res. Public Health* **2022,** *19* (11), 6674.
(10) Smith, H., Kim, S., Nguyen, L. Air Emissions from Natural Gas Combustion: A Comparative Review. *J. Clean. Prod.* **2020,** *251,* 119–132.
(11) U.S. Environmental Protection Agency (EPA). *Integrated Science Assessment for Carbon Monoxide*; EPA/600/R-15/044F; U.S. EPA: Washington, DC, **2022**. https://www.epa.gov
(12) U.S. Energy Information Administration (USEIA). *Electricity Explained: Electricity Generation, Capacity, and Sales in the United States*; U.S. EIA: Washington, DC, **2023.**

https://www.eia.gov/energyexplained/electricity/electricity-in-the-us-generation-capacity-and-sales.php

(13) World Health Organization (WHO). *WHO Global Air Quality Guidelines: Particulate Matter, Ozone, Nitrogen Dioxide, Sulfur Dioxide and Carbon Monoxide*; WHO: Geneva, **2021**,1-300.

(14) Zhang, X., Li, J., Wang, Y. Development and Application of Continuous Emissions Monitoring Systems for Power Plants in China. *Environ. Sci. Pollut. Res.* **2019,** *26* (24), 25012–25025.

(15) Zheng, X., Yang, H., Chen, L. Comparison of AERMOD and CALPUFF for Power Plant Environmental Impact Assessment in Complex Terrain. *Atmosphere* **2022,** *13* (5), 712.

ISBN: 978-978-68-0485-9 DOI: https://doi.org/10.55455/acsnigeria.1.2.142-148

Advancement of Artificial Intelligence in Chemical Sciences

Excellence Amaibiam Okonkwo[1]*, Kennedy Izuchukwu Ogunwa[1], and Linda Mgbo Ngumoha[2]

[1]Department of Industrial and Medicinal Chemistry, David Umahi Federal University of Health Sciences Uburu-Ohaozara, Ebonyi State, Nigeria.

[2]Department of Chemistry, Alex Ekwueme Federal University, Ndufu-Alike Ikwo, Ebonyi State

Corresponding Author's email: excelokonkwo@gmail.com; Phone: + 2348037737839

ABSTRACT

Artificial Intelligence (AI) is now being used in many areas of chemical sciences ranging from pharmaceutical chemistry, nanotechnology, analytical chemistry: faster and more precise compound identification in organic chemistry and easier complex organic synthesis. Integration of AI technologies in chemical sciences has enhanced reaction prediction, material design, drug discovery, and sustainability efforts. AI in chemical sciences has brought about a lot of transformation which is very essential for addressing global health, energy and environment challenges in line with sustainable development goals (SDGs). However, limitations such as data unavailability, difficult model interpretation, unreliability and scalability remain areas for further studies. This paper discusses the recent advancements, applications and future directions of AI in chemical sciences, highlighting its roles in shaping the future of chemical sciences.

KEYWORDS: Artificial Intelligence (AI), Chemical Sciences,Drug Discovery, Sustainability, Reaction Prediction.

1. INTRODUCTION

Artificial Intelligence is a field in computer science that is capable of performing tasks commonly associated with intelligent beings. It is programmed to carry out very complex tasks with great proficiency. It has emerged as developmental tool across numerous scientific disciplines of which chemical sciences is not an exception. The integration of artificial intelligence (AI) into the chemical sciences marks a paradigm shift in how chemistry is studied, understood, and applied.[1] The field has evolved from hypothesis-driven experimentation to data-driven discovery powered by computational intelligence.[2] A surge in AI-based research and tools have led to major advancements in various areas of chemistry, significantly, facilitating breakthroughs in molecular modeling, drug discovery, materials design, catalysis, environmental chemistry and beyond.[3] This sudden increase has been driven by the proliferation of large chemical datasets, advances in computational power, and the development of sophisticated algorithms capable of learning and predicting complex chemical phenomena.[4]

AI employs a lot of methods particularly machine learning (ML), deep learning (DL), neural networks, and natural language processing (NLP) which have enabled chemists to extract patterns from vast data repositories, automate experimental procedures, and design new molecules with unprecedented accuracy and efficiency.[1,5,6] These have caused changes to how chemists think about reaction mechanisms, molecular property prediction, and laboratory automation .[7] As AI continues to mature, its integration with chemical sciences is expected to deepen, potentially redefining the discipline's theoretical foundations and experimental methodologies. AI is becoming relevant in research, and very likely chemists that don't embrace it will be heavily disadvantaged.

Recent studies illustrate how AI has enhanced various areas of chemical sciences. In drug discovery, for instance, generative models have been used to propose novel drug candidates with desired active compounds and toxicity profiles, dramatically reducing the cost and time of development.[8,9] In catalysis, AI has facilitated the identification of optimal catalyst compositions and reaction conditions.[10,11] Similarly, materials informatics now leverages AI for the design of energy storage materials, semiconductors, and polymers with tailored properties.[12] AI stands as a key enabler in solving complex chemical problems and achieving the Sustainable Development Goals.[1,6]

Despite these advances, several challenges persist. Issues of data quality, impact of AI on jobs, inability of a human to understand a model's inner workings and reasoning process and the need for interdisciplinary collaboration continue to shape the discourse around AI in chemistry.[13] Another key

concern is on ethical considerations and the integration of AI into traditional laboratory practices. This paper summarizes recent advancements, applications, and future directions of AI in chemical sciences. It highlights the developmental potential of AI in driving innovation, improving research efficiency, and addressing longstanding challenges in the field.

2. METHODS

Research methods are a scientific way to obtain data with specific purposes and uses.[14] The method used in this research is descriptive qualitative which involves looking at several previous studies related to the research topic.[15]

3. ADVANCEMENTS AND APPLICATIONS OF ARTIFICIAL INTELLIGENCE IN CHEMICAL SCIENCES

The advancements and application of artificial intelligence (AI) have paved the way to a new era in learning of chemical sciences. Artificial Intelligence (AI) techniques are becoming valuable due to several reasons like easy to learn and use, simple implementation, easy designing, effectiveness, robustness, and flexibility; they are widely used in various areas of chemistry including molecular design, molecular property prediction, retro synthesis, reaction outcome prediction and reaction conditions prediction.[16]AI technology gives an avenue to process large chemical data with high accuracy, predict molecular properties with precision, and design new molecules efficiently with the help of artificial neural networks, evolutionary algorithms and fuzzy logic. Artificial Intelligence (AI) has become the main catalyst in drastic transformation in various fields of chemical sciences. It has opened the door to significant changes in the way we understand, analyze, and apply knowledge about the molecular structure, reactivity, and design of chemicals and has been widely applied in core domains of chemical sciences.

3.1 Chemical Science Education

In the context of chemical sciences, AI has opened the door to significant changes in the way we understand, analyze, and apply knowledge about the molecular structure, reactivity, and design of chemicals.[17] Teachers are desperate to be creative and innovative in teaching at this 21st-century era because they are faced with the challenges of producing students who are ready to face the reality in a developing world.[18] Artificial intelligence help students have better access to an enhanced personalized learning tool. AI technology has been a key in accelerating chemical research and has paved the way for breakthroughs in innovations that have change the paradigm in chemical sciences as a whole. Thus, AI can be a very useful tool in supporting the teaching and learning process of chemical sciences, allowing students to explore and understand difficult concepts in a more engaging and interactive way.[17]

3.2 Molecular Property Prediction

AI is able to accurately predict chemical properties based on molecular structure. With the integration of AI algorithms into structure modeling, chemical scientists can design molecular structures faster and more efficiently, speeding up the process of research and development of new chemicals for drug production.[19] The article "Chemception: A Deep Neural Network with Minimal Chemistry Knowledge matches the Performance of Expert-developed Quantitative Structure-Activity Relationship/Quantitative Structure-Property Relationship (QSPR) Models published in arXiv in 2017.[20] Machine learning algorithms such as support vector machines (SVMs), random forests (RF), and deep neural networks (DNNs) have also been employed for predicting molecular properties such as solubility, boiling point, and reactivity, a proof that technology makes chemistry easier to learn.[1,21,]

3.3 Reaction Outcome and Retrosynthesis

Retrosynthesis is a key process in organic chemistry that is used to determine the synthesis pathway from complex molecules to simpler molecules.[22]AI tools like IBM's RXN for Chemistry and MIT's Molecular Transformer model predict reaction outcomes and automate retrosynthetic pathway planning.[23,24] The work of Segler and Waller also show progress in modeling chemical reactions using this approach of machine learning which could have major implications in the understanding and design of molecular synthesis processes in organic chemistry. These researches reduce the need for trial-and-error approaches in organic synthesis.[25]

3.4 Chemical Process Optimization

AI having better prediction and modeling capabilities can help in optimizing chemical processes and improving production efficiency and product quality. The combination of AI and chemical sciences unlock the potential for breakthroughs in its understanding and applications thereby increasing the ability to design new molecules, predict chemical properties, and increase the efficiency of research and development in chemical sciences.[1, 26, 27]

3.5 Material Discovery

AI is transforming the discovery of materials by accelerating the process of finding new materials with desired properties.[1]Machine learning and high-throughput screening are enabling researchers to predict material behavior, optimize designs, and discover new materials faster and more efficiently than traditional methods.[28] This shift is crucial for addressing global challenges, accelerating the discovery of new materials like catalysts, polymers, and battery components and by analyzing large chemical datasets to predict novel combinations.[1] A typical example of AI used for material discovery is MatterGen, it works by generating novel materials, giving prompts of the design requirements for an application instead of screening the candidate thus enhancing advance development with improved characterization and autonomous experimentation. [29]

3.6 Reduction of Reliance on Experimentation

AI predictive capacity can help reduce repetitive experiments, saving time and resources in chemical research. This approach aims to automatically create new molecules with desired properties based on a continuous representation of the molecular structure.[30, 31]

3.7 Drug Discovery and Development

AI facilitates drug candidate screening, QSAR modeling, and toxicity prediction, significantly reducing the cost and time for drug development.[32] Artificial Intelligence (AI) is revolutionizing traditional drug discovery and development models by seamlessly integrating data, computational power, and algorithms. This synergy enhances the efficiency, accuracy, and success rates of drug research, shortens development timelines, and reduces costs.[33] Coupled with machine learning (ML) and deep learning (DL), AI has demonstrated significant advancements across various domains, including drug characterization, target discovery and validation; small molecule drug design, and the acceleration of clinical trials. Through molecular generation techniques, AI facilitates the creation of novel drug molecules, predicting their properties and activities, while virtual screening optimizes drug candidates. Additionally, AI enhances clinical trial efficiency by predicting outcomes, designing trials, and enabling drug repositioning. Majority of pharmaceutical companies have used AI to improve drug discovery. Verge Genomics uses AI to predict the effects of some new drugs on patients with Alzheimer's disease and Parkinson's disease.[34] In 2018, Bayer and Merck received Food and Drug Administration approval to use AI algorithms to support clinical decision making for chronic thromboembolic pulmonary hypertension.[1,35] Novartis currently uses AI algorithms to classify digital images of different cells.[36] In 2018, the biotech company Cyclica collaborated with Bayer, using AI machine learning to determine the polypharmacological profiles of small molecules and develop more affordable drugs.[37]

3.8 Spectroscopy and Analytical Chemistry

In recent years, artificial intelligence (AI) has offered transformative solutions to enhance the speed, accuracy, and efficiency of spectroscopic analysis. AI is revolutionizing the use of spectroscopy in

fields like pharmaceuticals, materials science, and environmental monitoring.[38] AI has helped to improve the accuracy of spectroscopic analysis by training algorithms to consistently detect discrepancies in spectral data, reducing the chances of misinterpretation, which is particularly relevant in industries like pharmaceuticals, where ensuring the quality and safety of products is paramount. AI improves spectral analysis (NMR, IR, MS) by automating peak identification, baseline correction, and compound classification.[39].

4. IMPACT OF AI ON GLOBAL CHALLENGES AND THE SUSTAINABLE DEVELOPMENT GOALS (SDGs)

AI serves as a catalyst for achieving the SDGs by providing innovative, data-driven solutions to some of the world's most pressing challenges. AI's integration into chemical sciences supports various global challenges in different ways, Its integration across sectors is significantly influencing key areas, particularly **SDG 3 (Good Health and Well-being)**[40,41,42]**; SDG 6 (Clean Water and Sanitation)** [43,44]**; SDG 7 (Affordable and Clean Energy)**[45]**; SDG 12 (Responsible Consumption and Production)** [46]**; and SDG 13 (Climate Action)** [47]**.**

5. CHALLENGES AND LIMITATIONS OF AI IN CHEMICAL SCIENCES

Despite its advantages, AI has brought a tremendous change to chemical sciences and this has positively affected most of the global challenges however limitations are inevitable and they include the following:data scarcity and quality Issues.[4,33,48]; inability of understanding AI results in a chemical context and integrating them with existing chemical knowledge; ethical, legal, and regulatory compliance[49], computational cost and infrastructure[39]; insecurity of data in chemical research; unfriendly AI platforms[1]; training of AI models on narrow data set[3]; limitations of AI Algorithms in understanding complex patterns in chemical data and difficult Interpretation of models and transparency.[50]

6. FUTURE DIRECTIONS OF AI TO CHEMICAL SCIENCES

The future development of chemical knowledge and AI technologies are likely to cause challenges to AI in chemical sciences thus a huge need for collaborations among chemists.computer scientist and AI experts to ensure constant update of AI models. This will directly improve interpretability,ensuring safety and ethics in the application of artificial intelligence thereby enhancing increased autonomy, sustainability, and deeper integration with emerging technologies. Among the developments,the emergence of autonomous laboratories**,** or self-driving experimental platforms, capable of designing, executing, and optimizing chemical experiments with minimal human intervention thereby accelerating discovery and reducing costs is very significant. Explainable AI (XAI)**,** which focuses on creating interpretable models that reveal underlying chemical reasoning, fostering trust and adoption, particularly in high-stakes domains such as drug discovery and toxicology remains another key trend.[50] The integration of AI with quantum computing is also expected to revolutionize molecular modeling and reaction prediction by enabling more efficient analysis of complex quantum systems.[52] Moreover**,** enhanced data infrastructure will be critical for the accuracy and reproducibility of AI models, with increasing emphasis on standardized, high-quality, and openly accessible datasets aligned with FAIR (Findable, Accessible, Interoperable, and Reusable) principles[53]. AI will further green and sustainable chemistry by aiding in the design of environmentally friendly materials and energy-efficient processes, thereby supporting circular economy practices and climate goals.[7] In addition**,** multimodal and multi-scale integration will allow AI systems to combine diverse data types such as text, spectra, and molecular structures across scales from the molecular to the process level, enabling more comprehensive chemical modeling.[39] Finally, the application of AI in education and collaborative research will democratize access to chemical knowledge and foster interdisciplinary innovation.[25]

7. CONCLUSION

The integration of artificial intelligence into chemical sciences represents a critical advancement in the 21st century. With applications ranging from drug discovery to environmental sustainability, AI offers powerful tools to address both long-standing and emerging challenges. However, to fully harness its potential, the chemical sciences community must overcome existing limitations in data quality, model transparency, and interdisciplinary collaboration. As AI continues to evolve, it is expected to redefine the boundaries of chemical research and contribute significantly to achieving global sustainability goals.

CONFLICT OF INTERESTS

The authors declare no conflict of interests.

REFERENCES

(1) Butler, K. T.; Davies, D. W.; Cartright, H.; Isayev, O.; Welsh, Aron. Machine Learning for Molecular and Materials Science. *Nature*, **2018**, 559(7715), 547–555.
(2) Mater, Adam C.; *Coote*, Michelle L. Deep Learning in Chemistry. *In: Journal of Chemical Information and Modeling*. **2019**, Vol.59,No.6.pp.2545-2
(3) Schneider, Sascha,; Beege Maik.; Nebel, Steve.: Rey, G.D. A meta-analysis of how signaling affects learning with media. *Educational Research Review* **2017**. 23 DOI: 10.1016/j.11.001
(4) Zeller, M.; Friedler, S.A.; Joshua, S.; Norquist, A. J. Machine-Learning-Assisted Materials Discovery Using Failed Experiments. *Nature*, **2016**, 533(7601), 73–76.
(5) Sanchez-Lengeling, B.; Outeiral, C.; Guimaraes, G.; AspuruGuzik, A. Optimizing Distributions over Molecular Space. An Objective-Reinforced Generative Adversarial Network for InverseDesign Chemistry (Organic). ChemRxiv. Preprint, **2017** DOI: 10.26434/chemrxiv.5309668.v3
(6) Aspuru-Guzik, A.; Tim, B.; Varinia, B.; Philip, C.; Biggin, F. B.; Itamar, B. J.; Ksenia, R.; Briling, et al. "Discovering chemical structure: general discussion." *Faraday Discussions*, vol. 256, **2025**, pp. 177-220.
(7) Schwaller, P.; Probst, D.; Vaucher A.C.; Nair , V.; Kreutter, D.; Laino, T. Mapping the Space of Chemical Reactions Using Attention-Based Neural Networks. *Nature Machine Intelligence*,
(8) Zhavoronkov, A.; Aspuru-Guzik, A. Reply to 'Assessing the impact of generative AI on medicinal chemistry'. *Nat. Biotechnol.* 2020. 38, 146
(9) Gangwal, A.; Ansari, A.; Ahmad, I.; Azad, AK.; Kumarasamy, V.; Subramaniyan, V.; Wong, L,S. Generative artificial intelligence in drug discovery: basic framework, recent advances, challenges, and opportunities. *Front Pharmacol*. **2024**;15:1331062.
(10) Mazheika, A.;Wang, Y.G.; Valero, R.; Viñes, F.; Illas, F.; Ghiringhelli, L..; Levchenko, S.V.; Scheffler, M. Artificial-intelligence-driven discovery of catalyst genes with application to CO_2 activation on semiconductor oxides. *Nat Commun*. **2022** ;13(1):419.
(11) Morán-González, L.; Burnage, A.L.; Nova, A.; Balcells, D. AI Approaches to Homogeneous Catalysis with Transition Metal Complexes. *ACS Catal.* 2025 15(11):9089-9105
(12) .Nematov, D.; Hojamberdiev, M. *Machine Learning-Driven Materials Discovery: Unlocking Next-Generation Functional Materials – A Minireview*. *arXiv* 2025, arXiv:2503.18975.
(13) Hrckova, A.; Renoux, J.; Tolosana Calasanz, R.; Chuda, D.; Tamajka, M.; Simko, J. AI Research Is Not Magic, It Has To Be Reproducible and Responsible: Challenges in the AI Field from the Perspective of Its PhD Students. *arXiv.* 2024, arXiv:2408.06847.
(14) Creswell, J. W.; Creswell, J. D. *Research Design: Qualitative, Quantitative, and Mixed Methods Approaches*, 5th ed.; Sage Publications: Thousand Oaks, CA, **2018.**
(15) Nassaji, H. Qualitative and descriptive research: Data type versus data analysis. *Language Teaching Research.* **2015***, 19*(2), 129–132.
(16) UKCI. Advances in Intelligent Systems and Computing, vol 1453. *Springer.* **2023**, Cham.
(17) Tasneem, S.; Saman, J. AI in Senior Chemistry Education: Enhancing engagement, Personalization and Pedagogical Practice. *Journal of Media Horizons* **2025**, *6* (2), 112-124.

(18) Iyamuremye, A., Niyonzima, F.N., Mukiza, J. *et al.* Utilization of artificial intelligence and machine learning in chemistry education: a critical review. *Discov Educ.* 2024 3, 95.
(19) Kokudeva, M.; Vichev, M.; Naseva, E.; Miteva, D.G.; Velikova, T. Artificial intelligence as a tool in drug discovery and development. *World J Exp Med.* **2024** 20;14(3):96042.
(20) Kearnes, S.; McCloskey, K.; Berndl, M.; Pande, V.; Riley, P. *Chemception: A Deep Neural Network with Minimal Chemistry Knowledge Matches the Performance of Expert-Developed Quantitative Structure–Activity Relationship (QSAR) / Quantitative Structure–Property Relationship (QSPR) Models. arXiv* **2017**, arXiv:1706.06689.
(21) Schütt, K. T.; Kindermans, P.-J.; Sauceda, H. E.; Chmiela, S.; Tkatchenko, A.; Müller, K.-R. *Quantum-Chemical Insights from Deep Tensor Neural Networks. Nat. Commun.* **2017**, *8* (1), 13890.
(22) Segler, M. H. S.; Waller, M. P. *Neural-Symbolic Machine Learning for Retrosynthesis and Reaction Prediction. Chem.–Eur. J.* **2017**, *23* (25), 5966–5971.
(23) Schwaller, P.; Vaucher, A. C.; Laino, T.; Reymond, J. L. *Prediction of Chemical Reaction Yields Using Deep Learning. Mach. Learn.: Sci. Technol.* **2021**, *2* (1), 015016. .
(24) Schwaller, P.; Laino, T.; Gaudin, T.; Bolgar, P.; Hunter, C. A.; Bekas, C.; Lee, A. A. *Molecular Transformer: A Model for Uncertainty-Calibrated Chemical Reaction Prediction. ACS Cent. Sci.* **2019,** *5* (9), 1572–1583.
(25) Segler, M. H. S.; Preuss, M.; Waller, M. P. *Planning Chemical Syntheses with Deep Neural Networks and Symbolic AI. Nature.* **2018**, *555* (7698), 604–610. Sanchez-Lengeling, B.; Aspuru-Guzik, A. *Engineering. Science* **2018**, *361* (6400), 360–365.
(26) Sanchez-Lengeling, B.; Aspuru-Guzik, A. *Engineering. Science* 2018, *361* (6400), 360–365.
(27) Häse, F.; Roch, L. M.; Aspuru-Guzik, A. *Next-Generation Experimentation with Self-Driving Laboratories. Trends Chem.* **2019**, *1* (3), 282–291.
(28) Schmidt, J.; Marques, M. R. G.; Botti, S.; Marques, M. A. L. Recent Advances and Applications of Machine Learning in Solid-State Materials Science. *npj Comput. Mater.* **2019**, *5* (1), 83.
(29) Stach, E.; DeCost, B.; Kusne, A. G.; Harrington, T.; Schrier, J.; Billinge, S. J. L.; Buonassisi, T.; Foster, I.; Hattrick-Simpers, J.; Mehta, A.; Montoya, J.; Olivetti, E.; Park, C.; Rotenberg, E.; Saal, J.; Smullin, S.; Srinivasan, V.; Suram, S. K.; Tabor, D. P. Autonomous Experimentation Systems for Materials Development: A Community Perspective. *Matter.* **2021**, *4* (9), 2702–2726.
(30) Gowda, S.; Tran, R.; Yang, J.; Zhang, Y.; Xu, Q.; Wood, B. C.; Wolverton, C.; Ong, S. P. MatterGen: A Generative Model for Inverse Materials Design. *npj Comput. Mater.* 2024, *10*, 35.
(31) Gómez-Bombarelli, R.; Wei, J. N.; Duvenaud, D.; Hernández-Lobato, J. M.; Sánchez-Lengeling, B.; Sheberla, D.; Aguilera-Iparraguirre, J.; Hirzel, T. D.; Adams, R. P.; Aspuru-Guzik, A. Automatic Chemical Design Using a Data-Driven Continuous Representation of Molecules. *ACS Cent. Sci.* **2018**, *4* (2), 268–276.
(32) Stokes, J. M.; Yang, K.; Swanson, K.; Jin, W.; Cubillos-Ruiz, A.; Donghia, N. M.; MacNair, C. R.; French, S.; Carfrae, L. A.; Bloom-Ackermann, Z.; Tran, V. M.; Chiappino-Pepe, A.; Badran, A. H.; Andrews, I. W.; Chory, E. J.; Church, G. M.; Brown, E. D.; Jaakkola, T. S.; Barzilay, R.; Collins, J. J. A Deep Learning Approach to Antibiotic Discovery. *Cell.* **2020***, 180* (4), 688–702.e13.
(33) Fu, C. Artificial Intelligence for Drug Discovery and Development. *Acta Pharm. Sin. B* **2022**, *12* (10), 3607–3616.
(34) Verge Genomics. Verge Genomics Uses AI to Tackle Neurodegenerative Diseases. *Verge Genomics* (accessed Aug 27, 2. U.S. Food & Drug Administration. FDA Permits Marketing of First AI-Based Device to Detect Certain Heart Problems. *FDA News Release* (2018).
(35) . U.S. Food & Drug Administration. FDA Permits Marketing of First AI-Based Device to Detect Certain Heart Problems
(36) Novartis. Harnessing Artificial Intelligence to Transform Drug Discovery. *Novartis* (accessed Aug 27, 2025).
(37) Cyclica. Cyclica and Bayer Partner to Apply AI in Drug Discovery. *Cyclica Press Release* (2018). https://www.cyclicarx.com
(38) Chen, J.;McCallum, A.; Achim, A.; He, Y. Artificial Intelligence in Spectroscopy: From Peak Assignment to Automated Spectral Interpretation. *TrAC Trends Anal. Chem.* **2021**, *143*, 116370.

(39) Zhou, Z.; Smith, A.; Johnson, B.; Patel, C.; Wang, D.; Martinez, E.; Gupta, F. AI-Driven Spectroscopy for Real-Time Chemical Analysis. *Anal. Chem.* **2022**, *94* (2), 789–796.
(40) Zhavoronkov, A., et al. Deep Learning Enables Rapid Identification of Potent DDR1 Kinase Inhibitors. *Nature Biotechnology*, **2019**, 37(9), 1038–1040.
(41) Topol, E. *Deep Medicine: How Artificial Intelligence Can Make Healthcare Human Again*; Basic Books: New York, **2019**. ISBN 9781541644632.
(42) Guégan J-F, Suzán G, Kati-Coulibaly S, Bonpamgue DN, Moatti J-P. Sustainable Development Goal 3, "health and well-being", and the need for more integrative thinking. *Veterinaria México OA*. **2018**,;5(2).doi:10.21753/vmoa.5.2.443
(43) Zou, S.; Ju, H.; Zhang, J. Water Quality Management in the Age of AI: Applications, Challenges, and Prospects. *Water* **2025**, *17*, 1641
(44) Jayakumar, D.; Bouhoula, A.; Al-Zubari, W.K. Unlocking the Potential of Artificial Intelligence for Sustainable Water Management Focusing Operational Applications. *Water* 2024, *16*, 3328.
(45) Razak, T. R.; Ismail, M. H.; Darus, M. Y.; Jarimi, H.; Su, Y. Artificial Intelligence in Renewable Energy: A Systematic Review of Trends in Solar, Wind, and Smart Grid Applications. *Research and Reviews in Sustainability* **2025**,Vol 1,No 1,p 1-22.
(46) United Nations. *Sustainable Development Goal 12: Ensure Sustainable Consumption and Production Patterns.* United Nations, **2015**. Available online: https://sdgs.un.org/goals/goal12 (accessed Aug 30, 2025).
(47) Rolnick, D.; Donti, P. L.; Kaack, L. H.; Kochanski, K.; Lacoste, A.; Sankaran, K.; Ross, A. S.; Milojevic-Dupont, N.; Jaques, N.; Waldman-Brown, A.; Luccioni, A.; Maharaj, T.; Sherwin, E. D.; Mukkavilli, S. K.; Kording, K. P.; Gomes, C.; Ng, A. Y.; Hassabis, D.; Platt, J. C.; Creutzig, F.; Chayes, J.; Bengio, Y. Tackling Climate Change with Machine Learning. *arXiv* [Preprint], arXiv:1906.05433, **2019**.
(48) Wu, Z.; Ramsundar, B.; Feinberg, E. N.; Gomes, J.; Geniesse, C.; Pappu, A. S.; Leswing, K.; Pande, V. MoleculeNet: A Benchmark for Molecular Machine Learning. *Chem. Sci.* **2018**, *9* (2), 513–530.
(49) Coley, C. W.; Eyke, N. S.; Jensen, K. F. Autonomous Discovery in the Chemical Sciences Part I: Progress. *Angew. Chem. Int. Ed.* **2020**, *59* (51), 22858–22893.
(50) Samek, W., et al. Explainable Artificial Intelligence: Understanding, Visualizing and Interpreting Deep Learning Models. *IEEE Signal Processing Magazine*, **2021**, 38(3), 88–92.
(51) Burger, B; Maffettone, P. M.; Gusev, V.V.; Aitchison, C. M.; Bai, Y.; Wang, X.; Li, X.; Alston, B. M.; Li, Bi; Clowes, R; Rankin, N.; Harris, B.; Sprick, R. S.; Cooper, A. I. A Mobile Robotic Chemist. *Nature* **2020**, *583* (7815), 237–241.
(52) Cao, Y.; Romero, J.; Olson, J. P.; Degroote, M.; Johnson, P. D.; Kieferová, M.; Kivlichan, I. D.; Menke, T.; Peropadre, B.; Sawaya, N. P. D.; Sim, S.; Veis, L.; Aspuru-Guzik, A. Quantum Chemistry in the Age of Quantum Computing. *Chem. Rev.* **2019**, *119* (19), 10856–10915.
(53) Wilkinson et al., The FAIR Guiding Principles for Scientific Data Management and Stewardship. *Sci. Data.* **2016,** *3*, 160018. .

ISBN: 978-978-68-0485-9 DOI: https://doi.org/10.55455/acsnigeria.1.2.149-154

Stacked Ensemble Machine Learning for Human Carbonic Anhydrase II Binding Affinity Prediction

[1]Miracle Olatilewa Olapade, [2]Olalekan Cosmas Ogundola, and [1]Dotun Solomon Akeju.
[1]Department of Chemistry, University of Ibadan, Ibadan, Nigeria
[2]Department of Chemistry, Federal University, Oye-Ekiti, Nigeria
Corresponding Author's email: olapademiracleo@gmail.com

ABSTRACT

Many diseases, such as glaucoma, epilepsy, and cancer, are associated with carbonic anhydrase II. This makes it an important therapeutic target for these diseases. A stacked ensemble machine learning model was built to predict the binding affinity of ligands with CA II. The dataset used consists of 6,530 compounds with experimental Ki values from ChEMBL. Each molecule was represented by a set of 1,420 molecular descriptors, including Morgan fingerprints, MACCS keys, and RDKit 2D descriptors, which were refined to 1,320 features through different feature selection procedures. A stacked ensemble model which makes use of LightGBM, ExtraTrees, and a Multi-Layer Perceptron (MLP) was developed, with ridge regression as the meta-learner. The model achieved a satisfactory performance on the test set, with a root mean square error (RMSE) of 0.68 pKi units and a coefficient of determination (R^2) of 0.76. SHAP (SHapley Additive exPlanations) analysis of the best-performing model provided important interpretability. The method identified some specific molecular substructures (e.g., Morgan_833), key pharmacophoric elements (MACCS_84, MACCS_33), and functional groups (e.g., primary amines) as the most impactful drivers of binding affinity. The outcome of the study aligns with established structure-activity relationships for CA II inhibitors; this validates the model's decision-making process. This work provides more than a tool for virtual screening but also offers interpretable insights to guide the rational design of novel CA II inhibitors.

KEYWORDS: Machine Learning, Binding Affinity, SHAP analysis, Carbonic Anhydrase II, Virtual Screening

1. INTRODUCTION

Human Carbonic Anhydrase II (hCA II) is a zinc-dependent metalloenzyme essential for physiological pH regulation and a well-established therapeutic target for conditions such as glaucoma and epilepsy, which drives the development of inhibitors like sulfonamides.[1,2,3] While experimental binding affinity measurements are resource-intensive,[4] conventional computational methods like molecular docking and dynamics are constrained by force-field approximations and high computational cost.[5,6,7,8] Machine learning (ML) offers a powerful alternative by learning structure-activity relationships directly from data, often surpassing the performance of classical scoring functions.[9]

Machine learning has been increasingly applied in carbonic anhydrase research, primarily focusing on classification tasks such as predicting inhibitor activity (active/inactive)[10] and identifying multi-target inhibitors.[11] Some studies have addressed the critical challenge of isoform selectivity, developing models to distinguish inhibitors of off-target isoforms like hCA II from therapeutic targets such as hCA IX,[12] with recent work incorporating explainable AI to elucidate the structural basis of these predictions.[13] Although these classification approaches are valuable tools for virtual screening, they offer limited utility for lead optimization, which requires quantitative potency measurements. Predicting continuous binding affinity (pKi) values represents a complex but practically important task which enables the precise ranking of compounds and also provides the avenue for quantitative structure-activity relationship analysis. To address this need, the present study developed a stacked ensemble model to improve predictive accuracy and generalization for binding affinity prediction. This approach provides both high-accuracy pKi values and interpretable insights into the molecular features governing binding affinity.

2. METHODOLOGY

2.1. Data Curation and Preprocessing

An initial dataset of 10,294 potential human Carbonic Anhydrase II (CA II) inhibitors was sourced from the ChEMBL database.[14] This raw data was rigorously curated to ensure data quality, retaining only entries with precisely defined equilibrium dissociation constant (K_i) values reported

in nanomolar (nM) units. Compounds annotated with inequality modifiers (e.g., '>', '<') were excluded. This filtration process resulted in a refined, high-confidence dataset of 6,539 compounds, each with a

defined ChEMBL identifier, SMILES string, and exact K_i value. For each unique canonical SMILES, only the entry with the lowest reported Ki value (indicating the highest potency) was retained to represent that compound, ensuring no data leakage between training and test sets. This process yielded a final curated dataset of 6,530 compounds. The Ki (nM) values were converted to pKi, the negative logarithm of the Ki in molar units, to create a more normally distributed target variable suitable for regression modeling, using the standard transformation:

$$\mathbf{pKi = 9 - \log_{10}(Ki\_nM)}$$

2.2. Molecular Feature Engineering and Selection

Molecular descriptors and fingerprints were computed for each compound using the RDKit library to numerically encode their structural and physicochemical properties. This included: (i) Morgan Fingerprints (ECFP4-like), configured with a radius of 2 and a fixed length of 1024 bits to capture atomic environments and molecular substructures; (ii) 167-bit MACCS keys, which are binary fingerprints which shows the presence of specific predefined structural fragments; and (iii) 208 RDKit 2D descriptors capturing key properties. The combination of these features resulted in an

initial high-dimensional feature matrix comprising 1,413 dimensions for each molecule and whereby after feature selection we have 1320 features for model development and evaluation.

2.3. Model Development and Evaluation

The curated dataset was partitioned using stratified random split into training set (60%), validation (20%), and test sets (20%). A stacked ensemble architecture was implemented, using three base learners (LightGBM, ExtraTrees, and MLP Regressor). Hyperparameter optimization was conducted through randomized search with 3-fold cross-validation over 25 iterations. Model performance was measured using root mean square error (RMSE), mean absolute error (MAE), and coefficient of determination (R^2) metrics. To enable interpretation of the model, SHapley Additive exPlanations (SHAP) analysis was applied to elucidate feature contributions to model predictions.[15]

3. RESULTS AND DISCUSSION

3.1 Results

3.1.1 Model Performance Evaluation

The performance of all models on both validation and test sets is summarized in Table 1. The Stacked Ensemble achieved the best performance as shown in Figure 1

Table 1. Performance metrics of models on validation and test sets

Model	Validation Set			Test Set		
	RMSE	MAE	R^2	RMSE	MAE	R^2
Extra Trees	0.7084	0.5006	0.7436	0.6895	0.4919	0.7571
LightGBM	0.7188	0.5257	0.7418	0.7052	0.5317	0.7459
MLP Neural Network	0.8144	0.6167	0.6610	0.7781	0.5910	0.6906
Stacked Ensemble	0.6920	0.5063	0.7553	0.6815	0.5033	0.7627

On the validation set, the stacked ensemble achieved the lowest RMSE (0.6920) and highest R^2 (0.7553),

outperforming all individual models. Extra Trees was the strongest base learner (RMSE = 0.7084, R^2 = 0.7436), followed closely by LightGBM (RMSE = 0.7188, R^2 = 0.7418). This performance hierarchy was maintained on the independent test set as shown in Figure 1, where the stacked ensemble further improved to RMSE = 0.6815 and R^2 = 0.7627, confirming robust generalization and the advantage of the ensemble approach.

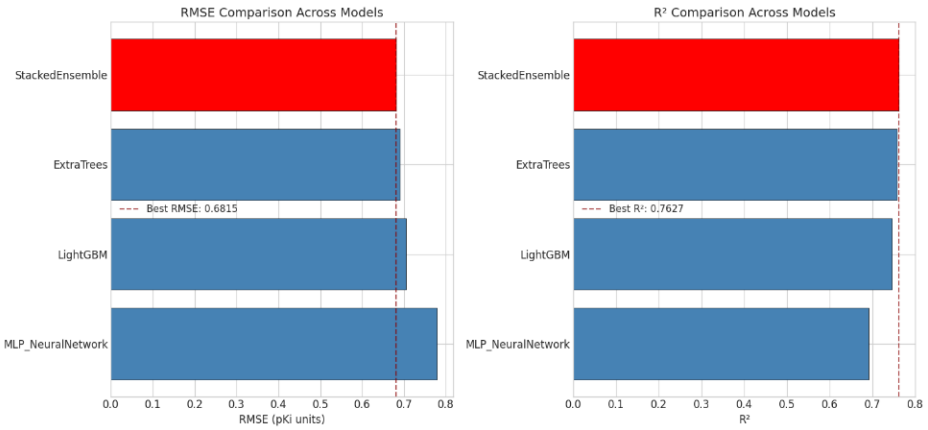

Figure 1: Comparative performance of individual models and stacked ensemble on the test set.

3.1.2. Model Interpretation via SHAP Analysis

SHAP analysis of the three individual models provided insights into binding affinity determinants.[15] The key molecular features driving predictions were identified through the SHAP analysis as shown in table 2.

Table 2. Top 5 Features by Model from SHAP Analysis

Rank	ExtraTrees	LightGBM	MLP Neural Network
1	Morgan_833 (0.3366)	SMR_VSA4 (0.4195)	fr_NH2 (0.1297)
2	MACCS_84 (0.3175)	Morgan_833 (0.1916)	SMR_VSA4 (0.0679)
3	MACCS_33 (0.0864)	MACCS_84 (0.1122)	fr_sulfonamd (0.0489)
4	fr_NH2 (0.0772)	MolLogP (0.0606)	NHOHCount (0.0258)
5	Morgan_583 (0.0501)	SPS (0.0453)	FpDensityMorgan3 (0.0227)

3.2 Discussion

This study reports the design and evaluation of a reliable predictive stacked ensemble model for predicting binding affinity (pKi) of ligands to human Carbonic Anhydrase II (CA II). The stacked ensemble model demonstrated strong predictive performance on the test set (RMSE = 0.68, R^2 = 0.76), confirming the efficacy of this approach for QSAR modeling. Consistent with our findings, previous QSAR studies have demonstrated that stacked ensemble approaches often outperform individual models in terms of predictive accuracy.[16,17,18] The stacked ensemble approach in this study leveraged the distinct strengths of its individual models: the gradient-boosting power of LightGBM,[19] the random feature selection and the use of random thresholds to split nodes in the decision trees in ExtraTrees,[20,21] and the ability of MLPs to capture complex non-linearities and complex feature interactions[22] that may be missed by tree-based methods. The meta-learner (Ridge regression) weighted these predictions, assigning the highest weights to the tree-based models, which individually performed best.

The curation process of the molecular data was a critical factor in the model's success. The steps taken

including SMILES standardization, removal of inorganic compounds, deduplication, and feature selections which are considered best practices in computational chemistry to ensure data quality and model reliability.[23] The removal of highly correlated features is crucial, as it reduces redundancy and multicollinearity, which can inflate variance and destabilize model coefficients. The model's performance on the test set (R^2 = 0.76, RMSE = 0.68) is consistent with the high standards seen in modern QSAR benchmarks. An RMSE of 0.68 log units, which corresponds to a less than 5-fold error in Ki value prediction on average, is considered highly accurate for practical applications in drug discovery, such as virtual screening and lead optimization prioritization.[24]

The SHAP analysis provided an important, experimentally actionable interpretation of the model predictions, this reveals the key structural drivers. A strong consensus across models on specific molecular features, particularly the Morgan_833 fingerprint and MACCS_84 key, suggests the identification of important substructures that are strong determinants of binding affinity. The outcome is consistent with the known structure-activity relationships of CA II inhibitors, which often rely on a zinc-binding group and specific aromatic moieties that fit into the hydrophobic pocket of the enzyme. [25, 26] Hydrogen-bonding features like the primary amine count (fr_NH2) and the primary sulfonamide group (fr_sulfonamd) serves as a strong validation of the model's ability to recapitulate known medicinal chemistry, as these groups are known to coordinate the active site zinc ion. Also, the impact of properties like MolLogP and SMR_VSA4 shows the model's recognition that overall physicochemical properties are vital for optimizing ligand efficiency and bioavailability.[27] These interpretability results significantly enhance the use of the model, as they provide medicinal chemists with specific guidance on which functional groups and properties to modify in order to optimize compound affinity.

4. CONCLUSION

This study presents a stacked ensemble model and interpretation of the three individual models used as the base learners. The SHAP analysis of the three individual models shows some important features which are critical for the prediction and also provide insight for the rational design of novel CAII inhibitors.

Code and dataset are available at https://github.com/miraculinp/CAII

CONFLICT OF INTERESTS

The authors declare no conflict of interests.

REFERENCES

(1) Tinazzi, E.; Patuzzo, G.; Lunardi, C. Autoantigens and Autoantibodies in the Pathogenesis of Sjögren's Syndrome. In *Sjogren's Syndrome*; Gerli, R., Bartoloni, E., Alunno, A., Eds.; Elsevier, 2016; pp 141–156.

(2) O'Herin, C. B.; Moriuchi, Y. W.; Bemis, T. A.; Kohlbrand, A. J.; Burkart, M. D.; Cohen, S. M. Development of Human Carbonic Anhydrase II Heterobifunctional Degraders. *J. Med. Chem.* **2023**, *66* (4), 2789–2803. https://doi.org/10.1021/acs.jmedchem.2c01843.

(3) Supuran, C. T.; Capasso, C.; De Simone, G. Carbonic Anhydrase II as Target for Drug Design. In *Carbonic Anhydrases as Biocatalysts*; Elsevier, 2015; pp 51–90.

(4) Yang, Y. X.; Zhu, B. T. Further Exploration of the Quantitative Distance-Energy and Contact Number-Energy Relationships for Predicting the Binding Affinity of Protein-Ligand Complexes. *Biophys. J.* **2025**, *124* (7), 1166–1177. https://doi.org/10.1016/j.bpj.2025.02.021.

(5) Mushebenge, A. G.-A.; Ugbaja, S. C.; Mbatha, N. A.; Khan, R. B.; Kumalo, H. M. Assessing the Potential Contribution of In Silico Studies in Discovering Drug Candidates That Interact with Various SARS-CoV-2 Receptors. *Int. J. Mol. Sci.* **2023**, *24* (21), 15518. https://doi.org/10.3390/ijms242115518.

(6) Guedes, I. A.; Pereira, F. S. S.; Dardenne, L. E. Empirical Scoring Functions for Structure-Based Virtual Screening: Applications, Critical Aspects, and Challenges. *Front. Pharmacol.* **2018**, *9*, 1089. https://doi.org/10.3389/fphar.2018.01089.

(7) Salmaso, V.; Moro, S. Bridging Molecular Docking to Molecular Dynamics in Exploring Ligand-Protein Recognition Process: An Overview. *Front. Pharmacol.* **2018**, *9*, 923. https://doi.org/10.3389/fphar.2018.00923.

(8) Challapa-Mamani, M. R.; Tomás-Alvarado, E.; Espinoza-Baigorria, A.; León-Figueroa, D. A.; Sah, R.; Rodriguez-Morales, A. J.; Barboza, J. J. Molecular Docking and Molecular Dynamics Simulations in Related to *Leishmania Donovani*: An Update and Literature Review. *Trop. Med. Infect. Dis.* **2023**, *8* (10), 457. https://doi.org/10.3390/tropicalmed8100457.

(9) Meli, R.; Morris, G. M.; Biggin, P. C. Scoring Functions for Protein-Ligand Binding Affinity Prediction Using Structure-Based Deep Learning: A Review. *Front. Bioinform.* **2022**, *2*, 885983. https://doi.org/10.3389/fbinf.2022.885983.

(10) Tinivella, A.; Pinzi, L.; Rastelli, G. Prediction of Activity and Selectivity Profiles of Human Carbonic Anhydrase Inhibitors Using Machine Learning Classification Models. *J. Cheminform.* **2021**, *13* (1), 18. https://doi.org/10.1186/s13321-021-00499-y.

(11) Kim, M.-J.; Pandit, S.; Jee, J.-G. Discovery of Kinase and Carbonic Anhydrase Dual Inhibitors by Machine Learning Classification and Experiments. *Pharmaceuticals* **2022**, *15* (2), 236. https://doi.org/10.3390/ph15020236.

(12) Galati, S.; Yonchev, D.; Rodríguez-Pérez, R.; Vogt, M.; Tuccinardi, T.; Bajorath, J. Predicting Isoform-Selective Carbonic Anhydrase Inhibitors via Machine Learning and Rationalizing Structural Features Important for Selectivity. *ACS Omega* **2021**, *6* (5), 4080–4089. https://doi.org/10.1021/acsomega.0c06153.

(13) Kırboğa, K. K.; Işık, M. Explainable Artificial Intelligence in the Design of Selective Carbonic Anhydrase I-II Inhibitors via Molecular Fingerprinting. *J. Comput. Chem.* **2024**, *45* (18), 1530–1539. https://doi.org/10.1002/jcc.27335.

(14) Zdrazil, B.; Felix, E.; Hunter, F.; Manners, E. J.; Blackshaw, J.; Corbett, S.; de Veij, M.; Ioannidis, H.; Lopez, D. M.; Mosquera, J. F.; et al. The ChEMBL Database in 2023: A Drug Discovery Platform Spanning Multiple Bioactivity Data Types and Time Periods. *Nucleic Acids Res.* **2023**, *52* (D1), D1180–D1192. https://doi.org/10.1093/nar/gkad1004.

(15) Lundberg, S. M.; Lee, S.-I. A Unified Approach to Interpreting Model Predictions. *Adv. Neural Inf. Process. Syst.* **2017**, *30*.

(16) Grenet, I.; Merlo, K.; Comet, J.-P.; Tertiaux, R.; Rouquié, D.; Dayan, F. Stacked Generalization with Applicability Domain Outperforms Simple QSAR on in Vitro Toxicological Data. *J. Chem. Inf. Model.* **2019**, *59* (4), 1486–1496. https://doi.org/10.1021/acs.jcim.8b00553.

(17) Schaduangrat, N.; Homdee, N.; Shoombuatong, W. StackER: A Novel SMILES-Based Stacked Approach for the Accelerated and Efficient Discovery of ERα and ERβ Antagonists. *Sci. Rep.* **2023**, *13* (1), 21166. https://doi.org/10.1038/s41598-023-50393-w.

(18) Sheffield, T. Y.; Judson, R. S. Ensemble QSAR Modeling to Predict Multispecies Fish Toxicity Lethal Concentrations and Points of Departure. *Environ. Sci. Technol.* **2019**, *53* (21), 12793–12802. https://doi.org/10.1021/acs.est.9b03957.

(19) Omotehinwa, T. O.; Oyewola, D. O.; Dada, E. G. A Light Gradient-Boosting Machine Algorithm with Tree-Structured Parzen Estimator for Breast Cancer Diagnosis. *Healthc. Anal.* **2023**, *4*, 100218. https://doi.org/10.1016/j.health.2023.100218.

(20) Sabherwal, G. Feature Selection Using Extra Trees Classifier for Parkinson's Disease Classification. *J. Mech. Cont. & Math. Sci.* **2024**, *Spl11* (1), 1–12. https://doi.org/10.26782/jmcms.spl.11/2024.05.00010.

(21) Ghazwani, M.; Begum, M. Y. Computational Intelligence Modeling of Hyoscine Drug Solubility and Solvent Density in Supercritical Processing: Gradient Boosting, Extra Trees, and Random Forest Models. *Sci. Rep.* **2023**, *13* (1), 22492. https://doi.org/10.1038/s41598-023-37232-8.

(22) Bagheri, S.; Taridashti, S.; Farahani, H.; Watson, P.; Rezvani, E. Multilayer Perceptron Modeling for

Social Dysfunction Prediction Based on General Health Factors in an Iranian Women Sample. *Front. Psychiatry* **2023**, *14*, 1283095. https://doi.org/10.3389/fpsyt.2023.1283095.

(23) Fourches, D.; Muratov, E.; Tropsha, A. Trust, But Verify: On the Importance of Chemical Structure Curation in Cheminformatics and QSAR Modeling Research. *J. Chem. Inf. Model.* **2010**, *50* (7), 1189–1204. https://doi.org/10.1021/ci100176x.

(24) Golbraikh, A.; Tropsha, A. Predictive QSAR Modeling Based on Diversity Sampling of Experimental Datasets for the Training and Test Set Selection. *Mol. Divers.* **2000**, *5* (4), 231–243. https://doi.org/10.1023/a:1021372108686.

(25) Ferraroni, M.; Cornelio, B.; Sapi, J.; Supuran, C. T.; Scozzafava, A. Sulfonamide Carbonic Anhydrase Inhibitors: Zinc Coordination and Tail Effects Influence Inhibitory Efficacy and Selectivity for Different Isoforms. *Inorg. Chim. Acta* **2018**, *470*, 128–132. https://doi.org/10.1016/j.ica.2017.03.038.

(26) Supuran, C. T. Carbonic Anhydrases: Novel Therapeutic Applications for Inhibitors and Activators. *Nat. Rev. Drug Discov.* **2008**, *7* (2), 168–181. https://doi.org/10.1038/nrd2467.

(27) Hopkins, A. L.; Keserü, G. M.; Leeson, P. D.; Rees, D. C.; Reynolds, C. H. The Role of Ligand Efficiency Metrics in Drug Discovery. *Nat. Rev. Drug Discov.* **2014**, *13* (2), 105–121. https://doi.org/10.1038/nrd4163.

ACS Chapter Nigeria
Book of Proceedings
15TH Annual SYMPOSIUM
ISBN: 978-978-68-0485-9 DOI: https://doi.org/10.55455/acsnigeria.1.2.155-158

Integrating Green Chemistry Approach in Teaching and Learning Esterification Among Senior Secondary Students in Uyo, Nigeria

Atim Sunday Johnson[a], Esther Raphael Etim[b*], Esther Silas Uwa[b], and Naomi Mattias Ekpenyong[b]
[a]Department of Chemistry, University of Uyo.
[b]Science Education Department, University of Uyo, Akwa Ibom State, Nigeria.
Corresponding Author's email: etimesther715@gmail.com

ABSTRACT

Traditional chemistry teaching methods often emphasize conventional techniques, which can overlook sustainability. Integrating Green Chemistry into the curriculum addresses this gap by promoting eco-friendly practices and enhancing students' critical thinking skills. This study aimed to examine the impact of the Green Chemistry (GC) approach on students' academic achievement in teaching esterification. The study was guided by two specific objectives, research questions, and hypotheses. A quasi-experimental control group design was employed, with post-test data. A sample of 120 students were drawn from a population of 3,246 students across 15 public secondary schools in Uyo. The experimental group, consisting of 28 urban and 30 rural students, was taught esterification using ethanol extracted from fermented palm wine and vinegar. The control group, comprising 62 students, was taught using conventional chemicals such as ethanol and ethanoic acid. Data were collected through the Chemistry Achievement Test (CAT) on esterification, with a reliability coefficient of 0.85. Analysis using mean, standard deviation, and independent t-tests revealed a significant difference in the academic achievement of students taught using the Green Chemistry approach compared to those taught using the conventional laboratory approach (CL). Furthermore, urban students outperformed rural students when both were taught using the Green Chemistry approach. Based on these findings, the study recommends that educational institutions adopt the Green Chemistry approach for teaching esterification and that teachers receive training to ensure its effective integration into classrooms.

KEYWORDS: Green chemistry education, esterification, students' academic achievement.

1. INTRODUCTION

The aim of chemistry education goes beyond merely preparing students for careers in the chemical sciences; it also seeks to help them understand the relevance of chemical applications and use of chemistry responsibly and sustainably. Unfortunately, the traditional way of teaching chemistry does not prioritize this aspect.Omoniyi[1] noted that, to meet the challenges of the 21st century, there is a need for an effectively implemented chemistry curriculum that inculcates in students the nature and benefits of chemistry to life and society. The current curriculum is designed to align with the objectives of science education as stated in the National Policy on Education[2], one of which is to foster critical thinking, problem-solving skills, and scientific attitudes in students. Achimugu[3] emphasized that, to achieve these objectives, chemistry teachers must effectively bridge curriculum and the students. Not only that they must also provide a grassroots approach to education -equipping young learners with advocacy skills, exposing them early to sustainable practices, and preparing them to contribute towards the achievement of the UN SDGs and to tackle environmental challenges in the future. This underscores the importance of Green Chemistry Education.

According to Achu[4], Green Chemistry in education is a novel approach to teaching chemistry that emphasizes risk mitigation and keeping hazardous substances out of the environment. Incorporating Green Chemistry into the chemistry curriculum at every level—beginning with secondary schoolis a strategic way to equip students with the knowledge and skills necessary to ensure environmental sustainability for both present and future generations. Similarly, Chen, Jeronen, and Wang [5] observed that demonstrating chemistry experiments using the principles of green chemistry fosters collaborative and problem-based learning. This approach engages students in real-world scenarios requiring critical thinking and teamwork, making chemistry more accessible, practical, and relevant to contemporary environmental issues.

Chemistry as a subject involves both theoretical content and practical skills learned through scientific methods such as experimentation. However, in Nigeria, many students perceive chemistry as abstract because they rarely have the opportunity to carry out experiments that make concepts tangible. The lack or insufficiency of chemicals and equipment for experiments has long hindered effective teaching and learning of chemistry [6] and is a contributing factor to the low academic achievement of secondary

school students in the subject. By applying the principles of Green Chemistry, both teachers and students can think critically about using readily available chemicals, improvised apparatus, natural catalysts, green solvents, renewable feedstocks, reused materials, cost-effective synthesis methods, microscale demonstrations, and energy-efficient workflows—all of which make learning more relevant and resourceful.

Furthermore, Green Chemistry demonstrations place a strong emphasis on safety, ensuring that experiments are conducted in ways that are environmentally friendly and non-hazardous to both students and teachers[7]. This intervention is particularly important in addressing the common situation where students shy away from practical work due to fear of accidents or exposure to toxic substances. Such fears have long hampered student-centered learning, as advocated in this contemporary era of education.

Researches have shown that green chemistry activities improve students' understanding of chemical principles and spark their interest in learning the subject, both of which are critical to their academic success [8,9]Ma and Shengli[10]investigated students' comprehension of green chemistry concepts. Grades 9–12 students were interviewed, and a semi-structured two-tier diagnostic instrument was developed. After revisions through pilot surveys, the final instrument was administered to examine students' understanding. Findings revealed that secondary school students have limited knowledge of green chemistry. This shows that the integration of green chemistry into the secondary school curriculum is still at its infancy stage in Africa.To facilitate this shift in Africa, there's a need to intergrate simple GC activities into the curriculum. This study explores the green alternative to demonstrating esterification which can be carried independently by students to help them better understand and appreciate this concept. The aim of this study is to determine to impact of this green demonstration on the academic achievement of students from both urban and rural school location.

2. RESEARCH HYPOTHESES

The following null hypotheses were generated and tested at 0.05 level of significance.

1. There is no significant difference between the achievement mean scores of students taught esterification using GC approach and those taught using CL approach.
2. There is no difference between the achievement mean scores of urban and rural school students taught esterification using GC approach.

3. RESEARCH METHODOLOGY

This study employed a quasi-experimental, posttest-only design to examine the effect of teaching esterification using the Green Chemistry approach compared to the conventional laboratory method. A total of 120 Senior Secondary School Two (SSS2) science students from two purposively selected public secondary schools formed the sample. One intact class from each school was randomly selected, with one class (58 students: 28 urban, 30 rural) assigned to the experimental group and the other (62 students: 30 urban, 32 rural) to the control group. The researcher-developed Chemistry Achievement Test (CAT) on Esterification, comprising 20 multiple-choice questions with a maximum score of 20 marks, was used for data collection. In the experimental group, the researcher guided the students on the demonstration of esterification using the Green Chemistry approach. In this approach, the mixture of fermented palm wine and yeast was distilled at about 78℃ to obtained ethanol. 10 drops of concentrated tetraoxosulphate (IV) acid was first added to 2ml of vinegar in a dry test tube and mixed followed by the addition of 4ml of the distilled ethanol. The mixture was warmed in a water - bath (hot but not bubbling) for 25 minutes and poured into a beaker partially filled with sodium chloride solution. The reaction yielded a fruity smell vapour tested to be ethyl ethanoate. Students in the control group with guidance, carried out the esterification demonstration using the conventional laboratory approach. Same procedures as in the GC approach was involved here but with the use of conventional chemicals namely; ethanol and ethanoic acid. The reaction also yield ethyl ethanoate. After the two-weeks treatment period, the CAT was administered to all 120 students. The test scripts were collected and analysed for assessment.

4. RESULTS AND DISCUSSION

4.1 Results

Table 1: Independent t-test analysis of mean achievement scores of students taught esterification using GC approach and those taught using CL approach

Variables	n	X	SD	df	t-cal	t-crit	Decision at p<.05
GC approach	58	14.18	2.52	118	13.19	1.98	Rejected
CL approach	62	7.65	2.91				

The findings in Table 1 above indicated that the calculated t-value of 13.19 is greater than the critical value of 1.98 at 0.05 level of significance. Based on this result, the null hypothesis earlier stated was rejected and the study claimed that there is a significant difference in students' academic achievement taught esterification using GC approach and those taught using CL approach.

Table 2: Independent t-test analysis of mean Achievement scores of urban and ruralstudents taught esterification using GC approach

Variables	n	X	SD	df	t-cal	t-crit	Decision at p<.05
Urban	28	15.46	2.08	56	2.12	2.00	accepted
Rural	30	13.00	2.91				

The findings in Table 2 above indicated that the calculated t-value of 2.12 is less than the critical value of 2.00 at 0.05 level of significance. Based on this result, the null hypothesis earlier stated was accepted. This means that there is no significant difference in academic achievement of urban and rural school students taught esterification using GC approach.

4.2 Discussion

The finding of this study as indicated in Table 1 shows that students taught esterification using GC approach performed significantly better than those taught using CL approach . The finding agrees with Karpudewan[8] who concluded that GC learning approach led to the highest learning outcomes among students than lecture learning approach. The finding also agrees with Umannah and Udo[9] who investigated the impact of GC approach on teaching Le chartler's principle among secondary schools students in Akwa Ibom State and concluded that GC approach does not only improve student engagement but also foster critical thinking skills, making chemistry more relevant and applicable to real-world scenarios.

The findings as shown in tables 2 shows that there is no significant difference in the mean achievement scores between urban and rural school students taught esterification using GC approach. This finding agrees with Karpudewan, Roth and Sinniah[8] who examined students' understanding of acid–base concepts and argumentation skill through GC approach and reported a no significant difference in the students' academic achievement between the two geographical locations of the schools taught using GC approach. The study contradicts the findings of Ovat, Nwogwugwu, and Idika[11], who found that school location has a significant impact on academic performance of upper basic nine students. Both groups performed well, but urban students outperformed rural students by a small margin. This is because the urban students are more frequently exposed to laboratory activities than the rural students.

5. CONCLUSION

The following conclusions were drawn from the findings of the study;

1. There is a significant difference between the mean achievement scores of students taught esterification using GC approach and those taught using CL approach .
2. There is no significant difference in the mean achievement scores of urban and rural school students taught esterification using GC approach

ACKNOWLEDGMENT

The authors wish to acknowledge with gratitude the contributions that made this study possible. In particular, we are grateful to the first author for her encouragement and dedicated support throughout the course of this work.

CONFLICT OF INTERESTS

The authors declare no conflict of interests.

REFERENCES

(1) Omoniyi, A.; Aarinola, A. Implementation of Chemistry Curriculum in Nigeria: Challenges for the 21st Century. *World J. Educ. Res.***2022**, *2* (1), 53–60.

(2) Federal Ministry of Education. *National Policy on Education*; 2023. https://education.gov.ng/wp-content/uploads/2020/09/Implementation-Guidelines-for-National-Policy-on-Science-and-Technology-Education (accessed Sept 18, 2025).

(3) Achimugu, L. Factors Affecting the Effective Implementation of Senior Secondary Education Chemistry Curriculum in Kogi State, Nigeria. *Int. J. Sci. Res. Publ.***2016**, *6* (5), 562–566.

(4) Achu, S. K. Teachers' Perception and Attitude toward the Integration of Green Chemistry Principles in the School Curriculum. *Int. J. Sci. Res. Arch.***2024**, *12* (01), 2489–2504.

(5) Chen, M.; Jeronen, E.; Wang, A. What Lies behind Teaching and Learning Green Chemistry to Promote Sustainability Education? A Literature Review. *Int. J. Environ. Res. Public Health***2020**, *17* (21), 7876.

(6) Anaso, J. N. Chemistry Laboratory Equipment and Senior Secondary School Students' Performance in North-West Nigeria: Implications for Counseling. *J. Curric. Instr.***2017**, *10* (2).

(7) O'Neil, N. J.; Scott, S.; Relph, R.; Ponnusamy, E. Approaches to Incorporating Green Chemistry and Safety into Laboratory Culture. *J. Chem. Educ.***2020**, *98* (1), 84–91.

(8) Karpudewan, M.; Roth, W. M.; Sinniah, D. The Role of Green Chemistry Activities in Fostering Secondary School Students' Understanding of Acid–Base Concepts and Argumentation Skills. *Chem. Educ. Res. Pract.***2016**, *17* (4), 893–901.

(9) Umanah, I.; Udo, E. Relationship between Green Chemistry and Traditional Laboratory Approaches on Students' Academic Achievement in Chemistry; **2021**. https://www.uniprojects.com.ng/2023/09/relationship-between-green-chemistry.html(accessed Sept 18, 2025).

(10) Ma, J.; Shengli, H. Evaluating Chinese Secondary School Students' Understanding of Green Chemistry. *Sci. Educ. Int.***2020**, *31* (2), 209–219.

(11) Ovat, S. V.; Nwogwugwu, C. E.; Idika, D. O. Assessment of School Location, Class Size and Academic Performance of Upper Basic Students in Cross River State, Nigeria. *Glob. J. Educ. Res.***2021**, *20* (2), 145–151.

ISBN: 978-978-68-0485-9 DOI: https://doi.org/10.55455/acsnigeria.1.2.159-168

Sustainable Nanohybrid Coating from Sugarcane-Bagasse Silica and *F. sycomorus* Extract for Long-Term Corrosion Resistance of Metal Surfaces

Thompson Izuagie[1], Yusuf Salihu[2], Shehu Umar[3], and Olumuyiwa Oyekunle Akintola[1]
[1]Department of Chemistry, National Open University of Nigeria, Abuja, Nigeria
[2]Department of Pure and Industrial Chemistry Sokoto State University, Sokoto, Nigeria
[3]Department of Energy and Applied Chemistry, UsmanuDanfodiyo University, Sokoto.
***Corresponding Author's email:** tomyi2012@yahoo.com

ABSTRACT

The study reports a sustainable nanohybrid coating that integrates biogenic silica nanoparticles (SiO_2 NPs) from sugarcane bagasse with *Ficus sycomorus* leaf extract in an epoxy matrix to protect metal surfaces against corrosion. Silica was prepared by a sol–gel route from acid-leached bagasse ash and characterized usingFT-IR, XRD and SEM. The SiO_2 NPs were amorphous and silanol-rich, forming strong interfacial interactions with epoxy and creating a dense, tortuous barrier. The *F. sycomorus* extract, rich in phenolics, flavonoids, and alkaloids, served as a green inhibitor via adsorption and metal-ion complexation. Coatings containing only extract (P), only silica (NP), and the combined nanohybrid (NH) were applied to tin-plate and evaluated by neutral salt spray (up to 360 h) and NaCl immersion. Relative to neat epoxy, all modified films reduced degradation, with NH performing best: rust creep <1 mm and corroded area ≤3% at 360 h, versus ~7 mm and >50% for the control; P and NP were intermediate (creep ≤3 mm, area ≤16–18%). Immersion testing showed corrosion-rate suppression from ~1.0×10^{-4} mm·h^{-1} (control) to <2.0×10^{-5} mm·h^{-1} (NH) with inhibition efficiency >80%; NP and P achieved ~60% and ~40%, respectively. Kinetic analysis confirmed diffusion-controlled growth for all systems, with parabolic rate constants k_p decreasing from 0.0998 (control) to 0.00007 mm^2·h^{-1} (NH), and power-law exponents n ≈ 0.4–0.5. The synergy between SiO_2-induced barrier densification and bio-extract chemisorption/passivation underpins the gains in durability. Leveraging agricultural waste and plant-derived inhibitors, this nanohybrid advances circular-economy coatings while delivering high corrosion resistance in saline environments.

KEYWORDS: Nanohybrid, coatings, anticorrosion, *Ficus sycomorus*, silica nanoparticles.

1. INTRODUCTION

Corrosion, the progressive deterioration of metals and alloys due to chemical or electrochemical interaction with their environment, remains a critical challenge across industries. Globally, corrosion-related losses are estimated at 3–4% of the world's gross domestic product (GDP), underscoring its severe economic and environmental consequences for infrastructure, energy, and manufacturing sectors.[1] Beyond the economic burden, corrosion can compromise structural integrity, cause catastrophic failures, and contribute to environmental contamination.[2]Consequently, the development of durable, sustainable corrosion-protection systems has become an essential research priority.

Conventional coatings such as chromate, phosphate, and solvent-based paints provide only short-term protection and frequently suffer from poor adhesion, brittleness, and the release of volatile organic compounds (VOCs), which pose ecological and health risks.[3] In response to increasingly strict environmental regulations, efforts have intensified to design green and high-performance alternatives, including hybrid nanocomposites and plant-based corrosion inhibitors.[4] These nanocomposite and nanohybrid coatings, in which organic polymers are reinforced with inorganic nanofillers, offer improved mechanical strength, thermal stability, and impermeability due to interfacial synergy and optimized dispersion of nanoparticles.[5,6]

Among the various nanofillers, silica (SiO_2) nanoparticles stand out for their abundance, low cost, non-toxicity, and chemical stability. When incorporated into epoxy or polymer matrices, silica nanoparticles generate tortuous diffusion pathways that slow the ingress of moisture, oxygen, and chloride ions, effectively increasing corrosion resistance.[3,7] Furthermore, biogenic silica derived from agricultural residues such as sugarcane bagasse provides a renewable alternative to conventional silica sources and aligns with circular economy principles.[4] The conversion of agro-waste into functional nanomaterials not only reduces environmental burden but also adds economic value to biomass waste streams.

In parallel, bioactive plant extracts have emerged as powerful corrosion inhibitors. These natural substances, that are rich in phenolics, flavonoids, tannins, and alkaloids, can adsorb on metallic surfaces, forming stable protective films that suppress both anodic and cathodic reactions.[1] Such adsorption typically involves π-electron and lone-pair interactions that hinder electrochemical activity

and reduce charge transfer.[2] For instance, *F. sycomorus* extract contains multiple polyphenolic compounds capable of complexing with metal ions and promoting passivation, making it a potential green corrosion inhibitor. When combined with epoxy resin, which is a matrix known for its strong adhesion, flexibility, and chemical resistance, the result is a nanohybrid coating that merges physical barrier effects, chemical inhibition, and hydrophobic sealing.[6]

Recent studies show that hybrid coatings containing nanosilica and plant-derived inhibitors significantly reduce corrosion rates and delay degradation under salt-spray and immersion conditions.[5,7] However, systematic investigations of biogenic silica–plant–epoxy nanohybrids remain limited. In this context, the present work focuses on synthesizing and characterizing an eco-friendly nanohybrid coating composed of silica nanoparticles derived from sugarcane bagasse, *F. sycomorus* extract, and epoxy resin. The study aims to elucidate the synergistic corrosion inhibition mechanisms arising from the combination of inorganic nanofillers and organic bio-inhibitors, thereby contributing to the advancement of green, high-performance coatings for industrial corrosion protection.

2. MATERIALS AND METHODS

2.1 Materials and Reagents

Analytical-grade reagents were used throughout the study. Sugarcane bagasse was collected from Ramin Kura Market (Sokoto, Nigeria) as a precursor for silica nanoparticles, while *F. sycomorus* leaves were obtained from Gida Bahure Farm, Runjin Sambo area, Sokoto. The epoxy resin system (two-pack resin + hardener; PPG Industries) served as the polymeric matrix. Chemicals used included sodium hydroxide (NaOH, 99.0 %), sodium chloride (NaCl, 99.5 %), and hydrochloric acid (HCl, 36 %), all supplied by Qualikems India and JHD China. Distilled water was used for washing and solution preparation.Equipment employed comprised a muffle furnace (Narange Medical Ltd., India), vacuum oven (Gallenkamp, UK), scout analytical balance (OHAUS SPU-202, USA), and Fourier Transform Infrared Spectrometer (FTIR), X-ray diffractometer (XRD), and Scanning Electron Microscope (SEM) for characterization.

2.2 Pretreatment of Raw Materials

2.2.1 Sugarcane Bagasse

Bagasse fibres were washed with distilled water to remove dirt and sugars, air-dried for 48 h, ground, and sieved to obtain fine powder. The sample was calcined in a muffle furnace at 650 °C for 2 h to yield silica-rich ash. This temperature range efficiently removes organic residues while preserving amorphous silica structure.[8,9]

2.2.2 *F. sycomorus* Leaves

Leaves were rinsed with distilled water, shade-dried for 5 days, pulverized, and sieved (250 µm). The powder was stored in airtight containers until extraction.[10]

2.3 Extraction and Screening of *F. sycomorus* Phytochemicals

Sequential solvent extraction was performed using hexane, chloroform and methanol via Soxhlet apparatus for 6 h per extraction step. Filtrates were concentrated under vacuum at 45 °C to yield the crude extracts. Phytochemical screening followed standard colour-test procedures: Dragendorff's reagent for alkaloids; ferric-chloride for phenolics/tannins; Shinoda reagent for flavonoids; and Kedde's reagent for glycosides.[11,12]

2.4 Synthesis of Silica Nanoparticles from Sugarcane Bagasse

Silica nanoparticles (SiO_2NPs) were produced via a sol–gel process adapted from Ni'mah *et al*. (2023). A 10 g sample of the calcined ash was leached with 1 M HCl at 100 °C for 1 h, filtered and washed. The residue was then dissolved in 250 mL of 1 M NaOH at 100 °C for 1 h under stirring to produce sodium silicate. The filtrate was neutralized with 1 M HCl until gelation (pH ≈ 7). The gel was aged for 24 h, washed with distilled water, dried at 100 °C, and ground to yield fine amorphous SiO_2 nanoparticles. This green route valorizes agricultural waste and aligns with sustainable nanomaterial synthesis.[13,14]

2.5 Characterization of Silica Nanoparticles

FTIR spectra were obtainedon a Bruker Alpha spectrometer fitted with a Platinum ATR module in the 4000–400 cm^{-1} range to identify characteristic vibrations. XRD patterns were recorded using XRD, Philips X' Pert Pro with Cu Kα radiation (λ = 1.5406 Å) at 2θ = 5°–80°. While surface morphology was analyzed on SEM (Phonem Prox, Malysia) at 10–20 kV acceleration voltage.

2.6 Formulation of Nanohybrid Coating

The nanohybrid composite was formulated by blending silica nanoparticles and *F. sycomorus* extract with the epoxy resin at a mass ratio of 4:1 (NP:extract). The resin : hardener ratio was 80 : 20. The mixture was mechanically stirred for 10 min to achieve homogeneous dispersion. Coatings were applied to degreased tin-plate panels (50 × 25 × 1 mm) using a film applicator and cured at ambient temperature for 24 h. Similar epoxy/nanoparticle and plant-extract hybridizations have been reported.[15]Coating codes are: P = Epoxy + *F. sycomorus* extract; NP = Epoxy + SiO_2 nanoparticles;NH = Epoxy + SiO_2 + *F. sycomorus* nanohybrid.

2.7 Corrosion-Resistance Evaluation

2.7.1 Accelerated Salt-Spray Test and Surface Examination

Corrosion performance of the coated and X-scribed panels was evaluated according to ASTM B117-23.[16] Samples were exposed to a continuous 5 wt % NaCl fog at 35 °C and 95 % relative humidity in a salt-spray chamber. At scheduled intervals (24, 48, 72, 96, 168, 240 and 360 h), panels were withdrawn, rinsed with deionized water, and air-dried for image analysis. Surface degradation was documented using a digital optical microscope (10×–200×, reflected bright-field illumination) following ASTM D1654 procedures.[17] Micrographs of the scribed regions were captured at fixed magnification and lighting to record rust propagation, blistering, and coating breakdown. Image analysis provided rust-creep length and corroded-area fraction, while time-to-first-rust and extent of film deterioration were noted visually. Prolonged resistance to rust initiation and lower rust-creep or corroded-area values were taken as indicators of superior coating protection.[17]

2.7.2 Immersion Test

Samples were immersed in 3.5 wt% NaCl solution at room temperature for 120 h. At intervals, specimens were cleaned, dried, and weighed. Corrosion rate (CR) was calculated by:

$$CR = \frac{87.6 \times W}{D \times A \times T}$$

where *W* = weight loss (mg), *D* = density (g cm^{-3}), *A* = area (cm^2), *T* = time (h).[18]The inhibition efficiency (η %) was derived as:

$$\eta = \frac{CR_0 - CR_i}{CR_0} \times 100$$

where CR_o = corrosion rate without inhibitor and CR_i = rate with inhibitor.[5]

2.9 Kinetic modelling and mechanism

Time-dependent rust-creep data were fitted to two common kinetic models to infer the rate-controlling process. (i) Parabolic (diffusion) law: $L^2 = k_p t + C$, where the slope provides the parabolic constant k_p(mm^2 h^{-1}). (ii) Power-law model: $L = k\, t^n$; linear regression of $\ln L$vs $\ln t$yields the exponent $n$and prefactor k. Goodness-of-fit (R^2) and the extracted parameters (k_p, k, n)were used to compare coatings and to classify the predominant mechanism (diffusion-limited vs. mixed/other), consistent with current practice in corrosion-protective coatings.[19]

2.8 Data Analysis

All tests were performed in triplicate. Data were expressed as mean ± standard deviation, and comparisons among coatings were made using one-way ANOVA ($p < 0.05$). Figures and statistical plots were generated using OriginPro 2024.

3. RESULTS AND DISCUSSION

3.1 Phytochemical screening of *F. sycomorus* extract

Colour-test assays (Table 1) indicated the presence of alkaloids, glycosides, phenolics/tannins, flavonoids, saponins, terpenoids, and steroids in the aqueous/methanolic extracts. These classes are well known to physisorb/chemisorb on metal surfaces via π-systems and heteroatom lone pairs, forming compact inhibitor films that diminish both anodic dissolution and cathodic oxygen reduction—often with additional antioxidant effects that suppress intermediate ROS (radical) pathways.[11,12]Literature on green inhibitors supports this multi-pathway protection for plant-derived polyphenols and alkaloids.[1]

Table 1. Phytochemical screening of *F. sycomorus*

Constituents	Alkaloids	Glycosides	Phenolics	Terpenoids	Saponins	Flavonoids	Tannnins	Steroids
Inference	+	+	+	+	+	+	+	+

3.2 Characterization of bio-derived Silica nanoparticles (SiO_2NPs)

The prepared silica nanoparticles were characterized using FTIR, XRD and SEM and the results are shown in Figure 1.

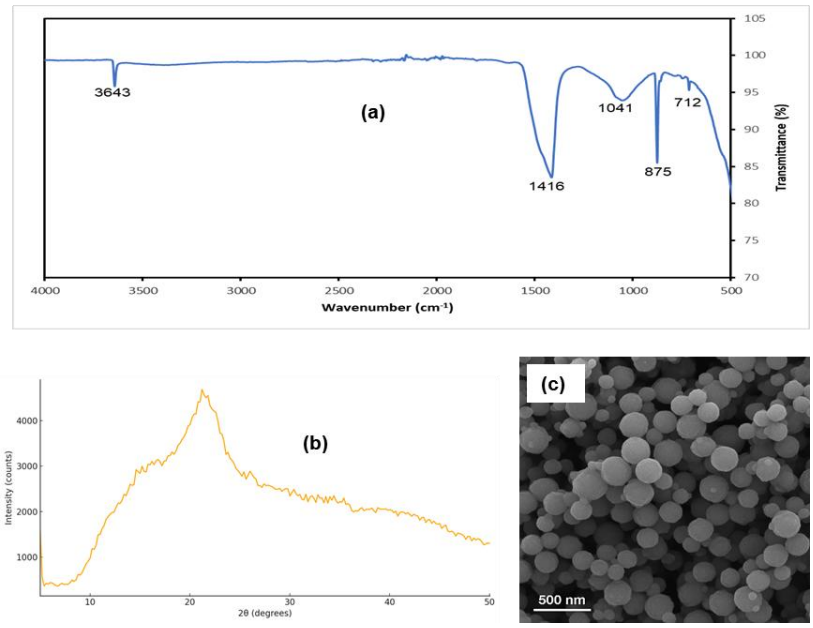

Figure 1. (a) FTIR of biogenic silica showing Si–O–Si (~1041 cm^{-1}) and Si–OH bands; (b) XRD with a broad halo at ~22° 2θ confirming amorphous SiO_2; (c) SEM revealing spherical, well-dispersed nanoparticles (~80–150 nm).

The FTIR spectrum of the synthesized silica nanoparticles (Figure 1(a))shows a prominent absorption at ~1041 cm^{-1}, which corresponds to the asymmetric stretching vibration of Si–O–Si linkages in the amorphous silica network.[20,21] Additionally, a distinct band at ~3643 cm^{-1} indicates the presence of isolated silanol (Si–OH) groups on the surface, which support the high surface reactivity and potential hydrogen-bond interactions in nanohybrid coatings.[22] Minor features at ~2326, ~1416, ~875 and ~712 cm^{-1} are attributed to adsorbed CO_2 and carbonate species, which are common in silica derived from agro-waste without extensive acid leachingand these signatures have been documented in biosilica from sugarcane bagasse and rice-husk sources.[9,23] Altogether, the FTIR data confirm formation of amorphous silica with active silanol surfaces suitable for composite coating development.

The XRD profile of the biogenic silica nanoparticles (Figure 1(b)) is dominated by a single broad diffuse halo centered near 2θ ≈ 20–22°, with no resolvable Bragg reflections at higher angles. This is a strong signature of amorphous SiO_2 formed by short-range order of Si–O tetrahedra rather than long-range

crystalline polymorphs (e.g., quartz, cristobalite). Such "amorphous hump" patterns are routinely reported for rice-husk-derived and other biosilicas and arise from medium-range correlations that produce the first-sharp diffraction peak in amorphous silica. Several studies have shown the same broad maximum at ~20–22° and used it to confirm the amorphous nature of nanosilica obtained under mild, biogenic/sol-gel conditions.[24–28] Collectively, the absence of sharp peaks and the prominence of the ~21° halo in the figure corroborate successful formation of amorphous biogenic silica with high surface area and short-range order suited for adsorption, catalysis, and biomedical functionalization.

The SEM image (Figure 1(c)) shows biogenic silica as predominantly smooth, spherical nanoparticles with limited necking or coalescence and a sub-200 nm size distribution (visually, most particles fall roughly ~80–150 nm from the 500 nm scale bar). This morphology—well-dispersed spheres produced under mild extraction/sol-gel routes—is widely reported for biosilica derived from agricultural precursors (e.g., rice husk, bamboo leaves) and is advantageous for high surface area and uniform surface silanols relevant to adsorption/catalysis and biomedical functionalization. Comparable SEM/TEM observations of spherical nanosilica are documented for rice-husk–derived mesoporous biogenic silica nanoparticles, for bamboo-leaf–derived silica synthesized via combustion–alkaline extraction, and for biosynthesized silica nanoparticles from rice husk ash, all confirming the characteristic near-monodisperse spherical morphology of amorphous SiO_2 formed via biogenic pathways.[29,30]

3.3 Corrosion performance

3.3.1 Salt-spray (fog) exposure

The salt spray test results (Figures 2 and 3) clearly demonstrate the progressive improvement in corrosion resistance achieved by the formulated coatings containing different additives (P, NP, and NH) relative to the control sample without additives.Across 360 h exposure, the control ("No additives") shows rapid underfilm attack: rust creep reaches ~7 mm/side and corroded area approaches ~50%, evidencing fast electrolyte ingress and poor barrier integrity. Adding the plant extract alone (P) markedly slows degradation (creep $\lesssim$3 mm; area $\lesssim$16–17%), consistent with adsorption of phytochemicals (tannins/polyphenols) that complex with Fe and suppress anodic/cathodic sites – aneffect reported for *F. sycomorus* leaves acting as an efficient green inhibitor on steel and Al in acid media (reduced rates vs. blank).[10] Incorporating nano-silica alone (NP) performs comparably to P (slightly lower creep/area early on), aligning with literature where SiO_2 nanoparticles dispersed in epoxy increase tortuosity, reduce porosity, and delay chloride transport, thereby improving salt-spray durability.[31]

The NH nanohybrid (SiO_2 + *F. sycomorus*) is the clear best performer (creep <1 mm; corroded area $\lesssim$2–3% at 360 h). This synergistic improvement is consistent with hybrid epoxy–silica systems where nanoparticles provide a dense, tortuous barrier while functional organics supply active inhibition/passivation and stronger interfacial adhesion; epoxy–silica hybrid/composite coatings routinely show superior long-term salt-spray responsescompared with either component alone[32] and with modern SiO_2-based nanocontainer strategies that deliver/retain inhibitors inside epoxy to sustain protection over hundreds of hours.[33] Overall, the ranking NH $\gg$ (P $\approx$ NP) $\gg$ No-additives indicates that combining nano-silica's barrier effect with *F. sycomorus*'s chemisorbed inhibition is additive (and likely synergistic), yielding minimal rust creep and the lowest corroded area in neutral salt spray.

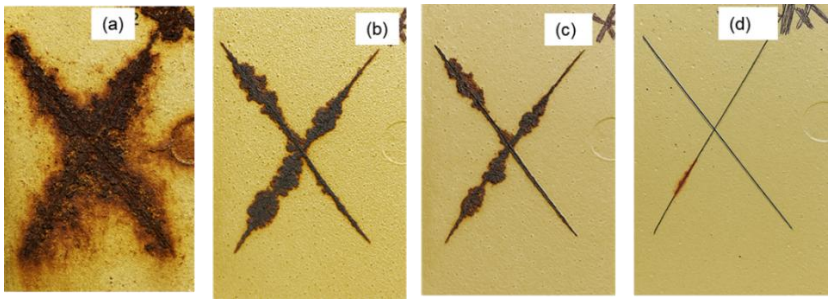

Figure 2. Visual comparison of corrosion resistance after salt spray exposure: (a) unmodified epoxy (No Additives); (b) P (epoxy + *F. sycomorus* extract); (c) NP (epoxy + SiO_2 NPs); (d) NH (epoxy + SiO_2 + *F. sycomorus* hybrid).

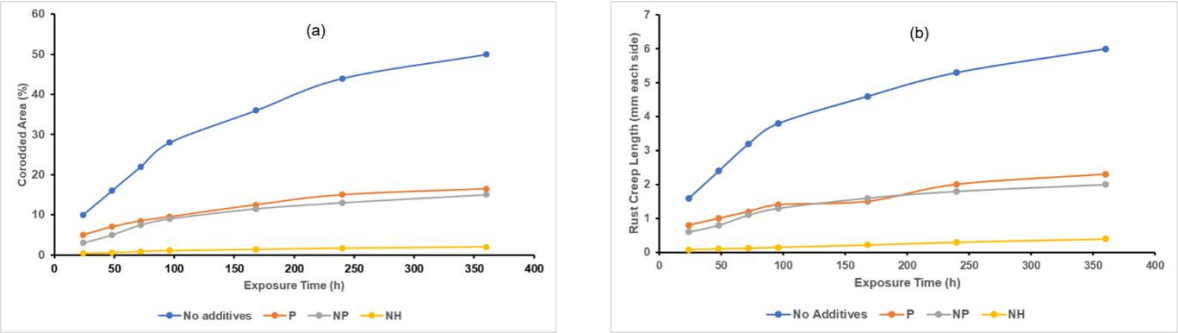

Figure 3. Salt spray test results showing (a) corroded area (%) and (b) rust creep length versus exposure time for coatings without additives, with *F. sycomorus* extract (P), SiO_2 nanoparticles (NP), and SiO_2 + *F. sycomorus* nanohybrid (NH).

3.3.2 Immersion tests (3.5% NaCl)

The immersion test data (Figure 4) reveal a clear trend consistent with the salt-spray results, confirming the synergistic corrosion protection effect of *F. Sycomorus* extract and SiO_2 nanoparticles in the epoxy matrix. The test shows a stepwise drop in corrosion rate and a matching rise in inhibition efficiency as the coating moves from unmodified epoxy to the extract-only (P), silica-only (NP), and finally the nanohybrid (NH) system. The P coating likely suppresses anodic/cathodic reactions via adsorption/complexation of polyphenolic constituents from *F. sycomorus* on the steel surface—consistent with broad evidence that plant extracts act as effective "green" corrosion inhibitors through surface adsorption and film formation on steels. The NP coating further lowers the rate by densifying the film and creating tortuous diffusion paths for water/ions; epoxy films filled with dispersed SiO_2 routinely show higher impedance and lower corrosion currents in NaCl immersion. The NH coating performs best (lowest rate, highest efficiency), reflecting complementary mechanisms: the SiO_2 nanofiller improves barrier integrity and interfacial adhesion while the bio-extract provides active inhibition at the metal/coating interface, a synergy that is well documented for epoxy–silica hybrid systems. Together, these results validate the ranking NH > NP ≳ P > No additives for immersion resistance and align with literature on plant-extract inhibitors and silica-reinforced epoxy barriers.[32,34,35]

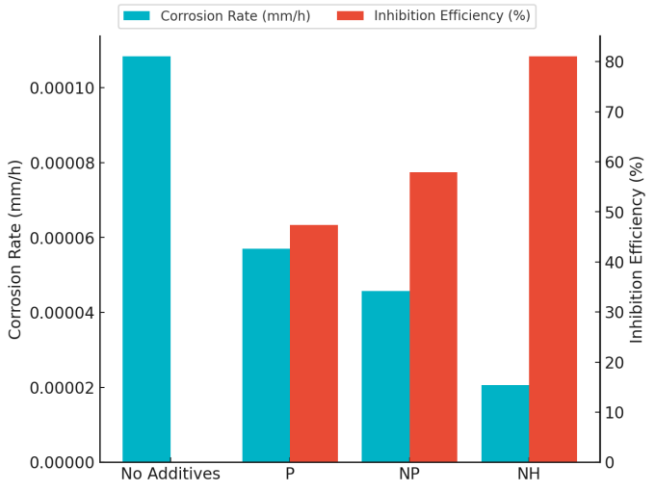

Figure 4. Corrosion rate and inhibition efficiency of epoxy coatings with and without *F. sycomorus* extract (P), SiO_2 nanoparticles (NP), and SiO_2 + *F. sycomorus* nanohybrid (NH).

3.3.3 Corrosion protection mechanism

Kinetic data (Figure 5) show that the parabolic plots (L^2 vs. time) are linear for all coatings, with strong fits (R^2 = 0.957–0.986) (Table 2), indicating diffusion-controlled rust growth through the corrosion product/coating.[19] The parabolic rate constants follow k_p: No-Additives (0.0998 mm² h^{-1}) ≫ P (0.0129) ≳ NP (0.0108) ≫ NH (7×10^{-5}). Thus, the unmodified film allows fast ionic transport through a porous rust layer, while the P film (epoxy + *F. sycomorus* extract) slows growth via an adsorbed, compact

organic inhibitor film at the steel interface. NP (epoxy + SiO_2 NPs) achieves a similar k_p by densifying the matrix and imposing a tortuous diffusion path for water/Cl^-. The NH hybrid (epoxy + SiO_2 + *F. sycomorus*) suppresses rust diffusion by ~3 orders of magnitude vs. the control, consistent with synergy: nanoparticles block transport and improve cohesion/adhesion, while phytochemicals passivate active sites.[32]

Power-law fits (ln L vs. ln t) (Figure 5(b) and Table 2) give exponents n ≈ 0.52 (No-Additives), 0.39 (P), 0.45 (NP), 0.41 (NH) with high R^2 (0.978–0.991). Exponents n ≈ 0.5 are diagnostic of diffusion-limited growth, while n ≈ 0.4 reflects even stronger transport limitation by a more compact protective film. The pre-exponential factors (k) decrease in the same order, confirming the progressive reduction in effective diffusivity within the rust/coating stack. Mechanistically, these trends match classical oxidation/corrosion kinetics – parabolic scaling when transport through the product layer controls, and contemporary coating science showing that epoxy–SiO_2 hybrids markedly slow ionic ingress, whereas plant-extract inhibitors lower the interfacial reaction rate via chemisorption.[36] Overall, the kinetic hierarchy and exponents demonstrate that NH drives the system deepest into the diffusion-limited regime, yielding negligible rust creep and the smallest corroded areas.

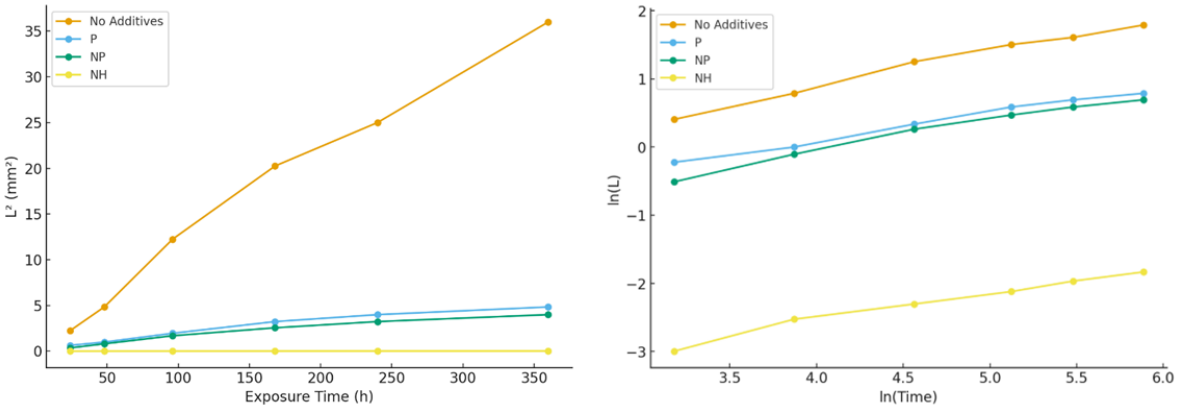

Figure 5. Kinetic analysis of rust growth for coated samples: (a) parabolic rate plots (L^2 vs. time) showing diffusion-controlled behaviour, and (b) power-law plots (ln L vs. ln t) confirming reduced corrosion rates for coatings with *F. sycomorus* extract (P), SiO_2 nanoparticles (NP), and SiO_2 + *F. sycomorus* nanohybrid (NH).

Table 2. Kinetic fit parameters (parabolic and power-law) for rust growth of epoxy coatings with *F. sycomorus* extract and SiO_2 nanoparticles (No Additives, P, NP, NH).

Sample	Model	Rate Constant	Exponent (n)	R^2
No Additives	Parabolic	k_p = 0.0998 mm² h^{-1}	–	0.986
P	Parabolic	k_p = 0.0129 mm² h^{-1}	–	0.957
NP	Parabolic	k_p = 0.0108 mm² h^{-1}	–	0.957
NH	Parabolic	k_p = 0.00007 mm² h^{-1}	–	0.982
No Additives	Power Law	$k = e^{-1.2} \approx 0.30$	n = 0.52	0.988
P	Power Law	$k = e^{-1.5} \approx 0.23$	n = 0.39	0.991
NP	Power Law	$k = e^{-1.9} \approx 0.16$	n = 0.45	0.981
NH	Power Law	$k = e^{-4.2} \approx 0.015$	n = 0.41	0.978

4. CONCLUSION

This work shows that epoxy coatings reinforced with biogenic silica nanoparticles and *F. sycomorus* extract deliver robust, sustainable corrosion protection. The bagasse-derived silica is amorphous and silanol-rich, promoting strong interfacial bonding and a dense, tortuous barrier within the epoxy. In parallel, the plant extract supplies green inhibition via adsorption and complexation at the metal surface. When combined, these functions act cooperatively – physically blocking chloride/oxygen ingress while chemically suppressing anodic/cathodic reactions. Thus, yielding markedly lower corrosion rates,

minimal rust creep, and superior stability in both salt-spray and immersion tests compared with single-additive or neat epoxy films.Beyond performance, the nanohybrid leverages agricultural waste and bio-derived chemistries, aligning with circular-economy goals and reducing dependence on synthetic inhibitors. To advance translation, future studies should apply electrochemical impedance spectroscopy for mechanism-resolved quantification, validate durability under outdoor exposure, and optimize nanoparticle and extract loadings to balance mechanical integrity with anticorrosion efficacy. Overall, *F. sycomorus*–silica–epoxy nanohybrids emerge as promising bio-inspired coatings for protecting metals in aggressive environments.

CONFLICT OF INTERESTS

The authors declare no conflict of interests.

REFERENCES

(1) Sheydaei, M. The Use of Plant Extracts as Green Corrosion Inhibitors: A Review. *Surfaces*2024, *7* (2), 380–403. https://doi.org/10.3390/surfaces7020024.

(2) Nwigwe, U. S.; Nwoye, C. I. Green Corrosion Inhibitors for Steel and Other Metals in Basic Media: A Mini-Review. *Research on Engineering Structures and Materials*2023. https://doi.org/10.17515/resm2023.643ma0116.

(3) Samad, U.; Alam, M.; Abdo, H.; Anis, A.; Al-Zahrani, S. Synergistic Effect of Nanoparticles: Enhanced Mechanical and Corrosion Protection Properties of Epoxy Coatings Incorporated with SiO2 and ZrO2. *Polymers (Basel)*2023, *15* (14), 3100. https://doi.org/10.3390/polym15143100.

(4) Hassan, I.; Baba, N. M.; Benin, M. E.; Labulo, A. H. Review on Green Synthesis of Silica Nanoparticle Functionalized Graphene Oxide Acrylic Resin for Anti-Corrosion Applications. *Journal of Umm Al-Qura University for Applied Sciences*2024, *10* (2), 379–397. https://doi.org/10.1007/s43994-023-00106-w.

(5) Ovari, T.-R.; Toth, T.; Katona, G.; Szabó, G. S.; Muresan, L. M. Epoxy Coatings Doped with (3-Aminopropyl)Triethoxysilane-Modified Silica Nanoparticles for Anti-Corrosion Protection of Zinc. *Coatings*2023, *13* (11), 1844. https://doi.org/10.3390/coatings13111844.

(6) López-Campos, J. E. D.; Mojica-Gómez, J.; Maciel-Cerda, A.; Castaño, V. M.; Hernández-Padrón, G. Hybrid Epoxy-SiO2/GO Nanosheets Anti-Corrosive Coating for Aeronautic Aluminum Al6061-T5. *J Coat Technol Res*2024, *21* (2), 559–574. https://doi.org/10.1007/s11998-023-00838-8.

(7) Olivieri, F.; Scherillo, F.; Castaldo, R.; Cocca, M.; Squillace, A.; Gentile, G.; Lavorgna, M. Effectiveness of Mesoporous Silica Nanoparticles Functionalized with Benzoyl Chloride in PH-Responsive Anticorrosion Polymer Coatings. *ACS Appl Polym Mater*2023, *5* (8), 5917–5925. https://doi.org/10.1021/acsapm.3c00585.

(8) Ni'mah, Y. L.; Muhaiminah, Z. H.; Suprapto, S. Synthesis of Silica Nanoparticles from Sugarcane Bagasse by Sol-Gel Method. *Nano Particle*2023, *4* (1). https://doi.org/10.35702/nano.10010.

(9) Nayak, P. P.; Datta, A. K. Synthesis of SiO2-Nanoparticles from Rice Husk Ash and Its Comparison with Commercial Amorphous Silica through Material Characterization. *Silicon*2021, *13* (4), 1209–1214. https://doi.org/10.1007/s12633-020-00509-y.

(10) Ogwo, K.; Osuwa, J.; Udoinyang, I.; Nnanna, L. Corrosion Inhibition of Mild Steel and Aluminium in 1 M Hydrochloric Acid by Leaves Extracts of Ficus Sycomorus. *Physical Science International Journal*2017, *14* (3), 1–10. https://doi.org/10.9734/PSIJ/2017/32708.

(11) Ogunleye, O. O.; Arinkoola, A. O.; Eletta, O. A.; Agbede, O. O.; Osho, Y. A.; Morakinyo, A. F.; Hamed, J. O. Green Corrosion Inhibition and Adsorption Characteristics of Luffa Cylindrica

Leaf Extract on Mild Steel in Hydrochloric Acid Environment. *Heliyon*2020, *6* (1), e03205. https://doi.org/10.1016/j.heliyon.2020.e03205.

(12) Bilgic, S. Plant Extracts as Corrosion Inhibitors for Aluminium and Steel in Acid Media. *DergiPark Journal,*2022, *64* (1), 20–79.

(13) Seroka, N. S.; Taziwa, R. T.; Khotseng, L. Extraction and Synthesis of Silicon Nanoparticles (SiNPs) from Sugarcane Bagasse Ash: A Mini-Review. *Applied Sciences*2022, *12* (5), 2310. https://doi.org/10.3390/app12052310.

(14) Seroka, N. S.; Taziwa, R.; Khotseng, L. Green Synthesis of Crystalline Silica from Sugarcane Bagasse Ash: Physico-Chemical Properties. *Nanomaterials (Basel)*2022, *12* (13). https://doi.org/10.3390/nano12132184.

(15) Mod, B.; Baskar, A. V.; Bahadur, R.; Tavakkoli, E.; Van Zwieten, L.; Singh, G.; Vinu, A. From Cane to Nano: Advanced Nanomaterials Derived from Sugarcane Products with Insights into Their Synthesis and Applications. *Sci Technol Adv Mater*2024, *25* (1). https://doi.org/10.1080/14686996.2024.2393568.

(16) Practice for Operating Salt Spray (Fog) Apparatus. ASTM International: West Conshohocken, PA November 1, 2019. https://doi.org/10.1520/B0117-19.

(17) Test Method for Evaluation of Painted or Coated Specimens Subjected to Corrosive Environments. ASTM International: West Conshohocken, PA September 1, 2024. https://doi.org/10.1520/D1654-24.

(18) Fontana, M. G. .*Corrosion Engineering*; Tata McGraw-Hill, 2005.

(19) Atkinson, A. Transport Processes during the Growth of Oxide Films at Elevated Temperature. *Rev Mod Phys*1985, *57* (2), 437–470. https://doi.org/10.1103/RevModPhys.57.437.

(20) Brinker, C. Jeffrey.; Scherer, G. W. .*Sol-Gel Science : The Physics and Chemistry of Sol-Gel Processing*; Elsevier Science, 2014.

(21) Socrates, George. *Infrared and Raman Characteristic Group Frequencies : Tables and Charts*; John Wiley & Sons, 2013.

(22) Zhuravlev, L. T. The Surface Chemistry of Amorphous Silica. Zhuravlev Model. *Colloids Surf APhysicochem Eng Asp*2000, *173* (1–3), 1–38. https://doi.org/10.1016/S0927-7757(00)00556-2.

(23) Azat, S.; Korobeinyk, A. V.; Moustakas, K.; Inglezakis, V. J. Sustainable Production of Pure Silica from Rice Husk Waste in Kazakhstan. *J Clean Prod*2019, *217*, 352–359. https://doi.org/10.1016/j.jclepro.2019.01.142.

(24) Khouchaf, L.; Boulahya, K.; Das, P. P.; Nicolopoulos, S.; Kis, V. K.; Lábár, J. L. Study of the Microstructure of Amorphous Silica Nanostructures Using High-Resolution Electron Microscopy, Electron Energy Loss Spectroscopy, X-Ray Powder Diffraction, and Electron Pair Distribution Function. *Materials (Basel)*2020, *13* (19). https://doi.org/10.3390/ma13194393.

(25) Biswas, P.; Dahal, D.; Elliott, S. R. Insights into the Origin of the First Sharp Diffraction Peak in Amorphous Silica from an Analysis of Chemical and Radial Ordering. *Phys Rev B*2024, *109* (10), 104207. https://doi.org/10.1103/PhysRevB.109.104207.

(26) Peralta, Y. M.; Molina, R.; Moreno, S. Chemical and Structural Properties of Silica Obtained from Rice Husk and Its Potential as a Catalytic Support. *J Environ Chem Eng*2024, *12* (2), 112370. https://doi.org/10.1016/j.jece.2024.112370.

(27) Aiello, I. W.; Höfig, T. W.; Riboulleau, A.; Teske, A. P.; Lizarralde, D.; Ash, J. L.; Bojanova, D. P.; Buatier, M. D.; Edgcomb, V. P.; Galerne, C. Y.; Gontharet, S.; Heuer, V. B.; Jiang, S.; Kars, M. A. C.; Kim, J.-H.; Koornneef, L. M. T.; Marsaglia, K. M.; Meyer, N. R.; Morono, Y.; Negrete-Aranda, R.; Neumann, F.; Pastor, L. C.; Peña-Salinas, M. E.; Pérez-Cruz, L. L.; Ran, L.; Sarao, J. A.; Schubert, F.; Khogenkumar Singh, S.; Stock, J. M.; Toffin, L.; Xie, W.; Yamanaka, T.;

Zhuang, G. Mineralization Kinetics of Biosiliceous Sediments in Hot Subseafloors. *GeochimCosmochim Acta*2024, *380*, 71–82. https://doi.org/10.1016/j.gca.2024.07.005.

(28) Falk, G.; Shinhe, G. P.; Teixeira, L. B.; Moraes, E. G.; de Oliveira, A. P. N. Synthesis of Silica Nanoparticles from Sugarcane Bagasse Ash and Nano-Silicon via Magnesiothermic Reactions. *Ceram Int*2019, *45* (17), 21618–21624. https://doi.org/10.1016/j.ceramint.2019.07.157.

(29) Pineda-Vásquez, T. G.; Casas-Botero, A. E.; Ramírez-Carmona, M. E.; Torres-Taborda, M. M.; Soares, C. H. L.; Hotza, D. Biogeneration of Silica Nanoparticles from Rice Husk Ash Using *Fusarium Oxysporum* in Two Different Growth Media. *Ind Eng Chem Res*2014, *53* (17), 6959–6965. https://doi.org/10.1021/ie404318w.

(30) Shrestha, D.; Nayaju, T.; Kandel, M. R.; Pradhananga, R. R.; Park, C. H.; Kim, C. S. Rice Husk-Derived Mesoporous Biogenic Silica Nanoparticles for Gravity Chromatography. *Heliyon*2023, *9* (4), e15142. https://doi.org/10.1016/j.heliyon.2023.e15142.

(31) Alam, M. A.; Samad, U. A.; Anis, A.; Alam, M.; Ubaidullah, M.; Al-Zahrani, S. M. Effects of SiO2 and ZnO Nanoparticles on Epoxy Coatings and Its Performance Investigation Using Thermal and Nanoindentation Technique. *Polymers (Basel)*2021, *13* (9), 1490. https://doi.org/10.3390/polym13091490.

(32) Abdollahi, H.; Ershad-Langroudi, A.; Salimi, A.; Rahimi, A. Anticorrosive Coatings Prepared Using Epoxy–Silica Hybrid Nanocomposite Materials. *Ind Eng Chem Res*2014, *53* (27), 10858–10869. https://doi.org/10.1021/ie501289g.

(33) Wang, J.; Tan, W.; Yang, H.; Rao, X.; Luo, X.; Ma, L.; Ren, C.; Mol, A.; Zhang, D. Towards Weathering and Corrosion Resistant, Self-Warning and Self-Healing Epoxy Coatings with Tannic Acid Loaded Nanocontainers. *Npj Mater Degrad*2023, *7* (1), 39. https://doi.org/10.1038/s41529-023-00360-7.

(34) Alam, M. A.; Samad, U. A.; Sherif, E.-S. M.; Poulose, A. M.; Mohammed, J. A.; Alharthi, N.; Al-Zahrani, S. M. Influence of SiO2 Content and Exposure Periods on the Anticorrosion Behavior of Epoxy Nanocomposite Coatings. *Coatings*2020, *10* (2), 118. https://doi.org/10.3390/coatings10020118.

(35) R. Holla, B.; Mahesh, R.; Manjunath, H. R.; Anjanapura, V. R. Plant Extracts as Green Corrosion Inhibitors for Different Kinds of Steel: A Review. *Heliyon*2024, *10* (14), e33748. https://doi.org/10.1016/j.heliyon.2024.e33748.

(36) Rani, B. E. A.; Basu, B. B. J. Green Inhibitors for Corrosion Protection of Metals and Alloys: An Overview. *International Journal of Corrosion*2012, *2012*, 1–15. https://doi.org/10.1155/2012/380217.

ISBN: 978-978-68-0485-9
http://acsnigeria.org/publications/proceedings

Comparative Assessment of Properties of Laterite and Clay of Otukpo in Benue State for Suitability in Making Bricks and Geopolymer Cement for A Green Environment

[1] Idongesit Nnammonso Akpan* and [2]Mutah Wadai
[1]Department of Chemistry, Federal University of Health Sciences, Otukpo, Benue State, Nigeria
[2]Department of Mathematics, Federal University of Health Sciences, Otukpo, Benue State, Nigeria
Corresponding Author's email: *aidongesit@yahoo.com. (+234-8039129014)*

ABSTRACT

As the cost of living is gradually becoming burdensome not only in the continent of Africa involving developing countries like Nigeria, but also in other continents of the world involving developed nations, efforts have been geared in recent years towards adequate utilization of cheap and readily available natural resources like laterites and clays as efficient substitutes and composites building materials for provision of affordable houses for the citizenry while maintaining eco-friendly green environment. Notably, governments at different levels have been saddled now more than ever with the responsibility of providing affordable housing to citizens due to the soaring cost of building materials. Thus, in this study, a comparative assessment of the suitability of properties of laterite and clay soils in Otukpo Local Government Area of Benue State has been carried out. The results of physico-chemical properties obtained were: particle size (mm) 1.66 (laterite)/0.006 (clay); pH = 6.68 (laterite)/ 6.15 (clay); geotechnical properties (specific gravity = 2.87(laterite) /3.80 (clay); moisture content = 29.6% (laterite) /50.6% (clay); bulk density (g/ml) = 1.10 (laterite) /1.80 (clay); plasticity indices (Ip) = 25.32% (laterite)/36.85% (clay); liquidity limits (WL%) = 38.97 (laterite) /59.70 (clay) and thermal properties (M.T ^{o}C = 55- 630 (laterite)/40-660 (clay), thermal conductivity = 34.98 $kgms^{-2}\Theta^{-1}$ (laterite)/ 107.8 (clay); resistivity (Ωm) = 0.0358 (laterite/0.0186 (clay). These results show that clay has light particles while laterite has heavy particles, and both have plastic behaviour and other excellent properties that guarantee them as suitable materials for making quality bricks for sustainable, eco-friendly green environments.

KEYWORDS: Citizenry, House, Building, Material, Green Environment, Eco-friendly.

1. INTRODUCTION

Before the advent of cement for molding blocks for building houses, man had primitively exploited clay and laterite soils for a long time for building local huts to provide shelter for himself and his family. Currently, not only in Nigeria, but in the whole of the African continent, laterite- and clay-based materials are emerging and sustaining as the new generation of building materials [1]. Unfortunately, now more than ever, the cost of purchasing bags of cement for molding blocks for building houses is quite exorbitant and burdensome. Consequently, houses, especially in rural areas, are no longer affordable to the common man due to the high cost of rent. Additionally, sand, as a highly demanding ingredient for concrete making, is regrettably costly even with its availability [2]. It is unarguably expected that the construction sector of the economy of most developing countries is currently facing a huge demand for sand due to the drastic growth of infrastructural development in the areas of roads, houses, and industrial constructions [3]. With this situation of high cost of materials for making concrete and blocks, it has become pressing necessary to utilize cheap and available alternatives or substitute materials for sand and cement for making bricks for building houses. Particularly, the prominent role that laterite and clay soils have continued to play in promoting the production of cheap bricks for the building of houses has led to a rising concern for their effective and maximum utilization. Essentially, laterite soils are rich in silica, and they are locally available material of low cost, and one of the major advantages is that they can be replaced with fine aggregate in concrete making [2].

Nevertheless, at present and in the past few decades, there has been a remarkable increase in the use of laterite soils as raw materials in various construction applications for enhancing social and ecological values, and a significant number of studies and reviews have explored the unique properties of laterite soils in various building products and road components [3]. Laterite soils are generally used as an alternative raw material for the production of fired and unfired bricks. Since the late 1970s, laterite soils have been used in place of stones as a base layer for low-volume roads with bituminous-surfaced asphalt or tar [1], and since then, they have been widely used to mold bricks, build roads, as aquifers in water supply, water treatment, manufacture of geo-polymeric products, etc. Being highly rich in iron content in addition to high content of corroded kaolinite of amorphous nature, laterite soils are equally used as precursor materials for making geopolymers through alkaline activation, thereby making it a

green, eco-friendly, and sustainable binder used in controlling the emission of CO_2 from the cement industry [4, 5].

On the other hand, considering clays as naturally occurring expansive soils, clay soils are abundantly found in various regions across the globe, including Nigeria in Africa [7], and the science of clay has been the interest of all kinds of people from different scientific backgrounds. However, clay in general consists of particles that are the smallest in the soil, with sizes less than 0.02 mm or less than 0.005 millimeter and the particles usually possess a net negative charge, and therefore can attract positive ions (cations), hold them, and then release them to the soil water when its cations have been lost through leaching or plant uptake [8, 9]. Perhaps for building, construction, and engineering purposes, clays have, in addition to the above-identified properties, mechanical and geotechnical properties. [10]. Additionally, it must however be pointed out that the most commonly occurring clay minerals are kaolinite, illite and montmorillonite, plus allophane and halloysite, which occur in active volcanic terrains and these minerals are not predominantly equidimensional, however, they may occur basically in flat plated, warped plated, tubular and in chain forms, giving the required characteristic properties of clays [11].

Essentially, there is a need to be aware that, in terms of applications, no other known earth material has so wide an importance or such extensive applications or uses as clays do. Clays and laterites commonly used in the manufacture of pottery and bricks must be made of fine grains and equally be sufficiently plastic to be molded when wet, and in addition, they must retain their shape when dried and sinter together to form a hard, coherent mass without losing their original shape when heated to a sufficient temperature [12]. On the strength of available extant evidence in terms of engineering significance, clay soil may cause regrettable damage to constructed structures in which it is used to form their foundation because of its inherent potential to react proportionately to changes in moisture regime and temperature [13, 14]. Equally worth mentioning is the fact that the uplift or elevated pressure due to a change in volume of clay often leads to structural foundation failure, with a resultant damage to the upper floors of a constructed building [13, 14].

Meanwhile, considering the fluctuating properties of clays, it is always essential for the characteristic properties of particular clay and laterite soils to be identified accurately before their utilization for any construction activities [13, 14], and that is therefore the primary focus of this study. Despite the extensive applications of laterites and clays, the abundant nature of the resources in Otukpo Local Government in Benue State, Nigeria, and the fact that the materials have been in used for long in the area, there is hardly any available reports in the literature on the suitability of properties of Otukpo laterites and clays for utilization for bricks production, except that very recently, Idongesit *et al*. [4], have reported the assessment of the mineralogical and elemental compositions of the clays of Otukpo, Benue State, Nigeria as potential raw materials for manufacturing of bricks, refractories and geopolymers. Therefore, this work was conducted to investigate the properties of lateritic and clay soils from three different sites in Otukpo Local Government Area of Benue State, Nigeria as potential raw materials for effective utilization for production of bricks, cements, and other building and construction materials and the findings achieved in the course of this study will be detailed below and we hope that the results of this investigation will also provide a valuable source of information about the laterite and clay resources of Otukpo for their effective utilization for value chain development for national and international recognition and utilization as good and efficient raw materials for production of bricks, cements, and other building and construction materials.

2. MATERIALS AND METHODS

2.1 Sample Collection

The 5.0 kg examples of lateritic soils and clay soils, respectively, were separately taken using a hand trowel at 1.0-meter depth from three different locations in Otukpo metropolis in sterilized polyethene bags and were transported to the point of analysis (Figure 1).

(a)  (b)  (c)  (d) 

Figures 1a & b: Plates of Image of Laterites, and **c & d** are Plates of Clays Used Sample Preparation

Up to 5.0 kg portions of each dry clay sample were sieved before they were ground using a jaw (10-300TPH concrete crusher, China) and roller crushers (2PG series, 350 x 350Jpeq, Japan). The samples were then riffled to obtain representative samples by using a Jones Riffler equipment and then followed by homogenization, and thereafter, each sample was divided into three equal portions and stored for analysis [4].

2.2 Determination of Physicochemical Parameters

2.2.1 Temperature Measurement

The temperature of the clay samples was taken in situ, at the point of collection of each sample. The temperature of each clay sample was taken in degrees Celsius but was converted to Kelvin using the relationship: T ^{o}C = (273 + T ^{o}C) K [4] ..... (Equ. 1)

2.2.2 pH Tests

In each case, 100 g of the laterite and clay samples was dissolved in distilled de-ionized water, and the resulting solution was first tested with litmus papers and then with a Digital pH meter (Lab Tech Model, USA), at a standard temperature of 298 K [4].

2.2.3 Electrical Conductivity Measurement

A sensitive electrical conductivity measuring meter, DDS meter (DDS 307), with the instrumental degree of accuracy of 0.001 and measuring range of 0.000$\mu S/cm$ to 199.90 $\mu S/c$m, was used to measure the electrical conductivity of the laterite and clay samples [4].

2.2.4 Particle Size Measurement

In each case, the laterite and clay particle sizes were determined using the sieve analysis method. Each of the laterite and clay samples was freed from debris, and stones were sieved using a mesh of known hole size between 0.02 - 70 µm, as reported in Idongesit *et al*. [4]. Hydrometer analysis was further employed to confirm the results obtained.

2.2.5 Thermal Properties Tests

Again, in each case, 100 g of homogenized composite form of the laterite and clay samples were subjected to a thermogravimetric test using a muffle electric furnace. Each sample was heated in the muffle electric furnace (SX-5-12; PC:22070222/2000 °C), and the weight loss behaviour of each sample was carefully monitored at various temperatures [4].

2.2.6 Specific Gravity Measurement

The measurement specific gravity of the samples was performed using a relative density glass bottle (50 ml/20 ^{o}C) to determine the ratio of the density of each sample compared to the density of pure water (ρl = 1000 kg/m^{3}), and the results were further confirmed using Archimedes' principle methodology [4].

2.2.7 Hardness Tests

Hardness tests were performed using indentation tests, and the results were further confirmed using scratch tests (Mohs) as described in [15, 16].

2.3 Mineralogical and Chemical Analysis

The XRF analysis was done with 100 g of fine powder of laterite and clay samples, respectively, where each sample was mixed with a binding aid and pressed to produce homogeneous sample pellets, and thereafter the samples were subjected to XRF analysis using a Thermo Fisher Scientific Machine (Ma 01876, USA; XL3-98293) model. Also, in each case, 100g of powdered laterite and clay samples were analyzed for structural arrangement of particles in the clay using Scanning Electron Microscope (Thermo Fisher Scientific, SEM, XL3-98293, USA) and for optical mineralogical properties [4, 17].

2.4 Analysis of Geotechnical Properties

2.4.1 Determination of Resistivity

The values of resistivity, as the ratio of resistance and cross-sectional area to the length of a material or resistivity (ρ), are often calculated as the product of resistance (R) and the cross-sectional area (A) divided by the length (l) of the material (ρ = RA/l). In this work, the resistivity of the samples was calculated as resistivity (ρ) = 1/σ, where σ stands for the conductivity of the samples [1].

2.4.2 Determination of Activity

Activity used as an index property to determine the swelling potential of soils was determined using this relationship: A = PI/C, where PI = Plasticity Index and C = % of laterite or clay–size fraction, by weight [15].

2.4.3 Determination of Activity of the Laterites and Clays

The activity (A) of the soil samples was obtained by dividing the plasticity index (PI) by the percent of clay-sized particles (less than 2 μm) present [15, 16].

2.4.4 Determination of Dry Unit Weight

Dry unit weights of the samples were determined using the formula as described by [15, 16]

Dry unit weight, γ_d (kN/m^3) = $\frac{\text{Weight of dry soil}}{Volume\ of\ soil}$; .....(Equ. 2)

2.4.5 Determination of Bulk and Wet Density

This formula was used: Bulk or wet density ρ_b (Mg/m^3) = $\frac{\text{Mass of wet soil}}{\text{Total volume of soil}}$; ..... (Equ. 3) [15].

2.4.6 Shear Strength Tests

Both in-situ and laboratory testing were performed to determine the shear strength of the samples. While the cone penetration test (CPT) technique was adopted for in-situ tests, direct shear box tests were employed for laboratory tests as described by [15, 16].

2.4.7 Plastic Limit (PL) Tests

The brittle or plastic behaviour of the samples was tested using the method described in [15], and a 3.0 mm diameter rod was used to gauge the thickness of the thread during the test, and the plastic limit test was defined by the ASTM standard test method [15, 16]

2.4.8 The Liquid Limit Tests

The test method for measuring the liquid limit used in this work was the fall cone test where the measurements were based on the penetration into the soil of a standardized cone of specific mass instead of Casagrande method because the results of the method are often considered to be a more consistent as the method often minimizes the possibility of human variations of results [15, 16]

2.4.9 Shrinkage Limit Tests

The tests to determine the shrinkage limit (SL) of the laterite and clay samples were performed to determine the water content at which further loss of moisture will not result in any more volume reduction in each of the samples, as described by [15, 16].

2.4.10 Determination of Moisture Content (%)

This formula was used: Moisture content w (%) = $\frac{\text{Mass of water in soil}}{\text{Mass of dry soil}}$ x 100; .....(Equ. 4) [16].

2.4.11 Determination of Liquidity Index

The liquidity index (LI) is often used for scaling the natural water content of a soil sample to the limits. In this work, it was calculated as a ratio of the difference between natural water content, plastic limit, and plasticity index: LI = (W-PL)/(LL-PL); where W is the natural water content [15, 16], PL is the plastic limit, and LL is the liquid limit.

2.4.12 Measurement of Unconfined Compressive Strength (UCS)

Unconfined compressive strength (UCS) measurements were made using an electronic servo-controlled MTS stiff testing machine with a capacity of 220 kips [15, 16]. The values were measured following the procedures given in ASTM D2938, with the length-to-diameter ratio of 2, by using NX-size core samples, and three UCS determinations were used to achieve statistical significance of the results [15, 16].

3. RESULTS AND DISCUSSION

3.1 Physicochemical Characteristics of Laterites and Clays

Table 1: Mean of Physicochemical Properties of Laterite and Clays

Property	Laterite	Clay
Temperature (°C)	49.6±0.010	55.0±0.001
Conductivity (mS/cm)	2.15 x 10^2 ± 0.01	2.13 x 10^2±0.01
Pore volume (mL g^{-1})	0.34±0.001	0.32± 0.001
Specific surface area (m2/g^{1})	150.9±0.002	158.20±0.005
pH	6.68±0.010	6.15±0.002
Particle size (mm)	1.66±0.001	0.006±0.001
Hardness (Mohr)	2.54±0.001	2.61±0.001
Specific gravity	2.87±0.005	3.80±0.002
Refractive index	0.99±0.001	1.55±0.001
Colour	Reddish brown	Grey

Idongesit *et al*. [4] and [17]

The results of the physico-chemical properties of the laterites and clays (Table 1) show that the laterites have moderately high conductivity, small pore volumes of 0.34±0.001, and high specific surface area 150.9±0.002. Comparatively, the clays have a higher specific surface area of 158.20±0.005, specific gravity of 3.80±0.002, refractive index of 1.55±0.001, and hardness of 2.61±0.001, than the laterites, but possess a lower pH of 6.15±0.002, particle size of 1.60±0.001, and pore volume 0.32± 0.001. In general, it is crystal clear and necessary to understand, in first instance that both the laterites pH (6.68±0.010) and the clays are slightly acidic (pH = 6.15±0.002), and the results are somewhat higher than the result of 5.59 achieved by [18] and 4.86, reported by [19], but lower than 6.7 reported in [20]. The specific gravity of 2.87±0.005 for laterites and 3.80±0.002 for clays obtained in this study is also higher than the previously reported value of 2.74 by [18], 2.75 by [19], and 2.61 acquired by [20] for laterites. The relatively higher specific gravity (2.87/3.80) obtained in this work may be attributed to low organic content and high percentage of fine particles (Figure 2a & b) of the soils used in the current study. Nevertheless, the pH and the specific gravity values obtained in the current study for both laterites and clays (6.68/6.15) and (2.87/3.80) are in the range of previously obtained results elsewhere for lateritic soils [18] and for clays [16].

3.2 Mineralogical/Chemical and Elemental Characteristics

Mineralogical and elemental compositions of lateritic soils and clays determine the type of clay minerals present in their soil disposal, and in addition to their geotechnical/mechanical properties. The results of mineralogical and elemental composition of the investigated laterite and clay soils are shown in Tables 2 and 3, respectively.

Table 2: Mineralogical Composition of Laterite and Clay

Mineral Composition	Percentage Composition (%)	
	Laterite	**Clay**
Al_2O_3	26.95	19.74
SiO_2	9.29	9.72
Fe_2O_3	7.49	6.39
MgO	3.06	2.02
CaO	2.79	2.80
TiO_2	2.35	1.12
$CaCO_3$	2.11	---
K_2O	1.61	0.201
Na_2O	0.169	0.067
LOI	5.99	14.62

LOI: Loss of Ignition During Heating at the Temperature of 1000 °C [4, 17]

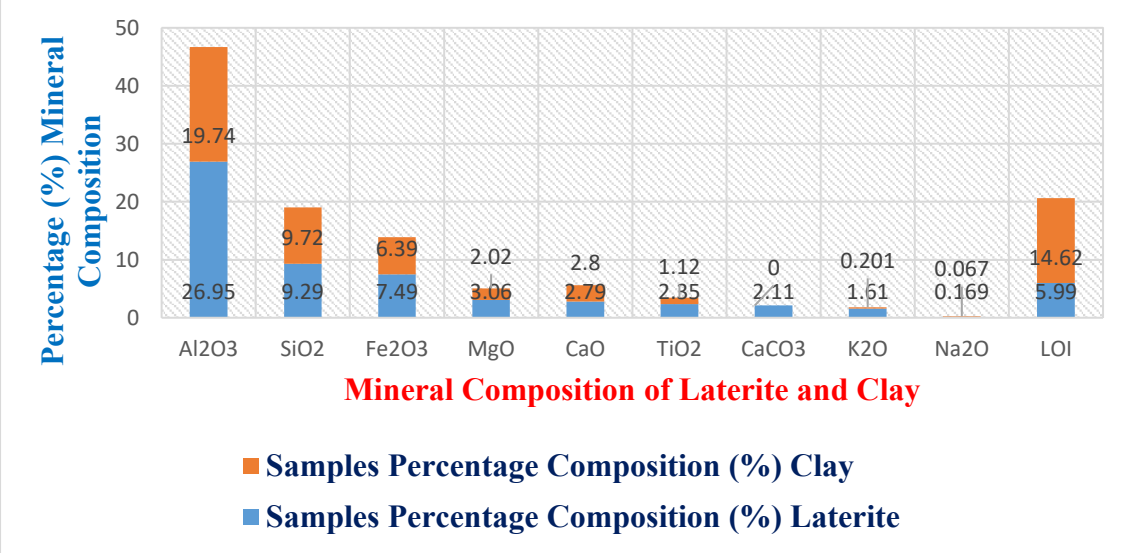

Figure 2: Chart of Percentage Mineral Compositions of Laterite and Clay Samples

The results of the mineralogical and elemental compositions of the laterites and clays investigated (Table 2) showed that the laterite contains approximately 1:3 silica-alumina ratio (SiO_2: Al_2O_3 = 1:3) and therefore it is high alumina-based laterite that is composed of kaolinite and illite minerals and the results obtained in this study are close to the results reported by [4, 21], while the clays also have high alumina to silica ratio of 2:1, hence, the clays are high kaolinite since high kaolinite clays have been reported to have alumina-to-silica ratio of 1:1 [4, 22, 23], and it contains also illite and may also contains small amount of montmorillonite which determines the swelling and the shrinkage of clays [4, 22]. The laterites and clays are enriched with major minerals such as alumina (Al_2O_3), silica (SiO_2), hematite (Fe_2O_3), magnesia (MgO), lime (CaO), and titania (TiO_2) with their percentage compositions as shown in Figure 2. The presence of calcium carbonate ($CaCO_3$) accounts for the major mineralogical difference between the laterites and the clays. Additionally, the specific surface area in the range of (5-20 m^2/g) is often attributed to kaolinite and (80-120 m^2/g) is for illite and the specific surface area of the studied laterite is (150.9±0.002) and that of clay is (158.20±0.005), it can be urged that the laterites and clays are rich in kaolinite and illite minerals (5-120 m^2/g) with small montmorillonite mineral. Interestingly, the results of mineralogical compositions obtained in this study are consistent with previously researched work reported by [4, 21, 22, 23].

Table 3: Elemental Composition of Laterite and Clay Samples

Elemental Composition	Laterite		Clay	
	% composition	± Error	% Composition	± Error
Al	14.62	± 0.089	----	----
Bal	81.246	± 0.002	95.719	± 0.023
Fe	8.932	±0.236	2.468	±0.055
Ti	0.174	±0.010	0.588	±0.012
Ca	0.060	±0.007	0.169	±0.008
Zr	0.059	±0.002	0.021	±0.001
Nb	0.004	±0.001	0.004	±0.001
Sr	0.003	±0.001	0.011	±0.001
Mo	0.001	±0.001	-----	-----
K	0.001	±0.001	0.973	±0.020
Na	0.001	±0.001	---	----
Cr	----	----	0.013	±0.001
V	----	----	0.015	±0.001
Rb	----	----	0.008	±0.001
Bi	----	----	0.010	±0.005

Idongesit et al. [4] and [17]

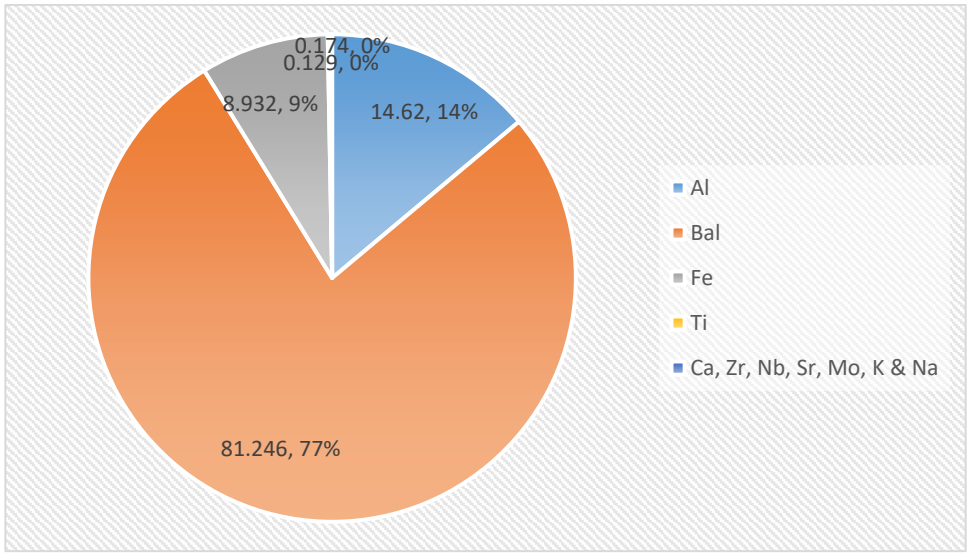

Figure 3: Chart of Percentage Elemental Composition of Laterite Samples

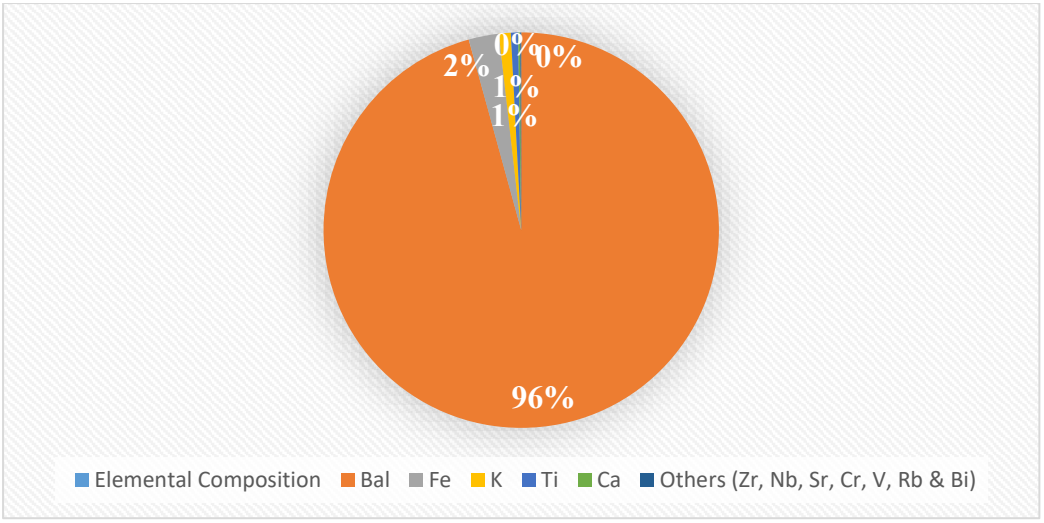

Figure 4: Chart of Percentage Elemental Composition of Clay Sample.

The XRF results (Table 3) show that the laterites and the clays of Otukpo in zone C of Benue State, Nigeria, used in this study contain significant percentages (81.246 %) and (95.719 %) of boron aluminide (Bal) as further presented in Figures 3 and 4 respectively. This alloy has no known historical report in the literature of its natural occurrence in mineral resources. However, the presence of Bal in the laterites and clays seems to add value to the samples as boron aluminide is an alloy of high demand in the aerospace industry. Meanwhile, further studies are required for the extraction of the alloy. In addition, the laterites also contain a significant amount of aluminum and iron. In contrast, the absence of aluminum in the clays may be attributed to the high percentage of Bal due to the bonding between aluminum and boron to form the alloy. Typically, the laterites and clays contain the prerequisite elements, Al, Fe, Ti, Ca, K, Zr, etc., and the results obtained are consistent with the results reported by [4, 16, 20, 21, 22]. Generally speaking, the presence of the elements makes the laterites and the clays suitable raw materials for the production of bricks and other building materials, as reported by [4].

Property	Laterite	Clay
Liquidity limits (W_L in %)	38.97±0.001	59.70±0.005
Plasticity limits (Wp in %)	20.44±0.02	29.93±0.010
Uniformity coefficient (Cu)	2.55±0.001	2.58±0.001
Coefficient of curvature (Cc)	4.375±0.005	4.570 ±0.01
Consistency	1.79±0.002	1.59±0.001
Plasticity indices (PI in %)	25.32±0.010	36.85±0.002
Hydraulic conductivity m/s	1.0 x 10^{-9}±0.01	1.0 x 10^{-8}±0.01
Sand equivalent (ES in %)	15.03±0.001	17.15±0.001
Moisture content (%)	29.60±0.002	50.60±0.001
Maximum dry density	1.41±0.001	3.02±0.002
Bulk density (g/cm^3)	1.10±0.005	1.80±0.001
Shear strength (KN/m^2)	24.89±0.001	29.95±0.01
Shrinkage Index	9.65±0.002	20.10±0.001
Dry unit weights (kg/cm^2)	1.32±0.001	1.59±0.005
Clay content %	28.90±0.05	68±0.002
Activity	0.98	1.09
Unconfined compressive strength (kPa)	249.80	78.90

The results of geotechnical properties of the laterites and clays (Table 4) show that the clay samples have high liquidity limit of 59.70±0.005, while the laterites (38.97±0.001) have medium and that is in agreement with the reports of Murali et al. [24], which reported that soils with high liquid content falls within the range of 40-60 % (W_L), and 30-40 % for medium. Also, the laterite samples have a medium plasticity limit of 20.44±0.02, while the clays have a high plasticity limit that falls within 20 -55 %, in agreement with the results reported by [24]. Furthermore, the shrinkage index of the laterites (9.651±0.002) is low, indicating a low degree of expansion (< 15), while that of the clay is 20.10±0.00, indicating also a medium degree of expansion in line with the (15-30) medium range reported by [24]. The results in Table 4 also showed that the moisture content of the laterites is 29.60 %, which is slightly higher than the 28 % reported by [18], 16-25 % reported in [25] and 10.1-20.6 % reported in [26], while that of the clay is 50.60 % and is higher than 16.9-33 % reported by [25]. Additionally, the plasticity indices of the laterites (25.32 %) are within the range of 13.5-26.5, reported by [27], and 8-24.1 % in [25], and that of the clays (36.85 %) is within the range of (23-45 %) reported in [27]. Furthermore, the unconfined compressive strength of the laterites (249.80 kPa) obtained is within the range of 71-375 reported by [26], and that of the clays (78.90 %), which is higher than 71.5 kPa reported in [28], and lower than 41.70 kPa reported in [29].

Meanwhile, from most research reports, the compressive strength of laterites or clays decreases as the plasticity index increases, and high plastic laterite and clay soils have stronger binding pressures, which may lead to an increase in the soil's shear strength [27, 29]. Also, it has been recognized that laterites and clays with high calcium carbonate content ($CaCO_3$) have lower plasticity indices and significantly higher shear strengths. That accounts for why the laterites used in this study had more unconfined compressive strength than the clays. For applications of laterites and clays, the determination of shear strength is often very critical to ensure that the produced structures of intention, like bricks, are secured against shear failure and excessive settlement [21]. The result also shows that the laterites have an

activity of 0.98, while the clays have 1.09, which is higher than 0.5 reported for kaolinite clays by [27]. The laterites and clays used in this study are normal in terms of their activity rating (i.e., 0.75 -1.25, range for normal) [18, 24, 28], assuming that in each case, the plasticity index is approximately equal to the laterite or clay fraction (A = 1).

Table 5: Thermal Properties of Laterite and Clay Samples

Property	Laterite	Clay
Melting temperature (°C)	55- 630	40-660
Thermal conductivity ($kgms^{-2}\Theta^{-1}$)	34.98	107.8
Resistivity (Ωm)	0.0358	0.0186
Thermal Temperature Range	49.6- 840 °C	55- 1320

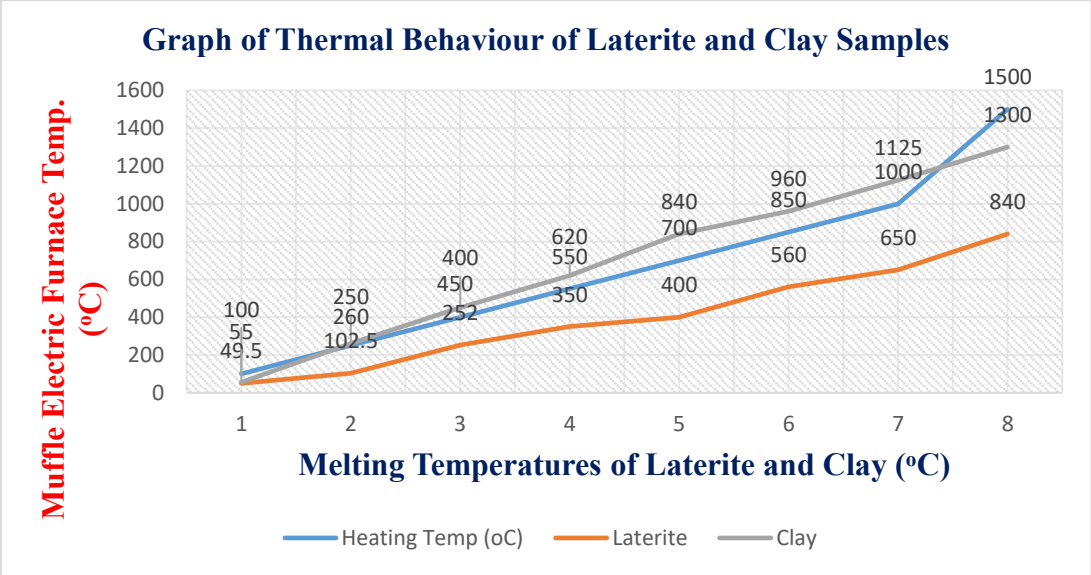

Figure 5: Graph of Thermogravimetric Analysis of Laterite and Clay Showing Their Thermal Behaviour

The results of electrical and thermal conductivity obtained (Table 5) revealed that the laterite soils have very low thermal conductivity of 3.498 x 10^1 $kgms^{-2}\Theta^{-1}$ and resistivity of 3.58 x 10^2 Ωm, while 1.078 x 10^2 $kgms^{-2}\Theta^{-1}$ and 1.86 x 10^2 Ωm were obtained for the clay samples. The resistivity values obtained in this study were much lower than the 340-5,500 reported by Mari [30]. Nevertheless, the low resistivity recorded in the present work could be attributed to the high temperatures of the laterites (49.6±0.010 °C) and clays (55.0±0.010 °C), since severe increases in resistivity often occur as the soil temperature decreases and past even the freezing point, or resistivity of soil samples often decreases with increase in the soil temperature [29]. However, the thermal conductivities according to Table 5 reveal that the laterite samples have the lowest thermal conductivity, while the clay samples have the highest as shown in Figure 5. In general, the low conductivity values obtained in our results indicate that both the laterites and the clays will be good heat-insulating materials for housing projects because of their low thermal conductivity, while the clay materials may conduct heat at a higher rate; however, their absorbent power may take a longer period to reach the steady state [1].

3.3 Microstructural and Optical Characterization

In addition to the mineralogical and elemental compositions, the microstructure of laterites and clays influences their geotechnical properties. Thus, the results of the scanning electron microscopic (SEM) analysis carried out to verify the microstructure of the samples showed that in both the laterite and clay soil, the particles are grain-like [19], and packed in wedge-like inter-aggregate pores. The soil particles' grains are connected face to face, edge to edge, and face to edge shapes with each other, as seen in Figure 6a & b [18]. Hence, the obtained microstructure can be considered matrix microstructure, in which the particles are connected irregularly to each other and the aggregation of the soil particles forms a rough surface, resulting in a well-interlocking arrangement between soil aggregates. The

obtained microstructure results in this work are consistent with previously researched reports [4, 18, 23].

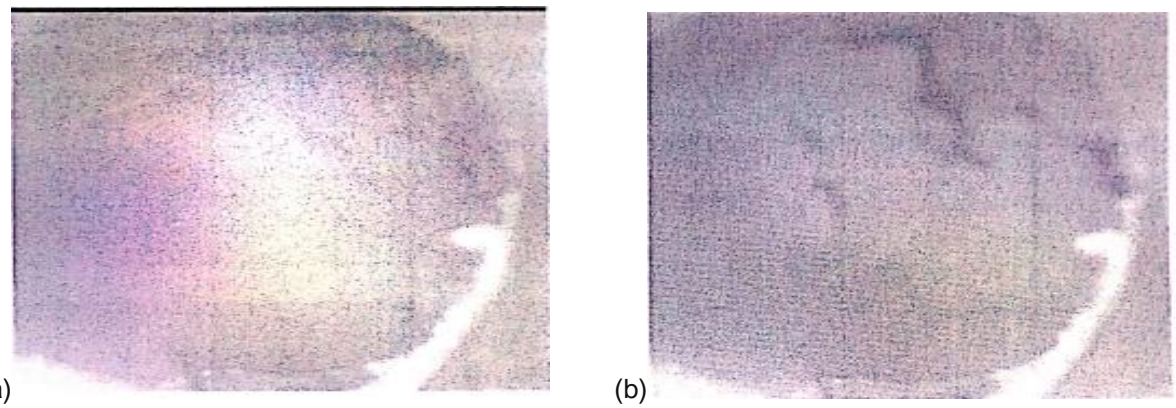

(a) (b)

Figures 6a: The Result of SEM Image of Laterite [17] and (b) The Result of SEM Image of Clay Adapted from [4] (10k magnification): Thermo Fisher Scientific, MA 01876 USA.

4. CONCLUSION

The studies were conducted on the various properties of the studied laterites and clays based on the new features of instrumental research methodologies and statistical calculations. The results of this study showed that both the laterites and clays contain kaolinite ($Al_2Si_2O_5(OH)_4$) mineral, alumina (Al_2O_3), silica (SiO_2), hematite (Fe_2O_3), magnesia (MgO), lime (CaO) and titania (TiO_2) among other minerals and elements, Al, Fe, Ti, Ca, K, Zr, etc. with good geotechnical properties. Since it has been repeated averred that the geotechnical/mechanical and thermal characteristics of laterite and clay soils varied considerably with climate, parent rock and formation process and the raw materials also possess inherent limitations [3, 24, 27], it is often expedient to verify and validate whether laterites and clays have the inherent prerequisite minerals, chemicals and properties like high thermal strength that would make them able to withstand stresses, pressures, high and low temperatures (temperature fluctuation) that they will be exposed to from the materials that they are intended to be used for. Because, early detection of inherent weaknesses of lateritic and clayey soils can be adequately addressed through supplementary provisions and limiting of their uses to what they are suitable for and based on that the determination of inherent properties of laterites and clays such as the shear strength has been a priority issue for engineers and mathematicians for more than 250 years as pressure due to volume change often experienced by soils especially clay can cause serious damage to concrete foundation, or failure and floor slabs as well as the rooms and upper building above them [24]. Therefore, it is usually essential to identify the characteristics of the soils before they are used for any construction activities to be carried out [23]. Overall, we have found experimentally through their properties that the laterites and clays have low thermal conductivity, high resistivity, good shear and compressive strength, high plasticity with moderate water content, high porosity, good shrinkage index, among other properties, and therefore, they have medium expansion and cracking potential in addition to their sufficient prerequisite mineral and elemental compositions. Hence, they are suitable raw materials for making cold and fired bricks, geopolymers, ceramics, and even tiles. We therefore call on the Federal Government of Nigeria, Benue State Government, Otukpo Local Government, industries, individual manufacturers and foreign investors to take advantage of this information to explore the possible maximum exploitation of the natural abundance laterite and clay raw materials of the area for economic benefit of Nigeria by joining countries like USA and become one of the exporters of laterites and clays for production of adsorbent, fillers, drain and roofing tiles, ceramics, organic pet litters, polymers, silica gel, sewer pipe etc.

CONFLICT OF INTERESTS

The authors declare no conflict of interests.

REFERENCES

[1] Adekunle, A., Ekandem, E. S., Ibe, K. E., Ananso, G. N., and Mondigha, E. B. (2014). Analysis of Thermal and Electrical Properties of Laterite, Clay, and Sand Samples and Their Effects on

Inhabited Buildings in Ota, Ogun State, Nigeria. Journal of Sustainable Development Studies, 6(2); pp. 391-412; ISSN 2201-4268.

[2] Jenifer, J. and Ramasundaram, S. (2015). Strength and durability characteristics of laterite sand mixed concrete. International Journal of ChemTech Research, 8(3): pp. 1253-1259.

[3] Kumar, G. S., Saini, P. K., Rajesh, D., Mishra, A. K., and Negi, S. K. (2022). Characterization of laterite soil and its use in construction applications: A review; CSIR-Central Building Research Institute. Roorkee, 247 667; Elsevier B.V.; Resources, Conservation & Recycling Advances; 2667-3789/© 2022 www.sciencedirect.com/journal/; https://doi.org/10.1016/j.rcradv.2022.200120; (http://creativecommons.org/licenses/by-nc-nd/4.0/.

[4] Idongesit, N. A., Ashishie, C.A., Muhammed, A.D, and Ambo, I. A. (2025). Assessment of the Mineralogical and Elemental Compositions of the Clays of Otukpo, Benue State, Nigeria as Potential Raw Materials for Manufacturing of Bricks, Refractories and Geopolymers. ChemClass Journal, 9(1); pp. 190-204; e-ISSN:0198-2734; p-ISSN:0198-5680; doi.org/10.33003/chemclas_2025_0901/016; https://chemclassjournal.com/;

[5] Kaze, C.R., Lemougna, P.N., Alomayri, T., Assaedi, H., Adesina, A., Das, S.K., Lecomte Nana, G.L., Kamseu, E., Melo, U.C. and Leonelli, C. (2021). Characterization and performance evaluation of laterite based geopolymer binder cured at different temperatures. Construction and Build. Mater. 270, 121443.

[6] Maiti, A., Thakur, B.K., Basu, J.K., and De, S. (2013). Comparison of treated laterite as arsenic adsorbent from different locations and performance of the best filter under field conditions. *J. Hazard. Mater*., 262, pp. 1176–1186.

[7] Chen, F.H. (2012). "Foundations on expansive soils", (ed), Elsevier, vol. 12.

[8] Brady, N.C. and Ray, R. W. (2008). The Nature and Properties of Soil, (14th ed): Upper Saddle River, NJ: Prentice Hall; pp. 1-95.

[9] Adam, A. (2008). Mineralogy. Encyclopedia Britannica (3rd Ed); Science and Tech; https://www.britannica.com/science/clay-geology#

[10] Parmar, H. (2023). 15 Characteristics of Clay Soil: Shree Ram Kaolin; An ISO 9001:2015 certified company; https://shreeramkaolin.com/characteristics-of-clay-soil/.

[11] Bell, F.G. (2002). The geotechnical properties of some till deposits occurring along the coastal areas of eastern England. *Engineering Geology*, 63, pp. 49-68.

[12] Chittoori, B.C.S. (2008). "Clay mineralogy effects on long-term performance of chemically treated expansive clays", ProQuest.

[13] Sirivitmaitrie, C., Puppala, A. J., Chikyala, V., Saride, S., and Hoyos, L. R. (2008). "Combined lime and cement treatment of expansive soils with low to medium soluble sulfate levels", *American Society of Civil Engineers, Proceedings of the Geo Congress*, pp. 646-653.

[14] Hui, Z. and Junhua, W. U. (2017). Study of soil pore fractal features in the process of soil consolidation and its impact on permeability. Ind. Constr. 8, 95–99. https ://doi.org/10.13204 /j.gyjz2 01708 018.

[15] LibreTexts (2021). The Delft Sand, Clay, and Rock Cutting Model (Miedema): Soil Mechanical Parameters. Engineering LibreTexts libraries; https://eng.libretexts; https://eng.libretexts.org/Bookshelves/Civil_Engineering/Book%3A_The_Delft_Sand_Clay_and_Rock_Cutting_Model_(Miedema)/02%3A_Basic_Soil_Mechanics/2.04%3A_Soil_Mechanical_Parameters.

[16] Singhal, S. (2010). "Expansive soil behavior: property measurement techniques and heave prediction methods", Arizona State University.

[17] Idongesit, N.A. and Wadai, M. (2024). Evaluation of the Mineral Contents of Lateritic Soils of Benue State, Nigeria for the Manufacture of Building Materials. *International Journal of Science and Society*, Yabatech (IJSCAS); 24-031.

[18] Roshan, M.J., Hezmi, M.A., Rashid, A.S.A., Ullah, R., and Ullah, A. (2022). Characterization of lateritic soil based on literature and lab testing. Research Square; DOI: https://doi.org/10.21203/rs.3.rs-1977542/v1; DOI:10.21203/rs.3.rs-1977542/v1 https://www.researchgate.net/publication/362850199.

[19] Eisazadeh, A., Kassim, K.A., and Nur, H. (2011). Characterization of phosphoric acid- and lime-stabilized tropical lateritic clay. Environ Earth Sci., 63: pp. 1057–1066. https://doi.org/10.1007/s12665-010-0781-2.

[20] Osinubi, K. J. and Eberemu, A.O. (2010). Unsaturated hydraulic conductivity of compacted lateritic soil treated with 451 bagasse ash. In: GeoFlorida. ASCE, pp 357– 369.

[21] Oyelami, C.A. and Van Rooy, J.L. (2018). Mineralogical Characterization of tropical residual soils from south-western Nigeria and its impact on earth building bricks. Environ. Earth Sci. 77 (5), 178.

[22] Adeniyi, F. I., Ogundiran, M. B., Hemalatha, T., and Hanumantrai, B. B. (2020). Characterization of Raw and Thermally Treated Nigerian Kaolinite Containing Clays Using Instrumental Techniques. *SN Appl. Sci.*, 2 (5), 1−14.

[23] Goracci, G., Ogundiran, M.B., Barzegar, M., Iturrospe, A., Arbe, A. and Dolado, J.S. (2024). Kaolin Clay-Based Geopolymer for Ionic Thermoelectric Energy Harvesting. ACS Omega, 9, pp. 13728−13737; CC-BY-NCND 4.0; https://doi.org/10.1021/acsomega.3c08257.

[24] Murali, K., Sambath, K., and Hashir, S. M. (2018). A Review on Clay and Its Engineering Significance. International Journal of Scientific and Research Publications, 8(2); https://www.researchgate.net/publication/322987497; ISSN:2250-3153.

[25] Kramarenko, V. V., Nikitenkov, A. N., Matveenko, I. A., Molokov, V. Y. and Vasilenko, Y.S. (2016). Determination of water content in clay and organic soil using a microwave oven. IOP Conf. Series: Earth and Environmental Science, 43; 012029; doi:10.1088/1755-1315/43/1/012029.

[26] Ojuri, O. O. (2013). Shear Strength Models for Tropical Lateritic Soils. Hindawi Publishing Corporation, Journal of Engineering, ID 595626; pp.1-8; http://dx.doi.org/10.1155/2013/595626.

[27] Firoozi, A.A., Firoozi, A. A., and Baghini, M.S. (2016). A Review of Clayey Soils. *Asian Journal of Applied Sciences*, 4(6); pp. 1319-1330; ISSN: 2321 – 0893; www.ajouronline.com; https://www.researchgate.net/publication/312027428.

[28] Hossain, S., Islam, A. and Fahim, F. (2021). Properties and Behaviour of Soil- Unconfined Compressive Strength Test. *Online Lab Manual*, https://uta.pressbooks.pub/soilmechanics/chapter/unconfined-compressive-strength- test/

[29] Widianti, A., Diana, W. and Fikriyah, Z. S. (2020). Unconfined Compressive Strength of Clay Strengthened by Coconut Fiber Waste. Advances in Engineering Research, vol. 199; Proceedings of the 4th International Conference on Sustainable Innovation 2020– Technology, Engineering and Agriculture (ICoSITEA 2020); CC BY-NC 4.0; Atlantis Press; http://creativecommons.org/licenses/by-nc/4.0/.

[30] Mari, L. (2020). An Introduction to Soil Resistivity-the soil's electrical characteristics: Technical Article.EEpower; https://eepower.com/author/Lorenzomari; https://eepower.com/technical-articles/an-introduction-to-soil-resistivity/.

ISBN: 978-978-68-0485-9 http://acsnigeria.org/publications/proceedings

Toxic Metals Contamination and Health Risk Assessment in Spices and Herbal Teas from Abuja, Nigeria

Adebisi Akinyemi Fagbohun[1], Toba Samuel Anjorin[2], and Mary Sunday Dauda[3]
[1]Chemistry Advanced Research Center, Sheda Science and Technology Complex, Abuja, Nigeria.
[2]Department of Crop Protection, Faculty of Agriculture, University of Abuja, Nigeria
[3]Chemistry Department, Faculty of Science, University of Abuja, Nigeria.
Corresponding Author's email: aa.fagbohun@shestco.gov.ng

ABSTRACT

Herbal teas and spices, valued for their nutritional, medicinal, and cultural significance in urban and peri-urban communities, can pose health risks due to heavy metal contamination. This study evaluates heavy metal levels in 12 herbal teas randomly purchased in Abuja and 11 spices, alongside their health risks, using AOAC 2000 analytical methods. Detectable concentrations of metals were found in all samples. Among spices, ginger powder showed the highest manganese (Mn: 598.8 mg kg^{-1}) and chromium (Cr: 15.13 mg kg^{-1}), while turmeric powder had elevated Mn (403.8 mg kg^{-1}) and Cr (12.96 mg kg^{-1}). Yellow pepper contained high lead (Pb: 7.89 mg kg^{-1}) and cadmium (Cd: 2.280 mg kg^{-1}), and garlic powder had notable Cr (10.88 mg kg^{-1}). In herbal teas, Top tea exhibited high Mn (1661 mg kg^{-1}) and Pb (35.12 mg kg^{-1}), while Moringa tea showed elevated Pb (77.00 mg kg^{-1}). Compared to WHO/FAO limits (Cd: 0.100 mg kg^{-1}; Co: 0.200 mg kg^{-1}; Cr: 2.000 mg kg^{-1}; Cu: 20.00 mg kg^{-1}; Mn: 0.120 mg kg^{-1}; Ni: 1.630 mg kg^{-1}; Pb: 10.00 mg kg^{-1}), Mn, Cr, and Pb frequently exceeded safe thresholds. Health risk assessment indicated a significant manganese hazard quotient (11.26), suggesting neurotoxicity risks, and a lead (1.11) slightly above safe limits, pointing to potential nervous, renal, and hematopoietic effects. Other metals (Cd, Co, Cr, Cu, Ni) had HQ < 1, indicating lower risk. These findings highlight significant contamination in widely consumed teas and spices, necessitating stricter regulatory measures to mitigate chronic dietary exposure risks and protect public health.

KEYWORDS: *Beverages, Condiment, Metals, Toxicity, Risk*

1. INTRODUCTION

Heavy metals, characterized by high atomic weights or densities, include toxic elements such as cadmium (Cd), lead (Pb), mercury (Hg), arsenic (As), and hexavalent chromium (Cr^{6+}), which are harmful even at low levels.[1] Spices and herbal teas, derived from plant parts like bark, rhizomes, and leaves, are valued for their culinary and medicinal properties, including antimicrobial, anti-inflammatory, and antioxidant effects. [2, 3] However, these products are susceptible to contamination from natural and anthropogenic sources, including soil bioaccumulation, industrial runoff, mining, pesticide use, and improper waste disposal. [4, 5, 6] Additional contamination arises from power plant emissions, vehicular exhaust, oil spills, and poor post-harvest handling. [7,8,9,10] While metals like iron, zinc, and copper are essential, excessive exposure to non-essential metals such as Cd and Pb can lead to osteoporosis, kidney and neurological disorders, cancers, and cardiovascular complications. [11,12,13] Heavy metals may also disrupt gut microbiota and mental health.[14] Accurate measurements use techniques such as Flame Atomic Absorption Spectrometry (FAAS) and Inductively Coupled Plasma Optical Emission Spectroscopy (ICP-OES) (Inobeme *et al.,* 2023). International safety is guided by ADI limits set by EFSA and FAO/WHO.[15] This study investigates the levels of selected heavy metals in spices and herbal teas sold in Abuja, FCT, Nigeria, against these standards.

2. MATERIALS AND METHODS

A total of 11 spices and 12 herbal tea brands were purchased randomly from different grocery stores and supermarkets within the Federal Capital Territory, Abuja (FCT), and were labeled accordingly. 2g ± 0.01g of each pulverized sample was digested using 20 mL of aqua regia, consisting of a 3:1 ratio of concentrated hydrochloric acid and nitric acid. The mixture was digested for 10 min at 155 °C for a further 7 min at 200 °C. The digested sample was filtered into a 50 ml standard volumetric flask and made up to the mark. The residual levels of 7 heavy metals in herbal teas and spices were determined using Solaar Elemental Thermo Scientific Atomic Absorption Spectrophotometry (AAS) located at Kembiz Scientific and Laboratories Nigeria Limited, Gwagwalada FCT, Abuja. Cadmium (Cd), Cobalt (Co), Lead (Pb), Chromium (Cr), Copper (Cu), Manganese (Mn), and Nickel (Ni). [16,17] The concentration of each metal was calculated using the following formula:

Final concentration $$n\,(mg/kg) = \frac{\text{Concentration of Metal ion} - \text{Blank}}{Weight\ of\ sample\ (g)} \times Dilution\ factor$$

Quality control measure was affected using blanks and performing a recovery study with spiked samples and blanks, equilibrated for 1 hour before digestion, and verifying method accuracy and precision. [18] Recovery was calculated from 4 replicates using the following formula:

$$\text{Percentage recovery} = \frac{Concentration\ of\ spiked\ sample - Concentration\ of\ unspike\ sample}{Amount\ added} \text{ X } 100$$

2.1 Assessment of Human Health Risk

The Food and Agriculture Organization (FAO) previously stated that Nigeria's annual food supply is 3.650 kg/capita for spices and 0.6 kg/capita for herbal teas, equating to food ingestion rates (FIR) of 0.01 kg/capita/day and 0.0016 kg/capita/day, respectively, as further illustrated in the equation below:

$$EDI = CXFIR/BW$$ .....Eqn I

Where C is the dry weight concentration of the residual heavy metals in the spice and herbal tea in mg kg^{-1}, FIR accuracy rate, and BW is the reference body weight of 60 kg for an adult human.

Hazard quotient: The hazard quotient (HQ) was regarded as the probable risk of undesirable health effects from pesticide mixtures to specify the long-term assessment of risk and was computed by dividing the EDI by the pertinent ADI and multiplying by 100, as stated in the equation below. [17]

$$HQ = EDI/ADI \times 100$$ ..... Eqn ii

3. RESULTS AND DISCUSSION

Heavy metal contamination in spices poses a significant public health concern due to their bioaccumulative and toxic nature. Table 1 depicts residual concentrations of seven heavy metals (Cd, Co, Cr, Cu, Mn, Ni, Pb) in eleven commonly consumed spices sold in FCT Abuja, Nigeria, with results compared against established regulatory limits.

Table 1: Residual Concentrations of Heavy Metals in Different Spices Sold in Abuja, Nigeria

Spices	Concentration (mg kg^{-1})						
	Cd	Co	Cr	Cu	Mn	Ni	Pb
Black pepper	1.640±0.011	0.960±0.01	BDL	58.30±0.02	157.95±0.02	6.110±0.00	6.830±0.00
Cayenne pepper	0.910±0.02	3.500±0.00	3.780±0.00	36.36±0.02	33.84±0.01	2.690±0.03	3.170±0.00
Nutmeg	0.720±0.00	BDL	3.320±0.01	55.36±0.03	54.72±0.00	4.070±0.01	3.740±0.00
Curry powder	0.930±0.01	0.660±0.00	4.650±0.01	29.78±0.01	51.59±0.00	3.070±0.00	2.520±0.01
Chicken season	0.840±0.03	BDL	6.080±0.00	22.35±0.00	52.18±0.00	4.190±0.02	2.870±0.02
Fried seasoning	0.680±0.00	BDL	9.170±0.00	4.380±0.01	15.53±0.01	3.670 ±0.01	1.750±0.03
Yellow pepper	2.280±0.01	1.310±0.01	8.100±0.00	23.51±0.01	20.06±0.00	2.460±0.00	7.890±0.02
Garlic powder	0.760±0.012	0.690±0.00	10.88±0.012	11.53±0.00	13.12±0.00	3.420±0.01	4.270±0.00
Turmeric powder	1.030±0.01	0.930±0.02	12.96±0.00	18.63±0.01	403.8±0.02	2.740±0.01	0.270±0.01
Ginger powder	1.270±0.00	0.000±0.00	15.13±0.00	27.53±0.00	598.8±0.03	3.710±0.00	3.120±0.00
Thyme leaves	1.230±0.011	0.000±0.01	18.40±0.00	31.84±0.02	69.89±0.02	4.140±0.00	3.370±0.01
Limit (mg kg^{-1})	0.100	0.200	2.000	20.00	0.120	1.630	10.00

BDL: Below detection limit (of 0.001), mg kg^{-1}: milligram per kilogram

Heavy metal contamination in packaged herbal teas raises public health concerns due to their potential bioaccumulation and toxicity. Table 2 displayed the residual levels of seven heavy metals (Cd, Co, Cr, Cu, Mn, Ni, Pb) in twelve commercial herbal tea varieties from Abuja markets, Nigeria, benchmarked against regulatory limits.

Table 2: Heavy Metal Concentrations (mg kg^{-1}) in Packaged Herbal Tea in Abuja Markets

Herbal tea	Concentration (mg kg^{-1})						
	Cd	Co	Cr	Cu	Mn	Ni	Pb
Green tea	0.790±0.03	BDL	21.52±0.00	55.94 ±0.00	505.2±0.11	6.48±0.00	5.090±0.01
Guava tea	0.390±0.02	0.850±0.01	22.76±0.01	23.06±0.01	31.19±0.02	3.59±0.02	6.16±0.01
Eyes bright	0.320±0.02	0.000±0.01	25.94±0.02	29.38±0.01	527.5±0.03	5.530±0.01	6.240±0.01
Moringa tea	0.600±0.01	BDL	5.930±0.01	15.63±0.00	50.05±0.02	2.940±0.01	77.00±0.01
Tummy and fat-reducing tea	1.450±0.00	BDL	BDL	12.65±0.01	58.64±0.00	4.220±0.01	5.340±0.01
Lipton tea	0.270±0.00	1.310±0.01	BDL	31.65±0.01	1369.±0.01	8.340±0.00	1.370±0.00
Nals pure natural mint l	0.620±0.01	BDL	10.41±0.01	33.74±0.02	110.9±0.02	5.940±0.00	1.680±0.00
Lemon-ginger tea	0.940±0.00	BDL	9.480±0.00	11.73±0.11	198.6±0.01	3.060±0.00	1.620±0.00
Top tea	0.690±0.00	BDL	11.23±0.01	42.87±0.01	1661±0.03	10.22±0.02	35.12±0.01
Mango tea	0.600±0.11	BDL	9.130±0.03	66.97±0.00	355.44±0.01	5.710±0.01	2.560±0.00
Highland tea	0.750±0.01	BDL	12.41±0.00	28.68±0.01	419.14±0.11	7.970±0.00	BDL
Beetroot tea	0.430±0.02	BDL	10.25±0.00	17.27±0.00	63.83±0.02	3.090±0.00	30.90±0.03
Limit (mg kg^{-1})	0.100	0.200	2.000	20.00	0.120	1.630	10.00

BDL: Below detection limit (of 0.001), mg kg^{-1}: milligram per kilogram

Table 1 revealed that manganese levels were notably high in spices, with ginger powder at 598.75 mg kg^{-1}, 4,989-fold exceedance of the 0.120 mg kg^{-1} MPL, and turmeric powder at 403.77 mg kg^{-1}. Some of the values reported in this current study far exceed those reported elsewhere, such as 45.8 mg kg^{-1} in turmeric,[18], and 93.70 mg kg^{-1} in ginger.[19] Herbal teas also showed extreme manganese contamination, with Top tea at 1,661 mg kg^{-1} (13,842-fold exceedance of the limit), Lipton tea at 1,369.04 mg kg^{-1}, and green tea at 505.2 mg kg^{-1}, surpassing ranges previously reported elsewhere (0–200 mg kg^{-1}) [20] and 62.1 mg kg^{-1} in green tea. [21] Elevated manganese levels, linked to neurotoxicity and manganism among other diseases [22,23], suggest localized contamination from soil, water, or industrial emissions. [24,25] Cadmium exceeded the 0.100 mg kg^{-1} maximum permissible limit (MPL) in all spice samples, notably yellow pepper (2.28 mg kg^{-1}) and fried seasoning (0.680 mg kg^{-1}), higher than values reported elsewhere. [26] In herbal teas, cadmium reached 1.45 mg kg^{-1} in Tummy and Body Fat-Reducing teas and 0.79 mg kg^{-1} in green tea. These levels, associated with renal dysfunction, bone demineralization, and carcinogenesis [27,28], indicate severe environmental or industrial contamination relative to previous findings [29].[30]. Copper levels exceeded the 20.00 mg kg^{-1} MPL in spices, with black pepper at 58.30 mg kg^{-1}, nutmeg at 55.36 mg kg^{-1}, and cayenne at 36.36 mg kg^{-1}, compared to 13.6–21.3 mg kg^{-1} obtained by [31]. Teas also showed elevated copper: Mango tea (66.97 mg kg^{-1}), green tea (55.94 mg kg^{-1}), and Top tea (42.87 mg kg^{-1}), surpassing 0.06–15.08 mg kg^{-1} [32], and 11.02–24.12 mg kg^{-1} earlier reported .[33] High copper levels, linked to oxidative stress, hepatotoxicity, and nephrotoxicity [34], may originate from processing or environmental sources. Nickel exceeded the 1.63 mg kg^{-1} MPL in spices: black pepper (6.11 mg kg^{-1}), ginger (3.71 mg kg^{-1}), and turmeric (2.74 mg kg^{-1}), higher than 1.2 mg kg^{-1} [35] In teas, nickel reached 10.22 mg kg^{-1} in Top tea and 8.34 mg kg^{-1} in Lipton tea, exceeding 1.2–3.0 mg kg^{-1} obtained previously [36]. These concentrations, linked to allergic dermatitis, respiratory complications, and renal damage. [37] align with Nigerian reports from Awka spices 0.34–2.89 mg kg^{-1} [38] and Ibadan teas 3.50–8.00 mg kg^{-1}. [39] Lead contamination was particularly severe in teas, with Moringa tea (77.00 mg kg^{-1}), Top tea (35.12 mg kg^{-1}), and Beetroot tea (30.90 mg kg^{-1}), exceeding the 10.00 mg kg^{-1} MPL, compared to 5.0–10.0 mg kg^{-1}.[40] Spices, such as yellow pepper (7.89 mg kg^{-1}) and black pepper (6.83 mg kg^{-1}), approached the limit, surpassing 5.0 mg kg^{-1}. [41] Lead, associated with neurotoxicity and developmental effects. [42, 43] were higher than Port Harcourt values (0.76–3.56 mg kg^{-1}). [44] Chromium exceeded the 2.00 mg kg^{-1} MPL in most spices (thyme leaves, 18.40 mg kg^{-1}; ginger, 15.13 mg kg^{-1}) and teas (Eyes Bright tea, 25.94 mg kg^{-1}; Guava tea, 22.76 mg kg^{-1}, far above 0.200 mg kg^{-1} [45]. These may include carcinogenic hexavalent chromium, exceeding Awka (0.001–3.81 mg kg^{-1}), [39] and Kano (0.6–6.5 mg kg^{-1}). [31] Cobalt, surpassing the 0.200 mg kg^{-1} MPL, was observed in cayenne pepper (3.50 mg kg^{-1}), Guava tea (0.850 mg kg^{-1}), and Lipton tea (1.310 mg kg^{-1}), higher than typical Nigerian levels 0.28–3.07 mg kg^{-1}, [39], raising concerns for cardiotoxicity and thyroid dysfunction [29] These findings, consistent with previous Nigerian studies [33,46], highlight the FCT as a contamination hotspot, particularly in teas, likely due to unique environmental, soil, and industrial factors. [25, 26]

Tables 3 and 4 present the health risk assessment (HRA) of heavy metals detected in spices and herbal teas sold across Abuja, FCT, Nigeria.

Table 3: Health Risk Assessment of Spices Sold in Abuja, Nigeria

Heavy Metal	Cd	Co	Cr	Cu	Mn	Ni	Pb
Avg	0.654	0.180	7.86375	30.80	445.9	5.590	14.42
Max	1.450	1.310	12.41	66.97	1660.79	10.22	77.00
Min	0.270	0	0	11.73	31.19	2.940	0
Sum	7.850	3.650	83.18	479.07	7488.1	85.84	264.5
ADI (mg/60day)	0.06	0.008	0.035	0.900	0.660	0.78	0.216
EDI	0.00010903	0.00003	0.001311	0.005133	0.07431	0.000932	0.002404
HQ	0.18171306	0.001667	0.007281	0.122212	11.25905	0.119462	1.112911

ADI: Acceptable daily intake, EDI: Estimated daily intake, HQ: Hazard quotient

Table 4: Health Risk Assessment of Herbal Tea Sold in Abuja, Nigeria

Heavy metals	Cd	Co	Cr	Cu	Mn	Ni	Pb
Max	2.280	3.500	18.40	58.30	598.75	6.110	7.890
Min	0.680	0	0	4.38	13.12	2.48	0.270
Avg.	1.1127	0.7665	8.406	29.05	133.76	3.661	3.618
ADI (mg/60 days)	0.060	0.008	0.035	0.900	0.660	0.780	0.216
EDI	2.9672E-05	2.04E-05	0.000224	0.000775	0.003567	9.76E-05	9.65E-05
HQ	0.04945333	0.001136	0.001245	0.018444	0.540444	0.012516	0.044667

ADI: Acceptable daily intake, EDI: Estimated daily intake, HQ: Hazard quotient

The Estimated Daily Intakes (EDIs) for all metals were considerably below their respective Acceptable Daily Intakes (ADIs), indicating minimal immediate exposure concerns. However, the hazard quotient (HQ) analysis revealed significant findings. Manganese recorded an exceptionally high HQ value of 11.26 above the allowable limit of less than 1, indicating a potential neurotoxic threat associated with long-term consumption. Lead also exhibited an HQ of 1.11, slightly exceeding the safe threshold, thereby suggesting possible nervous, renal, and hematopoietic complications on long-term consumption. In contrast, other metals, including cadmium (Cd), cobalt (Co), chromium (Cr), copper (Cu), and nickel (Ni), recorded HQ values were well below 1, reflecting minimal non-carcinogenic risk. The overall hazard index was well within the safety margin, except for manganese in spices (11.2590), where prolonged exposure may pose notable health hazards. These findings align with the observations made previously [47], who similarly reported hazard quotients below 1 in several Nigerian herbal beverages.

4. CONCLUSION

This study reveals significant public health risks from heavy metal contamination in Abuja's spices and herbal teas. Spices like ginger, turmeric, black pepper, and yellow pepper showed high manganese and lead levels, exceeding safe limits and posing risks of neurotoxicity and renal damage. Herbal teas had lower contamination, but cadmium, manganese, and lead were still detected. These findings underscore the need for stricter food safety regulations, continuous monitoring, and public awareness to reduce health risks from dietary exposure.

CONFLICT OF INTERESTS

The authors declare no conflict of interest.

ACKNOWLEDGMENTS

The authors would like to acknowledge the Institution-Based Research Grant (IBR) committee, University of Abuja, Nigeria, for financial aid.

REFERENCES

(1) Jadaa, W.; Mohammed, H. Heavy Metals–Definition, Natural and Anthropogenic Sources of Release into Ecosystems, Toxicity, and Removal Methods–An Overview Study. *J. Ecol. Eng.* **2023**, *24* (6), 249–271.

(2) Baig, J. A.; Bhatti, S.; Kazi, T. G.; Afridi, H. I. Evaluation of Arsenic, Cadmium, Nickel, and Lead in Common Spices in Pakistan. *Biol. Trace Elem. Res.* **2019**, *187* (2), 586−595.

(3) Winiarska-Mieczan, A.; Jachimowicz, K.; Kwiecień, M.; Krusiński, R.; Kislova, S.; Sowińska, L.; Yanovych, D. The Content of Cd and Pb in Herbs and Single-Component Spices Used in Polish Cuisine. *Biol. Trace Elem. Res.* **2023**, *201* (7), 3567−3581.

(4) Hu, Y.; Wang, J.; Yang, Y.; Li, S.; Wu, Q.; Nepovimova, E.; Kuca, K. Revolutionizing Soil Heavy Metal Remediation: Cutting-Edge Innovations in Plant Disposal Technology. *Sci. Total Environ.* **2024**, *918*, 170577.

(5) Yahaya, S. M.; Abubakar, F.; Abdu, N. Ecological Risk Assessment of Heavy Metal-Contaminated Soils of Selected Villages in Zamfara State, Nigeria. *SN Appl. Sci.* **2021**, *3* (2), 168.

(6) Kelle, H. I.; Ogoko, E. C.; Udeozo, P. I.; Fagbohun, A. A.; Ngbede, E. O.; Okopi, P. A.; Adamu, J. Investigation and Health Risk Assessment of Heavy Metals in Cattle from Slaughterhouses in the Federal Capital Territory (FCT), Abuja, Nigeria. *Rev. Colomb. Cienc. Quim.-Farm.* **2024**, *53* (3), 804−830.

(7) Ogoko, E. C.; Emeziem, D. Pollution Load Index and Enrichment of Heavy Metals in Soil within the Vicinity of Osogbo Power Station. *J. Chem. Soc. Nigeria* **2019**, *44* (4), 687−695.

(8) Umanah, I. A.; Awaka-ama, J. J.; Udo, G. J. Assessment of Heavy Metal and Polycyclic Aromatic Hydrocarbon (PAH) Levels in Drilling Fluids and Effluents from Niger Delta Oil Fields. *Res. J. Sci. Technol.* **2025**, *5* (3), 22−40.

(9) Uzoatu, C. A.; Osuji, L. C.; Onojake, M. C. Alterations in Physicochemical Properties of Soils Impacted by the Ahoada Oil Spill in Rivers State, Nigeria. *SSR J. Multidiscip.* **2025**, *2* (2), 95−101.

(10) Olatunji, A. S.; Kolawole, T. O.; Oloruntola, M.; Günter, C. Evaluation of Pollution of Soils and Particulate Matter around Metal Recycling Factories in Southwestern Nigeria. *J. Health Pollut.* **2018**, *8* (17), 20−30.

(11) Lawal, K. K.; Ekeleme, I. K.; Onuigbo, C. M.; Ikpeazu, V. O.; Obiekezie, S. O. A Review of the Public Health Implications of Heavy Metals. *World J. Adv. Res. Rev.* **2021**, *11* (2), 123−135.

(12) Budi, H. S.; Catalan Opulencia, M. J.; Afra, A.; Abdelbasset, W. K.; Abdullaev, D.; Majdi, A.; Mohammadi, M. J. Source, Toxicity, and Carcinogenic Health Risk Assessment of Heavy Metals. *Rev. Environ. Health* **2024**, *39* (1), 77−90.

(13) Munir, N.; Jahangeer, M.; Bouyahya, A.; El Omari, N.; Ghchime, R.; Balahbib, A.; Shariati, M. A. Heavy Metal Contamination of Natural Foods Is a Serious Health Issue: A Review. *Sustainability* **2021**, *14* (1), 161.

(14) Wang, Z.; Chen, W. H.; Li, S. X.; He, Z. M.; Zhu, W. L.; Ji, Y. B.; Han, Y. Gut Microbiota Modulates the Inflammatory Response and Cognitive Impairment Induced by Sleep Deprivation. *Mol. Psychiatry* **2021**, *26* (11), 6277−6292.

(15) Ayanniyi, O. A.; Ayeni, O. H.; Ibitoye, O. S.; Aremu, E. A.; Wealth, A. S.; Oyediji, O. T.; Aladeokin, B. O. Evaluating Estimated Daily Intake versus Acceptable Daily Intake of Heavy Metals in *Farfantepenaeus notialis* from Bodija Market, Ibadan: A Comprehensive Risk Assessment. *J. Res. For. Wildl. Environ.* **2024**, *16* (4), 29−38.

(16) AOAC International. *Official Methods of Analysis of AOAC International*, 17th ed.; AOAC International: Gaithersburg, MD, **2000**; Vols. 1−2.

(17) Kowalska, G. The Safety Assessment of Toxic Metals in Commonly Used Herbs, Spices, Tea, and Coffee in Poland. *Int. J. Environ. Res. Public Health* **2021**, *18* (11), 5779.

(18) Barriga-Vélez, M. A.; Ramírez-Vargas, L. C.; López-Barrera, E. A.; Peña-Rincón, C. A. Potential Ecological Risk Index for Metals in a Grazing Area, Guasca, Cundinamarca. *Rev. Fac. Ing. Univ. Antioquia* **2023**, *106*, 103−112.

(19) Karami, H.; Rasekh, M.; Mirzaee, M. Heavy Metal Content in Turmeric: A Case Study from Iran. *Food Sci. Technol. Int.* **2019**, *25* (4), 321–330.

(20) Sadeghi, M.; Karami, H.; Rasekh, M. Heavy Metal Residues in Ginger: Environmental and Health Implications. *J. Food Prot.* **2022**, *85* (3), 456–463.

(21) Wu, J.; Li, Z.; Chen, X. Manganese in Herbal Teas: A Global Survey. *J. Agric. Food Chem.* **2019**, *67* (12), 3456–3464.

(22) Ali, M.; Khan, S.; Rahman, A. Manganese Levels in Green Tea: A Case Study from Pakistan. *Food Chem.* **2020**, *312*, 126045.

(23) Peres, T.; Ong, C.; Costa, M. Manganese Toxicity: Neurological Impacts and Mechanisms. *Toxicol. Sci.* **2018**, *165* (2), 277–289.

(24) Kulshreshtha, D.; Sharma, S.; Singh, R. Manganese Neurotoxicity: Mechanisms and Implications. *Neurotoxicology* **2021**, *83*, 67–78.

(25) Ade, T.; Eze, C.; Musa, J. Environmental Contamination Sources in the Federal Capital Territory: Implications for Public Health. *J. Environ. Stud.* **2020**, *12* (3), 45–60.

(26) Musa, J.; Ade, T.; Idris, M. Industrial Emissions and Heavy Metal Contamination in the FCT: A Case Study. *Environ. Monit. Assess.* **2022**, *194* (5), 345.

(27) Marwat, S.; Khan, A.; Rehman, F. Cadmium in Chili Powder: A Comparative Study. *Food Control* **2020**, *112*, 107134.

(28) Chen, X.; Wang, Y.; Li, Z. Cadmium Toxicity: Renal and Skeletal Implications. *Environ. Health Perspect.* **2019**, *127* (6), 067008.

(29) Genchi, G.; Carocci, A.; Lauria, G. Cadmium: Environmental Exposure and Health Effects. *Int. J. Environ. Res. Public Health* **2020**, *17* (3), 987.

(30) Olumide, O.; Adeyemi, A.; Afolabi, O. Heavy Metal Profiles in Spices from Ado Ekiti: A Case Study. *J. Food Saf. Qual.* **2021**, *7* (2), 45–56.

(31) Idris, M.; Musa, J.; Ade, T. Heavy Metal Contamination in Spices from Kano, Nigeria. *J. Food Prot.* **2021**, *84* (6), 987–995.

(32) Sharma, R.; Singh, P.; Gupta, S. Copper in Spices: A Case Study from India. *Food Chem.* **2017**, *235*, 112–119.

(33) Onyekwere, P.; Chukwu, E.; Okeke, C. Manganese and Copper in Southeastern Nigerian Spices and Teas. *Food Chem.* **2019**, *288*, 178–185.

(34) Afolabi, O.; Okeke, C.; Mohammed, I. Heavy Metal Contamination in Herbal Teas and Spices in Ibadan: A Comparative Analysis. *Afr. J. Food Sci.* **2020**, *14* (5), 230–245.

(35) Borobia, A.; Lopez, M.; Garcia, R. Copper Toxicity: Mechanisms and Health Impacts. *Toxicol. Rev.* **2020**, *39* (1), 55–67.

(36) Ozdemir, N.; Kaya, S.; Yilmaz, A. Nickel in Spices: A Global Perspective. *J. Food Sci.* **2018**, *83* (10), 2456–2463.

(37) Zhang, Y.; Liu, X.; She, L. Nickel Contamination in Herbal Teas: Sources and Health Risks. *Food Control* **2020**, *118*, 107412.

(38) Filalova, T.; Chepak, V. Nickel Toxicity: Dermatological and Respiratory Effects. *J. Occup. Health* **2020**, *62* (1), e12145.

(39) Eze, A. N.; Okafor, C. E.; Nwankwo, S. I. Heavy Metal Contamination in Spices Sold in Awka, Nigeria. *J. Environ. Sci. Pollut. Res.* **2023**, *30* (1), 123–134.

(40) Ahmad, S.; Khan, M.; Ali, R. Lead Contamination in Herbal Teas: A Global Perspective. *J. Food Saf.* **2019**, *39* (4), e12678.

(41) Beatriz, L.; Souza, M.; Ferreira, J. Heavy Metal Residues in Spices: A Focus on Black Pepper. *J. Agric. Sci.* **2021**, *13* (7), 89–102.

(42) Mohammed, A.; Ibrahim, S.; Yusuf, M. Lead Toxicity in Food Products: Neurodevelopmental Risks. *J. Environ. Health* **2019**, *81* (9), 22−30.

(43) Okeke, C.; Mohammed, A.; Eze, C. Lead Contamination in Nigerian Food Products: Public Health Implications. *Afr. J. Public Health* **2020**, *12* (4), 156−167.

(44) Ukom, A.; Okeke, C.; Eze, C. Heavy Metal Contamination in Spices from Port Harcourt: A Comparative Analysis. *J. Food Saf.* **2022**, *42* (3), e12945.

(45) Hossain, M.; Ahmed, S.; Rahman, M. Chromium Levels in Tea Leaves: A Global Survey. *J. Food Compos. Anal.* **2018**, *73*, 112−118.

(46) Okwelle, A.; Pepple, G. Chromium Levels in Spices from Port Harcourt: A Comparative Study. *Niger. J. Food Sci.* **2020**, *10* (3), 88−95.

(47) Adepoju-Bello, A. A.; Issa, O. A.; Oguntibeju, O. O.; Ayoola, G. A.; Adejumo, O. E. Analysis of Some Selected Toxic Metals in Registered Herbal Products Manufactured in Nigeria. *Afr. J. Biotechnol.* **2012**, *11* (28), 6918−6922.

ISBN: 978-978-68-0485-9 DOI: https://doi.org/10.55455/acsnigeria.1.2.188-195

Comparative Analysis for Corrosion Inhibition on Mild Steel by Seed and Stem of *Anogeisuss leiocarpus* in Acidic Medium

Sunday John Ibejekwe[1,2], Uche Basil Eke [2], and Sunday Enenche Elaigwu[2]
[1]Department of Chemistry, Federal University of Education Pankshin, Pankshin: P.M.B 027, Nigeria.
[2] Chemistry Department, Faculty of Physical Sciences, University of Ilorin, P.M.B 1515, Ilorin, Nigeria
Corresponding Author's email: igweibejekwe@yaho.com; Phone: +2348060868701, +2349024857078.

ABSTRACT

This research work was investigated to compare corrosion inhibition by parts of *Anogeisuss leiocarpus* on mild steel in 0.5 M H_2SO_4 under temperature conditions of 30-60 ℃ and exposure time of 3-, 6- and 9-hours using weight loss, and PDP. The inhibition efficiencies of the parts follow the trend: seed (95.65 %) and stem-bark (88.09 %). Increase in the concentration (0.2 g/L, 0.4 g/L, 0.6 g/L and 0.8 g/L) of the methanol extracts resulted in % IE increase but decreased with temperature increase thus, increase in corrosion rate. The GCMS analysis of the extract reveals that 9-Octadecenoic acid (Z)-, methyl ester (45.2%), Hexadecanoic acid, methyl ester (18.09 %), 9,12-Octadecadienoic acid (Z,Z)-, methyl ester (17.38 %), Methyl stearate (12.43 %), Maltitol (18.74), 2-Quinazolineacetic acid, 6-chloro-1,2,3,4-tetrahydro-2-(methoxycarbonyl)-4-oxo-3-phenyl-, methyl ester (11.42 %), Ethyl Oleate (16.21%), and Oleic Acid (10.95 %) are prominent compounds. The Phytochemicals screening shows that following metabolites like saponinns, tannins, flavonoids, carbohydrates, steroids and cardiac glycosides are present in the extract. These metabolites may be responsible for inhibition.

KEYWORDS: *Anogeisuss leiocarpus,* weight loss, PDP, mild steel, IE %, Metabolites, GCMS.

1. INTRODUCTION

Long chain organic compounds have been reported to be efficient corrosion inhibitors due to their ability to cover the surface of mild steel and because of its hydrophobic nature thus preventing the metal surface from reacting with moisture within the environment. In addition, some of these compounds are attracted to functional groups such as nitrogen, sulphur and oxygen in conjugated systems thus blocking active sites or forming a protective barrier on steel surfaces [1,2,3]

Recent investigation have shown that most herbal plants for treatment of some diseases by traditionalist among our locals[4,5] are good sources of green inhibitor. *Anogeisuss leiocarpus* is one such medicinal plants used for the treatment of diseases like toothache, diarrhea, respiratory infections, jaundice, hepatitis, haemorrhoids and headache [6,4]. This plant is common in the middle-belt and in the far north of Nigeria[7,4]. The purpose of this investigation is to draw a comparative study on extracts from the seeds and stem of *Anogeisuss leiocarpus* to ascertain which has the highest inhibition efficiency, % IE on mild steel in 0.5M H_2SO_4 solution using weight loss and Potentiodynamic polarization (PDP) methods. This will also x ray the phyto-compounds present in both methanol extracts through photochemical analysis.

Fig 1: *Anogeisuss leiocarpus*, (DC) Guill & Perr Shere, Jos East, Plateau State

2. EXPERIMENTAL METHODS

2.1 **Gas Chromatography-Mass Spectroscopy (GC-MS)**

The sample was analyzed using Agilent technologies 7890A GC and 5977B MSD. The experimental conditions were set as follows: Hp 5-MS capillary standard non-polar column; Dimension: 30 m; ID: 0.25 mm; Film thickness: 0.5 µm. Flow rate of mobile phase (carrier gas: He) was set at 1.0 ml/min. Oven temperature was raised from 298 K to 313 K at 278 K/min, and injection volume was 1 µl. Samples dissolved in methanol were fully scanned at the range of 40-650 m/z and the results were compared by using NIST mass spectral library search programme.

2.2. Preparation of Specimen.

The composition of the mild steel used in this investigation are 0.226% C, 0.115% Si, 0.297% Mn, 0.032% P, 0.010% S, 0.034% Cr, 0.023% Ni, 0.0054% Al, 0.0096%Cu, 0.0035%Co, 0.0098%Nb, 0.0036%V, 0.0031% Pb, 0.0056% Sn, 0.015% As,0.0048%Ca, 0.0064%Ce, 0.0049% Zr, 0.0022 % La and 99.2 % Fe. This mild steel used in this research were obtained from building materials, Bukuru express, Jos south, Plateau state. And were cut into coupons with dimensions 2 x 2 x 0.14 cm size using mechanical cutter. The metals were abraded and polished with fine emery paper, washed with distilled water, degreased with ethanol and dipped in acetone to prevent corrosion. The coupons were kept in desiccators to dry prior to experiment.

2.3. Preparation of Plant Extract.

Anogeisuss lieocarpus used was obtained from Shere, Jos east and was taken to Federal college of Forestry Jos for identification with voucher number FHJ839. The Seed and Stem was washed thoroughly with distilled water to remove dirt, peeled to remove the thick back, sliced into pieces, dried thoroughly, pulverized to fine powder particle, stored in an air tight container and kept for corrosion studies. The prepared *Anogeisuss leiocarpus* samples (500 g) was introduced in 1000 mL of methanol in a beaker and allowed to stand for 72 h and kept in an aerated condition. The obtained filtrates were further subjected to evaporation at 352 K, in order to make them free of methanol. The extract stock solutions were used to prepare different extract concentrations, by dissolving 0.2 g, 0.4 g, 0.6 g and 0.8 g of it in 50 cm^3 of 0.5 M H_2SO_4 for gravimetric and electrochemical analyses [8].

2.4. Weight loss Measurement

This was carried out by carefully immersing the coupons which has been accurately weighed into a 100 mL beaker containing 100 mL 0f 0.5 M H_2SO_4 in the absence and presence of the different inhibitors concentration (g/L): 0.2 g/L, 0.4 g/L, 0.6 g/L and 0.8 g/L for an exposure period of 3 to 9 hours with temperature ranging from 303 K to 333 K. After the exposure time was reached, the samples were removed from the solution, washed with distilled water, dried and reweighed to the accuracy of four decimal places with which the Corrosion rate (CR) and inhibition efficiency were calculated using:

$$CR = \frac{wl}{A \times T} \times 1000\left(mgcm^{-2}\ hr^{-1}\right) \quad (1)$$

And

$$\%IE = \frac{w_1 - w_2}{w_1} \times 100 \quad (2)$$

where w, A and t are weight loss (mg), exposed area (cm^2) and minimum time (h), respectively, while w_1 and w_2 indicate the mild steel original weight and weight loss in either an uninhibited solution (blank) or an inhibited solution with the *Anogeisuss leiocapus* seed and stem extract [8].

2.5. Potentiodynamic Polarization Measurement

The electrochemical studies were performed using a VERSASTAT 400 complete dc voltammetry and corrosion system model with V3 Studio software. The mild steel was cut into a 1 cm^2 square area which was exposed to the corrosive media, with and without inhibitors, as working electrode, and an Ag/AgCl rod as counter electrode. A saturated calomel electrode (SCE) was used as reference electrode, and it was connected by a Luggin's capillary. The experiments were undertaken at room temperature (303K).

The working electrode was immersed in a test solution for 1hr, until a stable open circuit potential was attained. The Tafel analysis study was set from a cathodic potential of -250 mV to an anodic potential of +250 mV, with respect to the corrosion potential, at a sweep rate of 1mV/s. The linear Tafel segments of the anodic and cathodic curves were extrapolated to corrosion potential, to obtain the corrosion current densities (icorr). Each experiment was carried out three times to estimate the electrochemical parameters reproducibility and average values which are reported [8, 9].

$$\%IE = \frac{I^0_{corr} - I_{corr}}{I^0_{corr}} \times 100 \quad (3)$$

3. RESULTS AND DISCUSSION

3.1 Gas Chromatography-Mass Spectroscopy (GC-MS)

For the seed extract, 8 compounds were identified and their retention time, percentage area, compound name, are listed in Table 1a. 9-Octadecenoic acid (Z)-, methyl ester (45.2 %), Hexadecanoic acid, methyl ester (18.09 %), and 9,12-Octadecadienoic acid (Z,Z)-, methyl ester (17.38) are the abundant component. Table 1b shows the GCMS analyses for the stem extract and revealed 16 compounds with Maltitol (18.74 %) as the major component. Double bonds and heteroatoms are found in the structures of the identified compounds contain double bonds and oxygen, which suggests the use of the seed and stem extract of *Anogeisuss leiocarpus* as corrosion inhibitor.

Table 1a. GCMS Analysis for seed extract of *Anogeisuss leiocarpus*

Peak	Compound	RT	Area	Area %	Area Sum %
1	Diglycerol	2.9	536667.87	7.95	3.6
2	Hexadecanoic acid, methyl ester	13	2700493.51	40.02	18.09
3	Eicosanoic acid	13.5	67923.46	1.01	0.46
4	9,12-Octadecadienoic acid (Z,Z)-, methyl ester	14.7	2594057.17	38.45	17.38
5	9-Octadecenoic acid (Z)-, methyl ester	14.8	6747134.33	100	45.2
6	Methyl stearate	15	1854770.42	27.49	12.43
7	Palmitoleic acid	15.2	301625.86	4.47	2.02
8	Eicosanoic acid, methyl ester	17.7	123060.39	1.82	0.82

Table 1b. GCMS Analysis for stem extract of *Anogeisuss leiocarpus*

Peak	Compound	RT	Area	Area %	Area Sum %
1	3,4-Methylenedioxyamphetamine	11.2	6782570.38	35.93	6.73
2	4H-1,2-Diazepine, 5-(4-chlorophenyl)-3,7-diphenyl-	22.4	3291218.38	17.43	3.27
3	5β-Pregnane-3α,20α-diol	26.3	7042330.5	37.31	6.99
4	Maltitol	27.4	18877674.7	100	18.74
5	2-Quinazolineacetic acid, 6-chloro-1,2,3,4-tetrahydro-2-(methoxycarbonyl)-4-oxo-3-phenyl-, methyl ester	30	11506740.8	60.95	11.42
6	Pipercallpsine	31.8	582017.85	3.08	0.58
7	Benzoic acid, 2,4-bis[(trimethylsilyl)oxy]-, trimethylsilyl ester	32.5	720848.66	3.82	0.72
8	Methanone, (2-methoxyphenyl)phenyl-	33.3	2954761.84	15.65	2.93
9	Ethaneperoxoic acid, 1-cyano-1-[2-(2-phenyl-1,3-dioxolan-2-yl)ethyl]pentyl ester	33.7	1692350.33	8.96	1.68
10	Hexadecanoic acid, ethyl ester	33.9	5306309.57	28.11	5.27
11	2-Chloroethyl oleate	35.7	1306238.92	6.92	1.3
12	6-Octadecenoic acid	36.1	1067713	5.66	1.06
13	Oleic Acid	36.5	11031508.9	58.44	10.95
14	Ethyl Oleate	36.9	16323225.9	86.47	16.21
15	Octadecanoic acid, ethyl ester	37.3	6870794.72	36.4	6.82
16	Acetyldigitoxin	37.7	5370652.71	28.45	5.33

Table 2: Phytochemical Analysis of *Anogeisuss leiocarpus* (Seed and Stem-bark).

Parameters	Seed	Stem
Alkaloid	-	-
Saponins	++	+++
Tannins	+++	++
Flavonoids	+++	+++
Carbohydrates	+++	++
Steriods	++	++
Terpenes	++	-
Anthraquinones	-	-
Cardiac glycosides	++	+

Key: + = Trace amount
++ = Moderate amount
+++ = Appreciable amount
– = Absence

Tables 1 and 2, revealed that methanol extract of *Anogeisuss leiocarpus* contains phytochemical constituents reported as good corrosion inhibitors[10]. The corrosion inhibition of mild steel by methanol extract of *Anogeisuss leiocarpus* was due to the complex chemical compositions of some phytochemical constituents that contain hetero-atoms which forms chemical bonds between the iron in the mild steel and the extract[11,12]. Research in recent times has shown that effective organic compounds used for corrosion inhibition contains hetero-atoms like phosphorous, sulphur, oxygen and nitrogen[13,14]. These hetero-atoms have lone pair of electrons which forms a protective film on metal surfaces thereby decreasing the rate of corrosion[15]. In addition, phyto-componds of long hydro-carbon chains were also found in Anogeisuss leiocarpus which are hydrophobic (water resistant) in nature[16]. This suggests good potentials of the extract of *Anogeisuss leiocarpus* as a corrosion inhibitor.

Table 3: Average Values of C.R. (mpy) of Mild Steel Gained from ML Measurements, %IE, and θ of seed and stem with Various Concentrations at Diverse Temperatures.

			Temperature (K)											
P/P	**Time**		**303**			**313**			**323**			**333**		
Seed	3	Con (g/l)	C.R	θ	% IE	C.R	θ	% IE	C.R	θ	% IE	C.R	θ	% IE
		BK	5.8917			10.7083			21.7000			34.2750		
		0.2	3.1917	0.4583	45.83	5.6000	0.4770	47.70	15.2417	0.2976	29.76	28.3333	0.1734	17.34
		0.4	2.0083	0.6598	65.98	4.4250	0.5868	58.68	13.2500	0.3894	38.94	23.4583	0.3156	31.56
		0.6	1.4765	0.7494	74.94	3.6750	0.6568	65.68	11.5000	0.4700	47.00	19.0167	0.4452	44.52
		0.8	0.8833	0.8501	85.01	3.1833	0.7027	70.27	10.3667	0.5223	52.23	18.5500	0.4588	45.88
	6	BK	4.7917			9.8292			13.4333			30.1000		
		0.2	2.8833	0.3983	39.83	6.0750	0.3819	38.19	9.9625	0.2584	25.84	26.5083	0.1193	11.93
		0.4	2.3458	0.5104	51.04	5.3167	0.4591	45.91	9.0583	0.3257	32.57	23.2542	0.2274	22.74
		0.6	1.5894	0.6683	66.83	4.5000	0.5422	54.22	8.4458	0.3713	37.13	20.4042	0.3221	32.21
		0.8	1.1792	0.7539	75.39	3.2500	0.6693	66.93	7.3000	0.4566	45.66	17.0375	0.4340	43.40
	9	BK	4.6528			8.4500			11.5250			28.3472		
		0.2	3.0417	0.3463	34.63	5.3639	0.3652	36.52	8.9750	0.2213	22.13	26.9583	0.0490	4.90
		0.4	2.7222	0.4149	41.49	4.8222	0.4293	42.93	8.2944	0.2803	28.03	24.0361	0.1521	15.21

		0.6	2.3611	0.4925	49.25	4.2139	0.5013	50.13	7.8250	0.3210	32.10	22.1861	0.2173	21.73
		0.8	1.0389	0.5618	56.18	3.3806	0.5999	59.99	6.9361	0.3982	39.82	18.3250	0.3536	35.36
Stem	3	BK	5.8917			10.7083			21.7000			34.2750		
		0.2	3.0889	0.4757	47.57	5.7750	0.4607	46.07	14.0083	0.35.45	35.45	24.2000	0.2939	29.39
		0.4	2.1833	0.6294	62.94	4.5500	0.5751	57.51	11.7583	0.4581	45.81	23.2167	0.3226	32.26
		0.6	1.8917	0.6789	67.89	4.1833	0.6093	60.93	10.2667	0.5269	52.69	21.2967	0.3787	37.87
		0.8	1.7167	0.7089	70.86	3.9333	0.6327	63.27	9.3917	0.5672	56.72	19.2167	0.4393	43.93
	6	BK	4.7917			9.8292			13.4333			30.1000		
		0.2	2.6000	0.4574	45.74	7.1694	0.2706	27.06	10.0708	0.2503	25.03	22.2625	0.1607	16.07
		0.4	2.2250	0.5357	53.57	6.0375	0.3858	38.58	8.9083	0.3368	33.68	21.0125	0.3019	30.19
		0.6	1.9750	0.5878	58.78	5.6208	0.42.82	42.82	7.7958	0.4197	41.97	19.6917	0.3458	34.58
		0.8	1.5083	0.6852	68.52	4.8083	0.5108	51.08	7.1708	0.4662	46.62	17.5292	0.4118	41.18
	9	BK	4.6528			8.4500			11.5250			28.3472		
		0.2	2.7167	0.4161	41.61	6.1917	0.2673	26.73	8.5611	0.2572	25.72	26.2500	0.0740	7.40
		0.4	2.3481	0.4953	49.53	5.7500	0.3195	31.95	7.8639	0.3177	31.77	24.6222	0.1314	13.14
		0.6	2.0639	0.5564	55.64	4.8917	0.4211	42.11	7.1000	0.3839	38.39	19.7000	0.3050	30.50
		0.8	1.8750	0.5970	59.70	4.3778	0.4819	48.19	6.6250	0.4252	42.52	17.7833	0.3727	37.27

Key: P/P – Plant parts, Con. – concentration, %IE – Inhibition efficiency, Bk – Blank, C.R. – Corrosion rate, θ – Surface coverage.

Table 3, gives a general picture of the relationships that exist between the following parameters; corrosion rate, surface coverage, inhibition efficiency, temperature effect, exposure time effect and effect of concentration.

Figure 2, reveals the effect of temperature on inhibition efficiency. The inhibition efficiency decreases with increase temperature and this indicates physical adsorption[17,18]. The kinetic energy of the extracts increases due to the increase in temperature, thus, making adsorption insufficient between extract and surface of the mild steel at the binding sites[19,20].

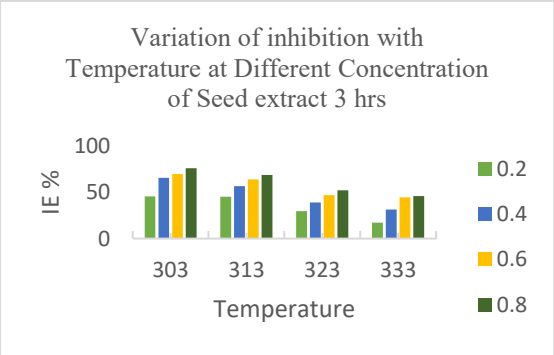

Fig 2a: IE % and Temperature

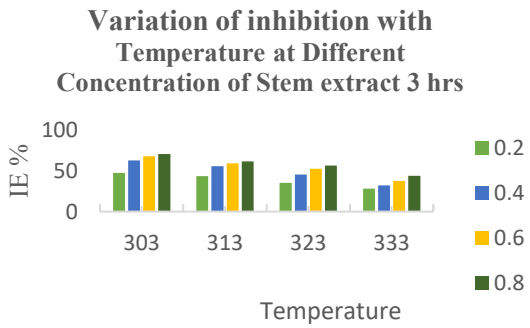

Fig 2b: IE % and Temperature

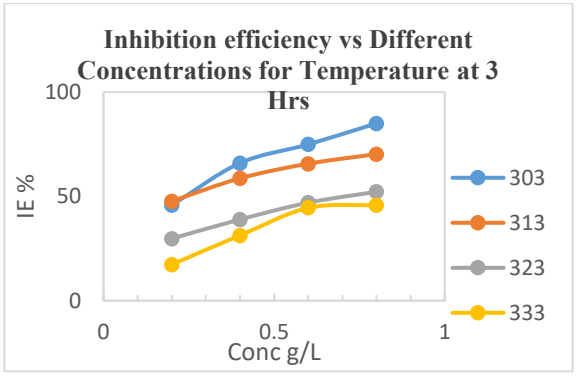

Fig 3a: IE % and Concentration.

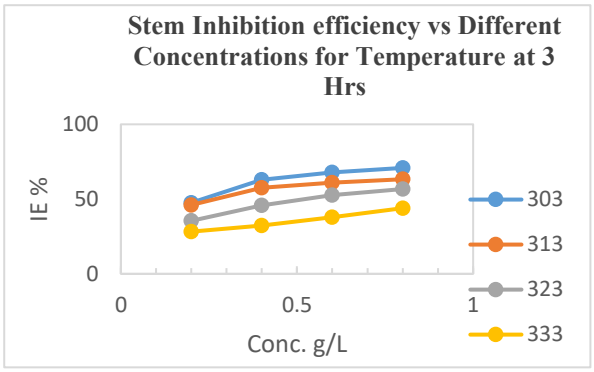

Fig 3b: IE % and Concentration.

For specific temperature, Fig 3, it was observed that with increase in the concentration of the extracts, the inhibition efficiency also increased to maximum of 70.86 % and 85.01 % for stem-bark and seed respectively. This implies that both extracts exhibited a good anticorrosion effect on the surface of the mild steel by forming films. The result clearly showed that the inhibition mechanism involves blocking of mild steel surface by inhibitor molecules via adsorption [21].

Also the corrosion rate decreases with increase in the inhibition efficiency due to increasing adsorption coverage of inhibitor molecules on the steel surface with their concentrations, which decreased the dissolution rates of mild steel [17]. But fig 4 revealed that with temperature increase, the corrosion rate also increased. The reason for this is due to acceleration of the hydrogen evolution reaction in acidic medium with rising temperature and thereby reducing the rate of inhibitor adsorption. This again is an indicator of physical adsorption mechanism of the extracts molecules on the electrode surface [18].

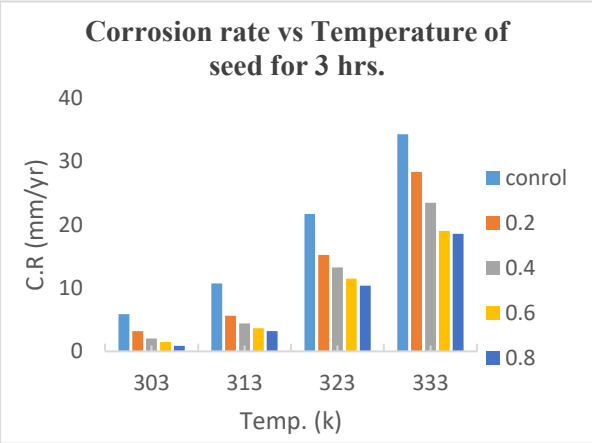

Fig 4a: Corrosion rate vs Temperature

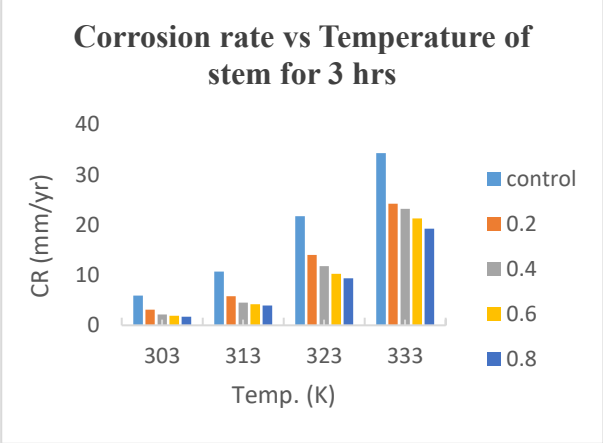

Fig 4b: Corrosion rate vs Temperature

3.2 Potentiodynamic Polarization Graph

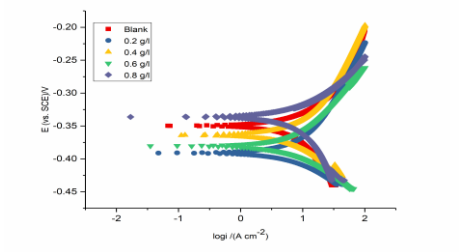

Fig 5a: Stem-bark

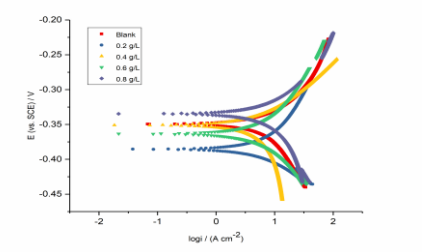

Fig 5b: Seed

Table 4: Potentiodynamic Polarization
Average Corrosion Parameters Acquired from PDP Curves in the Corrosion of Mild Steel in 0.5 M H_2SO_4 Solution without and with Various Concentrations of Seed and Stem 303K.

	Inch Conc (ppm)	$-E_{corr}$ (mV(SCE))	β_a (mV/dec)	$-\beta_c$ (mV/dec)	I_{corr} (µA/ cm²)	CR (mppy)	% IE	θ
BK	0	349.692	342.6	3292480.256	64844.258	75.0706	-	-
SE	200	385.501	174.8	91.0	11428.698	13.2311	82.38	0.8238
	400	351.127	91.7	1127.8	11501.781	13.3157	82.26	0.8226
	600	363.394	183.3	175.7	7398.728	8.5681	88.59	0.8859
	800	334.694	191.9	1295.2	2820.725	3.2645	**95.65**	0.9565
ST	200	343.306	155.3	405.1	20498.559	23.7313	68.39	0.6839
	400	363.989	207.3	141.7	15905.291	18.4137	75.47	0.7547
	600	380.232	115.2	80.9	9366.628	10.8438	85.56	0.8556
	800	396.118	101.6	65.6	7722.951	8.9409	**88.09**	0.8809

The result for inhibition efficiency in table 4 was computed using equation 3. Thus *Anogeisuss leiocarpus* extract is an organic inhibitor which has no heavy metal and is environmentally safe to use for minimizing corrosion of mild steel metals in acidic medium.

4. CONCLUSION

The methanol extracts for both seed and stem revealed high percentage of 9-Octadecenoic acid (Z)-, methyl ester (45.2 %), Hexadecanoic acid, methyl ester (18.09 %), 9,12-Octadecadienoic acid (Z,Z)-, and methyl ester (17.38 %), Maltitol (18.74 %) and Ethyl Oleate (16.21 %). These account for corrosion inhibition on the surface of the mild steel. The seed extract have higher inhibition efficiency compare to the stem due to the high presence of 9-Octadecenoic acid (Z)-, methyl ester (45.2 %) for both PDP and weight loss methods. Increase in concentration of both extract resulted in increase in IE %. Temperature and exposure time increase resulted in decrease in IE %, thus indicating physical adsorption mechanism.

CONFLICT OF INTERESTS

The authors declare no conflict of interests.

REFERENCES

(1) Dongqin Zhang, Yongming Tang, Sijun Qi, Dawei Dong, HuiCang, Gang Lu. The inhibition performance of long-chain alkyl-substituted benzimidazole derivatives for corrosion of mild steel in HCl. Corrosion Science 2016, vol.12, 517-522

(2)Tazouti, N. Errahmany, M. Rbaa, M. Galai, Z. Rouifi, R. Touir, A. Zarrouk, S. Kaya, M. EbnTouhami, B. El Ibrahimi, S. Erkan . Effect of hydrocarbon chain length for acid corrosion inhibition of mild steel by three 8-(n-bromo-R-alkoxy)quinoline derivatives: Experimental and theoretical investigations. Journal of molecular structure 2021, vol. 1244.

(3) F. E. Abeng, V. D. Idim, P. J. Nna**1**. Kinetics and Thermodynamic Studies of Corrosion Inhibition of Mild Steel Using Methanolic Extract of *Erigeron floribundus* (Kunth) in 2 M HCl Solution, WNOFNS 10 (2017) 26-38.

(4) Uche B. EKE, Elaigwu Sunday, Ibejekwe Sunday John, Godwin Agada, Denji Kitka Bulus and Bakji Gomerep. Comparative Study on Antimicrobial and Phytochemical Properties of Different Polar fractions Anogeisuss leiocarpus Root Extract from Langtang LGA Plateau State AJOCS 2025 vol. 15(1) pp.67-75.

(5) Ibejekwe S.J.I.1, Uche B. Eke2, Elaigwu Sunday1, Waziri J.R. Antimicrobial and Phytochemical Screening of Different Fractions of *Anogeisuss Leiocarpus* Guill and Perr Leaf Obtained From Langtang, Plateau State, Nigeria. *ChemClass Journal 2025 Vol. 9 Issue 1:313-325*

(6) Elsiddig, I. M. E., Muddather, A. K., Ali, H. A. R., &Ayoub, S. M. H. A comparative study of antimicrobial activity of the extracts from root, leaf and stem of *Anogeissus leiocarpus* growing in Sudan. *Journal of Pharmacognosy and Phytochemistry*, 2015, *4*(4), 107-113.
(7) Bello, A. A., &Jimoh, A. A.. Some physical and mechanical properties of *Anogeissus leiocarpus* timber. *Journal of Applied Science & Environmental Management*, 2018,*22* (1), 79-84.
(8) S.J.I Ibejekwe, U.B. Eke, S.E. Elaigwu, J.R. Waziri. Comparative Analysis of Corrosion Inhibition on mild steel by Parts of Anogeisuss leiocarpus in acdic medium. Proceedings of the Nigerian Society of Physical Sciences 2 (2025) 188
(9) I. B. Obot& N. O. Obi-Egbedi, ''An interesting and efficient green corrosion inhibitor for aluminium from extracts of *chlomolaenaodorata L.* in acidic solution'', J ApplElectrochem**40** (2009) 1977.
(10) Aralu Chiedozie, KovoAkpomie, Ho Chukwuemeka-okorie. Inhibition and adsorption potentials of mild steel corrosion using methanol extract of *Gongronemalatifoliuim.* Applied Water Science (2021) 11:22
(11) Ifeyinwa Calista Ekeke, Steve Efe, Felix Chigozie Nwadire. A review of amino acids used as corrosion inhibitors on iron metal/alloys in aggressive environments. Zastita Materijala, 2022, 63 (3) 318 – 340.
(12) Mabrouk, E. M.; Eid, S.; Attia, M. M. Corrosion inhibition of carbon steel in acidic medium using azochromotropic acid dye compound. J. Basic Env. Sci. 2017,4, 351.
(13) Palanisamy, K.; Kannan, P.; Sekar, A. Evaluation of chromotrope .FB dye as corrosion inhibitor using electrochemical and theoretical studies for acid cleaning process of petroleum pipeline. Surf. Interf. 2018, 12, 50−60.
(14) Ebenso EE, Murulana LC, Obot IB. Quinoline and its derivatives as effective corrosion inhibitors for mild steel in acidic medium.Int J Electrochem Sci., 2010, 5:1574–1586.
(15) Barouni K, Kassale A, Albourine A, Jbara O, Hammouti B, Bazzi L . Amino acids as corrosion inhibitors for copper in nitric acid medium: experimental and theoretical study. J Mater Environ Sci. 2014, 5(2):456–463.
(16) M.A. Bodude, H.O. Onovo, I.O. Adebayo. Study on Corrosion Inhibition Efficiency of *Solanum Erianthum* Extract on 6063 Aluminium Alloy in Different Sea Water. Diu Journal of Science and Technology, 2018, vol.13,Issue:1.
(17) Ahmed Fawzyand Arafat Toghan . Inhibition Evaluation of Chromotrope Dyes for the Corrosion of Mild Steel in an Acidic Environment: Thermodynamic and Kinetic Aspects. ACS Omega 2021, 6, 4051−4061
(18) Xu, B.; Liu, Y.; Yin, X.; Yang, W.; Chen, Y . Experimental and theoretical study of corrosion inhibition of 3-pyridinecarbozalde thiosemicarbazone for mild steel in hydrochloric acid. Corros. Sci. 2013,74, 206−213.
(19) Chiedozie C. Aralul, Helen O. Chukwuemeka-Okorie, Kovo G. Akpomie. Inhibition and adsorption potentials of mild steel corrosion using methanol extract of *Gongronemalatifoliuim.* Applied water science, 2021, 11:22
(20) Umoren SA, Ogbobe O, Ebenso EE, Ekpe UJ. Effect of halide ions on the corrosion inhibition of mild steel in acidic medium using polyvinyl alcohol. Pigment Resin Technol, 2006, 35:284–292.
(21) Anjali Peter, Sanjay K. Sharmal and Ime Bassey Obot. Anticorrosive efficacy and adsorptive study of guar gum with mild steel in acidic Medium. Journal of Analytical Science and Technology, 2016, 7:26.

ISBN: 978-978-68-0485-9 DOI: https://doi.org/10.55455/acsnigeria.1.2.196-205

Characterization and Evaluation of Kaolinite Clays from Bara, Kwi, and Wereng in Bauchi and Plateau States for Refractory Applications

Mohammed Ibrahim, Ser Nanriebet Goeffrey, Samuel Emmanuel Egga, John Rople Gungshik, Shangkum Yildun Goji, and Saraya Akubel Yakubu
Department of Chemistry, Faculty of Natural Sciences, University of Jos, P.M.B. 2084 Jos, Plateau State, Nigeria
Corresponding Author's Email: mibrahim@unijos.edu.ng

ABSTRACT

The evaluation of physical and chemical properties of clay deposits from Bara, Kwi, and Wereng villages in Bauchi and Plateau States, Northern Nigeria, with a focus on their potential as locally made refractory materials. The chemical composition of the clay was determined using Energy Dispersive X-ray Fluorescence Spectrophotometry (ED-XRF), while physical properties: moisture content (MC), color, pH, tapped density (TD), and refractoriness were determined using standard techniques. Clay bricks was fabricated from the clay samples and fired at intermittent temperature ranging from 150 °C to 600 °C for ten-minute intervals. The analysis of the chemical composition indicated Bara and Wereng clays contain over 70 % of SiO_2 and Al_2O_3, while Kwi clay comprises approximately 60 % of SiO_2 and Al_2O_3. The Physical properties range across the clay samples revealed pH(4.40-5.20), MC(3.30-4.40 %), TD(0.96-1.11 g/ml), (white to reddish-brown and near-white color), and refractoriness temperature (1526-1597 °C) for Bara, Kwi and Weng respectively. The firing of the sample bricks produced resulted in progressive weight losses. The findings unveiled the valuable potential of these clay deposits in refractory production for both domestic and industrial applications thereby cutting down the huge cost of imported refractory material and enhance their performance. Purifications and blend formulations studies of these clay materials can further enhance their refractory potential and properties. These studies lined with the MDGs/SDGs vision 2030 for social, environmental and global economic growth for industrial innovation and infrastructure development and sustainability.

KEYWORDS: Refractory, Characterization, kaolinite, Clay Deposits, Brick Kwi Clay, Alumina.

1. INTRODUCTION

Clay materials are formed from deposited component of the earth composed mainly of layers of fine particle with high characteristics of plasticity at suitable water mixed, turn completely hard when fired.[24,18] Materials of clay are classified into three groups which include, the kaolinites white, grayish-white or slightly colored which became more dark, with high plastic properties when wetted with water,[10,14,20] while the second group is composed majorly of montmorillonite and the intermediate product of the disintegration of mica into kaolin are the third group of clays.[20]

Hijioke *et al.*[8] reported several literature that define clay as a natural material used for the manufacture of many industrial products including the refractory materials that has proved to be reliable in the metallurgy processes.[4] Refractory product have the capacity to resist high temperatures both physically and chemically as such good refractories can withstand temperature variation between 1000 ^oC to1500 ^oC and also serves as better thermal and electrical insulator.[4] Kaolinites is composed of high content of alumina (up to 39.50 % by weight) among the clay minerals as shown by the chemical formula ($Al_2O_3.2SiO_2.2H_2O$) but the most suitable for refractory application must have high percentage of alumina (Al_2O_3) as well as very low impurity oxides of fluxes minerals (Na_2O, K_2O etc) and coloring (Fe_2O_3, TiO_2 etc) agents.[2] Complete chemical analysis of clays unveiled the true mineralogical composition and refractory materials are constructed in varying combinations and shapes depending on their applications.

The increasing demand for refractory products is associated the growth of metallurgical industries which required 80 % of all forms refractories for full operation.[9] The advancement in the areas of metallurgical processes in Nigeria recently has been the reason for the increasing demand for refractory materials[4] and a large proportion of it are currently being imported to meet this demand.[17] Following the development and revitalization of the iron and steel industry through the restoration of different inland rolling mills and conceived completion and commissioning of the multibillion-dollar Ajaokuta Steel Complex to produce 1.3 million tonnes of liquid steel, there will be further increasing demand for refractory materials locally.[5] The Ajaokuta iron steel industry is estimated to require bricks of refractory

materials in volume of over 36,000 tonnes with worth of over sixty million naira for furnace lining only and more than 80 % refractory bricks mostly required are fire clay.[13]

Nigerian four major refineries were reported to have cost more than $850 million dollars for turnaround maintenance (TAM) operation as from 1997 to 2002 and the main unit in the TAM process operation is the fluid catalytic cracking (FCC) which is made up with large quantity of different grades of refractory channels.[11] Omowumi[21] locally available raw material for the production of different types of refractory products include kaolinite ($Al_2O_3.2SiO_2.2H_2O$), chromite ($FeCrO_3$), magnesite ($MgCO_3$) etc and additives such as saw dust, graphite and binders. Studies reported by Nnuka and Enejor[19] on the characterization of Nigerian clays showed that the Otukpo clay can accommodate furnace temperature of 1710 ^oC which comparably can compete favorably with products of refractories imported from foreign countries. Research reported also by Amuda *et al*.[5] revealed the characterization and evaluation of some clay deposits in Southwest Nigeria to possess good refractory properties with performance results that agreed favorably with standard recommendations and suggest a blend of these clays for good furnace lining and performance.

This present study realized the vital need to further characterized the local clay materials from Plateau and Buachi state axis to explore their potentials to build good and quality refractories which could cut cost, reduced importation and saved foreign exchange rate.[12] Aside metallurgical industries, petrochemicals, chemicals, agrochemicals, oil and ceramic industries used refractory materials for various operational processes, but still yet there is no specialized industry for the production of refractory products in Nigeria, considering the abundant and availability of the clay rocks and other raw materials across the country.[1]

Hence, it becomes necessary to the essential need to expand the utilization of local raw content for the production of industrial equipment for application in various industrial operation processes necessitated the desire to study and characterize kaolinite clay samples obtained from Bara, Kwi and Wereng villages in Bauchi and Plateau States, Northern Nigeria. To equally assess and ascertain the suitability of the clay as refractory bricks for furnace linings and other domestics and industrial purposes due to the rich nature of the clays in this region in alumina and silica content.

2. MATERIALS AND METHODS

2.1 Study Area Description

Kwi and Wereng are located in Riyom Local Government Area of Plateau State, North central Nigeria. Riyom L.G.A has its headquarters in the town of Riyom to the North of the area at 9° 38' 00"N 8° 46'00" E. The L.G.A has boundaries with Kaduna and Nasarawa States. Bara is located in Kirfi Local Government Area of Bauchi State, Northeast Nigeria bordering Gombe State in the East. Its headquarters is in the town of Kirfi (or Kirfin kasa). The Northeasterly line of equal latitude and longitude passes through the L.G.A. It is located precisely around latitude 10° 24'N 10° 24'E.

2.2 Sample Collection and Preparation

The Clay samples were collected separately from the sampling sites in Kwi and Wereng villages of Riyom Local Government Area, Plateau State and Bara village of Kirfi Local Government Area, Bauchi State. The sample materials weight of 3 kg was randomly collected at a depth of 500 mm using pitch digger and shovel. The samples were air-dried for 3 days, finely crushed with a laboratory mortar and pestle to achieve homogeneity of particle sizes. Then sieved with a mesh size of 2.0 mm and collected for various physical and chemical analyses.

2.3 Methods and Experimental

The analysis of the physical properties of the clay was carried out at the Department of Chemistry, University of Jos, Nigeria whereas the chemical compositions of the clay were determined at the National Metallurgical Development Centre (NMDC) Jos, Plateau State.

2.4 Determination of Clay Chemical Compositions

The elemental analysis of the raw clay samples was determined using an Energy Dispersive X-ray Fluorescence Spectrophotometer (ED-XRF). The ground samples were filled each in a sample cup as

the ED-XRF spectrophotometer was turned on and allowed to stabilize the optics and X-ray tube for some period. The samples were place in the machine while in operation and ran using the prepared program. The concentration of the elements present in the samples were automatically calculated and displayed. The percentage composition of the various constituents was recorded from the print out.

2.5 Determination of Clay Physical Properties

The clay samples was taken for various physical analysis. The tests conducted were moisture content, pH, color, and tapped density. These tests were conducted using standard test procedures.

2.5.1 Color of the Clay Samples

The colors of the clay samples were determined using the Lovibond Comparator. The device is used to determine the color of liquids. The clay samples were prepared into solutions to unveil all the coloring particles by dispersion and thoroughly shaken in a volumetric flask. The sample solutions each were turned in glass tubes and inserted into the comparator one after the other and compared with series of colored glass disc until their nearest possible color matches were found. The colors for the three samples were recorded.

2.5.2 Moisture Content of the Clay Samples

The percentage moisture content of the clay samples was determined using a thermo-gravimetric approach whereby a sample is heated and the weight loss due to the evaporation of moisture were recorded. Three (3) petri dishes were properly washed and dried in an electric oven for 30 minutes at a temperature of 105 ^{o}C and transferred into a desiccator to cool. The dry weight of the petri dishes was taken using an analytical weighing balance and recorded as W_1. The samples each of weight 1g were transferred into the petri dishes and weighed as W_2. The petri dishes containing the samples were placed in the oven and heated to a temperature of 110 ^{o}C for 16-24 hours. The samples were then cooled in a desiccator. After the cooling process, they were reweighed and recorded as W_3. To calculate the percentage moisture content of the samples, equation 1 was used.

$$\%\ \text{Moisture Content} = \frac{W2-W3}{1\text{g of sample}} X\ 100 \quad ---------- 1$$

2.5.3 Clay pH Values

The pH for each of the kaolin clay samples were determined by the used of an electronic pH meter where a glass electrode was inserted into a mixture (suspension) of clay and distilled water to determine the pH which was then noted on a digital display screen and recorded.

2.5.4 Tapped Density

The tapped density of a powder is the ratio of mass of the powder to the volume occupied by the powder after been tapped for a defined period. The tapped density is obtained by mechanically tapping a 250 ml graduated cylinder containing 100g of each sample on a flat surface until a little further volume change is observed after been tapped for fifty (50) times. The tapped density was calculated using the equation 2 below;

$$\text{Tapped Density}\left(\frac{\text{g}}{\text{ml}}\right) = \frac{\text{M}}{\text{Vf}} ---------- 2$$

Where $\boldsymbol{M}$ = the mass of powder in g

$\boldsymbol{Vf}$ = the tapped volume in milliliters

2.6 Refractory Brick Production Process

The method prescribed by Kipsanai[12] was adopted for the bricks production. The grounded and sieved clay samples were mixed to form a thick paste using some quantity of water, then molded to obtain bricks using a wooden mold of dimension 6 cm x 3 cm x 2 cm. The mold was continuously lubricated with water to prevent the clay from sticking to the mold as the bricks were molded by hand. The bricks produced were then air-dried for about 3 days with a mass between 0.80 kg and 1.1 kg, oven dried under temperature of 110 ^{o}C for 8 hours.

Fig. 1: Molded bricks.

Fig. 2: Air dried bricks.

2.7 Firing of Clay Bricks at Intermittent Temperatures

The aired and oven dried brick samples were fired in a muffle furnace at intermittent temperatures of 150, 200, 300, 400, 500 and 600 ^{0}C. The firing was controlled at steady rate of 10 minutes followed by gradual cooling and weighing of fired bricks to obtain progressive weight losses at various temperatures. The weight losses in fired clay bricks were recorded.

Fig. 3: showing brick in the muffle furnace.

Fig. 4: Fired clay bricks.

2.8 Refractoriness

The prescribed by Shuaib-Babata *et al*.[24] and was used to determine the refractoriness of the clay materials. Refractoriness is the capacity of material designed to serve as refractory to withstand high range of temperature conditions under service operations without deforming. The refractoriness was estimated using the Shuen's formula in accordance with Bochraraov and Gemsimov.[7] Equation 3 below;

$$\text{Refractoriness (K)} = 360 + \text{Al2O3} - \text{RO} / 0.228 - 3$$

Where K = Refractoriness

Al_2O_3 = Percentage alumina content in the clay

RO = Sum of other oxides in the clay excluding SiO_2 and Al_2O_3 (%)

The value of 360 and 0.228 are constant.

3. RESULTS AND DISCUSSION

3.1 Chemical Composition of Kaolin Clay Samples

The chemical composition of the clay samples were presented in table 1

Table 1: Chemical Composition (wt %) of Kaolin clay samples

Composition (%)	Kwi	Wereng	Bara
Al_2O_3	24.70	27.80	25.90
SiO_2	38.60	43.70	52.40
P_2O_5	0.58	0.66	0.08
SO_3	<LOD	0.30	<LOD

K_2O	0.40	0.04	1.69
CaO	0.35	0.43	0.58
TiO_2	4.12	6.09	6.29
V_2O_5	0.21	0.20	0.21
Cr_2O_3	0.09	0.11	0.08
MnO	<LOD	0.03	0.03
Fe_2O_3	18.59	9.50	4.79
NiO	0.01	0.02	0.02
CuO	0.07	0.06	0.04
ZnO	0.03	0.04	0.03
Ga_2O_3	0.04	0.05	0.04
SrO	0.07	0.06	0.05
ZrO_2	0.81	0.74	0.95
Nb_2O_5	0.10	0.09	0.07
Au	<LOD	0.007	0.006
PbO	<LOD	0.09	0.06
Total	88.77	90.02	93.32
Al_2O_3 : SiO_2	0.64	0.64	0.49

Key: % = Percentage. <LOD = below limit of detection/Loss in ignition (LOI) was not determined

3.1 Chemical Properties

The key indicators for good refractory materials by chemical compositions are high Al_2O_3 content desirable for refractory applications, low Fe_2O_3 content is preferred to minimize fluxing effects and high SiO_2 content can contribute to refractoriness properties. Comparatively, Kwi sample contains; Al_2O_3(24.70 %), relatively high Fe_2O_3(18.59 %) and SiO_2(38.60 %). Wereng sample contains Al_2O_3 (27.80 %) moderate contamination of Fe_2O_3 (9.50 %) and high SiO_2(43.70 %) while Bara sample contains Al_2O_3(25.90 %), low Fe_2O_3(4.79 %) content and high SiO_2(52.40 %). Base on the refractory indicators, Bara samples is more favorable for refractory applications due to low Fe_2O_3 content and high SiO_2 content followed by Wereng sample with moderate refractory potential due to balanced Al_2O_3 and SiO_2 content while the Kwi sample is less favorable due to high Fe_2O_3 content (Fig 5). Therefore, Bara clay sample appears to have the most favorable refractory properties due to its low Fe_2O_3 content and high SiO_2 content.

Fig. 5: Chemical Composition of the Clay Samples

The chemical constituent of the clay samples (Table 1) to be principally SiO_2 and Al_2O_3 in which 80 % of the clay material were characterized by eight elements while the remaining were attributed to water, trace elements and organic matter. The result also reflects slight variability of average in values of silica

(SiO_2) and alumina (Al_2O_3) contents in Bara and Wereng clays, which constitute 70 % major constituents of the clay. Therefore, the clay samples were classified to belong to the aluminosilicate group. The clay sample from Bara contains high silicate with percentage silica of 52.40 % (Fig. 5) which agree with the standard recommended range of 46-62 % for a good refractory material as reported by Yami and Umaru.[27] This implies the clay can be built and designed to fit applications as refractories for linings in melting furnace for low melting temperature metals, heat treatment furnaces, aluminium ladle molds and blast furnaces.

3.2 Physical Properties of Kaolinite Clay Samples

The results of the physical properties of the clay samples are presented in table 2

Table 2: Physical Properties of Kaolinite clay samples

Sample location	Moisture Content (%)	Tapped Density (g/ml)	Color	pH
Bara	3.70±0.24	1.11±0.05	White	5.20
Kwi	4.40±0.33	1.00±0.09	Near White	4.70
Wereng	3.30±0.24	0.96±0.02	Reddish Brown	5.70

Values are expressed as mean ± SD, n=3 for each group

The physical Properties of the clay bricks revealed the moisture content (MC): Bara (3.70%), Kwi (4.40%) and Wereng (3.30%). Tapped Density (TD): Bara (1.11 g/ml), Kwi (1.00 g/ml) and Wereng (0.96 g/ml) and pH: Bara (5.20), Kwi (4.70), Wereng (5.70) which makes them acidic clays respectively. The refractory Properties (Refractoriness) shows Bara (1597 K), Kwi (1526 K) and Wereng (1575 K) respectively (Fig. 6).

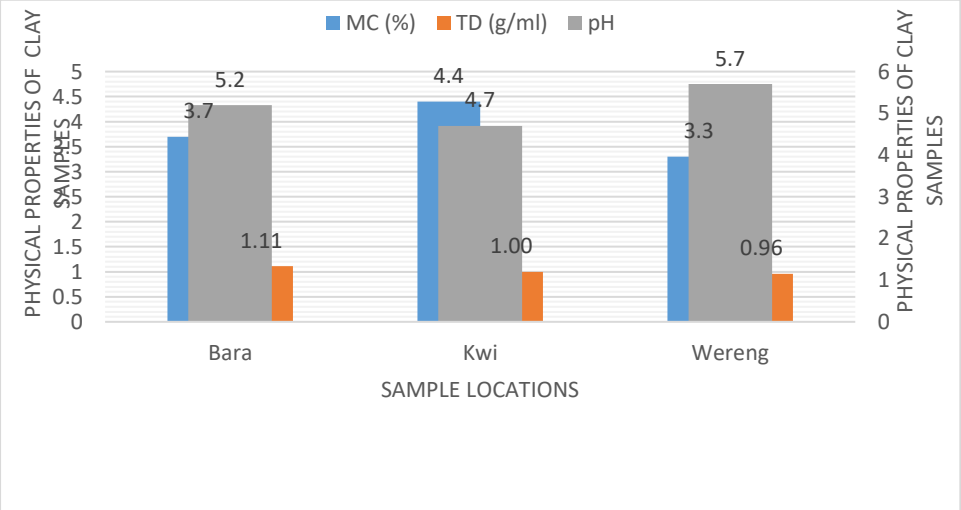

Fig. 6: Physical Properties of Kaolinite clay samples

Bara clay appeared whitish because of traces amount of iron (iii) oxides (4.79 %), Wereng clay contain more iron (9.50 %) with a near whitish color while high iron oxides (18.59 %) in Kwi clay resulted in a tinge of brown-reddish appearance.[16] The process of clay firing alter the color of the resulted clay brick samples slightly from light-brown to dark-brown in Kwi clay due to the presence of high amount of iron oxide and other impurities. The Tapped density for Bara, Kwi and Wereng clays are 1.11 g/ml, 1.0 g/ml and 0.96 g/ml respectively. The Tapped density tells the powder flow ability and compressibility of the clay samples. A more powder flow ability observed in Bara clay followed by Kwi and Wereng the least.

3.3 Refractory Properties of The Clay Brick Samples

The refractory results of the clay brick samples are presented in table 3.

Table 3: Refractoriness Properties of Kaolinite Brick Samples

S/N	Sample location	Refractoriness (K) °C
1	Bara	1597
2	Kwi	1526
3	Wereng	1575

The estimated refractory temperature for Bara clay was 1597 °C, Wereng was 1575 °C and Kwi 1526 °C which falls within standard value (1500-1750 °C) for refractories materials. The high refractoriness in Bara and Wereng clay (Fig. 7) resulted from high alumina contents of 25.90 and 27.80 respectively. The relatively low value of refractoriness in Kwi clay is because of lower content of alumina and silica and the high percentage content of flux materials. Impurities like Fe_2O_3 in aliminosilicate refractory lowers the refractoriness and service limits of bricks.

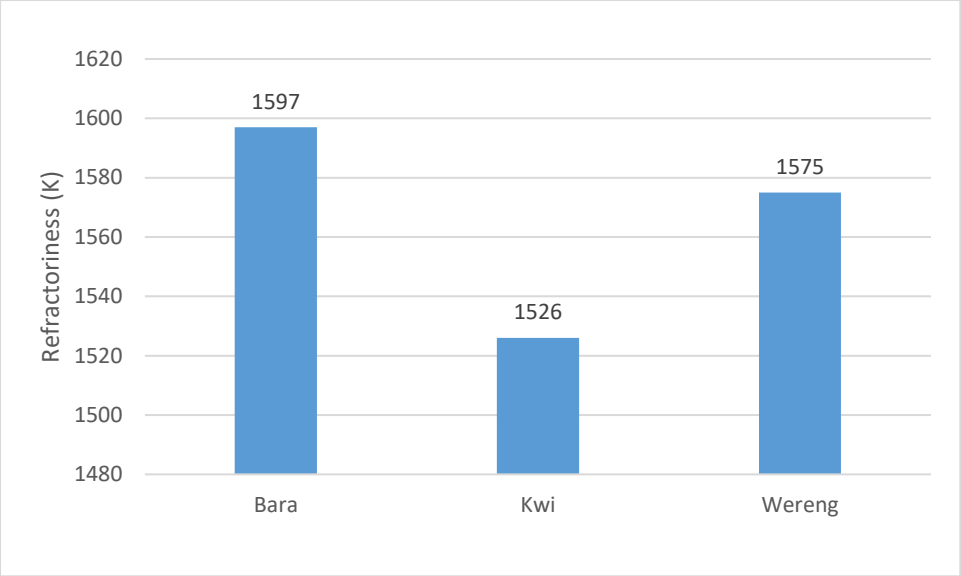

Fig.7: Refractoriness Properties of the Clay Samples (K)

3.4 Effect of Heat on Clay Brick Samples

The influence of heat on the brick samples are shown in table 4.

Table 4: Loss in weight of fired clay bricks at different temperatures

Sample location	Bara	Kwi	Wereng
Temperatures (°C)	Weight (g)	Weight(g)	Weight (g)
100	907.40	718.40	678.10
150	906.50	717.40	676.50
200	905.80	716.10	675.30
300	904.60	714.20	673.40
400	903.40	712.40	671.70
i500	902.40	710.30	670.10
600	900.20	706.80	666.00

The progressive loss in weight in fired clay bricks heated at intermittent temperatures of 100 °C, 150 °C, 200 °C, 300 °C, 400 °C, 500 °C, and 600 °C are because of further dehydration and escape of some impurities in the clay as temperature increases. The increase in the firing temperature resulted in the conversion of moisture within the bricks into vapor which diffuse out while creating vacant sites within the clay. The clay particles immediately then migrate and rearranged to occupy the vacant sites, which subsequently results to shrinkage and weight losses. This process consequently reduces porosity and enhances the mechanical strength of the bricks.

3.5 Correlation Relationship between Chemical Composition and Physical Properties

The correlation analysis between chemical composition and refractory properties at $P<0.05$ revealed percentage Al_2O_3 and SiO_2 in the samples to show positive significant correlation with the refractory properties. While the correlation of physical properties and refractory properties of the clay bricks revealed moisture content and tapped density to show no significant correlation with refractoriness.

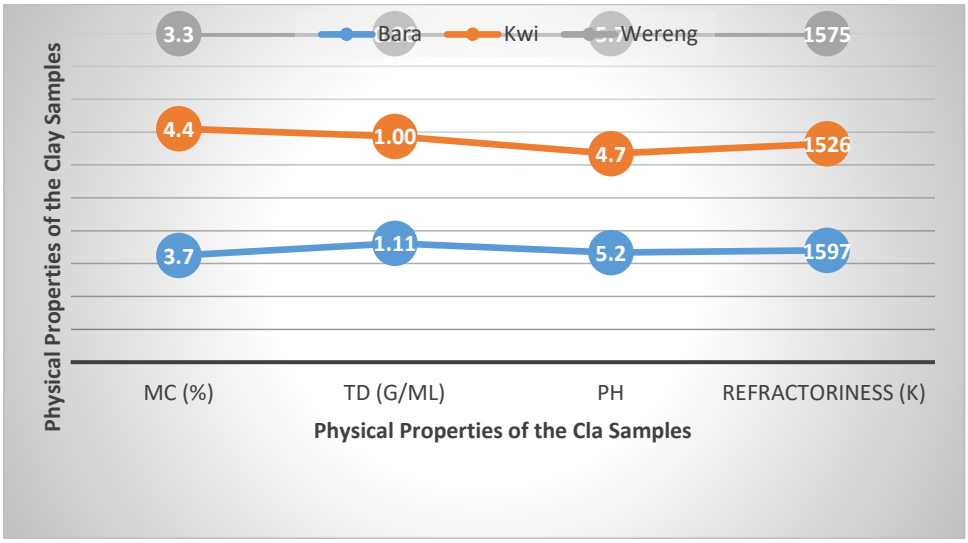

Fig. 8: correlation Between Physical Properties and Refractoriness

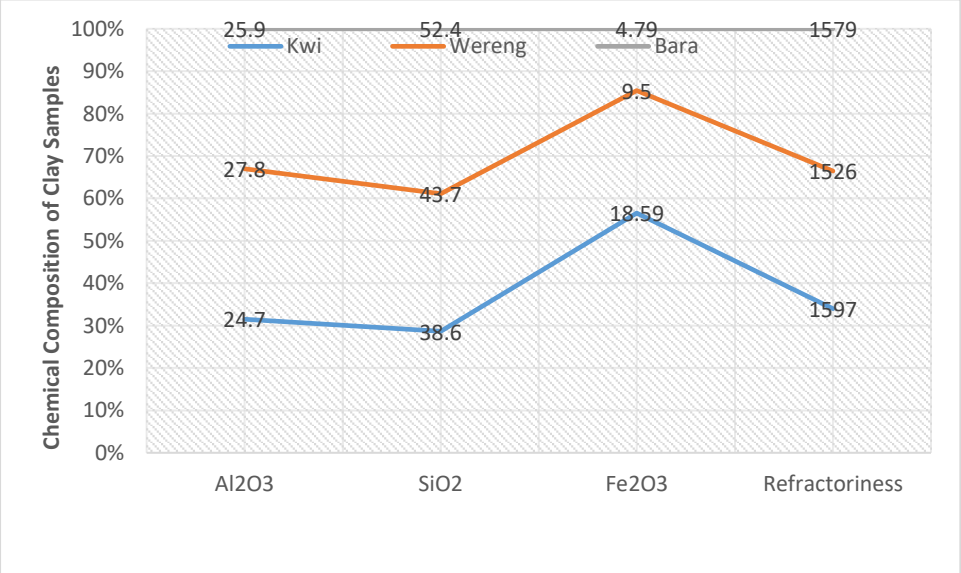

Fig. 9: correlation analysis between Chemical Composition Vs Refractioness

Chemical Composition and Refractory Properties (Fig. 9) - Al_2O_3 and Refractoriness shows positive correlation (r = 0.53), SiO_2 and Refractoriness also shows positive correlation (r = 0.76) while Fe_2O_3 vs. Refractoriness shows a negative correlation (r = -0.83). The correlation between physical properties and refractory properties (Fig. 8) shows moisture content vs. refractoriness to have no significant correlation (r = -0.21) and tapped density vs. refractoriness to show a positive correlation (r = 0.62) while pH vs. Refractoriness also shows no significant correlation (r = 0.35).

These correlations result strongly suggest that higher Al_2O_3 and SiO_2 content are associated with higher refractory properties while higher Fe_2O_3 content is associated with lower refractory properties. However, tapped density also shows a moderate positive correlation with refractoriness.
However, Clay samples from Bara, Kwi and Wereng can be considered as moderate alumina clay that agrees appreciably and consistently with value of 13-30 % alumina reported in a similar study by Ugwuoke[26] for good refractory materials. The presence of impurities in aluminosilicate refractory such as TiO_2, K_2O, P_2O_5, ZrO_2 lowers the refractory properties and operational durability of the bricks as all the three clay samples have significant amount of such impurities. Studies by Onyeji[22] showed that, clays materials with high content of iron could not be used to sources aluminium due to the deleterious

effects of iron on the extraction processes. The clay samples may not be fit for direct application as refractories in furnace linings as it contain high percentage range of iron (4.79-18.59 %) compared to the recommended range of 0.5-2.4 %.[24] The elemental composition of the clay samples in table 1 were not in conformity with Sanni's[23] report that suggest refractories clay should contain at least 30 % alumina (Al_2O_3) and less than 1.8 % iron (iii) oxide (Fe_2O_3). This indicates the clay samples are not suitable as refractories materials chemically, except subjected to certain pretreatments and purification processes.

4. CONCLUSION

The chemical characterization revealed the clay samples to contain the required percentages of alumina, silica, metal oxides and other flux minerals that can enhance refractory properties and performance while the evaluation of the clay physical properties revealed the parameters to fall within the range required for the designed and fabrication good refractory materials. The estimated refractoriness values of the clay samples also fall within standard recommended value (1500-1750 ^oC) for refractories. However, Bara and Weng recorded the higher value of refractories property, which correlated to the high amount of aluminosilicate and other flux mineral content in these clay samples. The progressive weight loss at intermediate temperature changes during firing was due to loss of water vapor and other volatile impurities contained in the clay samples. The process also help to reduce porosity and improve the mechanical properties of the bricks. The results revealed these clay samples to possess the potential to be consider as material for the designed and construction of fire refractory materials for applications in furnace and kiln lining. However, the three clay samples were limited as they contained significantly amount of iron and titanium oxides, which have deleterious effect on the refractory property of the clays. It is therefore, recommended that additives such as purified bauxite (fused alumina) can be controllably added to significantly reduced impurities such as iron and titanium oxides and to enhance the refractory property of the clays. In addition, geological survey of the study areas could also help to map out the substantiality of the deposits and inform the basis to building and designing refractory product markets in Northern Nigeria. This will, in a short run create more jobs opportunities and in a long run, save huge foreign exchange yearly by drastically reducing the importation of similar product materials and revitalized the fortunes for entire region and the country in a whole.

ACKNOWLEDGEMENT

The Authors wish to acknowledge Prof. M.B Dalen (of blessed memory) who supervised this research work, gave guidance and constructive criticism that led to the successful completion of this work.

CONFLICT OF INTERESTS

The authors declare no conflict of interests.

REFERENCES

(1). Afolabi, A.S and Osoba, L.O Suitability of Nigerian Rocks as Refractory materials for Monolithic Furnace Lining. Article in Particulate Science and Technology: *An International Journal*. **2012**, ISSN:0272-6351.

(2). Aliyu S., Garba B., Danshehu B.G., Argungu G. M., and Isah A. D. Physio- chemical Analysis of Gwarmi Clay Deposit, Wurno Local Government Area of Sokoto State, Nigeria. *The International Journal of Engineering and Science* (IJES), **2014**, 3(6):62-67.

(3). Aliyu, M.; Musa, U., Muhammed, I., and Sadiq, M., A Comparative Study on the Refractory Properties of Selected Clays in North Central Nigeria, *International Journal of Academic Research,* **2012**, 3(1):393-397.

(4). Ameh, E.M., & Obasi, N.W. Effect of rice husk on insulating bricks produced with Nafuta and Nsu clays. *Global Journal of Engineering and Technology*, **2009**, 2(4):661-668.

(5). Amuda, M.O.H., Lawal, G.I and Majolagbe, F.O. Characterization of some South West clay Deposits*. NSE Technical Transactions*, **2005**. 40:13-23.

(6). Aremu, D.A.; Aremu, J.O., and Ibrahim, U.H. Analysis of Mubi Clay Deposite as A Furnace Lining. *International Journal of Scientific & Technology Research,* **2013**, 2(12).

(7). Ogunro A.S, Usman M.A, Ikponmwosa E.E, Aribike D.S, Characterization of some clay deposits in southwest Nigeria for use as supplementary cementitious material in cement, Materials Today: Proceedings, **2023**.
(8). hijioke Peter Egole, Gaius Chukwuka Nzebuka, Chukwuzubelu Okenwa Ufodike, Rasaq Olawale Medupin, Chima Chinedu Ugwuegbu, Nnamdi Anthony Nnodum, Ugochukwu Philip Ochieze, Experimental characterization of two clay deposits blended with feldspar and quartz for building services and refractory applications, Journal of African Earth Sciences, **2024,** 218.
(9). Hassan M. Lomertwala*, Peter W. Njoroge, Sylvia A. Opiyo, Brian M. Ptoton Characterization of Clays from selected sites for Refractory Application, *International Journal of Scientific and Research Publications*, **2019,** 9(11):600-603.
(10). Kankara IA Geology and Geochemical Characterization of Rocks in Funtua Northeast, Sheet 78, Scale of 1:50,000, Northwestern Nigeria. An Unpublished PhD Thesis submitted to Department of Geology, Federal University of Technology, Minna Nigeria, **2014**.
(11). Kankara, I. A., and Yunusa, L. U. Behaviour and Effect of Clay Soils on Engineering Constructions in Nigeria: Implications for Geotectonism, Direct Research Journal of Engineering and Information Technology, **2020**, 7(5):84-96.
(12). Kipsanai, J. J., A Study of the Refractory Properties of Selected clay deposit in Chavakali, Kenya, *International journal of Scientific and Technical Research in Engineering*, **2018,** 3(1):19-24.
(13). Kipsanai, J. J.; Namango, S. S.; Muumbo, A. M., A study of Selected Kenyan Anthill clays for production of Refractory Materials, International journal of scientific and Research Publications, **2017**. 7(9):169-175.
(14). Lopez-Galindo, C. Viseras and Cerezo, P. Compositional, Technical and Safety Speciation of Clay to be used in pharmaceutical and cosmetic products. *Applied clay sciences*, **2007**. 36:51-63.
(15). Miranda-Trevino, J.C and Coles, C.A. Kaolinite properties, structure and influence of metal retention on pH. *Appl.Clay.Sci*., **2003**, 23(1):133-139.
(16). Musa U., Aliyu M., Mohammad I.A., Mohammad A.D., Sadiq M.M, and Isah A.G. A comparative study of the Refractory Properties of selected clays in Niger State, *Nigeria. Advances in Biotechnology and Chemicals Processes*, **2011**, 2:1-5.
(17). Mutembei, P. K.; Muthengia, J. W.; Muriithi, N. T., Iron enrichment in laterites soils from selected regions in Kenya using magnetic separation*. IOSR Journal of Engineering*, **2013**. 4(3), 42-48.
(18). Njoka, E.N., Ombaka, O., Gichumbi, J.M., Kibaara, D.I., Nderi, O.M. Characterization of clay from Tharaka Nithi County in Kenya for Industrial and Agricultural applications, *Afr. J. Environ. Sci. Technolog*y, **2015**, 9(3):228-243.
(19). Nnuka, E.E. and Enejor, C. Characterization of Nahuta clay for industrial and commercial applications. *Nigerian Journal of Engineering and Materials,* **2010**, 2(3):9-12.
(20). Nwoye, I.C. Effect of water steam transition temperature on evaporation of clay. *New York Science Journal*, **2010,** 3(4):33-38.
(21). Omowumi, O.J. Characterization of some Nigerian clays as refractory materials for surface lining. Mineral Raw Materials Department, Federal Institute of Industrial research, Ikeja, Lagos, Nigeria, **2001**.
(22). Onyeji, L.I. Analysis and Characterization of Nyinkangbe Clay, Chanchanga L.G.A., Niger State. *JMME*, **2010**, 55-62.
(23). A.S. Ogunro, M.A. Usman, E.E. Ikponmwosa, D.S. Aribike, Characterization of some clay deposits in southwest Nigeria for use as supplementary cementitious material in cement, Materials Today: Proceedings, **2023**,
(24). Shuaib-Babata Y. L., Yaru S. S., Abdulkareem S., Busari Y. O., Ambali I. O., Ajao K. S. and Mohammed G. A. Characterization of Baruten Local Government Area of Kwara State (Nigeria) Fireclays as Suitable Refractory Materials, *Nigerian Journal of Technology (NIJOTECH)*, **2018**, 37(2):374 – 386.
(25). Injor O. M., Sadiku E. R., Teffo M. L., Ramakokovhu M. M., Agbogo V. U., and Kupolati W. K., "Advances in the Development, Processing, and Application of Locally Sourced Clay-based Refractory Materials for Furnace Application in Nigeria", *Sci. Eng. Technol.*, **2025**, 5(2)
(26). Ugwuoke J. C. "Characterization Of Iboko And Nduage-Echara Clay Deposits In Ebonyi State, Nigeria For Refractory Applications. "*International Journal of Engineering Inventions*, **2018**, 07(9):55-60.
(27). Yami, A.M., and Umaru, S. Characterization of some Nigerian clays as refractory materials for furnace lining. *Continental Journal of Engineering Sciences*, **2007**, 30-35.

ISBN: 978-978-68-0485-9 http://acsnigeria.org/publications/proceedings

Monitoring of Dumpsite Gas Emission and Its Implications to Health

Etiowo George Ukpong*, Imo-obong Pius Etuk, Promise-Godsfavour Mfon Bobson, Ekaete Joseph Tom, Okon Effiong Okon, James Okon Effiong and Idongesit Ignatius Udo
Department of Chemical Sciences, Akwa Ibom State Polytechnic, Ikot Osurua, Ikot Ekpene.
Corresponding Author's email: etiowoukpong@gmail.com (08027957927)

ABSTRACT

This study monitored the emission of gases and particulate matter from a dumpsite in Ikot Ekpene L.G.A., Akwa Ibom State, using an Industrial Gas Analyzer FD 600 forensic detector. The measured concentrations were carbon monoxide (CO) at 2 ppm, carbon dioxide (CO_2) at 416 ppm, formaldehyde (HCHO) at 0.008 mg/m³, total volatile organic compounds (TVOCs) at 0.016 mg/m³, particulate matter $(PM)_{2.5}$ at 12 µg/m³, PM_{10} at 129 µg/m³, hydrogen sulfide (H_2S) at 0.2 ppm, ammonia (NH_3) at 0.2 ppm, and methane (CH_4) at 0.2%. The Air Quality Index (AQI) was 118, while the temperature and humidity were 30°C and 80%, respectively. Results show that H_2S and PM_{10} exceeded permissible limits, posing health risks, while other pollutants were within standard thresholds. The findings highlight the need for improved waste management practices to mitigate environmental and health impacts.

KEYWORDS: Gas emission, Dumpsite, Particulate Matter, Air Quality Index, Health Risk

1. INTRODUCTION

The practice of dumping solid waste in open space is still obtainable the world over, both in developed and developing countries. This system of open dumping of waste comes with its attendant impact on the environment and public health[1]. The rise in the production of municipal solid waste with its hazardous effect on the environment and public health in Bangladesh has been linked to rapid population growth and urbanization[2,3,4]. The prevalence of this open solid waste disposal in Nigeria has been attributed to insufficient waste management capacity and unplanned development amongst other factors[5]. Also lack of organized landfill sites, deficient urban planning and negligence in the enforcement of waste disposal regulations were observed as reasons why dumpsites are found in residential areas of developing countries[6].

The site where solid wastes are disposed without environmental controls is referred to as dumpsite[7]. One of the major challenges faced by developing countries is the disposal of waste[8]. Waste disposal to open dumpsites is a common practice in developing countries[9].

Effort had been made to design an engineered (Semi – aerobic) landfill in Akure with a view to motivate a shift from using dumpsite which had been the major waste disposal method in Nigeria amidst its negative impacts on the environment[10], but a study had noted lack of enough land for sitting landfill as a major issue[11].

Open dumping has been classified as a type of landfills in addition to semi-controlled landfill and the sanitary landfill[12]. Landfill gas and Biogas are produced through biological decomposition process produces biogas[13,14].

Microbial activity on biodegradable wastes is responsible for the continuous production of landfill gases[15]. Waste degradation in landfills produces leachate and gases such as methane, carbon dioxide and green-house gases[16,17]. Although landfill methane can help to produce electricity, generating CO_2 as by-product, which produces less effect of global warming[18], the emissions from landfills affect environmental quality and human health[16]. CO_2 emission into the atmosphere can lead to global warming and ozone layer depletion[19,20,17].

Open dumpsite causes air pollution issues as the biogenic hydrocarbon gases like polychlorinated dibenzo – p – dioxins, non-methanic volatile organic compounds, polycyclic aromatic hydrocarbon and dioxin, release during the anaerobic microbial attack on the solid waste are converted to gaseous pollutants like hydrogen sulphide, carbon monoxide, ozone, sulphur dioxide, carbon dioxide and oxides of nitrogen[21]. Particulate matters (PMs) are generated in dumpsites when decomposed wastes are disperse by wind and also due to certain anthropogenic activities such as sorting of waste, tipping and waste compaction by bulldozers, stock piling of soil and other related activities[22].

There is a certain claim by some environmentalist that the negative impact of PM on public health has caused premature deaths of about 22,000 adults and 700 teenagers[23].

Landfill areas produces foul smell and vermin which is the major cause of diseases. Respiratory illnesses and cancer are associated with landfill site exposure[24]. Landfill impact socioeconomic and public health as a result of groundwater contamination and the diffusion of leachate into the wider ecological system due to insufficient recycling site activities[25]. Research have shown that the quality of groundwater closed to dumpsite is affected by the subsurface percolation of the leachates[26]. With the dearth of data on dumpsite gas emissions in Ikot Ekpene and due to the proliferation of dumpsite in residential areas with its attendant impacts on public health and environment, this study was therefore carried out to monitor gas emissions from dumpsite and its implications to health, as it might be useful to the authorities concerned.

2. MATERIALS AND METHODS

2.1 Gaseous Emission Data Acquisition

The data were collected from a dumpsite along Aba road in Ikot Ekpene L.G.A of Akwa Ibom State, South South of Nigeria with the Global Position System (G.P.S) coordinates of N5^0 8^{1}17.05884" latitude and E 7^{o}42^{1}55.13724" longitudes. The research was carried out in the morning hours by 11am for a period of 1 hour during the dry season using an Industrial Gas Analyzer FD600 Forensic Detector. The air quality detector was used for the measurement of air quality index (AQI), carbon monoxide (CO), carbon dioxide (CO_2) total volalite organic compounds ($TVOC_S$), hydrogen sulphide (H_2S), ammonia (NH_3), methane (CH_4), fomaldehyde (HCHO), particulate matters ($PM_{2.5}$ and PM_{10})

2.2 Procedure for the operation of the Gas Monitor:

The unit was placed in normal air, and the switch was turned to the gas position. The red LED and the sounder was beeped three times every one second. The LED was displayed to show 0.00 or 20.9. If not, the ZERO was re-set to adjust until the display read 0.00, or the CAL preset was adjusted to read 20.9. At this instant, the detector was ready for use. The unit was held at arm's length at 1.5m about ground level, then the unit was adjusted to alarm position to check battery level and gas position was then turned then the reading was taken to the LED display.

3. RESULTS AND DISCUSSION

3.1 Results

The results for the monitoring of dumpsite gas emission in Ikot Ekpene L.G.A., Akwa Ibom is shown in Table 1.

Table 1 Results of dumpsite gas emission in Ikot Ekpene.

Pollutants	Concentration	FEPA		WHO	
CO (ppm)	2		10		9
CO_2 (ppm)	416		-		-
HCHO (mg/m^3)	0.008	0.1		0.1	
TVOC (mg/m^3)	0.016	0.5		0.3	
$PM_{2.5}$ (µg/m^3)	12		25		10
PM_{10} (µg/m^3)	129		50		50
H_2S (ppm)	0.2		0.005		-
NH_3 (ppm)	0.2		0.2		0.2
CH_4 (%)	0.2	-		-	
AQI	118		-		-
Temperature (^{o}C)	30		-		-
Humidity (%)	80		-		-

3.2 Discussion

The data obtained from this study confirmed the emission of various pollutants from the dumpsite in Ikot Ekpene, Akwa Ibom State, Nigeria. The observed pollutants are due to waste degradation in the dumpsite (Sallam, 2020). The pollutants monitored were CO, CO_2, HCHO, TVOC, $PM_{2.5}$ and PM_{10}, H_2S, NH_3, and CH_4. AQI of the location was also determined in addition to temperature and humidity. The concentrations of CO, CO_2, NH_3, CH_4, HCHO, and TVOCs were within acceptable thresholds.

Regarding particulate matter, the site presents mixed results. The $PM_{2.5}$ concentration of 12 µg/m³ is compliant with FEPA's 25 µg/m³ threshold but slightly exceeds WHO's more stringent 10 µg/m³ guideline. However, the PM_{10} concentration, recorded at 129 µg/m³, surpasses both FEPA and WHO recommended limits of 50 µg/m³, raising significant health concerns. Elevated PM_{10} levels are associated with respiratory and cardiovascular complications, especially among children, the elderly, and individuals with preexisting conditions[27,28]. Similarly, a study reported PM_{10} values averaging 130 µg/m³ around open dumpsites in Nigeria, attributing the cause to airborne dust and the uncontrolled combustion of waste[29]. Mitigation strategies such as establishing vegetative buffers and dust suppression systems could play a crucial role in controlling particulate spread[30].

The hydrogen sulfide (H_2S) concentration was found to be 0.2 ppm, which significantly exceeds the FEPA guideline of 0.005 ppm. H_2S, often released during the anaerobic breakdown of sulfur-rich organic materials, is a well-documented hazardous gas with a distinctive rotten egg odor. Short-term exposure to H_2S at such levels may cause mucosal irritation, respiratory distress, and nausea[31]. Comparative studies such as that by Musa *et al.*[32], confirmed elevated H_2S emissions in unmanaged landfill zones across southwestern Nigeria, reinforcing the necessity for gas collection and odor control systems. Reducing the volume of sulfur-containing waste and adopting anaerobic digestion technologies could mitigate such emissions.

The Air Quality Index (AQI) measured at 118 indicates that air conditions are "Unhealthy for Sensitive Groups." This classification reflects cumulative exposure to elevated particulate and gaseous pollutants and signals heightened risk to individuals with respiratory conditions, children, and older adults[33]. Recent work by Abubakar *et al.*[34] on peri-urban dumpsites in northern Nigeria observed similar AQI ranges, underlining the correlation between poor waste handling and degraded air quality. This necessitates urgent reforms in landfill management practices.

Environmental parameters recorded a temperature of 30°C and a relative humidity of 80%, which are characteristic of tropical regions. These climatic conditions are known to intensify microbial activity, thereby accelerating the decomposition of organic matter and the subsequent emission of gases such as CH_4, NH_3, and H_2S[35]. Efficient environmental controls and periodic aeration can help moderate these emissions.

Overall, the data point to specific pollutants—especially PM_{10} and H_2S—as major contributors to air quality degradation around the dumpsite. Coordinated efforts involving source reduction, improved waste segregation, vegetative buffers, and gas recovery technologies are imperative to mitigate both public health and environmental impacts.

4. CONCLUSION

The findings of this study reveal that gas emissions from the monitored dumpsite in Ikot Ekpene pose significant health and environmental concerns, particularly due to elevated levels of hydrogen sulfide (H_2S) and particulate matter (PM_{10}), which exceeded permissible limits. Although other pollutants such as CO, CO_2, NH_3, CH_4, HCHO, and TVOCs were within acceptable thresholds, the Air Quality Index (AQI) of 118 indicates that the overall air quality is unhealthy for sensitive groups. These results underscore the urgent need for effective waste management strategies and continuous environmental monitoring to safeguard public health and ensure sustainable urban living conditions.

ACKNOWLEDGEMENTS

We thanked Dr. E. J. Abai, the Head of Department of Environmental Science and Management Technology, Akwa Ibom State Polytechnic, Ikot Osurua, for providing the Industrial Gas Analyzer FD600 Forensic Detector for the study.

CONFLICT OF INTERESTS

The authors declare no conflict of interests.

REFERENCES

(1). Ezekwe, I. C.; Arokoyu, S. B. Landfill Emissions and Their Urban Planning and Environmental Health Implications in Port Harcourt, South-South Nigeria. Desenvolv. Meio Ambiente 2017, 42, 224–241.

(2). Shammi, A. T.; Hassan, N.; Golder, M. R.; Molla, H.; Islam, S. S. Health Status Assessment of People Adjacent to Temporary Waste Disposal Sites in Khulna City, Bangladesh. Heliyon 2023, 9(9), e19810.

(3). Abedin, M. A.; Jahiruddin, M. Waste Generation and Management in Bangladesh: An Overview. Asian J. Med. Biol. Res. 2015, 1(1), 114–120.

(4). Rahman, M. M.; Sultana, K. R.; Hoque, M. A. Suitable Sites for Urban Solid Waste Disposal Using GIS Approach in Khulna City, Bangladesh. Proc. Pak. Acad. Sci. 2008, 45(1), 11–22.

(5). Nasir, A. A.; Ebeinyamba, O. E.; Odiji, C.; Ahmad, B.; Kopteer, E. P.; Abdullahi, S. K.; Tukur, K. A.; Ibrahim, V. A.; Musa, R.; Amodu, P. O. Analysis of Dumpsites and Their Potential Health Risks to Residents of Jahi District, Federal Capital Territory (FCT), Nigeria. World J. Adv. Res. Rev. 2024, 23(2), 1020–1031.

(6). Orimisan, A. E.; Olarewaju, A. J.; Babaniyi, B. R.; Olumuyiwa, A. O. Heavy Metal Content in Dumpsite Soils and Vegetables: A Case Study of Ondo Town, Nigeria. GSC Adv. Res. Rev. 2024, 19(1), 97–104.

(7). Tse, A. C.; Adamu, C. I. Assessment of Anthropogenic Influence on Quality of Groundwater in Hand-Dug Wells in Parts of Makurdi Metropolis, North Central Nigeria. Ife J. Sci. 2012, 14(1), 123–135.

(8). Oyelami, A. C.; Aladejana, J. A.; Agbede, O. O. Assessment of the Impact of Open Waste Dumpsites on Ground Water Quality: A Case Study of the Onibu-Eja Dumpsite, Southwestern Nigeria. Proc. Earth Planet. Sci. 2013, 7(4), 648–651.

(9). Ferronnato, N.; Torrentta, V. Waste Mismanagement in Developing Countries: A Review of Global Issues. Inter. J. Environ. Res. Pub. Health, 16(6), 1060.

(10). Ojuri, O. O.; Ajijola, T. O.; Akinwumi, I. I. Design of an Engineered Landfill as Possible Replacement for an Existing Dump at Akure, Nigeria. Afr. J. Sci. Technol. Innov. Dev. 2018, 10(7), 835–843.

(11). Yazdani, M.; Monavari, M.; Omrani, G. A.; Shariat, M.; Hosseini, M. Municipal Solid Waste Open Dumping, Implication for Land Degradation. Solid Earth Discuss. 2015, 7, 1097–1118.

(12). Nwosu, C.; Gloria, O.; Tukur, A. An Assessment of Open Dumps and Landfill Management in the Federal Capital Territory, Nigeria – Using Scotland as a Case Study for Structural Development. J. Environ. Earth Sci. 2016, 6(7), 1–9.

(13). Rada, E. C.; Ragazzi, M.; Stefani, P.; Schiavon, M.; Torrenta, V. Modeling the Potential Biogas Productivity Range from a MSW Landfill for Its Sustainable Exploitation. Sustainability 2015, 7, 482–495.

(14). Shen, S.; Chen, Y.; Zhan, L.; Xie, H.; Bouazza, A.; He, F.; Zuo, X. Methane Hot Spot Localization and Visualization at a Large-Scale Xi'an Landfill in China: Effective Tool for Landfill Gas Management. J. Environ. Manag. 2018, 225, 232–241.

(15). Chiriac, R.; Carre, J.; Perrodin, Y.; Fine, L.; Letoffe, J. Characterisation of VOCs Emitted by Open Cells Receiving Municipal Solid Waste. J. Hazard. Mater. 2007, 149(2), 249–263.

(16). Sallam, R. M. A. Landfill Emissions and Their Impact on the Environment. Int. J. Chem. Stud. 2020, 8(2), 1567–1574.

(17). Ramprasad, C.; Teja, H. C.; Gowtham, V.; Vikas, V. Quantification of Landfill Gas Emissions and Energy Production Potentials in Tirupati Municipal Solid Waste Disposal Site by LandGEM Mathematical Model. MethodsX 2022, 9, 101869.

(18). Kivimägi, J. A Descriptive Analysis of Post-Closedown Environmental Monitoring and Maintenance of the Pääskula Landfill. Manag. Environ. Qual. 2011, 22(6), 769–786.

(19). Bruce, N.; Ng, K. T. W.; Vu, H. L. Use of Seasonal Parameters and Their Effects on FOD Landfill Gas Modeling. Environ. Monit. Assess. 2018, 190(5), 1–14.

(20). Hoque, M. M.; Rahman, M. T. U. Landfill Area Estimation Based on Solid Waste Collection Prediction Using ANN Model and Final Waste Disposal Options. J. Clean. Prod. 2020, 25, 120387.

(21). Salami, L.; Popoola, L. T. A Comprehensive Review of Atmospheric Air Pollutants Assessment around Landfill Sites. Air Soil Water Res. 2023, 16, 1–17.

(22). Chalvatzaki, E.; Kopanakis, I.; Kontaksakis, M.; Glytsos, T.; Kalogerakis, N.; Lazaridis, M. Measurement of Particulate Matter Concentration at a Landfill Site (Crete, Greece). Waste Manag. 2010, 30(11), 2058–2064.

(23). Hassan, A.; Ilyas, S. Z.; Agathopoulos, S.; Hussain, S. M.; Jalil, A.; Ahmed, S.; Baqir, Y. Evaluation of Adverse Effects of Particulate Matter on Human Life. Heliyon 2021, 7(2), e05968.

(24). Da Costa, F. M.; Daflon, S. D. A.; Bila, D. M.; Da Fonseca, F. V.; Campos, J. C. Evaluation of the Biodegradability and Toxicity of Landfill Leachates after Pretreatment Using Advanced Oxidative Processes. Waste Manag. 2018, 76, 606–613.

(25). Alobaid, F.; Al-Maliki, W. A. K.; Lanz, T.; Haaf, M.; Brachthauser, A.; Epple, B.; Zorbach, I. Dynamic Simulation of a Municipal Solid Waste Incinerator. Energy 2018, 149, 230–249.

(26). Inyang, N. E.; Ehibol, I. U.; Ekot, A. E.; Udo, I. G. An Environmental Assessment and A Priori Implications of Field Investigations of Older MSW at Uyo and Younger MSW at Eket, Akwa Ibom State, Southern Nigeria. Res. J. Sci. Technol. 2024, 4(1), 45–71.

(27). WHO. Global Air Quality Guidelines: Particulate Matter, Ozone, Nitrogen Dioxide, Sulfur Dioxide and Carbon Monoxide. World Health Organization, 2021.

(28). Brook R.D., Rajagopalan S., Pope C.A., 3rd, Brook J.R., Bhatnagar A., Diez-Roux A.V., et al. Particulate matter air pollution and cardiovascular disease: An update to the scientific statement from the American Heart Association. Circulation. 2010;121:2331–2378.

(29). Udo, E. J.; Okafor, A.; James, T. Particulate Matter Levels in Proximity to Open Dumpsites in Nigeria. Afr. J. Environ. Sci. 2022, 16(2), 95–108.

(30). IARC. Particulate Matter and Air Pollution: Human Carcinogenic Risks. Int. Agency Res. Cancer, 2019.

(31). Agency for Toxic Substances and Disease Registry (ATSDR). Toxicological Profile for Lead. Atlanta, GA: US Department of Health and Human Services, Public Health Service.

(32). Musa, L. A.; Bello, F.; Obaje, G. Hydrogen Sulfide Emissions from Domestic Landfills: A Case Study in Southwest Nigeria. J. Waste Manag. Res. 2022, 40(11), 1294–1303.

(33). USEPA. Technical AQI Standards for Ambient Air Quality. U.S. Environ. Prot. Agency, 2022.

(34). Abubakar, M. I.; Nuhu, A.; Lawal, K. Air quality dynamics in peri-urban Nigerian dumpsites. International J. Environ. Health, 2023, 15(2), 112–124.

(35). Kumar, D.; Sharma, R.; Patel, S. Impact of Tropical Climate on Gas Emission in Solid Waste Dumpsites. J. Environ. Eng. 2020, 146(9), 04020085.

ISBN: 978-978-68-0485-9 DOI: https://doi.org/10.55455/acsnigeria.1.2.212-218

Review of Emerging Trends in Surface Chemistry

[1]Raymond Bwano Donatus, [2]Blessed Dimas Jen, [3]Bala Joseph, [4]Tadzabia Kadam, and [2]Ernest Isaac

[1]Department of Chemistry, Federal University Wukari, Wukari-Taraba State, Nigeria
[2]Department of Chemistry, Taraba State University, Jalingo- Taraba State, Nigeria
[3]Department of Chemistry, University of Agriculture, Mubi-Adamawa State, Nigeria
[4]Department of Chemistry, Nigerian Army University, Biu-Borno State, Nigeria

Corresponding Author's email: dbwano@fuwukari.edu.ng, blesseddimas@gmail.com

ABSTRACT

Surface chemistry is a fundamental and radical science that forms the basis of modern materials and technologies. On a molecular level, it controls the behavior of matter because it determines adhesion, wetting, catalysis, and the energy conversion processe s that are the basis of innovations in medicine, renewable energy, environmental protection, and ordinary materials. Understanding of surface behaviour also helps the scientists to regulate reactivity, synthesize functional interfaces and develop materials that react best with their surroundings. The review follows the historical development of surface chemistry focusing on the pre-history of the field, current advances, and future developments. Theoretical foundations, e.g., adsorption isotherm of Langmuir and surface energy equation of Gibbs, laid the theoretical basis of explaining interfacial events and adsorption equilibria. Modern directions include nanostructured and biofunctional surfaces, stimuli-responsive interfaces, and environmental systems such as dispersion of oil-spills, control of pollution and purification of wastewater. Surface chemistry is being disrupted by the combination of artificial intelligence, machine learning, and the use of computational modelling to predictively design materials with customized interfacial characteristics. The directions of future research include sustainable and green surface chemistry, in particular bio-based surfactants, renewable nanomaterials and multifunctional hybrid systems to biomedical, catalytic and energy applications. Finally, advances in surface chemistry do not just stop in the laboratory environment; they offer cleaner water, more efficient energy storage, safe materials, and an improved quality of life, which has further supported its core contribution to more sustainable and human-centered technological future.

KEYWORDS: Artificial intelligence, Environmental remediation, Hybrid materials. Nanostructured surfaces, Smart materials, Surface chemistry.

1. INTRODUCTION

Surface chemistry is an interdisciplinary field of chemistry, which studies chemical reactions at the surface of solid materials. The field requires the study of adsorption, migration, assembly, activation, reaction, and desorption processes of atoms and molecules at the surface.[1] Surface chemistry has had a significant impact on numerous technologies due to the fundamental formation of surface chemistry. In the early days related to Langmuir and Ertl, the improvement of the performance of incandescent lamps was viewed as a key technological driving force, which triggered the intensive research of tungsten filament chemistry and the dynamics of molecules adsorbed onto and reacting with surfaces of transition metals; these concepts form the basis of heterogeneous catalysis.[2] The semiconductor surfaces did grow in popularity in the 1960s, thereby further enlightening the influence of the surface structural features in catalytic and semiconductor sciences. Surface chemistry has long been associated with a significant fraction of the world GDP over many years, and the wide range of applications with high impact has been driving the development of surface chemistry, including electronics, petrochemicals, fixing nitrogen on fertilisers, and automotive catalyst technology. Other upcoming fields are photovoltaics and a wide range of energy conversion technologies.[2]

Contemporary surface chemistry is based on a molecular level concept and exact control of surface based chemical reactions. Numerous surface-science methods have been developed in the past decades, and a large body of knowledge on surface chemistry has been accumulated.[3,4,5] This is a cumulative knowledge that forms the basis of many industrial technologies which manufacture chemicals, fuels, semiconductor devices and biomedical apparatus. Advancement in technology, in turn, contributes towards the further development of surface-characterization methods of increased space, time, and energy.[6] Recent publications have shown that operando and spatially resolved probing technology can be used to apply laboratory results to operational and that interface-specific structural and dynamical markers can be used to correlate the molecular orientation with functional

output with the aid of vibrational nonlinear optical methods that include the sum -frequency generation.[7,8] At the same time, operando X-ray and ambient-pressure photoelectron spectroscopies clarify the evolution of chemical states on catalytic surfaces under conditions that are realistic thus enhancing mechanistic understanding of reactions of relevance in industry.[9]

Surface chemistry is a crucial part of various scientific and industrial aspects, which disposes of material interactions on both molecular and macroscopic levels. Since the initial developments of adsorption and catalysis were first explained, the field has developed significantly to its current uses in nanotechnology, storing energy and environmental sustainability. This review discusses the history, current advances and future trends of surface chemistry. Surface chemistry in the present age is the source of innovation in nanostructured surfaces, self-assembled monolayers, and smart surfaces that have adjustable properties. It is noted that these materials find more and more applications in different fields such as energy conversion, environmental remediation, biomedical engineering, and industrial manufacturing.[10] In addition, the design and optimization of functional surfaces are also being turned by integrating artificial intelligence and computational.[11,12]

In the future, surface chemistry is expected to play a major role in the development of sustainable materials with particular applications in biodegradable surfactants, environmental friendlier coatings and multifunctional hybrid surfaces. This is a review that provides an in-depth discussion of the recent trends in surface chemistry covering past successes, present developments, and future directions of research.

2. HISTORICAL DEVELOPMENT OF SURFACE CHEMISTRY

The area of surface chemistry started with heterogeneous catalysis pioneered by Paul Sabatier on hydrogenation and Fritz Haber on the Haber process. Irving Langmuir was also one of the founders of this field, and the scientific journal on surface science, Langmuir, bears his name. The Langmuir absorption equation İs used to model monolayer adsorption where all surface adsorption sites have the same affinity for the adsorbing species and do not interact with each other.[13]

Gerhard Ertl in 1974 described for the first time the adsorption of hydrogen on a palladium surface using a novel technique called LEED. Similar studies with platinum, nickel, and iron followed. Most recent developments in surface sciences include the 2007 Nobel prize of Chemistry winner Gerhard Ertl's advancements in surface chemistry, specifically his investigation of the interaction between carbon monoxide molecules and platinum surfaces.[14]

The foundations of surface chemistry were laid by early studies on adsorption, catalysis and surface interactions. Langmuir's adsorption isotherm (1918) was a breakthrough in understanding gas adsorption on solid surfaces at different concentrations. While Langmuir's work laid the foundation for heterogeneous catalysis and surface modification, Freundlich's empirical model further contributed to the understanding of multilayer adsorption on heterogeneous surfaces.[15,16]

Later, the development of scanning probe microscopy (SPM) and X-ray photoelectron spectroscopy (XPS) provided detailed insights into surface structures at the atomic level.[17]

Early studies in surface chemistry were centered on adsorption, catalysis, and surface interactions. Langmuir[16] introduced the adsorption isotherm, which described how molecules adhere to surfaces at different concentrations. The development of the Gibbs adsorption equation explained how surfactants lower surface tension by accumulating at interfaces, influencing emulsification and wetting processes.[18] In the mid-20th century, advancements in surface spectroscopy techniques, such as X-ray photoelectron spectroscopy (XPS) and Auger electron spectroscopy (AES), enabled atomic-scale surface analysis, improving the characterization of catalytic and adsorption processes.[17]

2.1 Adsorption Isotherm

A variety of isotherms have been applied in adsorption systems, such as the Langmuir model, linear model, the Freundlich model, the Sips model, the Temkin model, and the Brunauer, Emmett, and Teller (BET) model.[19]

2.2 Langmuir Isotherm

The Langmuir isotherm was initially developed for gas–solid interaction but is also used for various adsorbents. It is an empirical model based on kinetic principles; that is, the surface rates of adsorption and desorption are equal with zero accumulation at equilibrium conditions. Based on the following assumptions, (a) monolayer adsorption, (b) homogeneous sites, (c) constant adsorption energy, and (d) no lateral interaction between the adsorbed molecules, the Langmuir isotherm can be written as

$$q_e = q_o K_L C_e / 1 + K_L C_e \quad \text{.....(1)}$$

where q_o is the maximum amount of adsorbed surfactant in and K_L is the Langmuir constant in. The linearized version of the equation is

$$C_e/q_e = 1/K_L q_o + C_e/q_o \quad \text{.....(2)}$$

A plot between C_e/q_e versus C_e will generate a straight line with a slope of $1/q_o$ and an intercept equals to $1/K_L q_o$.

The monolayer assumption requires identical adsorption sites, and only one molecule can be adsorbed at each site. There is no more adsorption in a site once a surfactant molecule has occupied it.

2.3 Freundlich Isotherm

Unlike the Langmuir isotherm, this empirical model can be used for multilayer adsorption on heterogeneous sites. It assumes that the adsorption heat distribution and affinities toward the heterogeneous surface are non uniform. The mathematical model can be shown as

$$q_e = bC_e^{1/n}$$

where b is the adsorption capacity and $1/n$ is the adsorption intensity or surface heterogeneity. When $0 < 1/n < 1$, adsorption is considered favorable. Unfavorable adsorption occurs when $1/n > 1$ and is irreversible at $1/n = 1$.

The linearized form can be written as

$$\ln q_e = \ln b + \frac{1}{n} \ln C_e$$

A plot of $\ln q_e$ versus $\ln C_e$ produces a straight line with a slope = $1/n$ and intercept = $\ln b$.

The linearized form is easy and straightforward. On the other hand, the linearization process generates propagating errors, which results in erroneous predictions of parameters. Therefore, the use of nonlinear regression to solve the nonlinear Freundlich model is recommended for the calculation of the model parameters.

The Freundlich isotherm describes multilayer adsorption and assumes exponential decay in the energy distribution of adsorbed sites. However, it is not valid for a large range of adsorption data.[20]

2.4 Applications of adsorption isotherms

There are several possible applications of adsorption isotherms. The following points introduce short key highlights on applications of adsorption isotherms:

To compute the capacity and percentage removal of adsorbates from a certain media or environment.

To acquire the greatest adsorbent absorption and affinity between adsorbent and adsorbate, Langmuir parameters can be applied.

Freundlich parameters can be used to obtain adsorption capacity of adsorbents.[21]

2.5 Surface chemistry in adsorption process

Adsorption process is a surface phenomenon in which adsorbates transfer onto adsorbents. Over the past decades, adsorption technology has been widely applied for the water and wastewater treatment because it is low-cost, efficient, simple, and environmentally friendly

Adsorption is the adhesion of an adsorbate such as a fluid, liquid, or gas, by creating a thin layer or film on the surface of an adsorbent whether it is a solid or liquid as shown on figure 1.

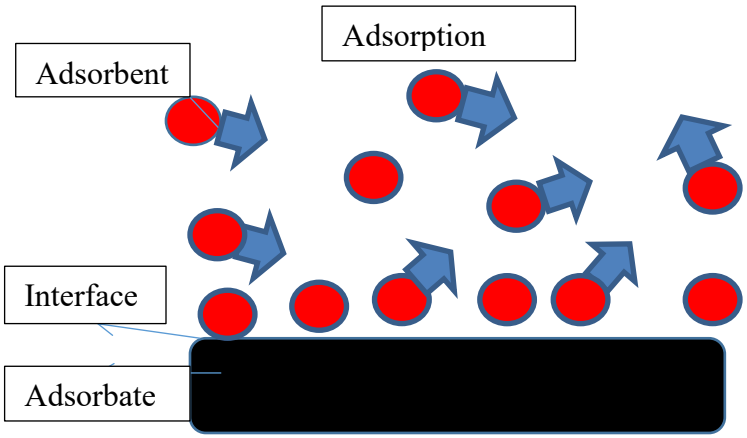

Figure 1 Adsorption on adsorbent

The bonding between adsorbate and adsorbent could be physical or chemical bonding as shown in figure 2.The adsorption mechanisms include chemical adsorption corresponding to the formation of chemical bonds, physical adsorption related to the van der Waals force, and the ion exchange. The knowledge of adsorption mechanisms is of great importance to design the adsorbents and the adsorption systems. The chemical bonding provides stronger bonding than physical bonding, layers. Adsorbate can be separated from the adsorbent and the process is called desorption. There are some factors influencing the adsorption process, but, at the basic level, the most widely studied is the influence of temperature and could be assumed as a monolayer. The adsorption process is usually studied at a given temperature and recognized as an adsorption isotherm.[22]

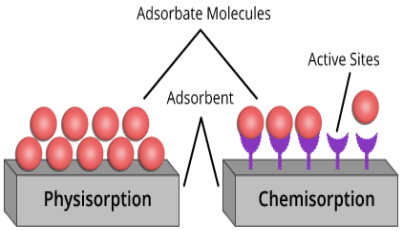

Figure 2 Physisorption and Chemisorption on adsorbent

3. PRESENT TRENDS IN SURFACE CHEMISTRY

3.1. Nanostructured and Functionalized Surfaces

Recent advances in nanotechnology have led to the development of nanostructured surfaces with tunable properties. Graphene-based coatings, metal-organic frameworks (MOFs), and self-assembled monolayers (SAMs) have shown promise in applications such as catalysis, biomedical engineering, and energy storage.[23] Studies by Zhang et al.[24] highlight the fabrication of bioinspired

superhydrophobic surfaces, mimicking the lotus leaf effect for antifouling and self-cleaning applications.

3.2. Surface Chemistry in Environmental Remediation

Surface chemistry is increasingly applied in oil spill remediation, wastewater treatment, and pollutant adsorption. Wang et al.[25] demonstrated that engineered surfaces with hydrophobic/hydrophilic balance enhance oil-water separation efficiency. Additionally, Jiang et al.[26] investigated surface-modified bioadsorbents for heavy metal and fluoride removal from contaminated water sources. The use of surfactant-functionalized nanomaterials has further improved adsorption capacity and selectivity for toxic pollutants.

3.3. Smart and Responsive Surfaces

Advancements in stimuli-responsive materials have enabled the development of smart surfaces that change their properties based on external triggers such as temperature, pH, or light.[27] Photo switchable molecular receptors have been explored for controlled adsorption and release of pollutants, offering potential applications in chemical sensing, self-healing coatings and drug delivery.[28]

3.4. Surface Chemistry in Energy Applications

Surface chemistry modifications play a crucial role in improving the efficiency of electrocatalysts for hydrogen production, fuel cells, and lithium-ion batteries. Zhao et al.[29] reviewed advancements in surface-engineered electrode materials that enhance charge transport and stability in energy storage systems. Similarly, surface-functionalized perovskite materials have shown promising efficiency in boosting solar cell.[30]

4. FUTURE PROSPECTS IN SURFACE CHEMISTRY

4.1. Sustainable and Green Surface Chemistry

As sustainability concerns grow, green chemistry approaches in surface engineering are gaining traction. The shift toward eco-friendly and biodegradable surfactants is gaining momentum, with researchers exploring plant-based and sugar-derived surfactants as sustainable alternatives to synthetic surfactants.[31] Bio-based coatings are also being developed for corrosion protection and antimicrobial applications.[32]

4.2. Advanced Computational Surface Chemistry

Computational modeling like, Machine learning and other Artificial Intelligence -driven approaches are transforming the way surface chemistry is studied. Computational simulations help predict surface interactions, optimize coatings, and design self-healing materials.[32] The application of density functional theory (DFT) has further improved the understanding of molecular-level surface modifications.[29]

4.3. Multifunctional and Hybrid Surface Materials

These are hybrid surfaces that focus on multifunctional hybrid materials, integrating self-cleaning, antibacterial, and conductive properties into a single surface.[30] These materials hold promise for applications in biomedical implants, electronic devices, and aerospace coatings.[30]

5. CONCLUSION

This study highlights the evolution of surface chemistry from classical adsorption theories to advanced functionalized materials. The field has witnessed a shift toward nanotechnology-driven surface

engineering, smart interfaces, and sustainable surface modifications. Future advancements are expected to integrate AI-driven material design and multifunctional hybrid surfaces, addressing critical challenges in environmental sustainability, energy efficiency, and biomedical applications.

CONFLICT OF INTERESTS

The authors declare no conflict of interests.

REFERENCES

(1) Xin L.; Zhen X.; Donglei B.; Jinming C.; Huamei C.; Qi C.; Ting C.; Fang C.; Lifeng C.; Wenjie D.; Zhenchao D.; Shixuan D.; Qitang F.; Xing F.; Qiang F.; Song G.; Jing G.; Weijun G.; Yang H.; Shimin H. Recent progress on surface chemistry I: Assembly and reaction, Chinese Chemical Letters. 2024, 35 (12),110055.

(2) Ertl, G. Reactions at surfaces: from atoms to complexity (Nobel Lecture). Angew. Chem. Int. Ed. 2008, 47, 3524–3535

(3) Bhattacharjee, S. and Prasad, V. Recent advances in single-atom catalysts for electrochemical CO_2 reduction: A computational perspective. ACS Catalysis. (2023, 13 (7), 4567–4589.

(4) Fellows, C. J. Machine learning accelerated discovery of earth-abundant oxygen evolution catalysts. Journal of the American Chemical Society. 2024, 146 (12), 7890–7901.

(5) Gabor, B., and Yimin, A. Density functional theory studies of methanol synthesis on Cu(111): Role of surface oxygen vacancies. The Journal of Physical Chemistry C. 2010, 114 (41), 17763–17770.

(6) Goodwin, C. M.; Cardon, S.T.; .Briton J.S. Scaling relations in heterogeneous catalysis: Beyond the d-band model. Angewandte Chemie International Edition, 2023, 63 (15),18765.

(7) Mattia, S.; Elena, A.; Igor, D.; Jurberg, C.C.; Paolo, M. Enantioselective Organocatalytic Alkylation of Aldehydes and Enals Driven by the Direct Photoexcitation of Enamines *J.American Chemical Society.* 2015,*137* (19), 6120-6123.

(8) Hepsiba, N.C.; Wei-Lun C.; Lee-Lee C.; Kuo-Lun T.; Chechia H. Gel-like Ag-Dicyandiamide Metal–Organic Supramolecular Network-Derived g-C3N4 for Photocatalytic Hydrogen Generation. ACS Sustainable Chemistry & *Engineering.* 2022, 10 (26), 8360-8369.

(9) Lee, J.; Xu, M.; Li, Z.; Liuing, M.; Zhou, W. Quantum dot-sensitized TiO_2 for visible-light-driven CO_2 reduction to methanol: Mechanism and efficiency. Nature Catalysis. 2023, 8 (3), 210–221.

(10) Nilsson, A.; Lars, G.m P.; Jens K.N. Chemical Bonding at Surfaces and Interfaces. Amsterdam: Elsevier Science & Technology. 2008.

(11) Jinxiu, H.; Ni, W.; Xialiang, L.; Haitao, L.; Yabo, W.; Hongbo, G.; Xiaotong, J.; Qingxin, Z.; Xinyang, P.; Xue-Peng, Z.; Wei Zhang, U-P.A.; Rui, Cao. Bioinspired iron porphyrins with appended polypyridine/amine units for boosted electrocatalytic CO2 reduction reaction.J. eScience. 2022, 06, 003.

(12) Wu, J.; Xu, M.; Li, Z.; Li, M.; Zhou, W. Dual Defect-Engineered $BiVO_4$ Nanosheets for Efficient Peroxymonosulfate Activation. Nanomaterials. 2025, *15* (5), 373.

(13) Nung, S.L; Yi, S.T.; Xialin, Z.; Jun, Y.; Jiali, L.; Binhang, Y.; Xiaonan W. Artificial Intelligence (AI) Workflow for Catalyst Designand Optimization. Ind. Eng. Chem. Res. 2023, 62, 17835−17848.

(14) Langmuir, I. The Adsorption of Gases on Plane Surface of Glass, Mica and Platinum". Journal of the American Chemical Society. 1918, 40 (9), 1361–1402.

(15) Chen, L.; Wang, X. Photoswitchable surface chemistry for environmental applications. *Journal of Surface Science*. 2021, 45 (2), 123-135.

(16) Hansraj V.P.; Nilesh P. B.; Suresh, R. D.; Kulkarni, K.N. Sustainable bio-based surfactants: Advances in green chemistry and environmental applications, Materials Today Communications. 2025, 48, 113583.

(17) Humaira, A.; Ali, U.; Shehla, H.; Mansour, M.; Mis bah, U.K.; Nazia, N.; Ghulam, A.; Mustansar, A.; Jehanzeb, S.; Moazam, A.; Shumaila A. Adsorbents for the Removal of Heavy Metals from Wastewater: A Review. Biomed J Sci & Tech Res BJSTR. 2024, 58 (3) 009151.

(18) Asan, G.; Arslan, O. Multifunctional, Biocompatible Hybrid Surface Coatings Combining Antibacterial, Hydrophobic and Fluorescent Applications. Polymers. 2025, 17, 2139.

(19) Neoh, K.G.; Kang, E.T. Responsive surfaces for biomedical applications. *MRS Bulletin.* 2022, **35**, 673–681.

(20) Bai, X.; Zhang, X. Artificial Intelligence-Powered Materials Science. *Nano-micro letters*. 2025, *17* (1), 135.

(21) Somorjai, G. A.; Li, Y. Introduction to Surface Chemistry and Catalysis. 2010, Wiley.

(22) Wang, Q.; Cui, Z.; Xiao, Y.; Chen, Q. Stable highly hydrophobic and oleophilic meshes for oil–water separation. Applied Surface Science. 2023, 253, 9054-9060.

(23) Freshteh, S.; Mahmood, M.S.; Nader, K.; Bok, J.L.; Abolfazli-Esfahani, J.; Mohammad,K.D M. Natural and synthetic superhydrophobic surfaces: A review of the fundamentals, structures, and applications, Alexandria Engineering J. 2023, 68, 587-609.

(24) Chen, Y.; Yao, Y.; Zhao, W.; Wang, L.; Li, H.; Zhang, J. Precise Solid-Phase Synthesis of CoFe@FeO_x Nanoparticles for Efficient Polysulfide Regulation in Lithium/Sodium-Sulfur Batteries. Nature Communications. 2023, 14. 7487.

(25) Yates, J.T.; Charles T.C. Surface Chemistry: Key to Control and Advance Myriad Technologies. Proceedings of the National Academy of Sciences of the United States of America, JSTOR. 2011, 108, (3) 911–16.

(26) Gabor, A. S.; Yimin, L. Impact of surface chemistry. Department of Chemistry and Lawrence Berkeley National Laboratory, University of California, Berkeley, CA 94720 Proc Natl Acad Sci U S A. 2010, 108 (3): 917–924.

(27) Maia, K. C.; B., Densy Dos Santos Francisco, A.; Moreira, M. P.; Nascimento, R. S. V.; Grasseschi, D. Advancements in Surfactant Carriers for Enhanced Oil Recovery: Mechanisms, Challenges, and Opportunities. *ACS omega*. 2024, *9* (35), 36874–3690.

(28) Xin, L.; Zhen, X.; Donglei, B.; Jinming, C.; Huamei, C.; Qi, C.; Ting, C.; Fang, C.; Lifeng, C.; Wenjie, D.Z. Recent progress on surface chemistry 1:Aseembly and reaction Chiness Chemical Letters. 2024, 35 (12),110055.

(29) Tawfik A.S Chapter 4 - Isotherm models of adsorption processes on adsorbents and nanoadsorbents. 2022, 99-126.

(30) Jailong, W.; Xuan, G. Review Adsorption isotherm models: Classification, physical meaning, application and solving method ,Chemospher. 2020, 258.127279.

(31) Patiha, E.; Heraldy, Y H.; Firdaus, M. The langmuir isotherm adsorption equation: The monolayer approach. IOP Conf. Ser. Mat. Sci. Eng. 2016, 107, 012067.

(32) Wennerström, H.; Lidin, S. Scientific Background on the Nobel Prize in Chemistry 2007 Chemical Processes on Solid Surfaces.

ISBN: 978-978-68-0485-9 DOI: https://doi.org/10.55455/acsnigeria.1.2.219-223

Cytotoxicity and Anti-cancer Effects of *Hibiscus sabdariffa* Leaf Extracts on Triple Negative Breast Cancer (TNBC) Cell Lines

Jemimah Simon Wakawa, Bilkisu Adedoyin, Umar Ahmed, Olutola Adeola Olayemi, Fagge Khadija Ali, and Okafor Lilian Chidera
Applied Chemistry Research Laboratory, University of Abuja, FCT, Abuja Nigeria.
Corresponding Author's email: simon.wakawa2020@uniabuja.edu.ng; **Tel:** 09038084193

ABSTRACT

Hibiscus sabdariffa belongs to the family of Malvaceae and is widely cultivated and used in traditional medicine for its antioxidant, anti-inflammatory, anti-obesity, and anti-cancer properties. This study aims to investigate the effects of *H. sabdariffa* leaf extracts using the brine shrimp Lethality Test (BSLT) and MTT assay against Triple-Negative Breast Cancer (TNBC) cell lines: MCF7 (invasive ductal carcinoma), MDA-MB-231 (adenocarcinoma), Hs578T (invasive ductal carcinoma), and SKBr3 (invasive ductal carcinoma). The Brine Shrimp Lethality test (BSLT) revealed significant cytotoxicity across all extracts, with mortality ranging from 27 to 30, where 30 brine shrimp larvae were used. The methanol extract exhibited the highest cytotoxic activity, indicating a higher concentration of potent cytotoxic compounds compared to the ethyl acetate and n-hexane extracts. The LC_{50} values for n-hexane, ethyl acetate, and methanol extracts are 72.26, 51.19, and 50.61 µL, respectively. The MTT assay was performed to assess the anti-cancer potential of the extracts. The assay revealed different IC_{50} values of the most potent extract on the cell line: MCF7 (n-hexane IC_{50}-77µM, etoposide IC_{50}-68µM), Hs578T (methanol IC_{50}-66µM, etoposide IC_{50}-78µM), SKBr3 (methanol IC_{50}-96µM, etoposide IC_{50}-70µM), and MDA-MB-231 (ethyl acetate IC_{50}-67µM, etoposide IC_{50}-69µM). These results suggest that the methanol extract exhibits strong anti-cancer activity against the Hs578T cell line, which outperformed the standard drug etoposide. Overall, *Hibiscus sabdariffa* leaf extracts showed significant medicinal properties and potential as a source of anti-cancer therapy for pharmaceutical development.

KEYWORDS: Cytotoxicity, Anti-Cancer Effects, TNBC, *Hibiscus sabdariffa* Leaves.

1. INTRODUCTION

Cancer is a critical health condition worldwide. Among various cancers, breast cancer is the most prevalent type and the second most common cause of death in women around the globe.[1] The World Health Organization reported 2.3 million women were diagnosed with breast cancer in 2020, and 685,000 deaths were recorded globally, making it the world's most prevalent cancer in the past five years.[2] Triple-Negative Breast Cancer (TNBC) is known as inflammatory and invasive breast cancer. It is resistant to therapies and occurs in 15 to 20% with a lower survival rate. TNBC lacks the three most common markers used for targeted therapies: estrogen receptors (ER), progesterone receptors (PR), and HER2, which are all negative. It is more common in younger women and often affects those with a BRCA1 gene mutation.[3] *H. sabdariffa* exhibits a wide range of biological activities, including antibacterial, antifungal, antiviral, anticancer, immunomodulatory, antioxidant, smooth muscle relaxant, gastrointestinal anti-inflammatory, wound healing, and cardiovascular protective effects.[4] *H. sabdariffa* aqueous extract (HSE) on a human breast adenocarcinoma cell line (MCF-7) and normal foreskin fibroblast cells (HFFF), apoptosis induction was assessed at a concentration of 0.5 mg/mL; the extract reduced the viability of MCF-7 cells to below 50% after 72 hours of incubation, demonstrating notable cytotoxic effects.[5] Despite *H. sabdariffa's* ethnomedicinal uses, there is limited literature on its cytotoxicity properties. This research aims at investigating the cytotoxicity of crude extracts from *H. sabdariffa* leaf against triple-negative breast cancer (TNBC) cell lines.

2. MATERIALS AND METHODS

2.1 Plant Collection and Identification

The fresh leaves of *H. sabdariffa* were collected randomly over a period of 5 days, verified, and authenticated (ABU02768) at the herbarium, Botany Section of the Department of Biological Sciences, Ahmadu Bello University, Zaria, Kaduna, Nigeria.

2.2 Sample Collection for Bioassay Analysis

In the Brine Shrimp Lethality (BSLT) assays, *Artemia salina* shrimp eggs were collected, and four Triple-Negative Breast Cancer (TNBC) cell lines were used in the study, namely invasive ductal carcinoma (MCF7), adenocarcinoma (MDA-MB-231), invasive ductal carcinoma (Hs578T), and invasive ductal

carcinoma (SKBr3), which were collected from the cell-culture laboratory, Centre for Natural Product Discovery, School of Biochemical Science, Liverpool John Moores University (LJMU), United Kingdom.

2.3 Brine Shrimp Lethality Test (BSLT) Assays Procedure

Brine shrimp (*Artemia salina*) eggs were hatched in seawater for 48 hours to obtain larvae. Extracts (0.2 g) were dissolved in 2 ml of solvent of extraction, and concentrations of 1000, 100, and 10 µg/ml were prepared in triplicate with controls. Ten larvae were introduced into each vial, and survival was recorded after 24 hours. LC_{50} values were calculated using Finney probit analysis software.

2.4 MTT (3-(4,5-dimethyl-2-thiazolyl)-2,5-diphenyl-2H-tetrazolium bromide) Assay procedure

Extract concentrations of 1.0, 0.5, and 0.25 mg/ml were prepared by dissolving measured amounts in 2 ml of extraction solvent, evaporating to dryness, re-dissolving in a drop of DMSO, and making up to 2 ml with distilled water. Cells were washed with phosphate buffer saline (PBS), harvested by trypsinization, plated in 96-well plates, and incubated at 37°C under 5% CO_2 for 24 hours. All concentrations of plant extracts were in triplicate on the same cell batch. Growth of tumor cells was quantitated by the ability of living cells to reduce the yellow dye 3-(4,5-dimethyl-2-thiazolyl)-2,5-diphenyl-2H-tetrazolium bromide (MTT) to a blue formazan product.

2.5 Extraction and Fractionation

The freshly collected leaves of *H. sabdariffa* were carefully separated and air-dried at room temperature and pulverized using a ball mill machine (Gilson Company INC). Cold extraction by the maceration method was used. A portion (500 g) of the powdered sample was soaked in 2000 ml of n-hexane, ethyl acetate, and methanol successively and allowed to stand for seven days, then decanted and filtered with 20 cm filtered paper and concentrated using a rotary evaporator at 30°C to 60°C (86°F to 140°F) and 10-50 mbar. The extraction yields were calculated.

3. RESULTS AND DISCUSSION

3.1 Results

3.1.1 Brine-Shrimp Lethality Test Results.

The lethal concentration of n-hexane, ethyl acetate, and methanol extracts of *H. sabdariffa* indicates its toxicity against brine shrimp larvae. The lower the LC_{50} value, the higher the toxicity showed in table 1 and figure.

Table 1: LC_{50} (µg/ml) of the Crude Extracts of *H. Sabdariffa* Leaves.

CRUDE EXTRACTS	SOLVENT OF EXTRACTION	LC_{50} (µg/ml)
001JN	n-Hexane	72.26 (83.79-491.63)
002JE	Ethyl Acetate	51.19 (42.13-558.11)
003JM	Methanol	50.61 (43.18-458.12)

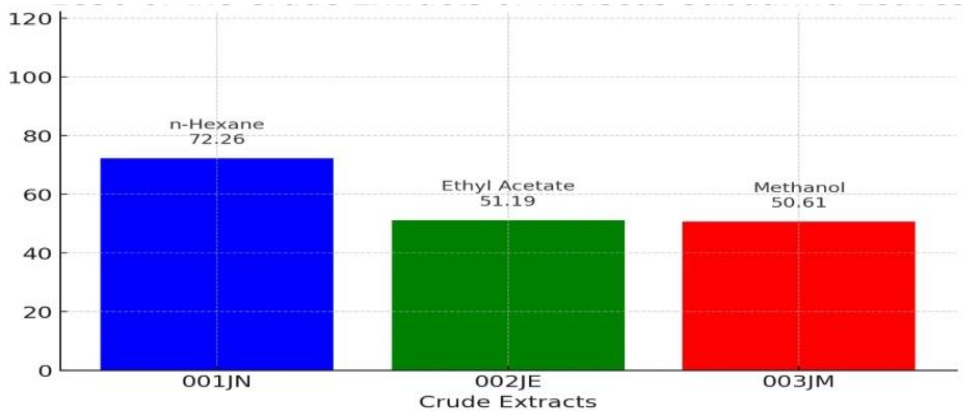

Figure 1: A bar chart showing LC_{50} of extracts from *H. sabdariffa* Leaf.

3.1.2 MTT Assay of N-Hexane, Ethyl Acetate, and Methanol Extracts.

Table 2a is the inhibitory activity of the extracts from *H. sabdariffa* Leaf against TNBC cell lines (Cell proliferation activity). The inhibition increases as the concentration of extracts increase on the four cell lines however; same action was noted on the control etoposide.

Table 2a: Inhibitory Activity of the extracts from *H. sabdariffa* Leaf against TNBC cell lines (Cell proliferation activity).

	Concentration µ/m	MCF7	Hs578T	SKBr3	MDAMB-231
001JN	0.25	246± 2.37	234.1 ±	306.6 ±	360.3 ± 2.144
	0.5	158.0± 2.370	1.273	2.571	268.0± 2.155
	1.0	77.3± 2.519	149.0±	265.0 ±	109.3± 3.132
002JE	0.25	197.6 ± 2.453	2.226	2.372	281.7± 2.140
	0.5	140.7± 2.519	90.3± 1.511	176.3 ±	199.0± 2.142
	1.0	98.5± 2.352	282.2±	2.271	67.2± 2.243
002JM	0.25	287.4 ± 2.271	2.401	227.2 ±	210.1± 2.230
	0.5	156.0 ± 2.361	171.3±	2.102	172.2± 2.145
	1.0	107.1± 1.283	2.360	201.1 ±	78.4± 2.167
Etoposide	0.25	144.3± 2.471	100.2±	2.305	144.3± 2.471
	0.5	105.7± 2.471	2.488	124.5±	105.7± 2.471
	1.0	68.9± 2.471	233.4±	2.472	68.9± 2.471
			2.461	211.4±	
			153.0±	2.412	
			2.981	175.0±	
			66.1± 2.743	2.312	
			144.3±	96 .1± 2.320	
			2.471	144.3±	
			105.7±	2.471	
			2.471	105.7±	
			78.9± 2.471	2.471	
				70.2± 2.471	

Table 2b presents the inhibitory activity of n-hexane, ethyl acetate and methanol extracts from *H. sabdariffa* leaves. The inhibitory activity compared well with the standard drug etoposide, revealing its potency. The lower the value of IC_{50} µ/ml the higher the potency of the extract against the four cell lines as shown in table 2b and figure 2.

Table 2b: IC_{50}µ/ml Values of extracts from *H. sabdariffa* Leaves.

Crude extracts	MCF7	Hs578T	SKBr3	MDAMB-231
001JN	77	90	>100	>100
002JE	98	100	>100	67
003JM	>100	66	96	78
Etoposide	68	78	70	69

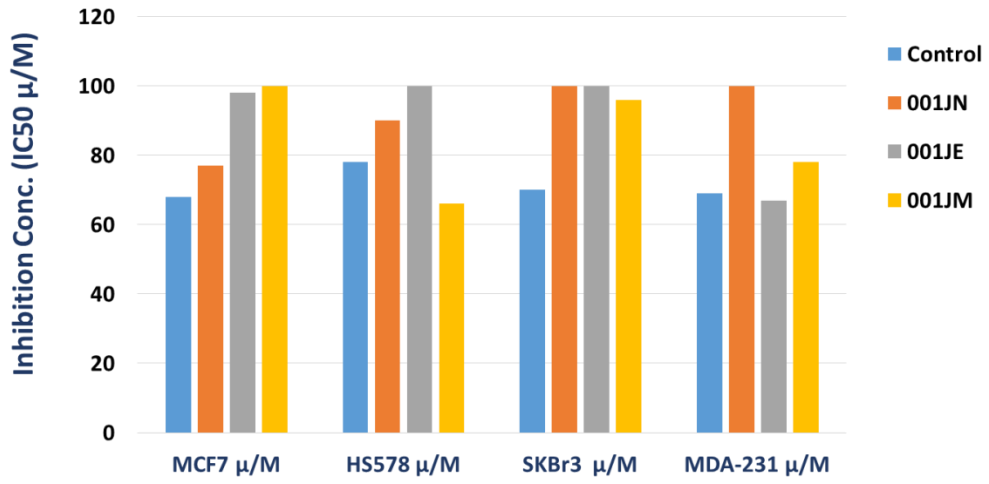

Figure 2: A bar graph of IC_{50} µ/ml Values of Extracts from *H. sabdariffa* leaves

3.2 Discussion

The Brine Shrimp Lethality Test (Table 1) showed high cytotoxicity across all extracts, with 27–30 mortality where 30 brine shrimp larvae were used. The methanol extract exhibited the highest cytotoxic activity, indicating potent cytotoxic compounds compared to ethyl acetate and n-hexane crude extract. The inhibition of methanol from Table 2b exhibited the cytotoxic effect of IC_{50} = 66 µM against the H_S578T cell line, outperforming etoposide (IC_{50} = 78 µM), and moderate activity of IC_{50} = 96 µM against the SKBr3 cell line; however, it was less potent than etoposide (IC_{50} = 70 µM). N-Hexane extract showed moderate activity (IC_{50} = 77 µM) against the MCF7 cell line; however, it was less potent than etoposide (IC_{50} = 68 µM), the standard drug. While ethyl acetate extract was most toxic (IC_{50} = 67 µM) against the MDA-MB-231 cell line, it was slightly more potent than etoposide (IC_{50} = 69 µM), the chemotherapy drug used as the standard. The cytotoxic effects of *H. sabdariffa* aqueous extract (HSE) on a human breast adenocarcinoma cell line (MCF-7) and normal foreskin fibroblast cells (HFFF) and apoptosis induction were assessed at a concentration of 0.5 mg/ml; the extract reduced the viability of MCF-7 cells to below 50% after 72 hours of incubation, demonstrating notable cytotoxic effects.[5] The cytotoxic activity of *H. sabdariffa* results showed IC_{50} 187.89 µg/ml against breast cancer cells (MDA-MB-231).[6] *H. sabdariffa* Linn flowers revealed cytotoxic activity with IC_{50} values of 719.28 µg/mL ethyl acetate and 906.57 µg/mL n-hexane, indicating weak cytotoxic activity.[7] In related research, the 95% ethanoic extract of *H. sabdariffa* dried leaves (HSDE95) demonstrated potent cytotoxicity with an IC_{50} of 8.58±0.68 µg/mL.[8] The cytotoxic potential of *H. sabdariffa* leaves showed an average IC_{50} of 43.48 µg/mL, indicating significant activity [9]

4. CONCLUSION

The study evaluated the cytotoxic effects of *H. sabdariffa* leaf extracts using n-hexane, ethyl acetate, and methanol extract against the Brine-Shrimp Lethality Test (BSLT) and four breast cancer cell lines (MCF7, MDA-MB-231, Hs578T, and SKBr3), comparing their efficacy to the standard chemotherapy drug etoposide. These findings highlight methanol extract's superior activity against H_S578T and SKBr3 cell lines, ethyl acetate's competitive efficacy against MDA-MB-231, and n-hexane's potency against MCF7. These may warrant further investigation for their potential in future breast cancer treatment strategies.

ACKNOWLEDGEMENT

The author gratefully acknowledges the Centre for Biotechnology Research and Development, Bayero University, Kano, for their support in the bioassay analysis. Appreciation is also extended to the Department of Chemistry, University of Abuja, for providing the necessary research facilities. Special thanks to my supervisor, mentors, family, and colleagues for their guidance and support.

CONFLICT OF INTERESTS

The authors declare no conflict of interests.

REFERENCES

(1) Esra, K. A.; Haroon, K.; Yaseen, H. Herbal Ingredients in the Prevention of Breast Cancer: Comprehensive Review of Potential Molecular Targets and Role of Natural Products. *ACS American Chemical Society.* **2022.**

(2) World Health Organisation (WHO), Breast Cancer. https://www.who.int. **2024.**

(3) Nicole, B. F. Understanding triple-negative breast cancer and its treatment. *Mayo Clinic Comprehensive Cancer Centre Blog*. **2024**

(4) Ali, E. A. Pharmacological and therapeutic importance of *Hibiscus Sabdariffa*. *ResearchGate.* **2018**. 10(3):451-475.

(5) Shahnaz, K.; Ahmad, S.; Parvin, P. Selective Cytotoxicity and Apoptogenic Activity of *Hibiscus Sabdariffa* Aqueous Extract against MCF-7 Human Breast Cancer Cell Line*. Journal of Cancer Therapy*. **2011**. 2, 394-400.

(6) Yuliastri, W. O.; Ajeng, D.; Isrul, M. Phytochemical Constituent and In-Vitro Cytotoxic Activity *of Hibiscus Sabdariffa L.* Calyx Fraction on Human Breast Cancer Cell Line MDA-MB-231. *ResearchGate: Journal of Chemistry.* **2022.** 15(03):1619-1625

(7) Qotrunnada, F.; Nadzila, A.; Norma, N. A. In vitro Cytotoxicity of *Hibiscus sabdariffa Linn* Extracts on A549 Lung Cancer Cell Line. *Pharmacognosy.* **2020.** 12(1): 1618-1623.

(8) Patsorn, W.; Arunporn I.; Srisopa, R. In vitro antioxidant, anti-inflammatory, and cytotoxic activity against prostate cancer of extracts from *Hibiscus sabdariffa* leaves. *PubMed.* **2014**. 8: S81-7.

(9) Formagio, A. S.; Foglio, M. A.; Carvalho, J. E. Phenolic compounds of *Hibiscus sabdariffa* and influence of organic residues on its antioxidant and antitumor properties. *PubMed*. **2015.** 75(1):6976.